



university of
groningen

faculty of science
and engineering

Time frequency analysis of the Kuramoto model

Master Project Mathematics

August 2017

Student: L.R. Zwerwer

Student number: 2183846

First supervisor: Prof.dr. H. Waalkens

Second supervisor: Prof.dr. E.C. Wit

Abstract

In this research we study the synchronization of the Kuramoto model. We discuss a threshold for synchronization of this model. Moreover, we discuss the stability of different states and reduce the Kuramoto model to a three dimensional system. Furthermore, we discuss chimera states. This is a state in which an array of oscillators splits into two (or more) groups; one group is completely synchronized in phase and frequency, while the other group is incoherent. For the chimera states we discuss a reduced system. Moreover, we discuss the bifurcations of chimera states. Subsequently we look deeper into the use of the wavelet transform as a tool to detect synchronization. Furthermore, we discuss time frequency plots for different situations. Using the time frequency analysis we confirm the threshold for synchronization and gain more insight into the process of synchronization. Finally, we discuss disadvantages and advantages of the wavelet transform as a tool to detect synchronization.

Contents

1	Introduction	5
2	The Kuramoto Model	7
2.1	Kuramoto Model	7
2.2	The order parameter and the critical coupling	8
2.3	Stability Analysis for the Distribution of the Oscillators	15
2.3.1	Discrete spectrum	17
2.3.2	Continuous spectrum	19
2.4	Stability Analysis for the order parameter	20
3	Reduction of the Kuramoto model with identical oscillators	23
3.1	Reduction of the general system	23
3.2	Reduction of the Kuramoto model	27
4	Chimera states	29
4.1	The phase equations	29
4.2	Reduced equations for the chimera states	30
4.3	Bifurcations of the chimera states	31
5	Time Frequency Analysis	33
5.1	Fourier Transform	34
5.2	Windowed Fourier Transform	34
5.3	Continuous Wavelet transform	36
6	Analysis of the Kuramoto Model	42
6.1	One Population of Oscillators	42
6.2	Two Populations of Oscillators	55
7	Time frequency analysis of chimera states	90
7.1	Two groups of two oscillators	90
7.2	Two groups of four oscillators	102
7.3	Two groups of hundred oscillators	114
8	Poincaré sections	126
9	Discussion	129
9.1	Numerical correctness	131

9.2	Advantages and disadvantages of the wavelet transform	131
9.3	Conclusion and further research direction	132
A	Appendix: Integration of the system	136
B	Appendix: Integration of the system for chimera states	140
C	Appendix: Calculating the wavelet transform	146
D	Appendix: Plot of the wavelet transform	152
E	Appendix: Poincaré map	156
F	Appendix: Calculating the two norm of the error for the numerical integration	162
G	Animation	168

1 Introduction

In the seventeenth century Huygens did a remarkable discovery about two pendula hanging next to each other against the wall. As Huygens watched the pendula oscillate, he found that the two pendula synchronized in time. He explained this phenomenon by a peculiar connection between the pendula. After Huygens many other scientists started to study synchronization.

Nowadays, three and a half centuries later, synchronization is still a frequently studied subject in physics, chemistry, biology, medicine and engineering, as it is recurrent in nature, society, and technology (Rodrigues, Peron, Ji & Kurths, 2016). We define synchronization as periods (or frequencies) that coincide. We will differentiate between two different types of locking; phase locking and frequency locking. Note that frequency locking implies phase locking. Examples of oscillators that synchronize are: networks of pacemaker cells in the heart, circadian pacemaker cells in the suprachiasmatic nucleus of the brain, metabolic synchrony in yeast cell suspensions, flashing of the fireflies, the chirps of crickets, arrays of lasers and microwave oscillators (cf. Strogatz, 2000).

Huygens was the first one to study synchronization of coupled oscillators (Rodrigues, Peron, Ji & Kurths, 2016). However, it was due to the work of Wiener (Wiener, 1961; Wiener, 1966), around 1960, that synchronization in large populations of oscillators obtained more attention (Rodrigues, Peron & Ji, 2016). Wiener showed interest in the generation of alpha rhythms in the brain and he hypothesized that this phenomenon was related to the same mechanism behind synchronization of other biological systems (Strogatz, 2000). Although Wiener's idea was correct, his idea was too difficult to obtain clear analytical results (Rodrigues, Peron & Ji, 2016).

Winfree proposed in 1967 a mathematical model which describes the synchronization of a population of oscillators or organisms (Oukill, Kessi & Thieullen, 2016). These oscillators or organisms have a simultaneous interaction. Winfree noticed that in order to simplify the model the coupling should be weak and the oscillators almost identical (Strogatz, 2000). Moreover, he found that spontaneous synchronization followed a threshold process (Rodrigues, Peron & Ji, 2016). More specifically, he found that when the spread of the frequencies of the oscillators is higher than the coupling between the oscillators, each oscillator continues to rotate with his own frequency. Hence, there is no synchronization of oscillators. This state is referred to as the incoherent state. When the coupling between the oscillators is higher than the spread of the oscillators the system will synchronize. This state is referred to as the synchronized state.

Kuramoto read the results of Winfree and started to simplify Winfree's model. His work

on the subject of synchronization led to a model that is now known as the Kuramoto model, which is seen as one of the most successful attempts to understand synchronization. The Kuramoto model is a model of phase oscillators that run at arbitrary intrinsic frequencies, and are coupled through the sine of the differences of their phase (Acebrón, Bonilla, Vicente, Ritort, & Spigler, 2005). For the Kuramoto model it is possible to exactly compute the critical coupling constant (Rodrigues, Peron & Ji, 2016; Strogatz, 2000). This makes the Kuramoto model attractive to use for research on synchronization. As for most coupled oscillators it is not that easy to compute a critical coupling, we have to use other methods to detect synchronization. One method to find out if the frequencies synchronized is time frequency analysis, which is further explained in Section 5.

Although global coupling is quite often explored (Bonilla, Perez Vincente, Ritort & Soler, 1998; Daido, 1996; Peleš & Wiesenfeld, 2003), there are still some interesting topics which can be discussed. An example of such a topic is applying time frequency analysis to multiple populations of oscillators.

Another interesting setup that is frequently studied in the last decade is an array of identical oscillators (the same frequency) with nonlocal coupling. Until ten years ago it was commonly believed that only systems of non identical oscillators exhibit interesting behavior like frequency locking, phase locking and partial synchronization. However, Kuramoto and Battogtokh (2002) found some intriguing solutions in systems of identical oscillators with nonlocal coupling. In these systems the array of oscillators splits into two (or more) groups; one group is completely synchronized in phase and frequency, while the other group is incoherent. Abrams and Strogatz (2004; 2006) named this phenomenon a chimera state. The name chimera comes from Greek mythology and refers to a fire spitting combination of a lion, a goat and a snake (Panaggio & Abrams, 2014).

Nonlocal interactions between oscillators are quite apparent in nature. One example of non locality may occur in the case of reaction-diffusion dynamics as a result of the disappearance of some rapidly diffusing components (Kuramoto & Battogtokh, 2002). Moreover there has been proof of chimera states in experiments with optical, chemical, mechanical, and electrochemical oscillators (cf. Panaggio, Abrams, Ashwin & Laing, 2016). It is logical to model the dynamics of such oscillators using a finite system of differential equations. However, finite systems exhibiting the behavior of chimera states are difficult to characterize because of fluctuations in the local synchrony (Panaggio, Abrams, Ashwin & Laing, 2016). As a result there was little progress in analyzing chimera states of finite systems for years. However, recently Ashwin and Burylko (2015) gave a formal definition of a weak chimera state, which allowed them to prove the existence and to investigate the stability and bifurcations of chimera states for finite networks. Even though chimera states look very closely

related to the questions about two groups of oscillators, recent research shows that a chimera state can not appear in a system that is globally coupled (Ashwin & Burylko, 2015).

The majority of the research on chimera state has been on a infinite network of oscillators (Panaggio, Abrams, Ashwin & Laing, 2016). In an infinite network the order parameter is stationary. As a consequence it is possible to analyze the chimera states using the Ott Antonsen Ansatz (The Ott Antonsen Ansatz is discussed in Section 2.4). This reduces the problem to an eigenvalue problem. However, as the problem is still difficult to solve most researchers discretize the solution and use numerical simulations to analyze the stability (Panaggio, Abrams, Ashwin & Laing, 2016). Although it is widely assumed that the systems for infinite and finite networks behave the same, this is not correct for all coupling schemes.

In this research we will look further into the Kuramoto model, time frequency analysis as a method to detect synchronization and chimera states. In Section 2 we will discuss the Kuramoto model; we will show the derivation of the critical coupling and discuss the stability of the Kuramoto model. After that, in Section 3, we will show a method to reduce the Kuramoto model with identical oscillators (i.e. all oscillators start with the same frequency) to a three dimensional system. Subsequently, in Section 4, we will discuss chimera states and we will show that in a chimera state the dynamics of each group are governed by three equations per group. Moreover, we will discuss the bifurcations of chimera states for different group sizes. In Section 5 we will discuss time frequency analysis and show a short example. After that, in Section 6 we will attempt to confirm the analytical results of the Kuramoto model using time frequency analysis. Furthermore, we will perform a time frequency analysis on two groups of oscillator and observe if there is a critical value in this case too. In the next Section (7) we will show time frequency analyses of chimera states for different group sizes and different parameters. In Section 8 we will look further into chimera states using a Poincaré section. Subsequently, we will discuss our results in Section 9. More specifically, we will have a closer look at the correctness of the numerical results, discuss the advantages and disadvantages of time frequency analysis, give a conclusion of our results and suggest further research directions.

2 The Kuramoto Model

2.1 Kuramoto Model

The Kuramoto model was defined in the eighties of the last century (Strogatz, 2000). The model assumes equally weighted oscillators, who are sinusoidally coupled. The phase equations are given by

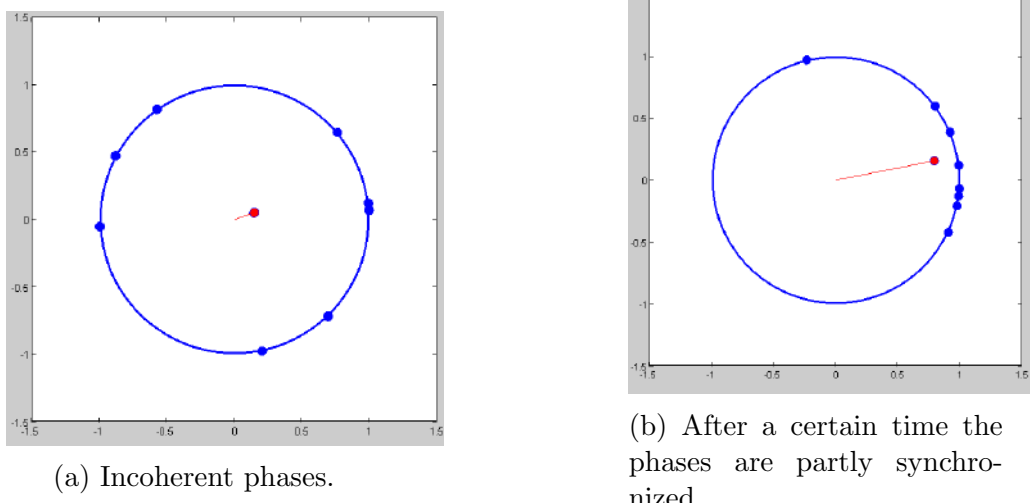


Figure 1: The phases of different oscillators running around on the unit circle. The order parameter is represented by the distance from the red dot to the origin.

$$\dot{\theta}_i = \omega_i + \sum_{j=1}^N \frac{K}{N} \sin(\theta_j - \theta_i), \quad i = 1, \dots, N, \quad (1)$$

where $\theta_i \in \mathbb{R}/2\pi\mathbb{Z}$ is the phase of oscillator i , ω_i its natural frequency, $K \geq 0$ the coupling strength and N the number of oscillators.

The frequencies ω_i are drawn from a probability density $g(\omega)$. This is an unimodal frequency distribution (i.e. there is just one local maximum). Moreover, the frequency distribution is assumed to be symmetric around the mean frequency Ω (this means that $g(\Omega+\omega) = g(\Omega-\omega)$ for all ω). Switching to a rotating frame with frequency Ω gives:

$$g(\omega) = g(-\omega).$$

2.2 The order parameter and the critical coupling

The order parameter, introduced by Kuramoto (Kuramoto, 1984), is a tool to find out if the phases of the oscillators are synchronized (Rodrigues, Peron & Ji, 2016). It can be seen as a collective rhythm of all the oscillators (Strogatz, 2000). According to Strogatz, to visualize the idea of the order parameter one has to imagine the phases of the oscillator running around on the unit circle (see Figure 1). The order parameter is given by

$$Re^{i\psi} = \frac{1}{N} \sum_{j=1}^N e^{i\theta_j}, \quad (2)$$

where ψ is the average phase of all oscillators. Moreover, $R \approx 0$ when the phases are equally divided around the unit circle and $R \approx 1$ when the phases are synchronized.

Kuramoto rewrote Equation (1) using the order parameter in such a way that the oscillators are only interacting through the quantities R and ψ (Strogatz, 2000). This can be done in the following way: multiply Equation (2) with $e^{-i\theta_i}$. This gives:

$$Re^{i(\psi-\theta_i)} = \frac{1}{N} \sum_{j=1}^N e^{i(\theta_j-\theta_i)}. \quad (3)$$

Only considering the imaginary part of Equation (3), we obtain:

$$R \sin(\psi - \theta_i) = \frac{1}{N} \sum_{j=1}^N \sin(\theta_j - \theta_i). \quad (4)$$

We recognize the same summation of sinusoid terms on the right hand side in both Equations (1) as well as (4). Hence, we can substitute the left hand side of Equation (4) in the right hand side of Equation (1). This results in:

$$\dot{\theta}_i = \omega_i + KR \sin(\psi - \theta_i), \quad i = 1, \dots, N. \quad (5)$$

Observe that each oscillator is attracted to the mean frequency ψ , where before each oscillator was drawn to the phase of any other oscillator. Note that the oscillators are more synchronized when the value R increases. Hence, the degree of synchronization R influences the system greatly.

The angular velocity of ψ equals the mean frequency Ω . Moreover we assume that we have a frame that rotates with velocity Ω . In this frame ψ is considered as a constant. Hence, without loss of generality we can take $\psi = 0$. Therefore, we obtain:

$$\dot{\theta}_i = \omega_i - KR \sin(\theta_i), \quad i = 1, \dots, N. \quad (6)$$

Looking further into the coupling, we differentiate between three different situations, namely $K \rightarrow 0$, $K \rightarrow \infty$ and $K_c < K < \infty$, where K_c is the critical coupling. If $K \rightarrow 0$, the solution of Equation (5) is $\theta_i \approx \omega_i t + \theta_i(0)$. Hence, when there is no coupling between the oscillators each oscillator rotates at its own frequency and has its own phase. Thus the phases and frequencies of the oscillators are incoherent.

In order to discuss the other situations we rewrite the order parameter (2) as

$$Re^{\psi i} = \int_{-\pi}^{\pi} e^{i\theta} \left(\frac{1}{N} \sum_{j=1}^N \delta(\theta - \theta_j) \right) d\theta. \quad (7)$$

Note that $e^{\psi i} = 1$, because we are in a rotating frame with $\psi = 0$. When $N \rightarrow \infty$, the mean over the delta functions in Equation (7) can be rewritten. We assume that the oscillators are distributed by a probability density $\rho(\theta, \omega, t)$, where $\rho(\theta, \omega, t)d\theta$ represents the fraction of oscillators between θ and $\theta + d\theta$ at time t with natural frequency ω . Hence, Equation (7) can be rewritten as

$$R = \int_{-\pi}^{\pi} \int_{-\infty}^{\infty} e^{i\theta} \rho(\theta, \omega, t) g(\omega) d\omega d\theta. \quad (8)$$

Note that inserting $\theta \approx \omega t$ (i.e. this is equivalent with $K \rightarrow 0$) in Equation (8) gives the inverse of the Fourier transform of $\rho(\theta, \omega, t)g(\omega)$ (see Section 5). Moreover, $\rho(\theta, \omega, t)g(\omega) \in L^1(\mathbb{R})$. Hence, the inverse of the Fourier transform of $\rho(\theta, \omega, t)g(\omega)$ is in $L^1(\mathbb{R})$ too. Therefore as $t \rightarrow \infty$ we obtain that $R \rightarrow 0$, which is in line with our expectation. Hence, we find no synchronization when $\theta \approx \omega t$.

When $K \rightarrow \infty$ the oscillators will synchronize to the average phase ψ with frequency Ω . Observe that setting θ equal to $\psi = 0$ in Equation (2), gives $R \rightarrow 1$.

Finally, when $K_c < K < \infty$ we find a state that is called partial synchronization, in which part of the oscillators are phase locked to the average phase $\psi = 0$ and the other part is moving out of synchrony with the locked part. This results in an order parameter that is between zero and one.

To find these fixed points we set $\dot{\theta} = 0$ in Equation (6). From this we find that oscillators that satisfy $|\omega| < KR$ have fixed points. However, we are only interested in stable fixed points. It turns out that for $-\pi/2 < \theta < \pi/2$ we find a stable fixed point. To see this we look at $\theta_i(t) = \theta'_i + u_i(t)$, where θ'_i is a fixed point and u_i is a small perturbation. Substituting θ_i into Equation (6) and rewriting using the Maclaurin series gives:

$$\begin{aligned}
\dot{u}_i &= \omega_i - KR \sin(\theta'_i + u_i) \\
&= \omega_i - KR \sin(\theta'_i) - KR \cos(\theta'_i)u_i \\
&= -KR \cos(\theta'_i)u_i,
\end{aligned}$$

for $i = 1 \dots N$. Hence, $\dot{u}_i = -Cu_i$, where $C = KR \cos(\theta'_i)$ is a constant. Solving this gives:

$$u_i = u_i(0)e^{-Ct}. \quad (9)$$

Analyzing Equation (9) we note that the perturbation shrinks for $C > 0$. Thus we have stable fixed points for $-\pi/2 < \theta < \pi/2$. Oscillators that satisfy $|\omega| \geq KR$ have no fixed points. These oscillators can not be phase locked and are out of synchrony with the locked oscillators.

To see what happens to their stationary density we look at the equations that contain the density. First of all the probability density $\rho(\theta, \omega, t)$ obeys the continuity equation

$$\frac{\partial \rho}{\partial t} + \frac{\partial v \rho}{\partial \theta} = 0, \quad (10)$$

where v is the angular velocity given by $\omega - KR \sin(\theta)$. Moreover, as $\rho(\theta, \omega, t)$ is a probability density, it follows the normalization condition

$$\int_{-\pi}^{\pi} \rho(\theta, \omega, t) d\theta = 1. \quad (11)$$

From Equation (10) we can conclude that the stationary density satisfies $\frac{\partial v \rho}{\partial \theta} = 0$. Therefore, $v \rho = C(\omega)$, where C is a constant value with respect to θ . From this we find that $\rho = C(\omega)/v$. This results in two options. If $C(\omega) \neq 0$ the oscillators are in the incoherent state with stationary density, this means that $|\omega| \geq KR$. In the case of a stationary density and $C(\omega) = 0$ ρ should be a delta function to obey the normalization condition (11). This situation corresponds to natural frequencies satisfying $|\omega| < KR$, and θ satisfying $-\pi/2 < \theta < \pi/2$. For this case we solve: $\frac{\partial v \rho}{\partial \theta} = 0$. This implies that $\omega_i - KR \sin(\theta_i) = 0$ for $i = 1, \dots, N$. Solving for θ gives: $\theta = \sin^{-1}(\frac{\omega}{KR})$. To fulfil the normalization condition (11) we get $\rho = \delta(\theta - \sin^{-1}(\frac{\omega}{KR}))$ whenever $|\omega| < KR$ and $-\pi/2 < \theta < \pi/2$. Hence, we can write the stationary density as follows:

$$\rho(\theta, \omega) = \begin{cases} \delta\left(\theta - \sin^{-1}\left(\frac{\omega}{KR}\right)\right)H(\cos(\theta - \psi)), & |\omega| < KR \\ \frac{C}{|\omega - KR \sin(\theta)|}, & |\omega| \geq KR, \end{cases} \quad (12)$$

where $H(x)$ is the Heaviside function, that is $H(x) = 1$ if $x > 0$ and $H(x) = 0$ when x is nonpositive. Hence the Heaviside function plays the role of the condition that was put on θ in order to find stable fixed points. Using the normalization condition (11) we can find the constant value C for each frequency, by solving for C in $\int_{-\pi}^{\pi} \frac{C}{|\omega - KR \sin(\theta)|} = 1$. This yields: $C = \sqrt{\omega^2 - (KR)^2}/(2\pi)$.

Finally, to find the critical value for K we substitute Equation (12) into Equation (8). This yields:

$$R = \int_{-\pi/2}^{\pi/2} \int_{-\infty}^{\infty} e^{i\theta} \delta\left(\theta - \sin^{-1}\left(\frac{\omega}{KR}\right)\right) g(\omega) d\omega d\theta + \int_{-\pi}^{\pi} \int_{|\omega| > KR} e^{i\theta} \frac{C}{|\omega - KR \sin(\theta)|} g(\omega) d\omega d\theta. \quad (13)$$

First we concentrate on the second part of this Equation. Recall that $g(\omega) = g(-\omega)$. Furthermore, we have the symmetry relation $\rho(\theta + \pi, -\omega) = \rho(\theta, \omega)$. This gives:

$$\begin{aligned} & \int_{-\pi}^{\pi} \int_{|\omega| > KR} e^{i\theta} \frac{C}{|\omega - KR \sin(\theta)|} g(\omega) d\omega d\theta \\ &= \int_{-\pi}^{\pi} \int_{KR}^{\infty} (e^{i\theta} \rho(\theta, \omega) g(\omega) + e^{i(\theta+\pi)} \rho(\theta + \pi, -\omega) g(-\omega)) d\omega d\theta \\ &= \int_{-\pi}^{\pi} \int_{KR}^{\infty} (e^{i\theta} \rho(\theta, \omega) g(\omega) - e^{i\theta} \rho(\theta, \omega) g(\omega)) d\omega d\theta \\ &= 0. \end{aligned}$$

Hence, Equation (13) becomes:

$$\begin{aligned} R &= \int_{-\pi/2}^{\pi/2} \int_{-\infty}^{\infty} e^{i\theta} \delta\left(\theta - \sin^{-1}\left(\frac{\omega}{KR}\right)\right) g(\omega) d\omega d\theta \\ &= \int_{|\omega| < KR} e^{i \sin^{-1}(\frac{\omega}{KR})} g(\omega) d\omega \\ &= \int_{|\omega| < KR} \left(\cos\left(\sin^{-1}\left(\frac{\omega}{KR}\right)\right) + i \frac{\omega}{KR} \right) g(\omega) d\omega. \end{aligned} \quad (14)$$

The integral over the imaginary part equals zero as this is an integral over an odd function. Therefore, we have:

$$R = \int_{|\omega| < KR} \cos\left(\sin^{-1}\left(\frac{\omega}{KR}\right)\right) g(\omega) d\omega.$$

Changing variables to $\theta = \sin^{-1}\left(\frac{\omega}{KR}\right)$ yields:

$$\begin{aligned} R &= \int_{-\pi/2}^{\pi/2} \cos(\theta) g(KR \sin(\theta)) KR \cos(\theta) d\theta \\ &= KR \int_{-\pi/2}^{\pi/2} \cos^2 \theta g(KR \sin \theta) d\theta. \end{aligned}$$

First of all there is the trivial solution $R = 0$ (i.e. the incoherent state), which corresponds to the uniform distribution $\rho = 1/(2\pi)$. The other solution corresponds to the partially synchronized oscillators and satisfies:

$$1 = K \int_{-\pi/2}^{\pi/2} \cos^2 \theta g(KR \sin \theta) d\theta. \quad (15)$$

To find the critical coupling K_c for which the solution bifurcates from $R = 0$, we substitute $R = 0$ in Equation (15). This gives:

$$K_c = \frac{2}{\pi g(0)}.$$

Hence, taking $K \geq K_c = \frac{2}{\pi g(0)}$ results in (partially) synchronized oscillators.

For the Lorentzian distribution it is possible to calculate the integral given by Equation (14). This distribution is given by:

$$g(\omega) = \frac{\gamma}{\pi(\gamma^2 + \omega^2)}. \quad (16)$$

First we substitute $\omega = KR \sin(u)$. This gives:

$$R = KR \int_{-\frac{\pi}{2}}^{\frac{\pi}{2}} e^{iu} \cos(u) g(KR \sin(u)) du \quad (17)$$

$$= \frac{KR}{2} \int_{-\pi}^{\pi} e^{iu} \cos(u) g(KR \sin(u)) du \quad (18)$$

$$= \frac{KR}{2} \int_{-\pi}^{\pi} e^{iu} \frac{e^{iu} + e^{-iu}}{2} g(KR \frac{e^{iu} - e^{-iu}}{2i}) du. \quad (19)$$

Next we substitute $z = e^{iu}$. This gives:

$$\begin{aligned} R &= \frac{KR}{2} \int_{|z|=1} \frac{z}{2} \left(z + \frac{1}{z} \right) g\left(\frac{KR}{2i}(z - \frac{1}{z})\right) \frac{dz}{iz} \\ &= \frac{1}{4i} \int_{|z|=1} G(z) \frac{z^2 + 1}{z} dz, \end{aligned} \quad (20)$$

where $G(z) = KRg(\frac{KR}{2i}(z - \frac{1}{z}))$. Substituting the Lorentzian distribution $g(\omega)$ into Equation (20) gives:

$$R = i\gamma KR \int_{|z|=1} \frac{z(z^2 + 1)}{\pi K^2 R^2 (z^2 - 1)^2 - 4\pi^2 \gamma^2 z^2} dz. \quad (21)$$

Next we use $\alpha = \gamma/(KR)$. We obtain:

$$R = \frac{i\alpha}{\pi} \int_{|z|=1} \frac{z(z^2 + 1)}{(z^2 - 1)^2 - 4\alpha^2 z^2} dz \quad (22)$$

$$= \frac{i\alpha}{\pi} \int_{|z|=1} \frac{z(z^2 + 1)}{(z^2 - 2\alpha z - 1)(z^2 + 2\alpha z - 1)} dz. \quad (23)$$

Using calculus of residues we obtain:

$$\begin{aligned} R &= -\alpha + \sqrt{\alpha^2 + 1} \\ &= \sqrt{1 + \left(\frac{\gamma}{KR}\right)^2} - \frac{\gamma}{KR}. \end{aligned} \quad (24)$$

Solving Equation (24) for R :

$$R = \sqrt{1 - \frac{K_c}{K}}, \quad (25)$$

where $K_c = 2\gamma$. Hence, for the Lorentzian distribution the critical value is given by $K_c = 2\gamma$. Moreover, we found an explicit expression for R . Equation (25) clearly shows that the order parameter grows as the spread of the Lorentzian distribution decreases. However, we still need to look at the relation between the distribution of the oscillators on the unit circle and the stability of these states while varying the coupling.

2.3 Stability Analysis for the Distribution of the Oscillators

In this subsection we will discuss the stability of the incoherent state. We will follow the article of Strogatz and Mirollo (1991). Note that it is possible to look at the stability of two different variables, namely the distribution of the oscillators $\rho(\theta, \omega, t)$ and the order parameter R . We will not discuss the stability of the synchronized state. A discussion about the stability of the synchronized state can be found in an article of Mirollo and Strogatz (2005).

To obtain results for the linear stability for the distribution of the incoherent state (i.e. $\rho(\theta, \omega, t)$) we use the continuity equation (10) (Strogatz, 2000). Recall that for the incoherent state we have the uniform distribution $\rho = \frac{1}{2\pi}$. Consider a perturbation of this distribution:

$$\rho = \frac{1}{2\pi} + \epsilon\eta(\theta, t, \omega) \quad (26)$$

Moreover, dividing Equation (8) on both sides by $e^{-i\theta}$ and considering the imaginary parts we obtain:

$$R \sin(\psi - \theta) = \int_{-\pi}^{\pi} \int_{-\infty}^{\infty} \sin(\theta' - \theta) \rho(\theta', \omega', t) g(\omega') d\omega' d\theta'.$$

Hence, substituting this into the expression of the angular velocity gives:

$$v = \omega + K \int_{-\pi}^{\pi} \int_{-\infty}^{\infty} \sin(\theta' - \theta) \rho(\theta', \omega', t) g(\omega') d\omega' d\theta'. \quad (27)$$

We substitute Equations (26) and (27) into the continuity Equation (10). We obtain:

$$\frac{\partial \eta}{\partial t} + \frac{\partial}{\partial \theta} \left[\omega \eta + \frac{K}{2\pi} \int_{-\pi}^{\pi} \int_{-\infty}^{\infty} \eta(\theta, t, \omega) g(\omega') \sin(\theta' - \theta) d\omega' d\theta' \right] = 0. \quad (28)$$

Inserting the Fourier series of $\eta(\theta, t, \omega)$ and interchanging the integrals gives:

$$\frac{\partial \eta}{\partial t} + \frac{\partial}{\partial \theta} \left[\omega \eta + \frac{K}{2\pi} \int_{-\infty}^{\infty} \int_{-\pi}^{\pi} \sum_{n=1}^{\infty} (c_n(t, \omega) e^{in\theta'} + \bar{c}_n(t, \omega) e^{-in\theta'}) \sin(\theta' - \theta) d\theta' g(\omega') d\omega' \right] = 0 \quad (29)$$

First we consider the inner integral. We rewrite the sine as complex exponentials. Moreover, recall that $\int_{-\pi}^{\pi} e^{im\theta'} e^{-in\theta'} d\theta'$ gives π whenever $m = n$ and zero when m equals n . We obtain the following:

$$\int_{-\pi}^{\pi} \sum_{n=1}^{\infty} (c_n(t, \omega) e^{in\theta'} + \bar{c}_n(t, \omega) e^{-in\theta'}) \sin(\theta' - \theta) d\theta' = \begin{cases} -2\pi \text{Im}(c_1(t, \omega) e^{in\theta}) & \text{if } n = 1 \\ 0 & \text{if } n = 0. \end{cases}$$

We obtain the following differential equations:

$$\begin{cases} \frac{\partial c_n(t, \omega)}{\partial t} + i\omega c_n(t, \omega) - \frac{K}{2} \int_{-\infty}^{\infty} c_n(t, \omega') g(\omega') d\omega' = 0 & \text{for } n = 1 \\ \frac{\partial c_n(t, \omega)}{\partial t} + in\omega c_n(t, \omega) = 0 & \text{for } n \geq 2 \end{cases} \quad (30)$$

The second equation (i.e. $n \geq 2$) can be solved directly and gives: $c_n(t, \omega) = c_n(0, \omega) e^{-in\omega t}$. The first equation has a remarkable structure; for a fixed frequency ω the evolution in time depends on all the other frequencies. However, this relation is the same for each frequency as there is no dependency of ω in the integral. We can rewrite the first equation using an operator A that acts on $c_1(t, \omega)$. We define operator A as follows:

$$Ac_1(t, \omega) = -i\omega c_1(t, \omega) + \frac{K}{2} \int_{-\infty}^{\infty} c_1(t, \omega') g(\omega') d\omega'.$$

This gives:

$$\frac{\partial c_1(t, \omega)}{\partial t} = Ac_1(t, \omega).$$

The spectrum of A consist of a continuous and discrete part. In the following subsection we will discuss both parts separately.

2.3.1 Discrete spectrum

We find the discrete eigenvalues through the Ansatz: $c_1(t, \omega) = b(\omega)e^{\lambda t}$, where λ is an eigenvalue. This gives:

$$\lambda b(\omega) = -i\omega b(\omega) + \frac{K}{2} \int_{-\infty}^{\infty} b(\omega') g(\omega') d\omega'. \quad (31)$$

Let: $B = K/2 \int_{-\infty}^{\infty} b(\omega') g(\omega') d\omega'$. This gives the following expression for $b(\omega)$:

$$b(\omega) = \frac{B}{\lambda + i\omega}, \quad (32)$$

where we assumed that $\lambda + i\omega \neq 0$. In Subsection 2.3.2 we will show that $\lambda + i\omega = 0$ belongs to the continuous spectrum. Rewriting Equation (31) using (32) gives:

$$\lambda \frac{B}{\lambda + i\omega} = -i\omega \frac{B}{\lambda + i\omega} + \frac{K}{2} \int_{-\infty}^{\infty} \frac{B}{\lambda + i\omega'} g(\omega') d\omega'. \quad (33)$$

This gives $B = 0$ or $1 = K/2 \int_{-\infty}^{\infty} \frac{g(\omega')}{\lambda + i\omega'} d\omega'$. However, B can not equal zero as in that case Equation (32) implies that $b(\omega)$ is zero and this implies that $c_1(t, \omega) = 0$ for all ω . This is a contradiction as $c_1(t, \omega)$ is an eigenfunction. Therefore we only consider:

$$1 = K/2 \int_{-\infty}^{\infty} \frac{g(\omega')}{\lambda + i\omega'} d\omega'. \quad (34)$$

Substituting the Lorentzian distribution into Equation (34) gives:

$$\begin{aligned} 1 &= \frac{K}{2} \int_{-\infty}^{\infty} \frac{\gamma}{\pi(\lambda + i\omega)(\omega^2 + \gamma^2)} d\omega \\ &= \frac{K\gamma}{2\pi i} \int_{-\infty}^{\infty} \frac{1}{(\omega - i\lambda)(\omega^2 + \gamma^2)} d\omega. \end{aligned} \quad (35)$$

We solve the right hand side of Equation (35) using the calculus of residues. The integrand has poles at λi , γi and $-\gamma i$. The pole with lambda can be on the lower half plane or on the upper half plane. In case of a negative lambda we close the integration path with a half circle on the upper half plane. This gives a contradiction:

$$1 = \frac{K}{2(\lambda - \gamma)} < 0.$$

For a positive λ we close the integration path with a half circle on the lower half plane. This gives:

$$1 = \frac{K}{2(\lambda + \gamma)}. \quad (36)$$

We obtain:

$$\lambda = \frac{K - K_c}{2}.$$

Hence, small perturbations grow exponentially for $K > K_c$. This means that the incoherent state becomes unstable when $K > K_c$.

In case of a different distribution Equation (34) should be solved differently. Recall that $g(\omega)$ is a symmetric and unimodal distribution. Strogatz and Mirollo (1990) proved that under the assumptions for $g(\omega)$ mentioned above, Equation (34) has at most one solution (proof of Theorem 2). Moreover, in case that a solution exists it should be real. They also showed that Equation (34) becomes:

$$1 = \frac{K}{2} \int_{-\infty}^{\infty} \frac{\lambda}{\lambda^2 + \omega'^2} g(\omega') d\omega'. \quad (37)$$

Analysis of Strogatz and Mirollo on Equation (37) provided the first proof for general distributions that the incoherent state becomes unstable when $K > K_c$. The proof is relatively simple and goes as follows: Let $\lambda \rightarrow 0^+$, as a result the function $\lambda/(\lambda^2 + \omega'^2)$ will continue to sharpen about $\nu = 0$. However, the integral of this function over the real line equals π for all $\lambda > 0$. Hence, this function goes to $\pi\delta(\nu)$ as $\lambda \rightarrow 0^+$. We can conclude that the right hand side of (37) goes to $(K/2)\pi g(0)$. Thus $\lambda > 0$ for $K > 2/(\pi g(0))$ as desired. The results of Strogatz and Mirollo are quite surprising as Equation (37) shows that $\lambda > 0$, which implies that the incoherent state is never linearly stable.

2.3.2 Continuous spectrum

The continuous part of the spectrum of A is defined as the set of complex numbers such that the operator $A - \lambda I$ is not surjective (Strogatz & Mirolo, 1991). Hence, we need to consider:

$$-(\lambda + i\omega)b(\omega) + \frac{K}{2} \int_{-\infty}^{\infty} b(\omega')g(\omega')d\omega' = f(\omega) \quad (38)$$

for fixed λ and any function $f(\omega)$. In case that Equation (38) is solvable for all $b(\omega)$ λ is not in the spectrum. Note that the integral does not depend on ω . Therefore when $\lambda + i\omega = 0$ Equation (38) is not solvable for all $f(\omega)$. Thus we can conclude that the continuous spectrum contains $\{i\omega : \omega \in \text{support}(g)\}$. It turns out that this forms the whole continuous spectrum of A . To show that nothing else is contained in the continuous spectrum we suppose that λ is in the continuous spectrum and not in $\{i\omega : \omega \in \text{support}(g)\}$. As $\lambda + i\omega \neq 0$ it is possible to solve Equation (38) for $b(\omega)$. We obtain:

$$b(\omega) = \frac{B - f(\omega)}{\lambda + i\omega}, \quad (39)$$

where $B = K/2 \int_{-\infty}^{\infty} b(\omega')g(\omega')d\omega'$. Next we will show that B can be determined self consistently. Substituting Equation (39) into the expression for B we obtain:

$$\begin{aligned} B &= \frac{K}{2} \int_{-\infty}^{\infty} \left[\frac{B - f(\omega')}{\lambda + i\omega'} \right] g(\omega')d\omega' \\ &= \frac{BK}{2} \int_{-\infty}^{\infty} \left[\frac{g(\omega')}{\lambda + i\omega'} \right] d\omega' - \frac{K}{2} \int_{-\infty}^{\infty} \left[\frac{f(\omega')}{\lambda + i\omega'} \right] g(\omega')d\omega'. \end{aligned}$$

This gives:

$$B \left(1 - \frac{K}{2} \int_{-\infty}^{\infty} \frac{g(\omega')}{\lambda + i\omega'} d\omega' \right) = -\frac{K}{2} \int_{-\infty}^{\infty} \left[\frac{f(\omega')}{\lambda + i\omega'} \right] g(\omega')d\omega'. \quad (40)$$

We assumed that λ was not in the discrete spectrum. Therefore by Equation (34) it follows that the coefficient of B is nonzero. This means that Equation (40) is solvable for B . Thus λ is not in the continuous spectrum. Hence, the continuous spectrum is given by $\{i\omega : \omega \in \text{support}(g)\}$. This implies neutral stability.

Hence, we showed that the distribution of the oscillators for the incoherent state is neutrally stable for $K < K_c$ and unstable for $K > K_c$.

2.4 Stability Analysis for the order parameter

In Subsection 2.2 we discussed two different branches of the order parameter. In this subsection we will discuss the stability of these branches. In order to find the stability of these branches we use the continuity Equation (10). Substituting the expression of the angular velocity (Equation (27)) into the continuity equation gives:

$$\begin{aligned} 0 &= \frac{\partial \rho}{\partial t} + \frac{\partial}{\partial \theta} \left[\rho \left(\omega + K \int_{-\pi}^{\pi} \int_{-\infty}^{\infty} \sin(\theta' - \theta) \rho(\theta', \omega', t) g(\omega') d\omega' d\theta' \right) \right] \\ &= \frac{\partial \rho}{\partial t} + \frac{\partial}{\partial \theta} \left[\rho \left(\omega + K \operatorname{Im} \int_{-\pi}^{\pi} \int_{-\infty}^{\infty} e^{i(\theta' - \theta)} \rho(\theta', \omega', t) g(\omega') d\omega' d\theta' \right) \right] \\ &= \frac{\partial \rho}{\partial t} + \frac{\partial}{\partial \theta} [\rho (\omega + K \operatorname{Im}(Re^{i\psi} e^{-i\theta}))]. \end{aligned} \quad (41)$$

Next we use the Fourier expansion of $\rho(\theta, \omega, t) = 1/(2\pi) \sum_{n=-\infty}^{\infty} c_n(t, \omega) e^{in\theta}$. In this expansion we have $c_{-n} = \bar{c}_n$. Moreover, because of the normalization condition (11) $c_0 = 1$. Substituting this in the expression for $Re^{i\psi}$ (Equation (8)) gives:

$$\begin{aligned} Re^{i\psi} &= \frac{1}{2\pi} \int_{-\pi}^{\pi} e^{n\theta'} e^{i\theta'} d\theta' \int_{-\infty}^{\infty} \sum_{n=-\infty}^{\infty} c_n(t, \omega) g(\omega') d\omega' \\ &= \int_{-\infty}^{\infty} \bar{c}_1(t, \omega') g(\omega') d\omega'. \end{aligned} \quad (42)$$

Substituting the Fourier expansion of ρ into Equation (41) and rewriting gives the following relation:

$$\frac{\partial c_n(t, \omega)}{\partial t} + in(\omega c_n + \frac{KRe^{i\psi}}{2i} c_{n+1} - \frac{KRe^{-i\psi}}{2i} c_{n-1}) = 0. \quad (43)$$

The next step is to use the Ott Antonsen Ansatz. This Ansatz only considers distributions that obey $c_n(t, \omega) = \alpha(t, \omega)^n$ for $n > 1$. For $n < 1$ this means $c_n = c_{|n|} = \bar{\alpha}^{|n|}$. Combining this with Equation (42) gives:

$$Re^{-i\psi} = \int_{-\infty}^{\infty} g(\omega') \alpha(t, \omega') d\omega'.$$

We assume that α is analytic in the lower half complex plane. Moreover, we choose again the Lorentzian distribution for the frequency distribution. Now it is possible to analyze the integral of $Re^{-i\psi}$ using residues. There are two poles; $-i\gamma$ and $i\gamma$. We will analyze the integral via a path on the lower half of the complex plane. This gives:

$$Re^{-i\psi} = -2\pi i \text{Res}(i\gamma) \quad (44)$$

$$= \alpha(-i\gamma, t). \quad (45)$$

Furthermore, substituting the expression for (45), $c_n(t, \omega) = \alpha(t, \omega)^n$ and $\omega = -i\gamma$ into Equation (43) gives:

$$\begin{aligned} 0 &= \frac{d}{dt} Re^{-i\psi} + \gamma Re^{-i\psi} + \frac{K Re^{-i\psi}}{2} [R^2 - 1] \\ &= e^{-i\psi} \frac{dR}{dt} - iR \frac{d\psi}{dt} e^{-i\psi} + \gamma Re^{-i\psi} + \frac{K Re^{-i\psi}}{2} [R^2 - 1]. \end{aligned}$$

From this we obtain two ordinary differential equations. The first one is $R\dot{\psi} = 0$. The second differential equation is given by:

$$\frac{dR}{dt} + \gamma R + \frac{KR}{2} (R^2 - 1) = 0. \quad (46)$$

We define $f(R) = -\gamma + -(KR)/2(R^2 - 1)$. The equilibria of this equation are the two branches of R ; 0 and $\sqrt{1 - K_c/K}$. The linear stability can be determined using the derivative of $f(R)$;

$$f'(0) = -\gamma + \frac{K}{2} \quad (47)$$

$$= \frac{K - K_c}{2}. \quad (48)$$

Hence, for the incoherent state whenever $K < K_c$ the derivative is negative. This implies stability for $K < K_c$. In the case that $K > K_c$, the incoherent state is unstable as $f'(0) > 0$. For the locked state we obtain:

$$\begin{aligned}
f'(\sqrt{1 - 2\gamma/K}) &= -\gamma + \frac{K}{2} - \frac{3K(1 - 2\gamma/K)}{2} \\
&= 2\gamma - K \\
&= -(K - K_c).
\end{aligned}$$

Therefore, the branch of the locked state is stable for $K > K_c$. Moreover, for $K < K_c$ this branch does not exist.

At last we will show that as t goes to infinity we will see the behavior mentioned above. We will use the substitution $u = R^2$ to solve the differential equation of (46). Multiplying Equation (46) by $2R$ and substituting u gives:

$$\frac{du}{dt} = (K - K_c)u - Ku^2.$$

We define $\delta = 1 - K_c/K$ and obtain:

$$\frac{du}{dt} = K(\delta u - u^2) \quad (49)$$

We obtain: $u/(u - \delta) = Ce^{\delta K t}$. Which can be rewritten as:

$$u = \frac{\delta}{1 - \frac{1}{C}e^{-(K-K_c)t}}. \quad (50)$$

We define the initial value $u(0) = u_0$, solving the constant gives: $C = u_0/(u_0 - \delta)$. We obtain the following expression for u :

$$u = \frac{\delta u_0}{u_0 - (u_0 - \delta)e^{-(K-K_c)t}}. \quad (51)$$

The limit of $t \rightarrow \infty$ has three cases; $K - K_c < 0$, $K - K_c > 0$ together with $u_0 \neq 0$ and $u_0 = 0$.

The first case gives $u = 0$. Hence, as expected, when the coupling strength is smaller than the critical coupling, the order parameter R is zero in the limit of $t \rightarrow \infty$. The second limit gives: $u = \delta$. Therefore, in line with our previous calculations, in the case that the coupling is greater than the critical coupling and $u_0 \neq 0$ we obtain $\sqrt{1 - K_c/K}$ as t goes to infinity. Finally, when $u_0 = 0$ then $u(t) = 0$, $t \in [0, \infty)$.

3 Reduction of the Kuramoto model with identical oscillators

In the previous section we discussed the Kuramoto model as a N -dimensional system. This system is significantly large when the number of oscillators is big. However, we will show that this system possess $N - 3$ constants of motion. Hence, the N -dimensional system can be rewritten as a three dimensional system. Unfortunately, this reduction is only possible for a system with identical oscillators (i.e. the frequency ω must be identical for all oscillators). Moreover, the number of oscillators has to be greater than three.

The idea of this section is based on the work of Watanabe and Strogatz, who discovered the reduction of the Kuramoto model in 1994 (Watanabe & Strogatz, 1994). To rewrite the Kuramoto model to a three-dimensional system, they suggested the use of a nonlinear transformation, also referred to as the Watanabe and Strogatz transformation. They started from the most general form of equations which this transformation applies to. These equations can easily be rewritten to the Kuramoto model. We will start this section by showing the reduction of the general system of N equations to a three dimensional system and towards the end of this section we will show the reduction of the Kuramoto model.

3.1 Reduction of the general system

Assume we have N identical phase oscillators. The equations of these phase oscillators are governed by:

$$\dot{\theta}_i = f + g \cos(\theta_i) + h \sin(\theta_i), \quad i = 1, \dots, N, \quad (52)$$

where the functions f , g and h , depend on $\theta_1, \theta_2, \dots, \theta_N \in \mathbb{Z}/2\pi\mathbb{Z}$ and maps these variables to \mathbb{R} . The functions f , g and h must not depend on the subscript i . Hence, these functions must be the same for all oscillators. Now consider the following change of variables:

$$\tan \left[\frac{1}{2}(\theta_i(t) - \Theta(t)) \right] = \sqrt{\frac{1 + \gamma(t)}{1 - \gamma(t)}} \tan \left[\frac{1}{2}(\psi_i - \Psi(t)) \right], \quad i = 1, \dots, N, \quad (53)$$

where ψ_i are constants depending on the oscillator and $0 \leq \gamma(t) < 1$. The functions $\Theta(t)$, $\Psi(t)$ and $\gamma(t)$ are unknown for now and their evolution will be derived later on in this section. It turns out that an arbitrary solution $\theta_i(t)$ of Equation (52) has the form of (53).

This transformation is called the Watanabe and Strogatz transformation. To motivate this transformation we consider a special case of Equation (52) in which f , g and h are constants. Then the solution of (52) has the form of (53) with $\Theta(t)$ and $\Psi(t)$ proportional to t . Moreover, $\gamma(t)$ is constant. By variation of parameters one finds (53).

The Watanabe and Strogatz transformation basically relabels the phases θ_i to ψ_i . It starts by going into a rotating reference frame $\Theta(t)$. Subsequently the circle is reparametrized with a nonlinear transformation, which is characterized by $\gamma(t)$. After that we go into a rotating reference frame $\Psi(t)$. Now all oscillators look motionless.

To reduce the System (52) we need to rewrite Equation (52) to the new variables ψ_i , $\Psi(t)$ and $\gamma(t)$. For this we need to find an expression for $\sin \theta_i$, $\cos \theta_i$ and $\dot{\theta}_i$. We start by rewriting Equation (53) to $\sin(\theta_i - \Theta)$ and $\cos(\theta_i - \Theta)$. This can be done using the identity $\tan(\frac{1}{2}x) = +/ - \sqrt{\frac{1-\cos x}{1+\cos x}}$. Hence, this gives:

$$\begin{aligned} \frac{1 - \cos \left[\frac{1}{2}(\theta_i - \Theta) \right]}{1 + \cos \left[\frac{1}{2}(\theta_i - \Theta) \right]} &= \frac{(1 + \gamma)(1 - \cos(\psi_i - \Psi))}{(1 - \gamma)(1 + \cos(\psi_i - \Psi))} \\ \implies \cos(\theta_i - \Theta) &= \frac{\cos(\psi_i - \Psi) - \gamma}{1 - \gamma \cos(\psi_i - \Psi)}. \end{aligned} \quad (54)$$

From the expression of $\cos(\theta_i - \Theta)$ we can find the expression of $\sin(\theta_i - \Theta)$ using the identity $\cos^2 x + \sin^2 x = 1$. This yields:

$$\sin(\theta_i - \Theta) = \frac{\sqrt{1 - \gamma^2} \sin(\psi_i - \Psi)}{1 - \gamma \cos(\psi_i - \Psi)}. \quad (55)$$

To obtain the expression of $\cos \theta_i$ we multiply Equation (54) by $\cos \Theta$ and Equation (55) by $\sin \Theta$. Subsequently we subtract these equations. Using the angle transformation formula, this gives:

$$\cos \theta_i = \frac{[\cos(\psi_i - \Psi) - \gamma] \cos \Theta - \sqrt{1 - \gamma^2} \sin \Theta \sin(\psi_i - \Psi)}{1 - \gamma \cos(\psi_i - \Psi)}. \quad (56)$$

A similar calculation yields the expression for $\sin \theta_i$:

$$\sin \theta_i = \frac{[\cos(\psi_i - \Psi) - \gamma] \sin \Theta + \sqrt{1 - \gamma^2} \cos \Theta \sin(\psi_i - \Psi)}{1 - \gamma \cos(\psi_i - \Psi)}. \quad (57)$$

Hence, we can rewrite the right hand side of (52). However, we still need an expression for the left hand side of (52). This can be obtained by solving Equation (53) for θ_i and differentiating with respect to t . We obtain:

$$\frac{d}{dt}\theta_i = \frac{d}{dt}\Theta + 2\frac{d}{dt}\left[\arctan(\Gamma \tan\left[\frac{1}{2}(\psi_i - \Psi)\right])\right],$$

where $\Gamma = \sqrt{(1 + \gamma)/(1 - \gamma)}$. Working out the differentiation gives:

$$\begin{aligned}\dot{\theta}_i &= \dot{\Theta} + \frac{2}{1 + \Gamma^2 \tan^2\left[\frac{1}{2}(\psi_i - \Psi)\right]} \left(\dot{\Gamma} \tan\left[\frac{1}{2}(\psi_i - \Psi)\right] + \frac{\Gamma}{\cos^2\left[\frac{1}{2}(\psi_i - \Psi)\right]} (-\frac{1}{2}\dot{\Psi}) \right) \\ &= \dot{\Theta} + \frac{\Gamma\left(\frac{\dot{\Gamma}}{\Gamma} \sin(\psi_i - \Psi) - \dot{\Psi}\right)}{\cos^2\left[\frac{1}{2}(\psi_i - \Psi)\right] + \Gamma^2 \sin^2\left[\frac{1}{2}(\psi_i - \Psi)\right]}. \end{aligned} \quad (58)$$

Moreover, we have:

$$\begin{aligned}\frac{\dot{\Gamma}}{\Gamma} &= \frac{1}{2\Gamma^2} \frac{d\Gamma^2}{dt} = \frac{\dot{\gamma}}{\Gamma^2(1 - \gamma)^2} \\ &= \frac{\dot{\gamma}}{1 - \gamma^2}, \end{aligned} \quad (59)$$

and we also have:

$$\begin{aligned}\cos^2\left[\frac{1}{2}(\psi_i - \Psi)\right] + \Gamma^2 \sin^2\left[\frac{1}{2}(\psi_i - \Psi)\right] &= \frac{1}{2}(\cos(\psi_i - \Psi)(1 - \Gamma^2) + \Gamma^2 + 1) \\ &= \frac{1 - \gamma \cos(\psi_i - \Psi)}{1 - \gamma}. \end{aligned} \quad (60)$$

Substituting Equations (59) and (60) into Equation (58) gives:

$$\begin{aligned}\dot{\theta}_i &= \dot{\Theta} + \frac{\Gamma(1 - \gamma)\left(\frac{\dot{\gamma}}{1 - \gamma^2} \sin(\psi_i - \Psi) - \dot{\Psi}\right)}{1 - \gamma \cos(\psi_i - \Psi)} \\ &= \dot{\Theta} + \frac{\dot{\gamma} \sin(\psi_i - \Psi) - (1 - \gamma^2)\dot{\Psi}}{\sqrt{1 - \gamma^2}(1 - \gamma \cos(\psi_i - \Psi))}. \end{aligned} \quad (61)$$

Hence, we have got an expression for $\cos \theta_i$, $\sin \theta_i$ and $\dot{\theta}_i$. The next step is to substitute these expressions into Equation (52) and from this we can derive the reduced system, which

contains three differential equations that do not depend on i . Substituting Equations (54), (55) and (61) into Equation (52) gives:

$$\begin{aligned} \dot{\Theta} + \frac{\dot{\gamma} \sin(\psi_i - \Psi) - (1 - \gamma^2)\dot{\Psi}}{\sqrt{1 - \gamma^2}(1 - \gamma \cos(\psi_i - \Psi))} &= f + g \frac{(\cos(\psi_i - \Psi) - \gamma) \cos \Theta}{1 - \gamma \cos(\psi_i - \Psi)} \\ &\quad - g \frac{\sqrt{1 - \gamma^2} \sin(\psi_i - \Psi) \sin \Theta}{1 - \gamma \cos(\psi_i - \Psi)} \\ &\quad + h \frac{(\cos(\psi_i - \Psi) - \gamma) \sin \Theta - \sqrt{1 - \gamma^2} \sin(\psi_i - \Psi) \cos \Theta}{1 - \gamma \cos(\psi_i - \Psi)}, \end{aligned} \quad (62)$$

for $i = 1, \dots, N$. Observe that all denominators have a factor $1 - \gamma \cos(\psi_i - \Psi)$. Therefore we multiply both sides of Equation (62) with $1 - \gamma \cos(\psi_i - \Psi)$. Moreover, we write all expressions on one side and rearrange them in such a way that they are of the form (52). This yields:

$$\begin{aligned} 0 &= (\dot{\Theta} - \sqrt{1 - \gamma^2}\dot{\Psi} - f + g\gamma \cos \Theta + h\gamma \sin \Theta) \\ &\quad + (-\gamma\dot{\Theta} + f\gamma - g \cos \Theta - h \sin \Theta) \cos(\psi_i - \Psi) \\ &\quad + \left(\frac{\dot{\gamma}}{\sqrt{1 - \gamma^2}} + g\sqrt{1 - \gamma^2} \sin \Theta + h\sqrt{1 - \gamma^2} \cos \Theta \right) \sin(\psi_i - \Psi). \end{aligned} \quad (63)$$

Note that the coefficients of Equation (63) are independent of i , which means that they are the same for all oscillators. Hence, for Equation (63) to be satisfied for all i and t the coefficients have to be zero. This gives:

$$\sqrt{1 - \gamma^2}\dot{\Psi} = \dot{\Theta} - f + g\gamma \cos \Theta + h\gamma \sin \Theta \quad (64)$$

$$\gamma\dot{\Theta} = f\gamma - g \cos \Theta - h \sin \Theta \quad (65)$$

$$\frac{\dot{\gamma}}{\sqrt{1 - \gamma^2}} = -g\sqrt{1 - \gamma^2} \sin \Theta - h\sqrt{1 - \gamma^2} \cos \Theta. \quad (66)$$

Note that Equation (64) contains two differentials. Therefore we multiply this equation by γ and then substitute Equation (65) into (64). Moreover, we multiply Equation (66) by $\sqrt{1 - \gamma^2}$. This gives the following system of differential equations:

$$\begin{aligned}
\gamma \dot{\Psi} &= -\sqrt{1-\gamma^2}(g \cos \Theta + h \sin \Theta) \\
\gamma \dot{\Theta} &= f\gamma - g \cos \Theta - h \sin \Theta \\
\dot{\gamma} &= -(1-\gamma^2)(g \sin \Theta + h \cos \Theta).
\end{aligned} \tag{67}$$

In this system ψ_i is a parameter, that depends on the oscillator. Whenever the above differential equations are satisfied, $\theta_i(t)$ will satisfy all N equations of System (52).

Observe that there are some issues with the system (67). First of all note that whenever $\gamma = 0$, it is possible for $\dot{\gamma}$ to be negative. This implies that γ could be negative at some point, which is a contradiction with its definition. Another problem is that the equations of (52) cannot be valid when $\gamma = 0$ except when $f \rightarrow 0$, $g \rightarrow 0$ and $h \rightarrow 0$. Observe that whenever $\gamma = 0$ both $\dot{\Theta}$ and $\dot{\Psi}$ are singular. Watanabe and Strogatz thrived to solve this singularity by using a change to a Cartesian type of coordinate system. However, they made a small error in a sign in (67). Whenever the sign is changed, the coordinate change suggested by Watanabe and Strogatz does not resolve the singularity any more. Hence, more research is required to solve this singularity. For now, we have to keep in mind that we may run into some problems whenever $\gamma = 0$.

3.2 Reduction of the Kuramoto model

In the previous subsection we derived the reduction for the general system (52). In this section we will specify this to the Kuramoto model. We are looking at the Kuramoto model with identical oscillators and a phase delay δ , switching to a rotating frame with angular velocity ω gives us:

$$\dot{\theta}_i = \sum_{j=1}^N \frac{K}{N} \sin(\theta_j - \theta_i - \delta), \quad i = 1, \dots, N. \tag{68}$$

Equation (68) has the form of Equation (52) with:

$$f = 0, \quad g = \frac{1}{N} \sum_{j=1}^N \sin(\theta_j - \delta), \quad h = -\frac{1}{N} \sum_{j=1}^N \cos(\theta_j - \delta).$$

Inserting this into the reduced system (67) gives:

$$\begin{aligned}
\dot{\gamma} &= \frac{K}{N}(1 - \gamma^2) \sum_{j=1}^N \cos(\theta_j + \Theta - \delta) \\
\gamma \dot{\Psi} &= -\frac{K}{N} \sqrt{1 - \gamma^2} \sum_{j=1}^N \sin(\theta_j - \Theta - \delta) \\
\gamma \dot{\Theta} &= -\frac{K}{N} \sum_{j=1}^N \sin(\theta_j - \Theta - \delta).
\end{aligned} \tag{69}$$

Substituting Equations (54) and (55) into the last two equations of this system yields:

$$\begin{aligned}
\dot{\gamma} \dot{\Psi} &= \frac{K}{N}(-\cos \delta(1 - \gamma^2) \sum_{j=1}^N \frac{\sin(\psi_j - \Psi)}{1 - \gamma \cos(\psi_j - \Psi)} + \sin \delta \sqrt{1 - \gamma^2} \sum_{j=1}^N \frac{\cos(\psi_j - \Psi) - \gamma}{1 - \gamma \cos(\psi_j - \Psi)}), \\
\dot{\gamma} \dot{\Theta} &= -\frac{K}{N}(\cos \delta \sqrt{1 - \gamma^2} \sum_{j=1}^N \frac{\sin(\psi_j - \Psi)}{1 - \gamma \cos(\psi_j - \Psi)} - \sin \delta \sum_{j=1}^N \frac{\cos(\psi_j - \Psi) - \gamma}{1 - \gamma \cos(\psi_j - \Psi)}).
\end{aligned}$$

Note that Θ has disappeared from the right hand side in these equations. As Equation (69) contains a plus sign within the brackets this case is a bit more complicated. However, we can rewrite this equation using the angle transformation formula and then insert Equations (56) and (57) into Equation (69). This gives:

$$\begin{aligned}
\dot{\gamma} &= \frac{-K(1 - \gamma^2)}{N} \left(- \left(\frac{[\cos(\psi_i - \delta - \Psi) - \gamma] \sin \Theta + \sqrt{1 - \gamma^2} \cos \Theta \sin(\psi_i - \delta - \Psi)}{1 - \gamma \cos(\psi_i - \delta - \Psi)} \right) \sin \Theta \right. \\
&\quad \left. + \left(\frac{[\cos(\psi_i - \delta - \Psi) - \gamma] \cos \Theta - \sqrt{1 - \gamma^2} \sin \Theta \sin(\psi_i - \delta - \Psi)}{1 - \gamma \cos(\psi_i - \delta - \Psi)} \right) \cos \Theta \right).
\end{aligned}$$

Hence, the differential equation of γ is the only equation that depends on Θ on the right hand side.

4 Chimera states

In the Introduction we defined chimera states as a system of identical oscillators that splits up in two groups; one group of oscillators is perfectly synchronized, while the other group is incoherent. Figure 2 shows an example of a chimera state. In this section, we will give the differential equations that the oscillators should follow to obtain a chimera state. We will discuss the bifurcations of this system for $N \rightarrow \infty$ and $N = 4$. Furthermore, similarly to the Kuramoto model (see Section 3.2), we will show the equations of the reduced system.

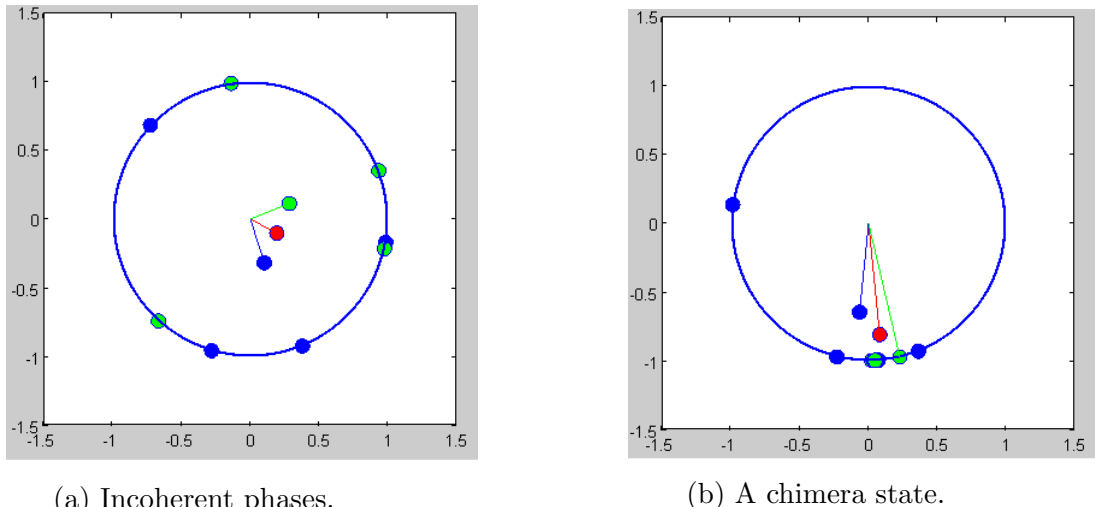


Figure 2: The phases of different oscillators running around on the unit circle. The order parameter of all oscillators is represented by the distance from the red dot to the origin. The order parameter per group is represented by the distance from the dot with the group color to the origin.

4.1 The phase equations

In this research we will look into a system consisting out of two groups of N phase oscillators. Both groups start from the same frequency ω . Moreover, we define an intergroup coupling strength of $\nu = (1 - A)/2$ and an intragroup coupling strength of $\mu = (1 + A)/2$, where $0 \leq A \leq 1$. Hence, the intragroup coupling strength is stronger than the intergroup coupling strength. Next to this we introduce a phase lag β . The phase equations of the two groups of oscillators are given by:

$$\frac{d\theta_i}{dt} = \omega - \left(\frac{1+A}{2N}\right) \sum_{j=1}^N \cos(\theta_i - \theta_j - \beta) - \left(\frac{1-A}{2N}\right) \sum_{j=1}^N \cos(\theta_i - \phi_j - \beta) \quad (70)$$

$$\frac{d\phi_i}{dt} = \omega - \left(\frac{1+A}{2N}\right) \sum_{j=1}^N \cos(\phi_i - \phi_j - \beta) - \left(\frac{1-A}{2N}\right) \sum_{j=1}^N \cos(\phi_i - \theta_j - \beta) \quad (71)$$

4.2 Reduced equations for the chimera states

Pikovsky and Rosenblum (2008) generalized the work of Watanabe and Strogatz to systems with multiple groups. They showed that the dimension of the system can be reduced to three for each group, provided that the minimum group size is bigger than three. Panaggio, Abrams, Ashwin and Laing (2016) analyzed this system of differential equations more closely. In our research we will follow their work and extend this work by doing time frequency analysis. The equations of the reduced system for each group are:

$$\begin{aligned} \frac{d\rho_j}{dt} &= \frac{1-\rho_j^2}{2} \operatorname{Re}(Z_j e^{-i\phi_j}) \\ \frac{d\psi_j}{dt} &= \frac{1-\rho_j^2}{2} \operatorname{Im}(Z_j e^{-i\phi_j}) \\ \frac{d\phi_j}{dt} &= \omega + \frac{1+\rho_j^2}{2\rho_j} \operatorname{Im}(Z_j e^{-i\phi_j}), \end{aligned} \quad (72)$$

with $j = 1$ or $j = 2$ and where

$$\begin{aligned} Z_1 &= \frac{-i(1+A)e^{i\beta}\rho_1 e^{i\phi_1}\gamma_1 - i(1-A)e^{i\beta}\rho_2 e^{i\phi_2}\gamma_2}{2} \\ Z_2 &= \frac{-i(1+A)e^{i\beta}\rho_2 e^{i\phi_2}\gamma_2 - i(1-A)e^{i\beta}\rho_1 e^{i\phi_1}\gamma_1}{2}, \end{aligned}$$

where γ_j is given by:

$$\gamma_j = \frac{1}{N\rho_j} \sum_{k=1}^N \frac{\rho_j + e^{i(\psi_k^{(j)} - \psi_j)}}{1 + \rho_j e^{i(\psi_k^{(j)} - \psi_j)}}.$$

The constants $\psi_k^{(j)}$ are the parameters given by the Watanabe and Strogatz reduction for population j (see Section 3). The variable ρ_j in system 72 measures the degree of synchrony

in population j . It is similar to the order parameter but not equivalent. Moreover, ϕ_j is related to the mean phase of the oscillators for each group and ψ_j is related to the spread of the phases of the oscillators for each group. Suppose we are in a chimera state. We assume that the first group is perfectly synchronized. Hence, $\rho_1 = 1$ and $\gamma_1 = 1$. Furthermore we define $\Delta = \phi_1 - \phi_2$, this reduces the whole system to:

$$\begin{aligned}\frac{d\rho_2}{dt} &= \frac{1 - \rho_2^2}{4} \left((1 + A)\rho_2\gamma_2 \sin \beta + (1 - A) \sin(\Delta + \beta) \right) \\ \frac{d\psi_2}{dt} &= - \left(\frac{1 - \rho_2^2}{4\rho_2} \right) \left((1 + A)\rho_2\gamma_2 \cos \beta + (1 - A) \cos(\beta + \Delta) \right) \\ \frac{d\Delta}{dt} &= \frac{1 + A}{2} \left(-\cos \beta + \frac{1 + \rho_2^2}{2\rho_2} \rho_2\gamma_2 \cos \beta \right) \\ &\quad + \frac{1 - A}{2} \left(-\cos(\beta - \Delta)\rho_2\gamma_2 + \frac{1 + \rho_2^2}{2\rho_2} \cos(\beta + \Delta) \right)\end{aligned}\tag{73}$$

Moreover, Pikovsky and Rosenblum (2008) showed that γ_2 can be rewritten as:

$$\gamma_2 = 1 + \frac{(1 - \rho_2^2)(-\rho_2 e^{-i\psi_2})^N}{1 - (-\rho_2 e^{-i\psi_2})^N}\tag{74}$$

Hence, we obtained a system that is independent of j .

4.3 Bifurcations of the chimera states

Abrams, Mirocco, Strogatz and Wiley (2008) studied Equations (70) and (71) in the limit of $N \rightarrow \infty$. Using the Ott-Antonsen ansatz, they derived a two-dimensional system, which enabled them to calculate analytically a saddle node and a supercritical Hopf bifurcation line. Moreover, they found numerically a homoclinic bifurcation line. The bifurcations are shown in Figure 3. Figure 3 shows that the stability of the chimera is dependent on the difference between the intragroup and intergroup coupling and the phase lag. Whenever the phase lag is small and the difference between the intragroup and intergroup coupling is increased from zero, two chimera states emerge in a saddle node bifurcation. One of these states is stable (stationary) and one is a saddle. When the difference in the coupling is increased even more the stable chimera undergoes a supercritical Hopf bifurcation. In this bifurcation a chimera that oscillates is created, which we refer to as a breathing chimera. Increasing the difference between the intergroup coupling and the intragroup coupling above the homoclinic bifurcation results in a collision of the breathing chimera with a saddle chimera. After this

there are no stable chimeras left. Hence, this means that in our research selecting a small phase lag and increasing A should result in these different chimera state whenever $N \rightarrow \infty$.

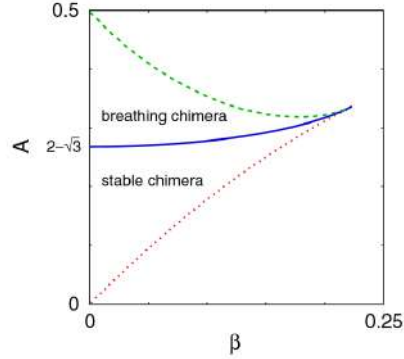
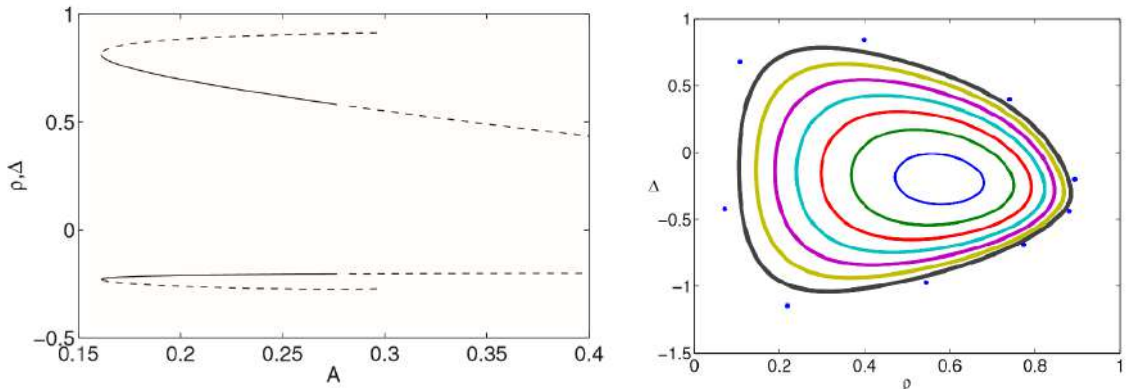


Figure 3: Bifurcations of chimeras for $N \rightarrow \infty$. Red: saddle node bifurcation line, blue: Hopf bifurcation line, green: homoclinic bifurcation line. Source: Abrams, Mirolo, Strogatz and Wiley (2008)

Panaggio, Abrams, Ashwin and Laing (2016) generated initial conditions, which were equivalent with the stable chimera for $N \rightarrow \infty$ and varied the group size N . Even though the order parameter in the incoherent group of the stable chimera is stationary for $N \rightarrow \infty$, the behavior of the order parameter for the incoherent group in smaller groups ($N \leq 10$) was dominated by fluctuations. Moreover, they found that for $N \geq 50$ the order parameter of the incoherent group is stationary.

As discussed before increasing A above the Hopf bifurcation gives a breathing chimera. According to the research of Panaggio, Abrams, Ashwin and Laing (2016) this is also true for group sizes bigger or equal to 10. However, for smaller group sizes they found that this oscillating state was not stable.

Next to this Panaggio, Abrams, Ashwin and Laing (2016) looked more closely at the case of $N = 4$. For this they used the reduced equations for the chimera states (see 73). They placed a Poincaré section at $\Psi = \pi$ and record the values of Δ and ρ while intersecting this Poincaré section. They set $\beta = 0.1$. Moreover, they increased A from zero and looked for periodic solutions of the reduced equations and obtained Figure 4a. This shows that above the Hopf bifurcation the stable point of the reduced system becomes unstable. Furthermore, for $0.28 \leq A \leq 0.35$ (above the Hopf bifurcation) they also showed the Poincaré section (see Figure 4b). This section showed stable limit cycles indicating that the Hopf bifurcation was supercritical. Moreover, for $A = 0.35$ the points show resonance. Finally, they plotted the bifurcation lines for $N = 4$ (see Figure 5). Note the similarities between the bifurcation plot for $N \rightarrow \infty$ and $N = 4$.



(a) Values of Δ (negative) and ρ (positive) on the Poincaré section ($\psi = \pi$) for $N = 4$ and $\beta = 0.1$. The solid lines show stable fixed points while the dashed lines show unstable fixed points.

(b) Values of Δ and ρ on the Poincaré section $\psi = \pi$ for $A = 0.28$ (inner) to 0.35 (outer) in steps of 0.01 with $N = 4$ and $\beta = 0.1$

Figure 4: Source: Panaggio, Abrams, Ashwin and Laing (2016)

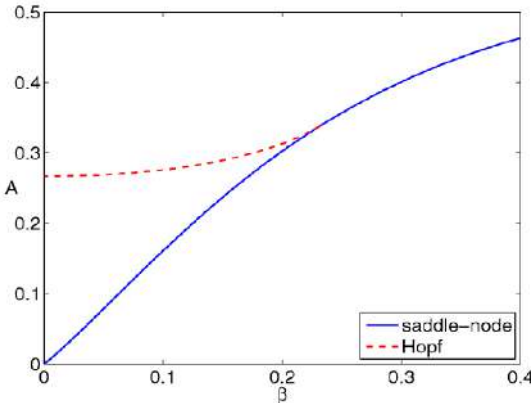


Figure 5: Bifurcations of chimeras for $N = 4$. Source: Panaggio, Abrams, Ashwin and Laing (2016)

5 Time Frequency Analysis

Recall that in Section 2, we calculated for the Kuramoto model the critical coupling analytically. For other models this critical value could be difficult to find. Moreover, the order parameter of the Kuramoto model provides a degree of synchronization too. However, not all models have a parameter which indicates the degree of synchronization. Therefore, we have to look at other tools to detect synchronization. In the following Section we will discuss time frequency analysis as such a tool. Time frequency analysis studies a signal in both the

time and frequency domains. We distinguish between three different time frequency analyses (Carmona, Hwang & Torrsani, 1998; Chandre, Wiggins & Uzer, 2003; Kaiser, 1994). We will discuss the basic Fourier transform, the windowed Fourier transform, and the continuous wavelet transform.

5.1 Fourier Transform

If $f \in L^1(\mathbb{R})$ is a signal, then the *Fourier transform* \hat{f} is defined as:

$$\hat{f}(\omega) = \int_{-\infty}^{\infty} f(t)e^{-i\omega t} dt, \quad \omega \in \mathbb{R}.$$

Hence, the Fourier transform takes a function that depends on time and transforms it into a function that depends on the frequency. The inverse is given by:

$$f(x) = \int_{-\infty}^{\infty} \hat{f}(\omega)e^{i\omega t} d\omega, \quad t \in \mathbb{R}.$$

The power of the signal at frequency ω is given by $|\hat{f}(\omega)|^2$. Moreover, we refer to the function $\omega \rightarrow |\hat{f}(\omega)|^2$ as the power spectrum. The power spectrum of a signal shows peaks at frequencies that are present in the signal. However, nothing can be said about the time of the frequencies nor about the duration of the frequencies. This is important as there are signals for which in some sense the frequencies are changing in time. An example of such a signal is the chirp of a bird, which we will simulate in Subsection 5.3. Therefore other tools might be helpful.

5.2 Windowed Fourier Transform

Another method is the *windowed Fourier transform*. This method uses a *window*, which localizes the signal in time. The windowed Fourier transform divides a signal into shorter segments by sliding the window over the time axis. The Fourier transform is then computed for each of these segments. This gives insight in how the Fourier spectrum changes in time. The windowed Fourier transform is given by:

$$\hat{f}_t(\omega, u) = \int_{-\infty}^{\infty} e^{-i\omega t} \bar{g}(t-u) f(t) dt, \quad (75)$$

where $g \in L^2(\mathbb{R})$ is the window function and $f \in L^1(\mathbb{R})$. Computing the windowed Fourier transform is equivalent to computing a Fourier transform of $f(\cdot + u)g(\cdot)$ at each time u . This can be seen by substituting $\tau = t - u$ in Equation (75), which gives:

$$\hat{f}_\tau(\omega, u) = e^{-i\omega u} \int_{-\infty}^{\infty} f(\tau + u)\bar{g}(\tau)e^{-i\omega\tau}d\tau.$$

Moreover, the power spectrum can be found by computing: $|\hat{f}_t(\omega, u)|^2$. The time spread at a point (u, ω) is defined by:

$$\sigma_{time}(u, \omega) = \left(\int_{-\infty}^{\infty} (t - u)^2 |g(t - u)e^{i\omega t}|^2 dt \right)^{1/2},$$

and the frequency spread is given by:

$$\sigma_{frequency}(u, \omega) = \left(\frac{1}{2\pi} \int_{-\infty}^{\infty} (\zeta - \omega)^2 |\hat{g}(\zeta - \omega)e^{iu(\omega - \zeta)}|^2 d\zeta \right)^{1/2}.$$

When the window function is well chosen, that is well localized in both time as well as frequency, the windowed Fourier transform will provide a local time frequency analysis (Kaiser, 1994). This means that the windowed Fourier transform will give information in both the frequency and time domain. However, according to the Heisenberg uncertainty principle sharp localisations in frequency and time are incompatible. According to Heisenberg, multiplication of the time spread with the frequency spread at a given point (u, ω) in the time-frequency plane (i.e. the time-frequency resolution) gives a constant value that is larger than $1/2$ (Chandre, Wiggins & Uzer, 2003). This means that choosing a window function that is too small may result in inaccurate information in the frequency domain, and the other way around too. Hence, choosing a window function that is too large, results in accurate information in the frequency domain, but in inaccurate information in the time domain. This means that it might be hard to find the time of each frequency. Figure 6 shows an example of a resolution of a windowed Fourier transform. In this example the time and frequency resolution are equally good.

One specific window function is the Gaussian function (i.e. $g(t) = e^{-t^2\sigma^2}/(\sigma^2\pi)^{1/4}$). The time and frequency spread of this transform are respectively: $\sigma/\sqrt{2}$ and $1/\sigma\sqrt{2}$. It follows that the time-frequency resolution equals $1/2$. Hence, this transform has minimal time-frequency resolution. However, a problem with the windowed Fourier transform is that the time resolution and frequency resolution stay fixed on both the time and frequency axis. In

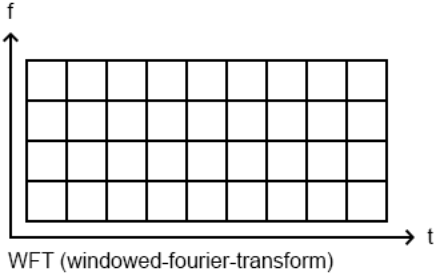


Figure 6: Time and frequency resolution for the windowed Fourier transform. In this example the time and frequency resolutions are equal.

case of a low frequency we need a good frequency resolution (i.e. the frequency resolution is small). Hence, the time resolution is of poor quality, meaning that the time resolution is high. For low frequencies this is not a big problem as they are slow. However, in the windowed Fourier transform the same resolutions are used for the higher frequencies as well. Higher frequencies might need a better time resolution as they are faster. Therefore, other methods might provide a better time frequency analysis.

5.3 Continuous Wavelet transform

Finally, the *continuous wavelet transform* is an alternative to the (windowed) Fourier transform for time frequency analysis. Wavelets are non zero on a finite time interval. The wavelets are translated across time. Moreover, they are rescaled to the window. This guarantees that the window is adjusted to the frequency of the signal. This is an advantage for detecting low frequencies, as in the windowed Fourier transform the window might be too short to detect these frequencies. Consequently, these frequency are missed by the windowed Fourier transform. Hence, the continuous wavelet transform assures a good time frequency resolution everywhere. Therefore the continuous wavelet transform is especially good for signals with frequencies that have big differences, because the variable window sizes make it possible to analyze different frequency components within one signal (cf. Gao & Yan, 2011). Figure 7 shows an example of the time and frequency resolution for the wavelet transform. Note the difference between Figures 6 and 7. The time and frequency resolution of Figure 7 is very good for detecting high frequencies.

In order to introduce the continuous wavelet transform, we have to discuss a few basics, these basics can be found in more detail in the book of Carmona, Hwang and Torrsani (1998). We define the *mother wavelet* as a fixed function $\psi \in L^1(\mathbb{R}) \cap L^2(\mathbb{R})$. A family of wavelets $\{\psi_{(b,a)}; b \in \mathbb{R}, a \in \mathbb{R}_+^*\}$ is created by translating and scaling the mother wavelet ψ . Taking

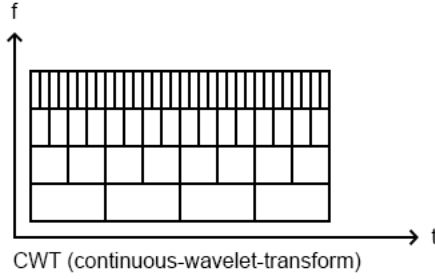


Figure 7: Time and frequency resolution for the wavelet transform. Note how the time resolution increases for high frequencies.

$b \in \mathbb{R}$ and $a \in \mathbb{R}_+^*$, we define the family of wavelets as:

$$\psi_{(b,a)}(t) = \frac{1}{\sqrt{a}}\psi\left(\frac{t-b}{a}\right), \quad t \in \mathbb{R}.$$

This wavelet is the mother wavelet rescaled by factor \sqrt{a} and centered around the time b . Now we can define the continuous wavelet transform:

Definition 1. Let $\psi \in L^1(\mathbb{R}) \cap L^2(\mathbb{R})$ be the mother wavelet. Then the continuous wavelet transform of a signal $f \in L^2(\mathbb{R})$ is defined by:

$$T_f(b, a) = \frac{1}{\sqrt{a}} \int_{-\infty}^{\infty} f(t) \bar{\psi}\left(\frac{t-b}{a}\right) dt.$$

This transform contains information of the signal f at scale \sqrt{a} around point b .

Furthermore the center frequency of the wavelet is given by:

$$\eta = \frac{1}{2\pi} \int_{-\infty}^{\infty} \omega |\hat{\psi}_{b,a}(\omega)|^2 d\omega.$$

We define $\zeta = \frac{\eta}{a}$. Now the time spread around a point (b, a) in the time-frequency plane is defined as follows:

$$\sigma_{time}(b, a) = \left(\int_{-\infty}^{\infty} (t-b)^2 |\psi_{b,a}(t)|^2 dt \right)^{1/2}.$$

Moreover, the frequency spread is defined as:

$$\sigma_{frequency}(b, a) = \left(\frac{1}{2\pi} \int_{-\infty}^{\infty} (\omega - \zeta)^2 |\hat{\psi}_{b,a}(\omega)|^2 d\omega \right)^{1/2}$$

In our research we will use the Morlet-Grossman wavelet given by:

$$\psi(t) = \frac{1}{\sigma\sqrt{2\pi}} e^{2\pi i \lambda t} e^{-t^2/2\sigma^2}.$$

The time-frequency spread is minimal for the Morlet-Grossman wavelet. Hence, the Morlet-Grossman wavelet is a nice wavelet as it has little uncertainty in both the time as well as the frequency domain. We take $(\lambda, \sigma) = (1, 2)$. To get a better understanding of the continuous wavelet transform, we will look at an example (Chandre, Wiggins & Uzer, 2003):

Example 1. *Continuous wavelet transform Suppose we have a signal $f(t) = e^{i2\pi\nu t}$. Then the continuous wavelet transform with the Morlet-Grossman wavelet is given by:*

$$\begin{aligned} T_f(b, a) &= \frac{1}{\sqrt{a}} \int_{-\infty}^{\infty} e^{i2\pi\nu t} \bar{\psi}\left(\frac{t-b}{a}\right) dt \\ &= \frac{1}{\sigma\sqrt{a}2\pi} \int_{-\infty}^{\infty} e^{2\pi i \nu t} e^{-2\pi i \lambda \left(\frac{t-b}{a}\right)} e^{-\frac{(t-b)^2}{a^2 2\sigma^2}} dt \end{aligned}$$

Changing variables to $s = (t - b)/a$ gives:

$$\begin{aligned} T_f(b, a) &= \frac{\sqrt{a}}{\sigma\sqrt{2\pi}} \int_{-\infty}^{\infty} e^{2\pi i \nu (as+b)} e^{-2\pi i \lambda s} e^{-\frac{s^2}{2\sigma^2}} ds \\ &= \frac{\sqrt{a}}{\sigma\sqrt{2\pi}} e^{2\pi i \nu b} \int_{-\infty}^{\infty} e^{2\pi i (\nu a - \lambda)s} e^{-\frac{s^2}{2\sigma^2}} ds \\ &= \frac{\sqrt{a}}{\sigma\sqrt{2\pi}} e^{2\pi i \nu b} \int_{-\infty}^{\infty} e^{-\frac{(-4\pi i \sigma^2(\nu a - \lambda)s + s^2)}{2\sigma^2}} ds \\ &= \frac{\sqrt{a}}{\sigma\sqrt{2\pi}} e^{2\pi i \nu b} \int_{-\infty}^{\infty} e^{-\frac{(s-2\pi i \sigma^2(\nu a - \lambda))^2}{2\sigma^2}} e^{\frac{-4\pi^2 \sigma^4(\nu a - \lambda)^2}{2\sigma^2}} ds \\ &= \frac{\sqrt{a}}{\sigma\sqrt{2\pi}} e^{2\pi i \nu b} e^{-2\pi^2 \sigma^2(\nu a - \lambda)^2} \int_{-\infty}^{\infty} e^{-\frac{(s-2\pi i \sigma^2(\nu a - \lambda))^2}{2\sigma^2}} ds \end{aligned}$$

Finally, we make a substitution $x = \frac{(s-2\pi i \sigma^2(\nu a - \lambda))}{\sigma\sqrt{2}}$. This gives:

$$\begin{aligned}
T_f(b, a) &= \frac{\sqrt{2a}\sigma}{\sigma\sqrt{2\pi}} e^{2\pi i\nu b} e^{-2\pi^2\sigma^2(\nu a - \lambda)^2} \int_{-\infty}^{\infty} e^{-x^2} dx \\
&= \sqrt{a} e^{2\pi i\nu b} e^{-2\pi^2\sigma^2(\nu a - \lambda)^2}
\end{aligned} \tag{76}$$

Hence, the modulus for the wavelet transform of $e^{2\pi i\nu t}$ is given by

$$|T_f(b, a)| = \sqrt{a} e^{-2\pi^2\sigma^2(\nu a - \lambda)^2}. \tag{77}$$

Hence, the wavelet transform is a complex valued function. We can consider the wavelet transform in polar representation $T_f(b, a) = |z(b, a)|e^{i\phi(b, a)}$, where the absolute value or amplitude $|z(b, a)|$ represents the angular frequency ω and the argument or phase $\phi(b, a)$ represents the phase of the signal $f \in L^2(\mathbb{R})$. Hence, or Example 1 the angular frequency is given by Equation (77) and the phase of the signal is given by $\phi = 2\pi\nu b$.

Next we want to find the relation between the angular frequency ω and the scale a . Note that the angular frequency ω of the signal of Example 1 equals $2\pi\nu$. Therefore, the maximum with respect to a of the modulus of the wavelet transform of Example 1 should equal $\omega = 2\pi\nu$. The global maximum for the modulus of the wavelet transform is at: $a = \frac{\pi}{2\pi\nu}(\lambda + \sqrt{\lambda^2 + \frac{1}{2\pi^2\sigma^2}})$. Therefore we associate with the angular frequency

$$\omega = \frac{\pi}{a} \left(\lambda + \sqrt{\lambda^2 + \frac{1}{2\pi^2\sigma^2}} \right). \tag{78}$$

Another important observation of the wavelet transform with this signal is that according to Equation (76) the phase is independent of the frequency parameter a . Hence, a time frequency plot for the phase of a signal with just one frequency is independent of the frequency.

In a time frequency plot we will find on the x -axis the time (i.e. b) and on the y -axis the frequencies (i.e. ω given by Equation (78)). How often a certain combination of time and frequency occurs is shown by color. The "warmer" the color the higher is the weight of the corresponding frequency. It is possible to generate such plots using two different methods. The first method uses the global maximum to normalize color assignment of the wavelet transform. In the other method the normalization is done within each slice of a constant time. Thus for this method: $|T_f(b, a_b)| = \max_a |T_f(b, a)|$. Both ways have their benefits and disadvantages. For example if one wants to know exactly what frequency is the most common for each time, the second method would be the best. However, in this method it

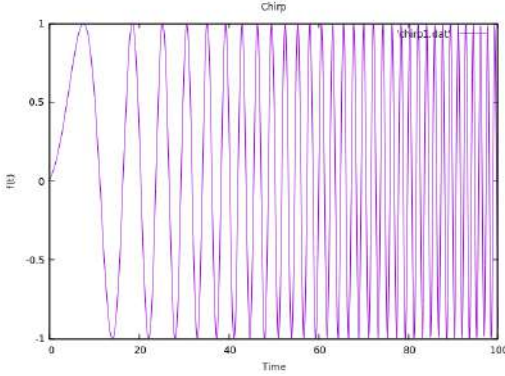


Figure 8: A plot of the chirp (i.e. $\sin(0.05t + 0.02t^2)$).

is not possible to see how the distribution of frequencies changes in time. For this the first method is more suitable. However, according to Carmona, Hwang and Torréssani (1998) the first method can be problematic in the presence of noise as this can create additional local maxima, which can give a biased view.

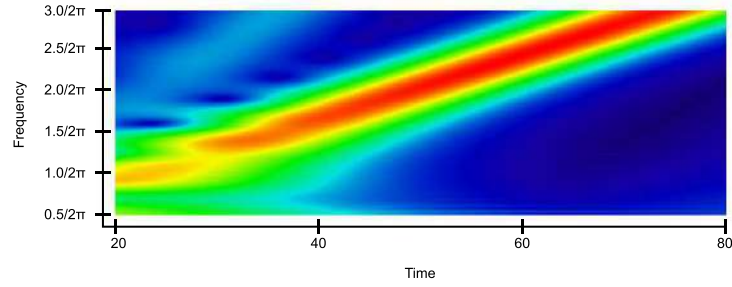
Another option is to plot the phase of the wavelet transform. In this plot not only the warmth of the color plays a role but also the brightness of the color. The brighter the color the more oscillators are present there. Hence, at places where the colors are very dark there are almost no oscillators. The darker the spot the less meaning it gives for the phase, as the modulus can be too small.

We will end this section with an example of a time frequency analysis for a chirp signal.

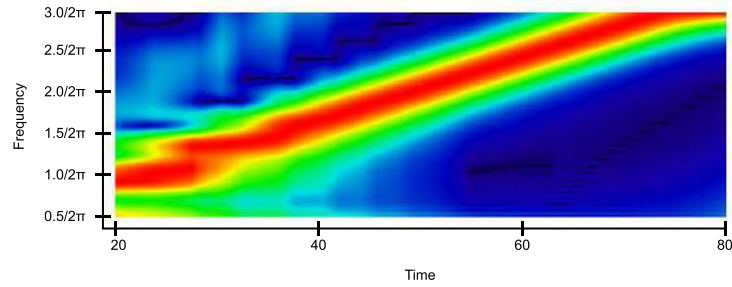
Example 2. In our example the chirp is given by: $f(t) = \sin(0.05t + 0.02t^2)$. A plot of this function is given in Figure 8. Observe that the frequency of this function increases.

Next we will perform a time frequency analysis (see Figure 9). Observe how the frequencies in Figures 9a and 9b increase in time. This is in agreement with Figure 8. At the beginning it looks like there is some disturbance of the wavelet. This is because the time frequency analysis starts already at time 20. Note that at the end the phases show vertical lines indicating that for each frequency we have the same mean phase at each time t (see Figure 9c).

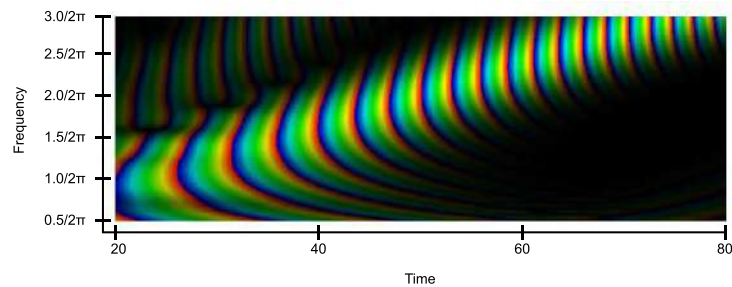
Figure 9: Time frequency analysis for $\sin(0.05t + 0.02t^2)$.



(a) Time frequency analysis of the chirp. This plot is made using the local maximum.



(b) Time frequency analysis of the chirp. This plot is made using the maximum per time.



(c) Time frequency analysis of the phases.

6 Analysis of the Kuramoto Model

6.1 One Population of Oscillators

The next step in our research is to find the critical coupling numerically. We take a group of 250 oscillators with the naturally frequencies being distributed by a Lorentzian distribution with modus 0.3 and scale 0.025. For the wavelet transform we took $\sigma = 2$ and $\lambda = 1$. We looked at 600 time units, with time steps of $dt = 0.3$. The first 60 and last 60 time units of the wavelet transform are not considered as it may be possible that the wavelet is not completely contained in the interval of the first or last 60 time units. Analytically the critical coupling should be equal to twice the scale (i.e. $2\gamma = 0.05$). Moreover, the order should be equal to: $R = \sqrt{1 - 0.05/K}$.

For different couplings we will show five figures. One figure contains a plot of the order parameter against the time, the second figure is a 3D plot with the time, the imaginary part of the order parameter and the real part of the order parameter. The third figure contains a time frequency analysis of the frequencies, produced using local maxima. The fourth figure contains a time frequency analysis of the frequencies with the maxima per time. Finally, the fifth figure shows the phase of the wavelet transform. Recall that in the case of a single frequency the phase of the wavelet transform is independent of the frequency. Therefore we expect that whenever the Kuramoto model synchronizes we see vertical lines in the time frequency plot (the same mean phase for all frequencies).

First we analyze the case of no coupling. Thus, all oscillators move out of synchrony with different frequencies. We expect the order parameter to be 0 with fluctuations of $1/\sqrt{250}$. Moreover, we expect that the time frequency plot showing the local maxima will look a bit stained. For the plot with the maxima per time we expect to see a line that is approximately straight and has a horizontal orientation. This line should appear around the frequency 0.3. Finally, for the phases we expect an unordered image.

When we run the program we obtain Figure 10. The order parameter oscillates between 0 and 0.1. Hence, the order parameter is small for all time t . However, the fluctuations are sometimes a bit bigger than expected. We can conclude that the oscillators are in the incoherent state ($R \approx 0$). As the incoherent state is stable for $K < K_c$ we expect that the system will keep behaving in the same way over time.

The next step is to look at the frequencies using the the wavelet transform. This will result in three figures per coupling. Figure 11 shows the time frequency analysis. Moreover, Figure 11a is the time frequency analysis obtained using local maxima with $K = 0$. As expected the figure is a bit stained. There is not yet a clear structure in the frequencies. Hence, according to the time frequency analysis the frequencies did not synchronize. The figure generated

using the maxima of the modulus of the wavelet transform per time (Figure 11b) starts with a maximum frequency around $0.3/2\pi$. This is in line with our expectations. However, the maximum frequency bifurcates from $0.3/2\pi$ on times 180 and 400. We hypothesize that this might have to do with fluctuations in the order parameter. Figure 11c shows the phase of the wavelet transform. This figure shows incoherence of the phases as we have different average phases for different frequencies.

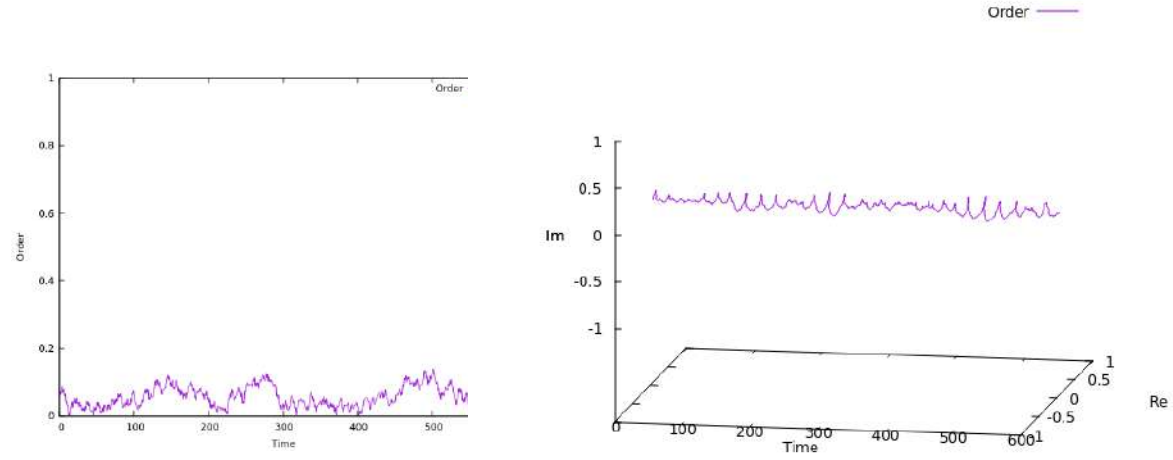
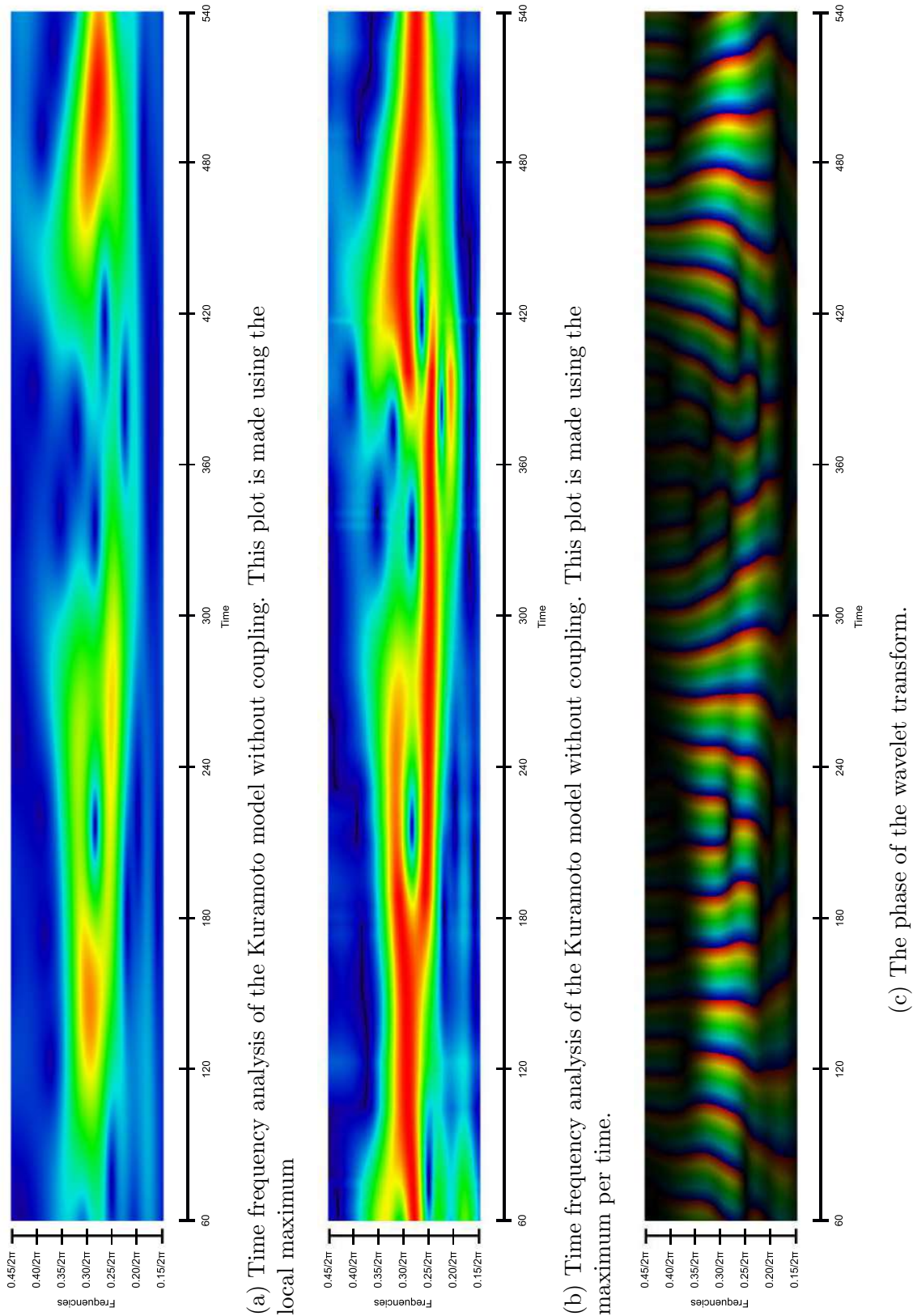


Figure 10: Order parameter for the Kuramoto model with 250 oscillators, without coupling (i.e. $K = 0$).

Figure 11: Time frequency analysis for $K = 0$



Increasing the coupling to $K = 0.025$ should still give an incoherent state. Thus we expect that the order parameter is close to zero. Moreover the time frequency plot obtained using local maxima should still look stained. For the time frequency plot obtained using maxima per time we expect an approximately straight line with a horizontal orientation around the frequency 0.3. Finally, for the time frequency plot of the phases we expect again an unordered plot.

The results of the order parameter are shown in Figure 12. The order parameter lies in between 0 and 0.2. This is higher than for the case without coupling, and that feels intuitively correct. The time frequency plot for local maxima (Figure 13a) looks again stained. However, it looks like the frequencies of the oscillators are a bit more concentrated in the middle than in the case of no coupling. The time frequency plot obtained using the maximum per time looks more concentrated around $0.3/2\pi$ than for no coupling. Finally, Figure 13c shows the time frequency analysis for the phases. One can see that the phases are still incoherent.

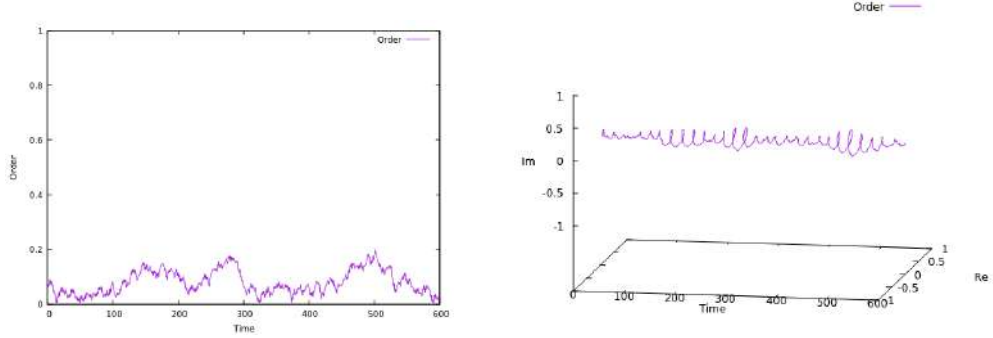
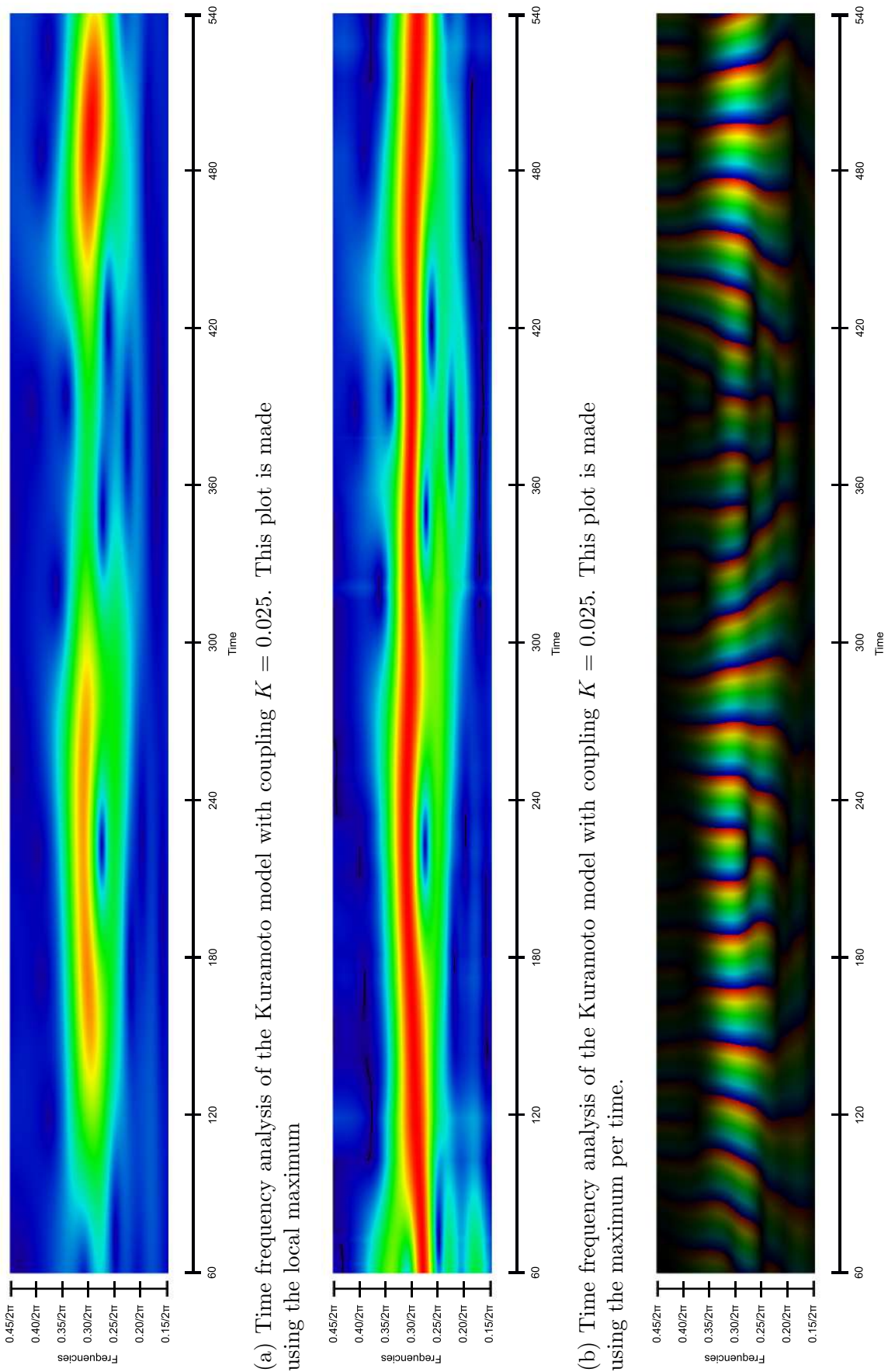


Figure 12: Order parameter for the Kuramoto model with 250 oscillators, with coupling $K = 0.025$.

Figure 13: Time frequency analysis for $K = 0.025$



When we increase the coupling to $K = 0.045$. We expect the order parameter to be approximately zero. However, in Figure 14 it shows a slight bifurcation from $R = 0$. Therefore we conclude that numerically the critically value equals $K = 0.045$. Analytically this should be $K = 0.05$. Note that for the numerically simulations we took $n = 250$ and analytically we assumed that $n \rightarrow \infty$. Hence, we expect to find $K = 0.05$ with a larger number of oscillators. In Figure 15a we can notice that the frequency start to synchronize. However, the frequencies still pulsate. Note that at these times (i.e. around $t = 300$ and $t = 540$) the order parameter increases (see Figure 14). Figure 15b shows clearly that for all times most oscillators are around a frequency that is approximately $0.29/2\pi$. Finally, note in Figure 15c that at the brightest places of the time frequency plot (i.e. the parts where the frequencies are a bit synchronized) the lines look vertical. One could say that in these parts there is one dominant frequency and therefore it might be possible to compare this with the situation of a signal with just one frequency.

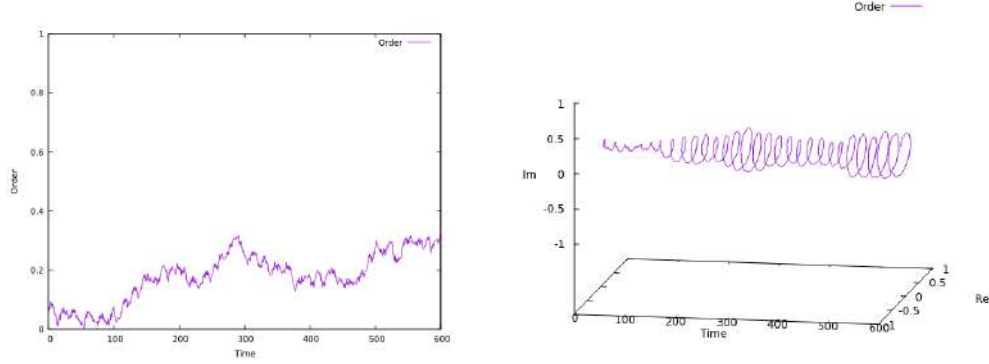
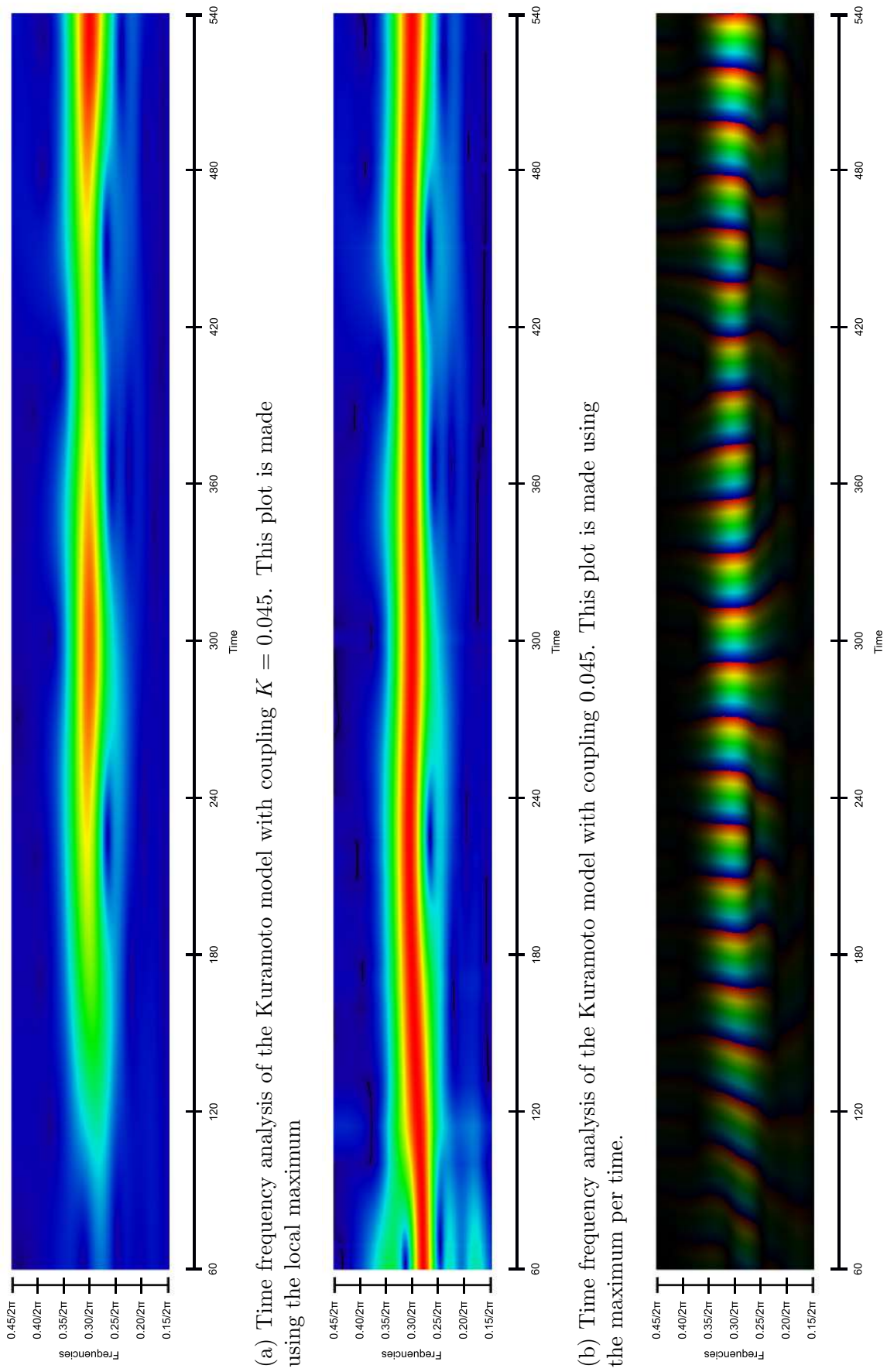


Figure 14: Order parameter for the Kuramoto model with 250 oscillators, with coupling $K = 0.045$.

Figure 15: Time frequency analysis for $K = 0.045$



Next we increase the coupling above the critical value K_c to $K = 0.075$. Analytically we would expect the order parameter to increase in the beginning till $R = \sqrt{1 - (0.05/0.075)} \approx 0.58$. After it reaches this value we expect small oscillations around $R = 0.58$. In the 3D plot of the order parameter we expect that the circles increase in the beginning strongly in diameter and after that it should stay relatively constant. Finally, practically we expect partial synchronization; some oscillators are locked while others are still incoherent. Figure 16 shows the expected behavior. The value for R is a bit higher then expected because we do not have an infinite number of oscillators. For the time frequency plots we expect to see some synchronization. Figure 17 shows the time frequency plots. In the time frequency plot with the local maximum (Figure 17a) we see that as time increases the frequencies of the oscillators tend to synchronize more and more to a frequency of $0.3/2\pi$. Figure 17b shows that from the beginning onwards the most prominent frequency is around $0.29/2\pi$ and increases slightly towards $0.3/2\pi$. Finally, for the phases (Figure 17c) we see the same pattern as for a coupling of $K = 0.045$, namely the more the frequencies synchronize the more the phases show a vertical pattern. Note again the connection between Figure 16 and Figures 17a and 17c, at the moment the order parameter grows both time frequencies plots show synchronization; Figure 17a shows synchronization for the frequencies, while Figure 17c shows synchronization for the phases. Figure 17b shows that from the beginning onwards the most common frequency is $0.3/2\pi$.

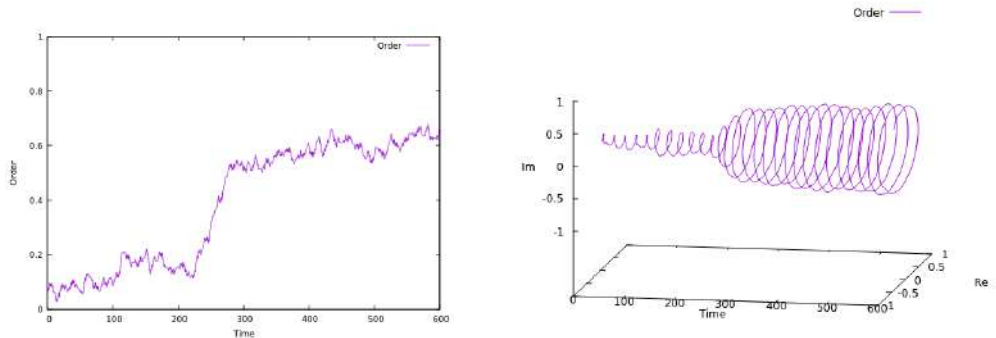
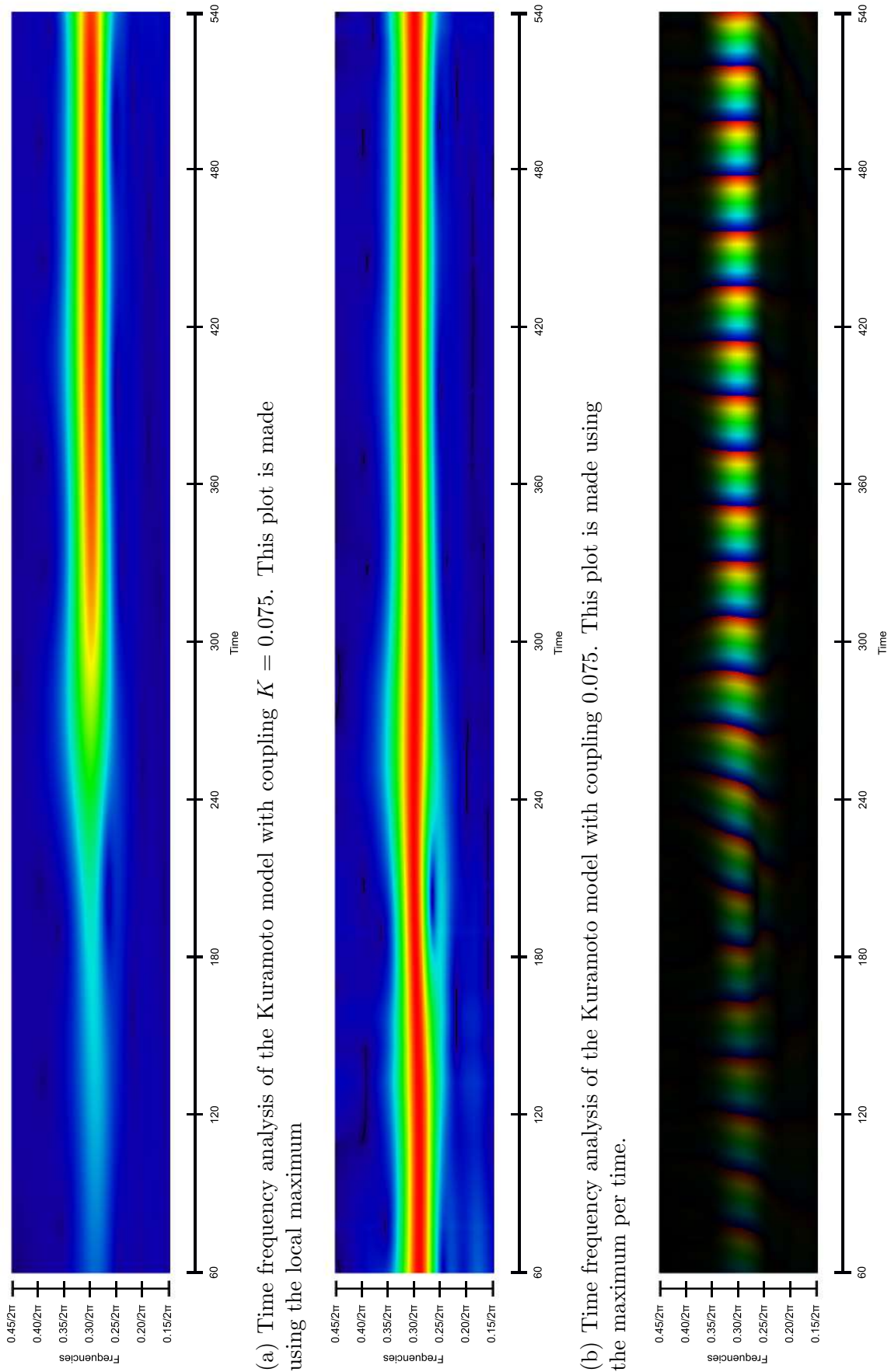


Figure 16: Order parameter for the Kuramoto model with 250 oscillators, with coupling $K = 0.075$.

Figure 17: Time frequency analysis for $K = 0.075$



Next we increase the coupling to $K = 0.1$. This should result in an order parameter that increases to a value of $R = \sqrt{1 - 0.05/0.1} \approx 0.71$. This should also be clear in the 3D plot as the order parameter grows rapidly in the beginning. Figure 18 shows both plots. The order parameter is again a bit higher than expected due to the fact that we do not have an infinite number of oscillators. However, both plots are still very close to our expectation. Hence, we have partial synchronization; most oscillators are phase locked and a few are incoherent.

As there are already many oscillators phase locked after $t = 120$ time units (see Figure 18), we know that there are also many oscillators frequency locked. Therefore we expect that the time frequency analysis will show synchronized frequencies from $t \approx 110$ time units onwards. Figure 19 shows the time frequency analyses. Note in Figure 19a that from $t = 120$ time units the frequencies starts to synchronize. Moreover, Figure 19b shows clearly that the most often occurring frequency throughout time is $0.3/2\pi$. Finally, Figure 19c shows again that as the frequency synchronizes the phases show a vertical pattern. Thus for each often appearing frequency we have the same mean phase at each point in time.

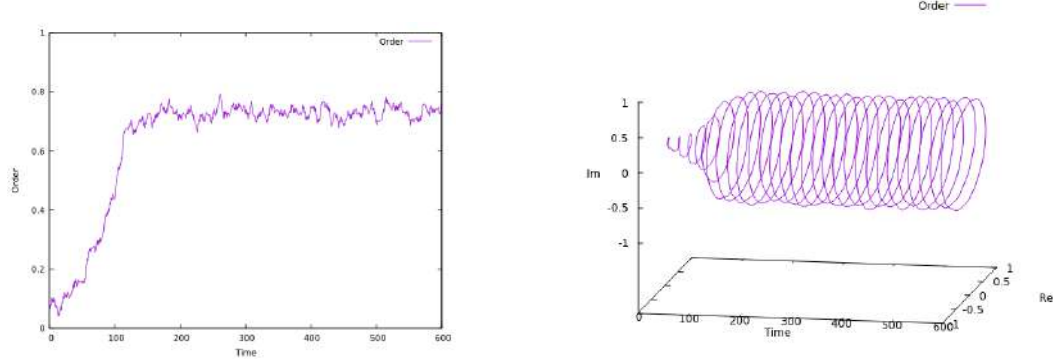
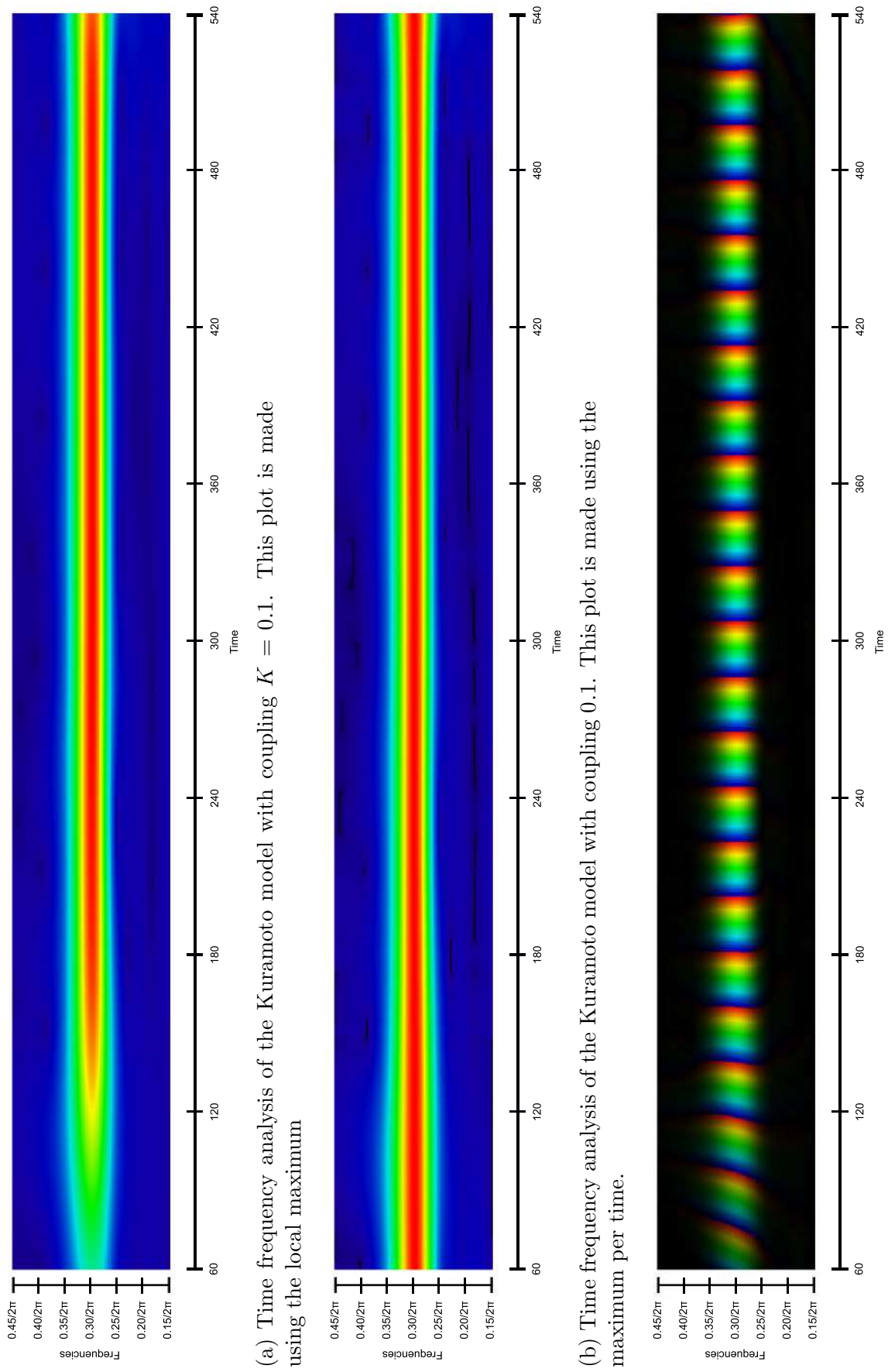


Figure 18: Order parameter for the Kuramoto model with 250 oscillators, with coupling $K = 0.1$.

Figure 19: Time frequency analysis for $K = 0.1$



At last we increase the coupling to $K = 1.0$. We expect that almost all oscillators will be synchronized. Analytically we get: $\sqrt{1 - 0.05/1.0} \approx 0.97$. Moreover, we expect the frequencies to synchronize relatively fast. In Figure 20 one can see that the order parameter is exactly as expected. Moreover, Figure 21 shows the time frequency analysis with this coupling. Note that the more we increased the coupling strength the less difference there is between the time frequency analysis with the local maxima and the time frequency analysis made using the maxima per time. This is because in case of high coupling the frequencies synchronize fast. Therefore the global maxima is from the beginning onwards around $0.3/2\pi$. In contrast with Figure 19a as in this figure the local maximum is after $t = 120$ time units. Hence, in the case of a high coupling the local maxima equals the maxima per time. Note that in Figure 21c the pattern of the phases is almost directly vertical. Hence, it looks like the phases synchronize very fast, which is in agreement with Figure 20.

In short, we found a critical value of $K_c = 0.045$. This is lower than the critical value that is expected analytically ($K_c = 0.05$). However, we assume that whenever we would take $n \rightarrow \infty$ the critical value would converge to $K_c = 0.05$. Furthermore, we saw that when $K > K_c$ the frequencies and phases synchronize fast. We confirmed that in that case the order parameter R goes to $R = \sqrt{1 - K_c/K}$. Moreover, we saw that the phases and frequencies synchronize at approximately the same moment in time. At last, we saw that whenever the oscillators synchronized to one frequency, the plot of the phase of the wavelet transform shows vertical lines.

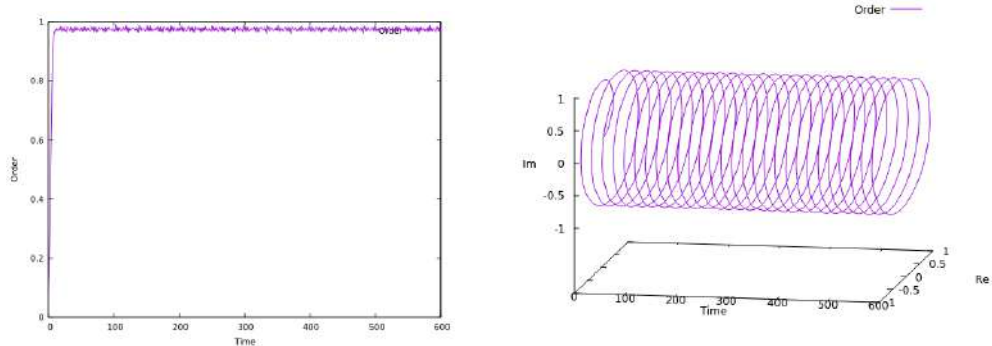
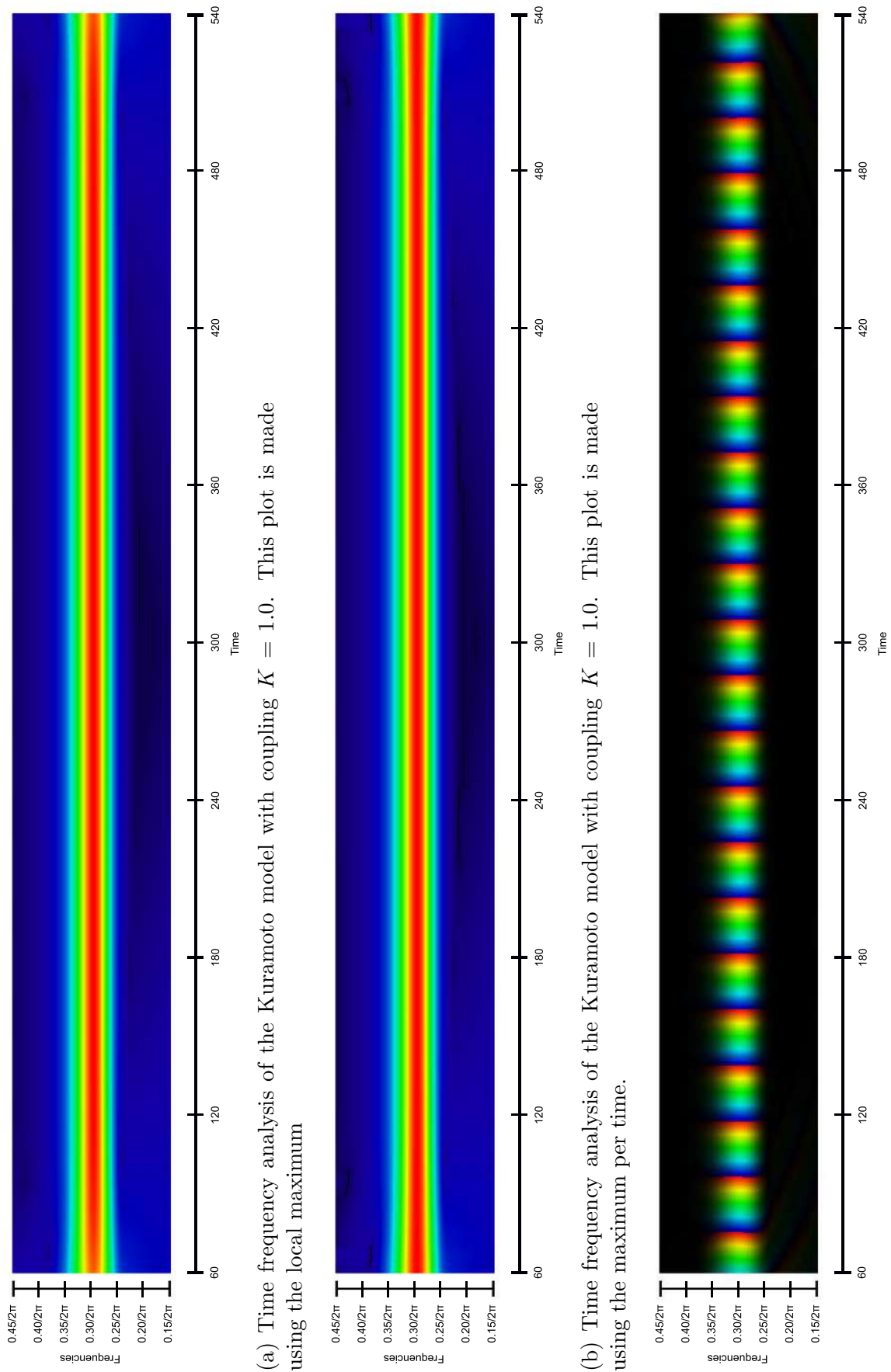


Figure 20: Order parameter for the Kuramoto model with 250 oscillators, with coupling $K = 1.0$.

Figure 21: Time frequency analysis for $K = 1.0$



6.2 Two Populations of Oscillators

In the previous section we looked at one population of oscillators distributed by the Lorentzian and we obtained the critical coupling. The next step is to look at two populations of oscillators both of $n = 50$ oscillators. Both groups are distributed by the Lorentzian with scale 0.015. However, the modus of one group is 0.2 and the modus of the other group is 0.5. For this situation, we show three plots of the order parameter one of each group and one plot of the order parameter for the total system. The order parameter per group is calculated by first calculating the trajectories of all oscillators and after that this trajectory is used to calculate the order parameters of the three different situations.

In a situation of one population of oscillators the critical value would be $K_c = 0.03$. However, in the case of two populations of oscillators we expect that the spread between the two groups plays a role too. What kind of role it will play is unclear.

When there is no coupling we expect the order parameter to be small in all three plots. Moreover, in the time frequency plot we expect to see two groups of frequencies that both look a bit stained.

Figure 22 shows the different plots of the order parameters. As expected the order parameter is small for all t . The order parameter for all oscillators is in general a bit lower than for group one and two. This is quite logical as those frequencies are closer to each other.

Figure 23 shows the time frequency analyses for two populations of oscillators without coupling. The time frequency analysis with the local maxima shows that the frequencies are spread around $0.2/2\pi$ and $0.5/2\pi$. The same information can be extracted from Figure 23b. However, Figure 23b also shows that the frequencies are the most concentrated around $0.2/2\pi$. Note that according to Figure 23a at the beginning the distribution of the frequencies of the oscillators is the most dense around $0.2/2\pi$. As the frequencies are divided by a distribution with the same scale we conclude that this happened by chance. Figure 23c shows the time frequency analysis for the phases. Note that at every point in time the mean phases are different for the different frequencies. Hence, also the time frequency plot of the phases shows that the phases are not synchronized.

It is also possible to perform a time frequency analysis for each group apart. This gives more insight in the process of synchronization. These time frequency plots are shown in Figures 24 and 25. In Figures 24a and 24b one can see that the frequencies for the first group are mostly concentrated around $0.2/2$. The frequencies for the second group are not this concentrated (see Figures 25a and 25b). This confirmed what we saw in Figure 22. As there is no coupling in this situation we can conclude that the frequencies of the oscillators of the first group are from the beginning onwards more synchronized than in the second group.

Figure 24c shows that although the frequencies of the first group are more concentrated, the phases are not synchronized at all. This is in agreement with the plot of the order parameter for the first group (see Figure 22b). The phases of the second group are incoherent too (see Figure 22c and 25c).

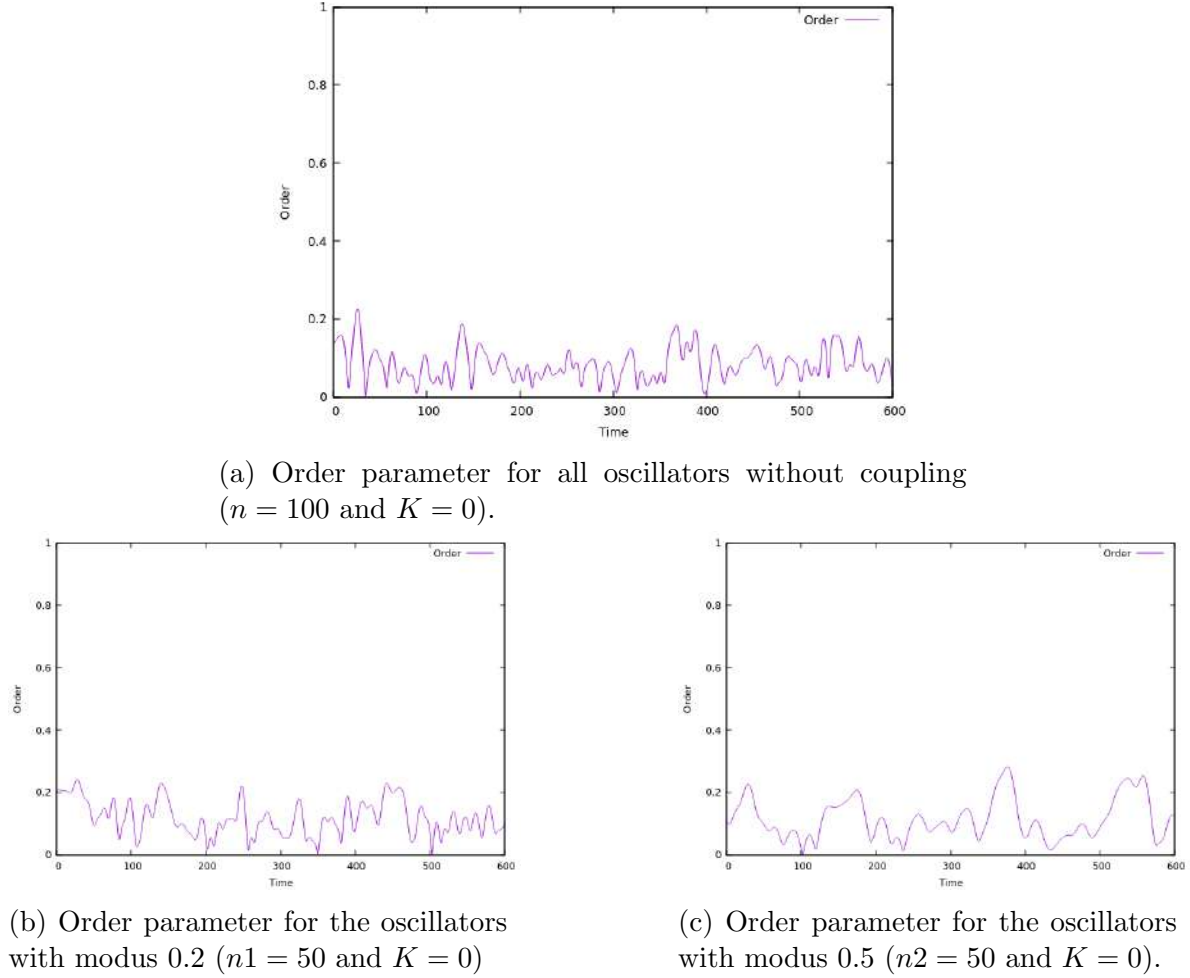


Figure 22: Order parameter for the Kuramoto model with coupling $K = 0$.

Figure 23: Time frequency analysis for $K = 0$

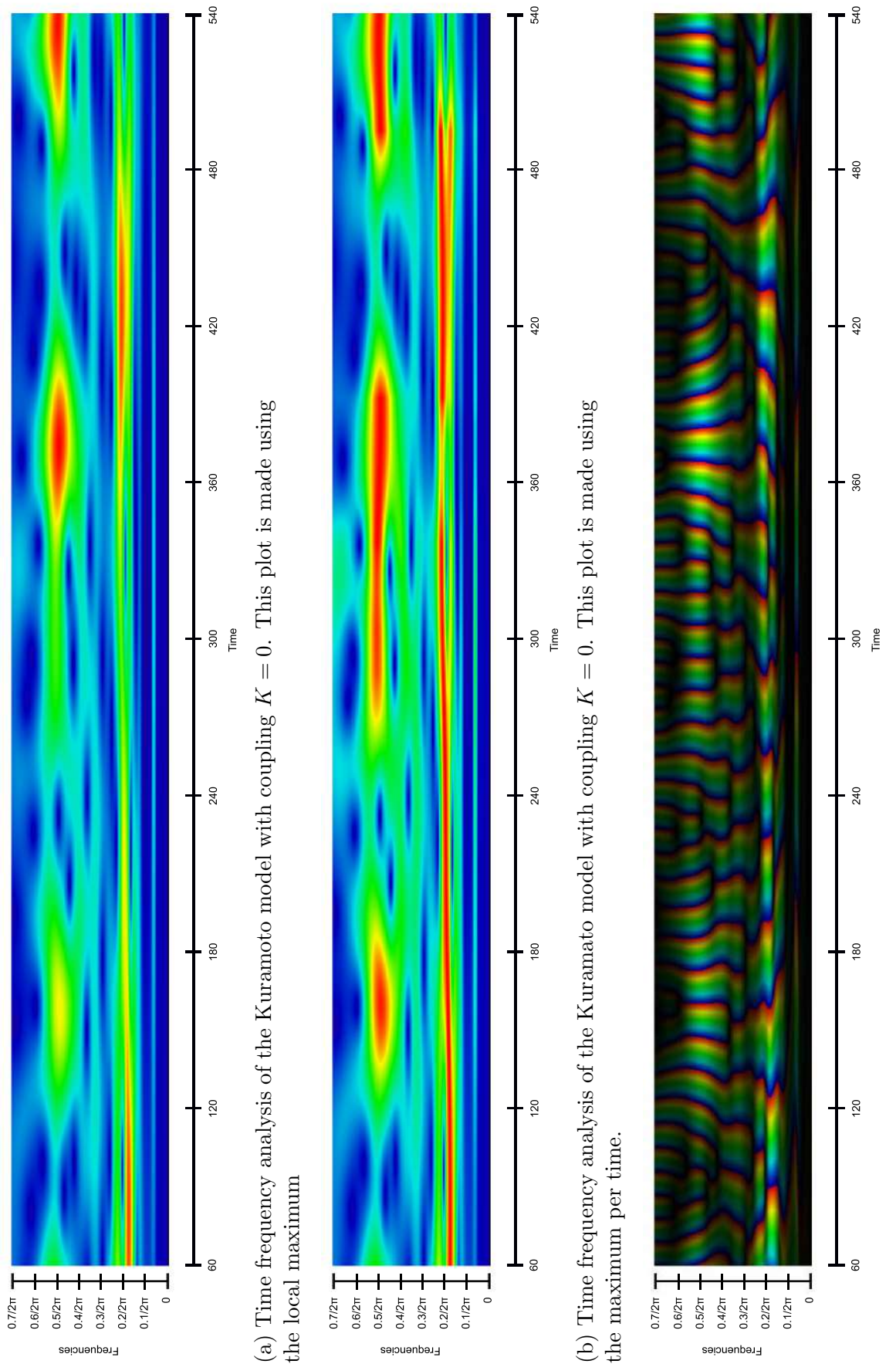


Figure 24: Time frequency analysis for the first group of oscillators (modus is $0.2/2\pi$) with coupling $K = 0$

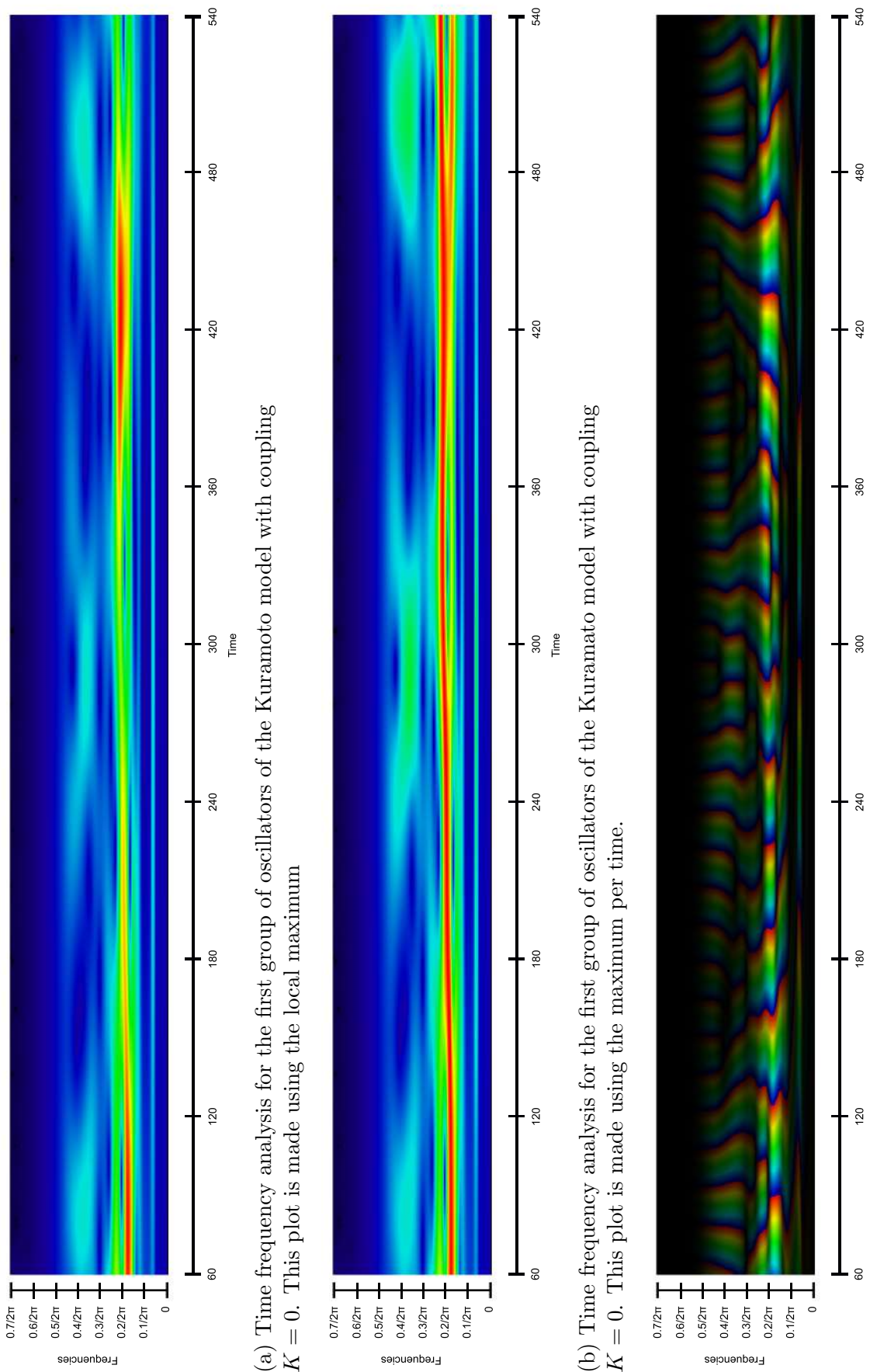
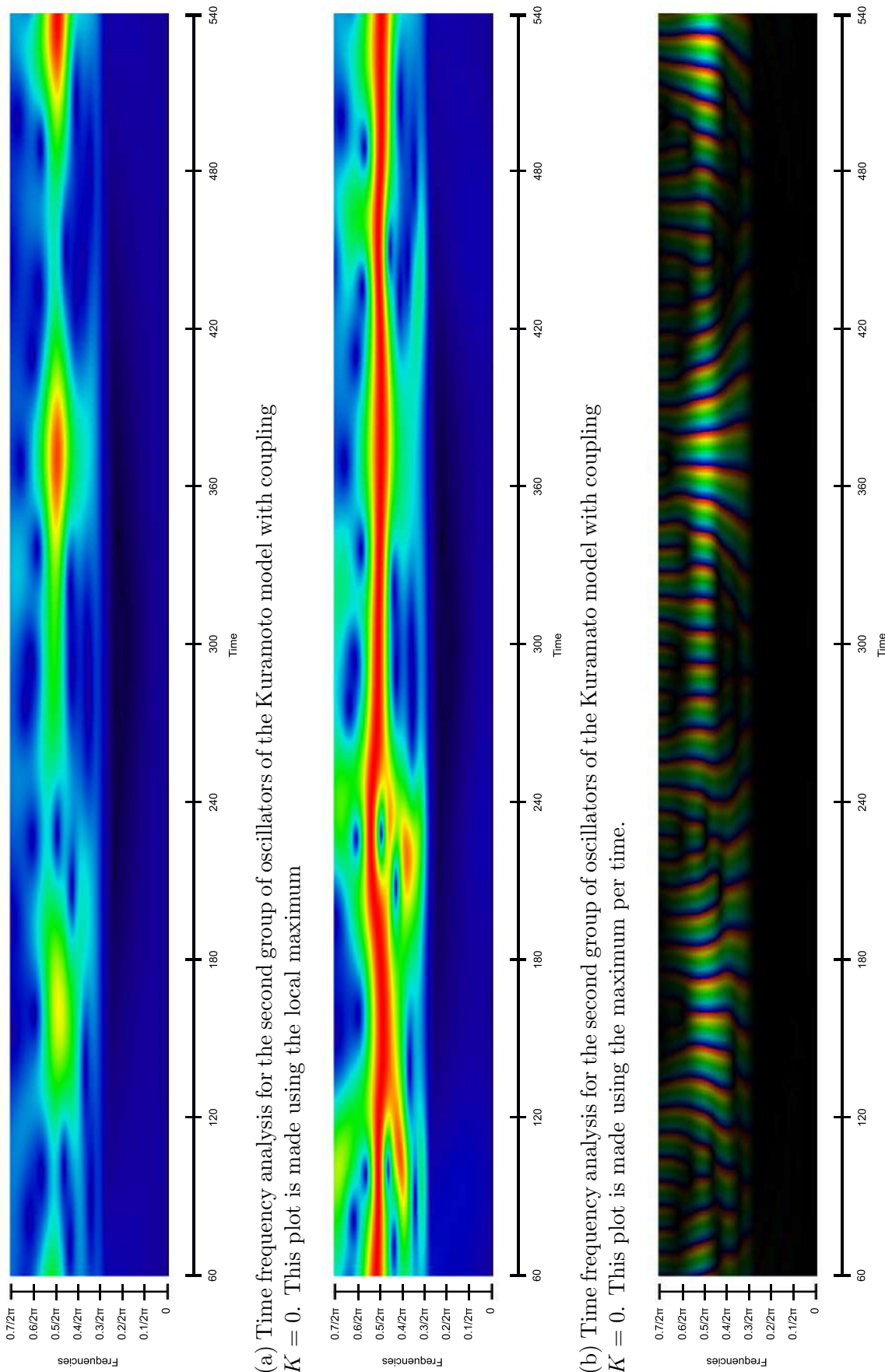


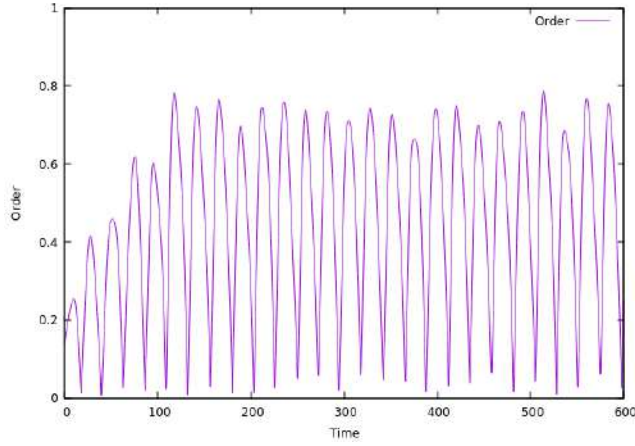
Figure 25: Time frequency analysis for the second group of oscillators (modus is $0.5/2\pi$) with coupling $K = 0$



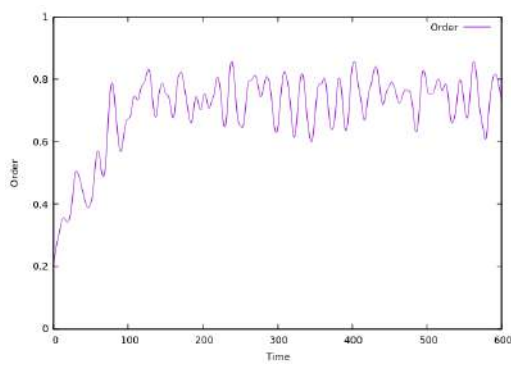
Next we increase the coupling strength to $K = 0.15$. We expect the frequencies and the phases to get more dense, which will result in higher values for the order parameter. We expect that this will also be apparent in the time frequency plots. Figure 26 shows the plots of the order parameter. In Figure 26a we see that the order parameter for the whole population oscillates heavily; sometimes the whole population is partially synchronized and on other times it is incoherent. However, the order parameters per group show that both groups are partially synchronized (see Figure 26b and 26c). Although both groups show some small oscillations, we conclude that within the groups the majority of oscillators did lock their phase and frequency.

Figure 27 shows the time frequency analyses for two population of oscillators with a coupling strength of 0.15. In Figure 27a one can see that the frequencies of both groups synchronized. Figure 27b shows that most frequencies are again around $0.2/2\pi$. Furthermore, Figure 27c shows clearly the behavior of the order parameter for all oscillators (Figure 26a). Note that in Figure 27c the phases change much slower for the lower frequency than for the higher frequency. Moreover, one can see that at a certain point in time the mean phases are the same in each group or they are different. For example at $t = 180$ the plot of the order parameter shows a minimum, and the time frequency plot shows that the mean phases of both groups are very different. Also at $t = 120$ Figure 27c shows that the mean phases of both groups are almost the same, and this is exactly peaked in Figure 26a. We can conclude that the order parameter for the two groups oscillates this heavily, because the frequencies of the two groups are far apart; sometimes the phases are synchronized (the peaks in the plot of the order parameter) while at other moments the phases are totally incoherent (the minima in the plot of the order parameter). Thus, for a coupling of 0.15 most oscillators in each group are phase and frequency locked. However the groups did not synchronize with each other.

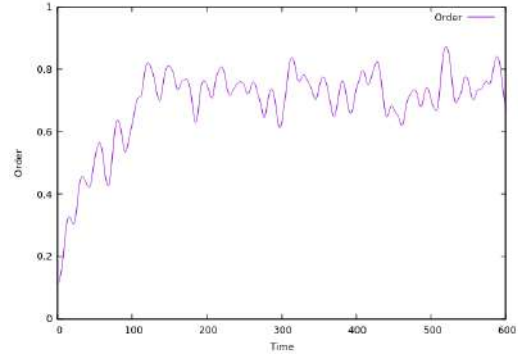
The time frequency plots for group one and two separated can be found in Figures 28 and 29. The time frequency plots of the frequencies show that in both groups the frequencies synchronized (see Figure 28a and 29a). However, in both Figures it looks like there are some oscillators that adjusted their frequencies to the other group. This is also visible in the plots with the maximum per time for both groups (see Figures 28b and 29b). The plots of the phase of the wavelet transform show that the phases of the oscillators within the groups are synchronized. However, the oscillators who adjusted their frequencies to the other group are not synchronized in phase with the group they belonged to (see Figures 28c and 29c).



(a) Order parameter for all oscillators ($n = 100$ and $K = 0.15$).



(b) Order parameter for the oscillators with modus 0.2 ($n1 = 50$ and $K = 0.15$)



(c) Order parameter for the oscillators with modus 0.5 ($n2 = 50$ and $K = 0.15$).

Figure 26: Order parameter for the Kuramoto model with coupling $K = 0.15$.

Figure 27: Time frequency analysis for $K = 0.15$

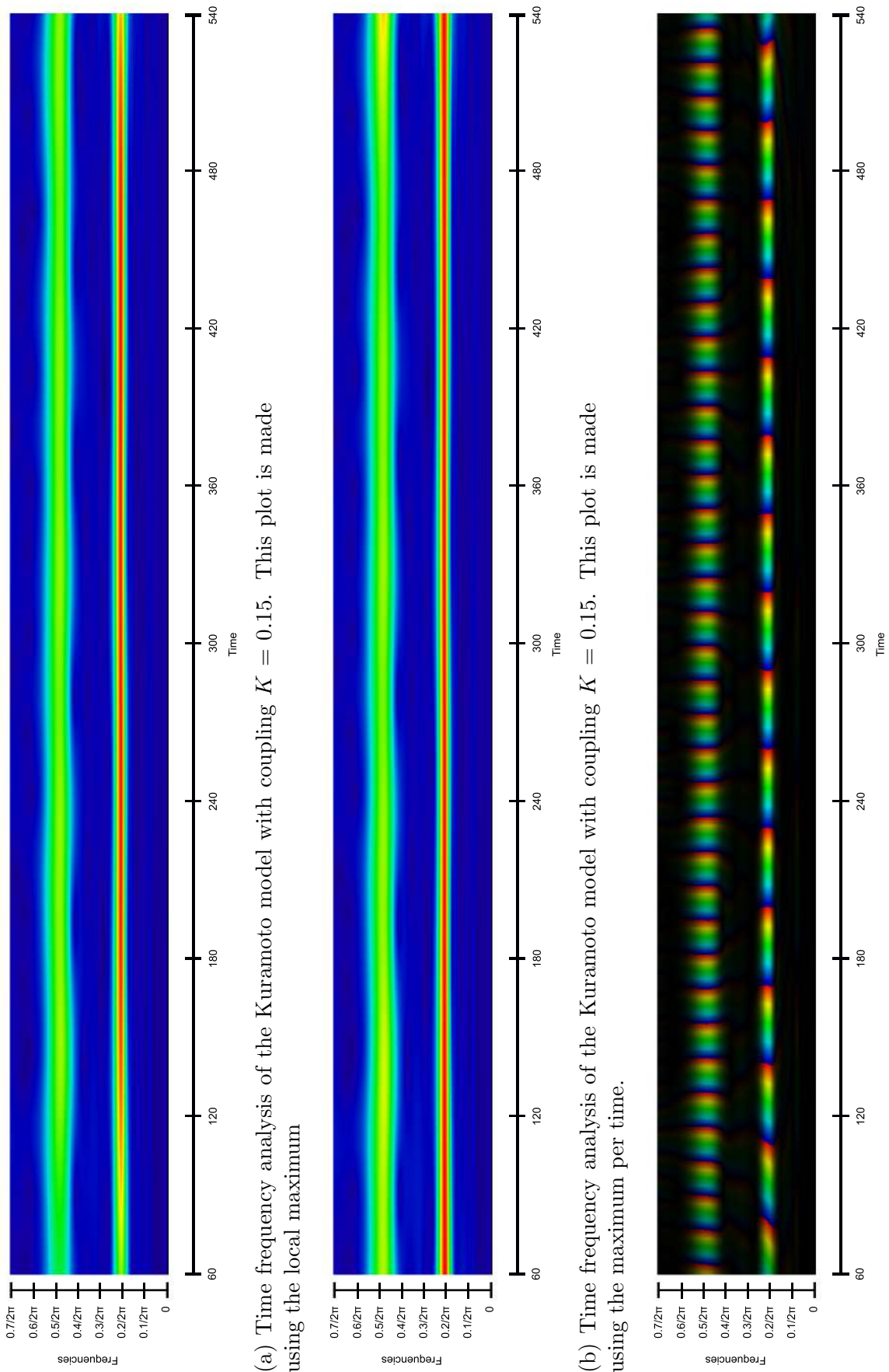


Figure 28: Time frequency analysis for the first group of oscillators (modus is $0.2/2\pi$) with coupling $K = 0.15$

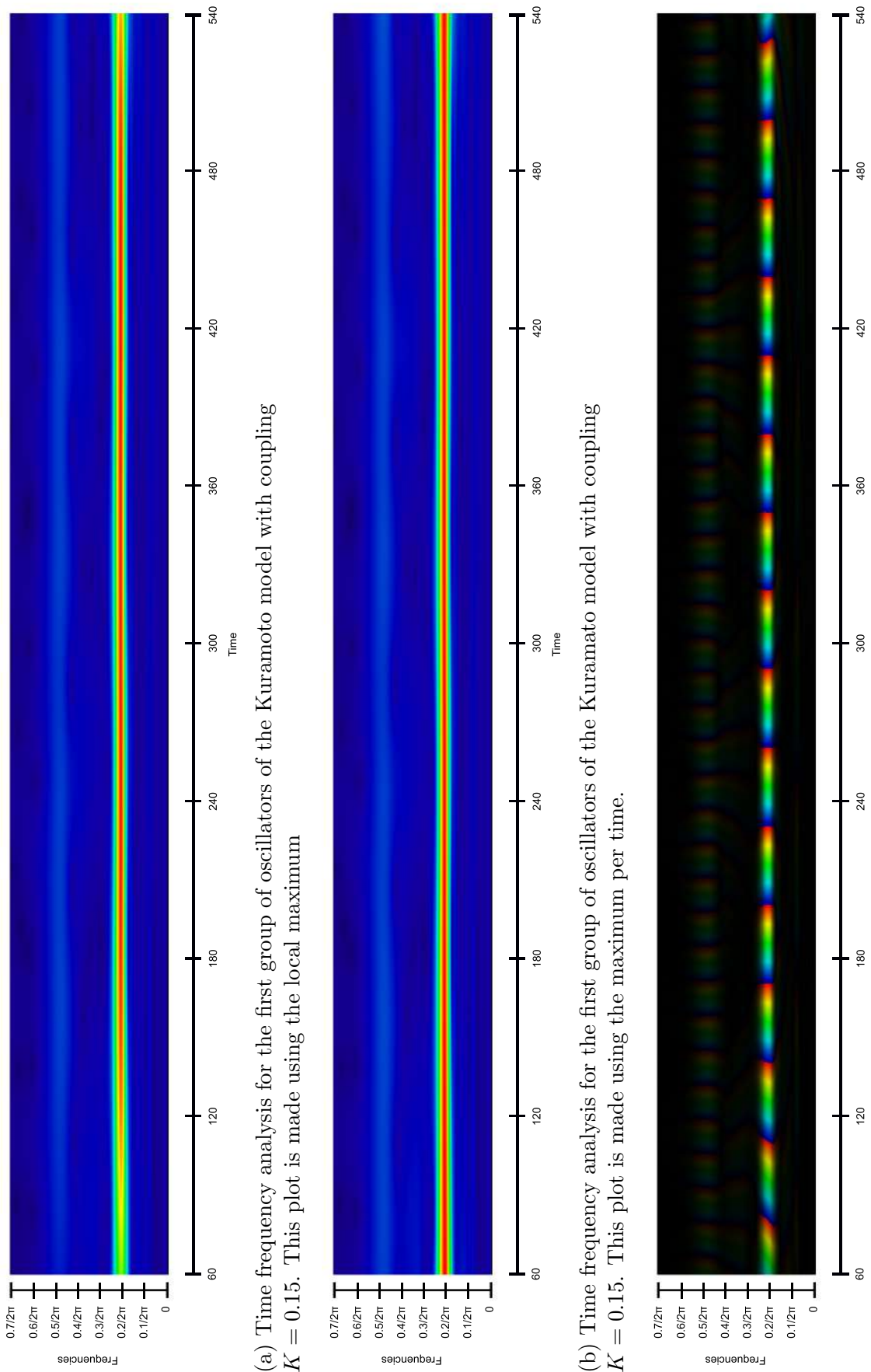
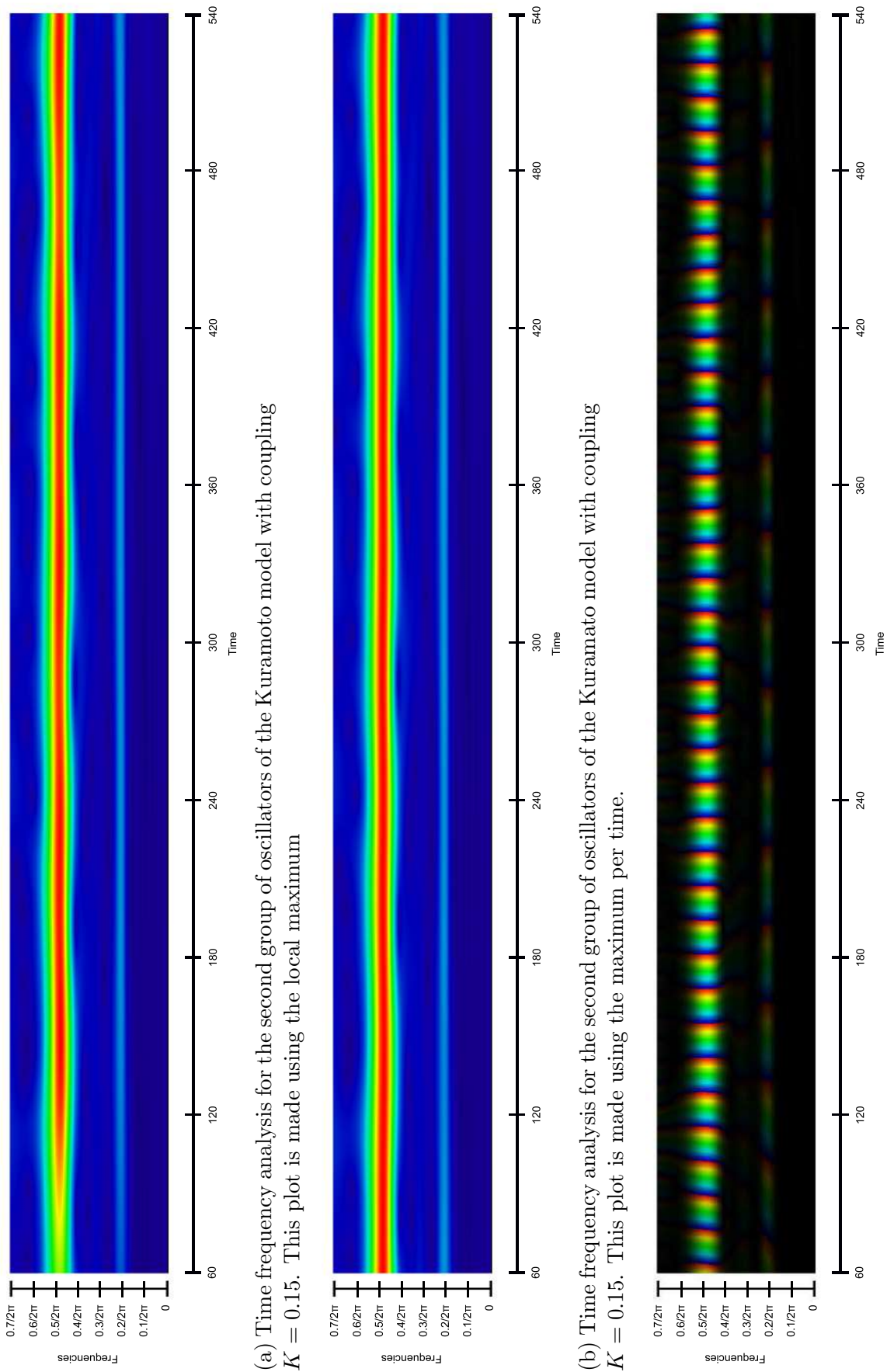


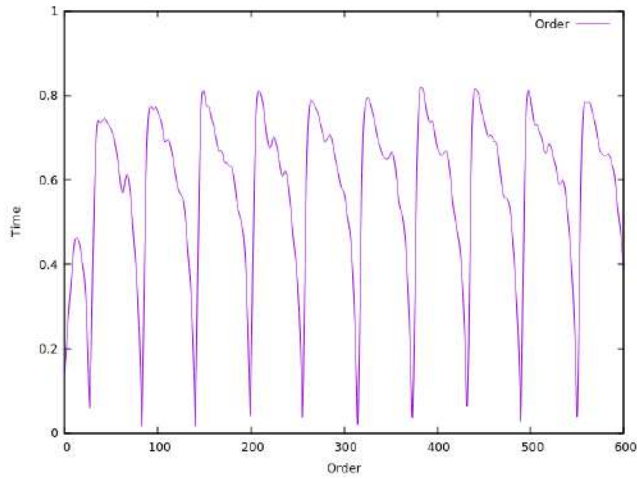
Figure 29: Time frequency analysis for the second group of oscillators (modus is $0.5/2\pi$) with coupling $K = 0.15$



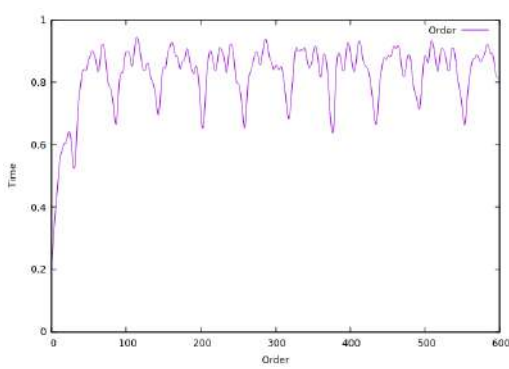
Next we double the coupling strength and we observe what happens to the phases and the frequencies. We expect that both groups might start to influence each other and some oscillators might adjust their frequencies. Figure 30a shows that the order parameter oscillates less heavily than before. Moreover, Figure 30b and Figure 30c show that the phases of both groups are more synchronized than for a coupling of $K = 0.15$. This gives the impression that when the coupling increases the groups of oscillators adjust their phases and frequencies to each other as a group rather than as individual oscillators. The time frequency analysis shown in Figure 31 shows the same pattern. Most frequencies are now concentrated around $0.4/2\pi$ and $0.3/2\pi$. Hence, the two populations of oscillators are drawn to each other. Note that this process happens extremely fast, because the two populations start at $t = 0$ with a modus of $0.2/2\pi$ and $0.5/2\pi$. Finally, Figure 31c shows some clarification for the changes in the order parameter. At some points in time the phases are clearly synchronized, while at others (due to the difference in frequencies) they are still incoherent.

Figures 32 and 33 show the time frequency analysis for each group separately. Both groups show interesting behavior; the frequencies of both groups tend to each other. Note that due to these plots of each group separately, this behavior is now better separable to each group. This gives much more insight in the process of synchronization. In Figure 32a one can see that the frequencies of most oscillators in the first group increased to $0.3/2\pi$. There are also some oscillators with a frequency of $0.4/2\pi$. Next to this, there are still some oscillators in the first group with a frequency of $0.2/2\pi$. Figure 32b confirms this behavior. The frequencies of the second group of oscillators decreased (see Figure 33a). Most oscillators have a frequency of $0.4/2\pi$. There are also some oscillators with a frequency of $0.3/2\pi$ and $0.2/2\pi$. Hence, it looks like for $K = 0.3$ the frequencies of the different groups start to merge into one group.

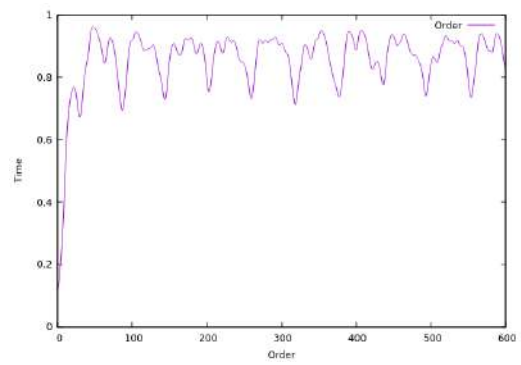
Although Figures 32 and 33 show that the frequencies of the different groups start to synchronize, the phases between the groups are still incoherent. However, within the groups the phases show synchronization. This is also visible in Figures 32c and 33c. Note that the synchronization within the groups is not yet perfect.



(a) Order parameter for all oscillators ($n = 100$ and $K = 0.30$).



(b) Order parameter for the oscillators with modus 0.2 ($n_1 = 50$ and $K = 0.30$)



(c) Order parameter for the oscillators with modus 0.5 ($n_2 = 50$ and $K = 0.30$).

Figure 30: Order parameter for the Kuramoto model with coupling $K = 0.3$.

Figure 31: Time frequency analysis for $K = 0.30$

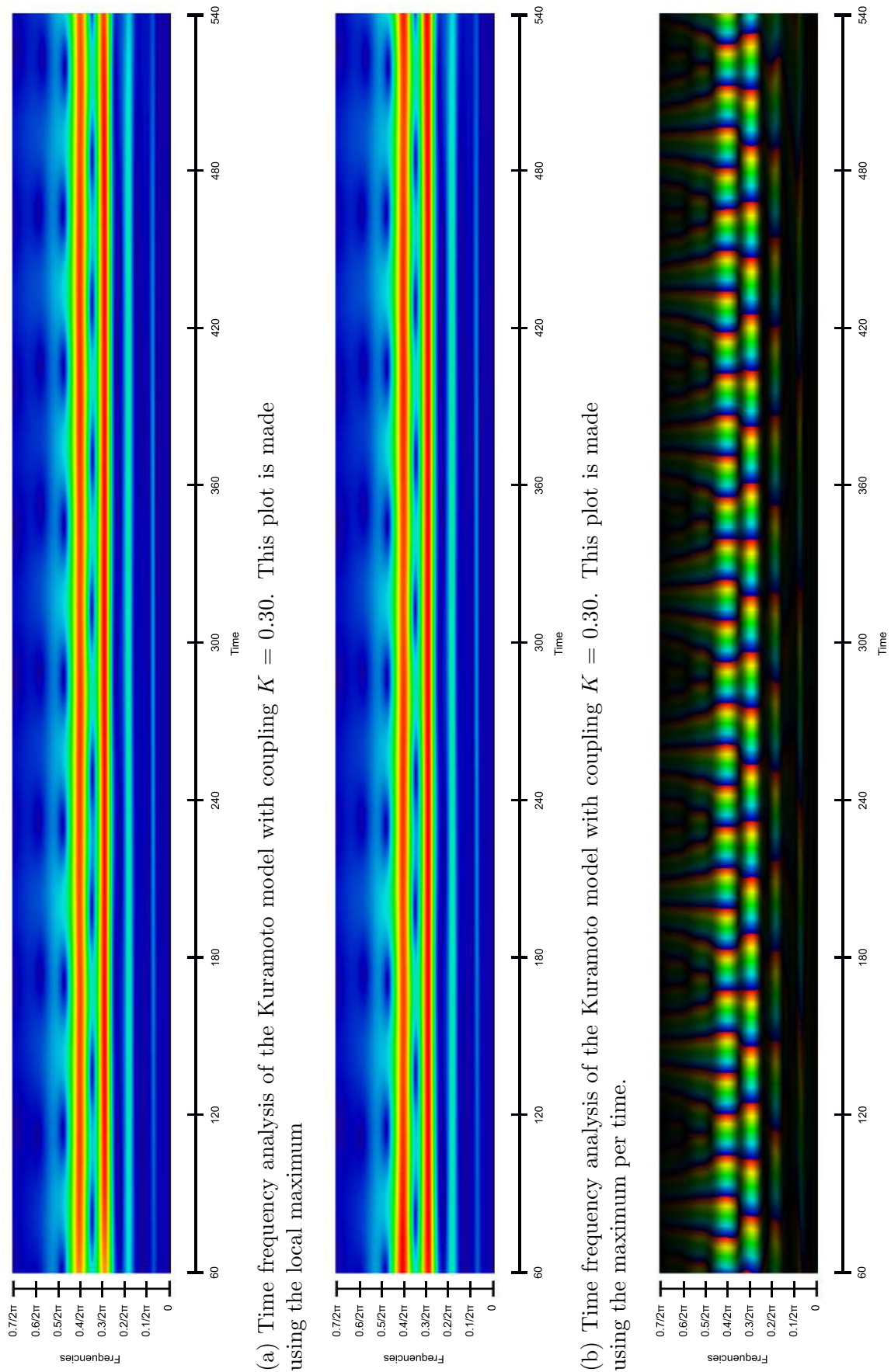


Figure 32: Time frequency analysis for the first group of oscillators (modus is $0.2/2\pi$) with coupling $K = 0.30$

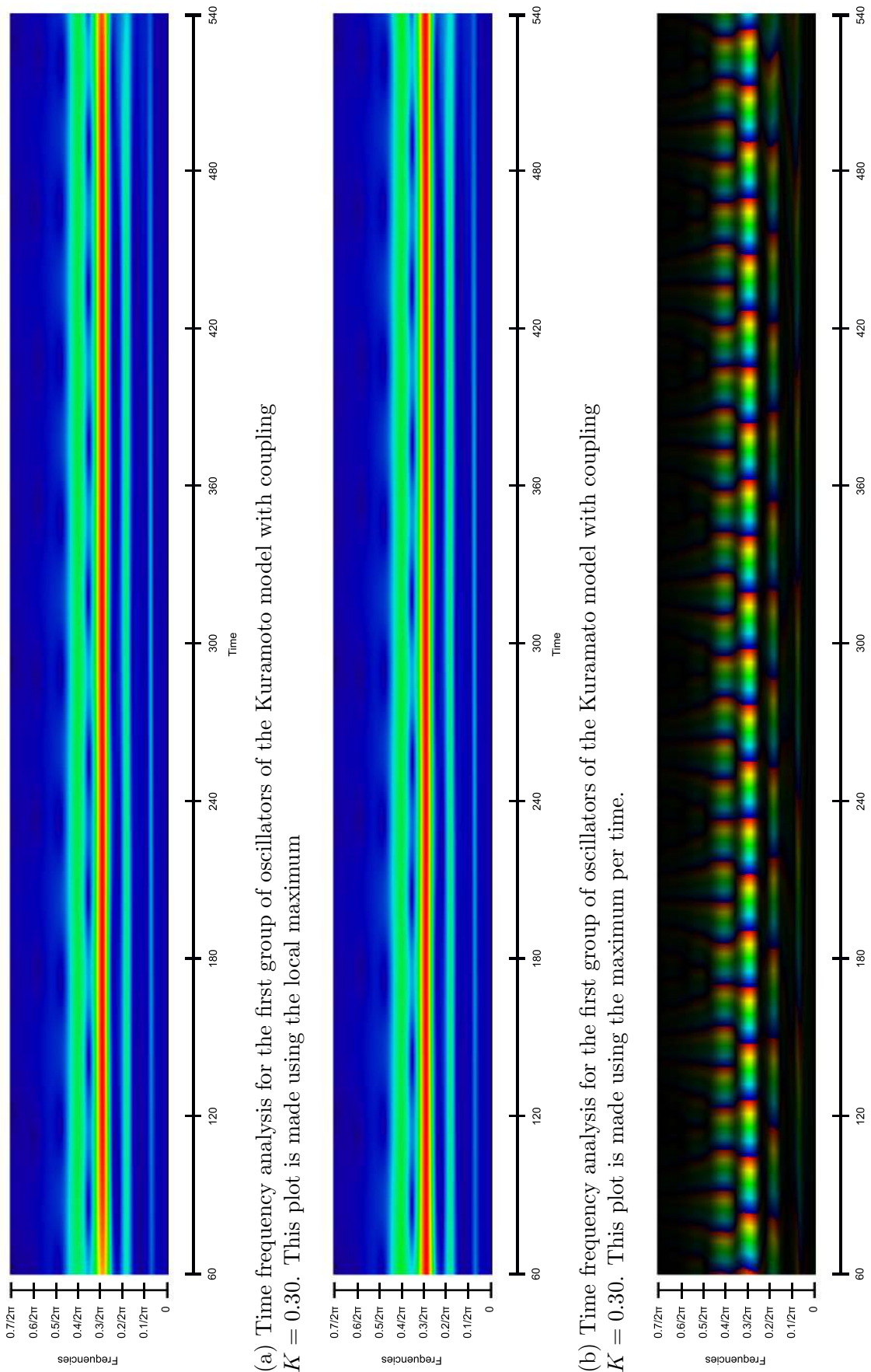
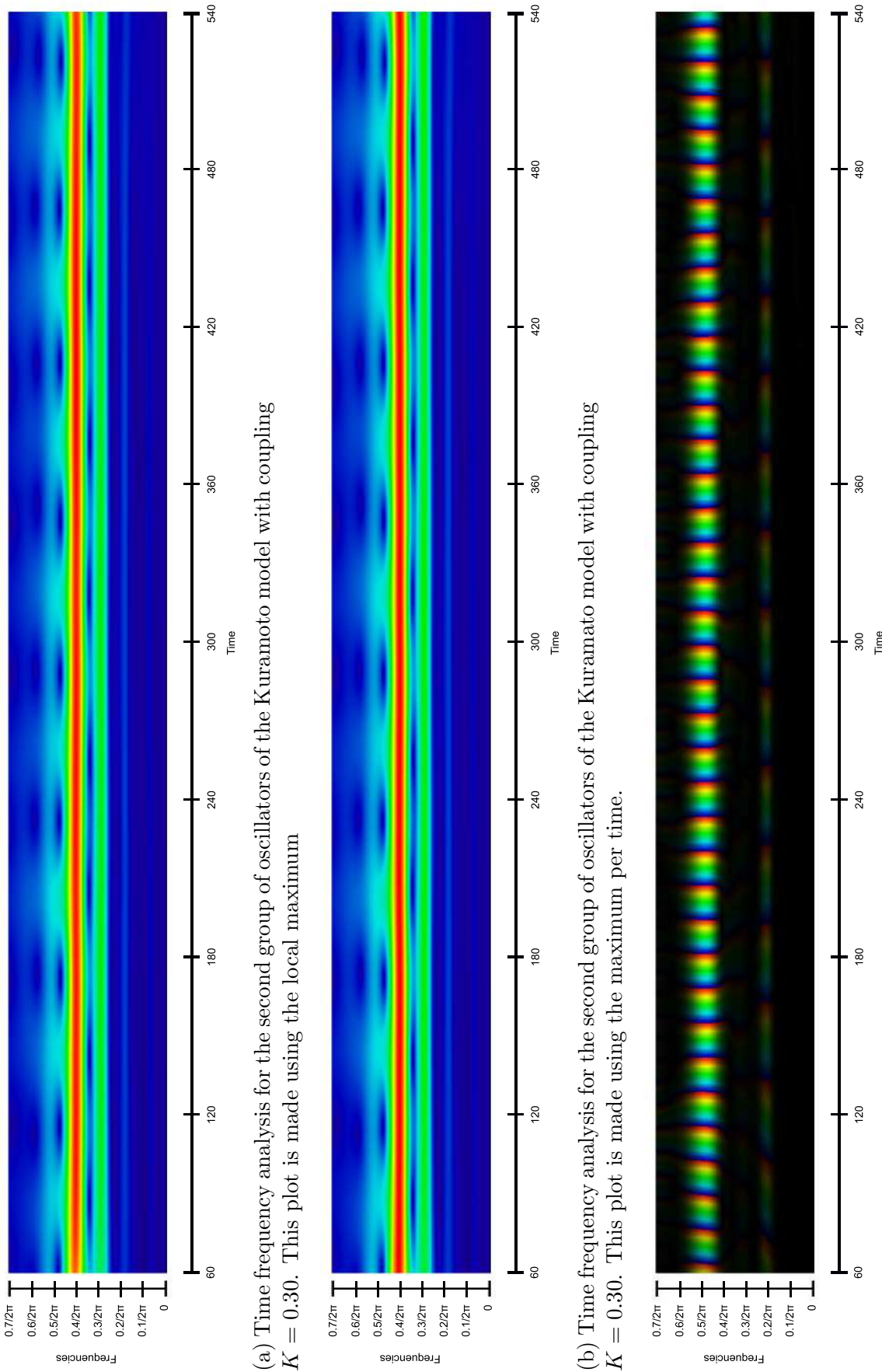


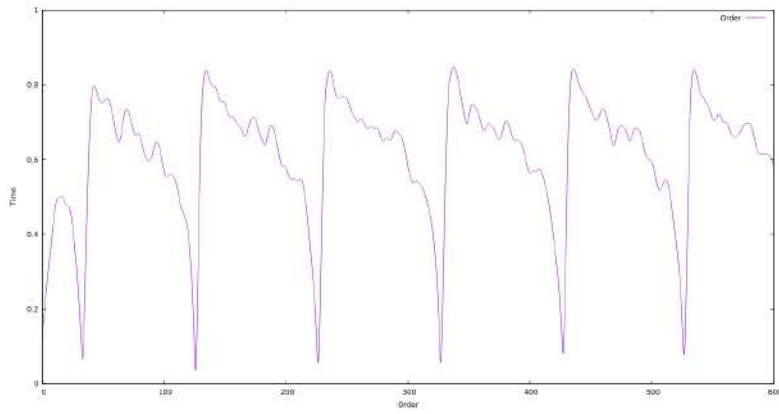
Figure 33: Time frequency analysis for the second group of oscillators (modus is $0.5/2\pi$) with coupling $K = 0.30$



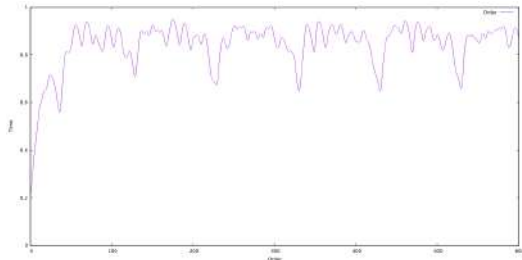
As $K = 0.3$ is clearly an interesting coupling we increase the coupling slightly to $K = 0.315$. Figure 34a shows that the order parameter for all oscillators oscillates less than before. Moreover, both groups synchronized a bit more (see Figures 34b and 34c). The time frequency analysis shows clearly that the groups of frequencies merge into one as the coupling grows (see Figure 35). Note the similarities between Figure 34a and Figure 35; when the order parameter reached a maximum the frequencies are synchronized, while when the order parameter decreases the frequencies bifurcate. The same pattern can be found in the plot of the phase of the wavelet transform (see Figure 35c). We can conclude that when the phases of the two groups are incoherent to each other the frequencies are adjusted. This is also clear in Equation (1).

In Figure 36 and 37 one can find the time frequency analysis for each group separately. Observe that in the first group the frequencies look more synchronized, but at higher value than the oscillators started (i.e. from $0.2/2\pi$ to $0.32/2\pi$). Moreover, the frequencies in the first group are more synchronized with a coupling of 0.315 than with a coupling of 0.3 (see Figures 32a and 36a). This is confirmed by the time frequency plots that is made using the maximum per time (see Figures 32b and 36b). Figure 37a shows that the second group lowered their frequencies from $0.5/2\pi$ to $0.38/2\pi$ (this process occurs in the first 60 time units). Note that the frequencies in the second group tend to go to $0.3/2\pi$.

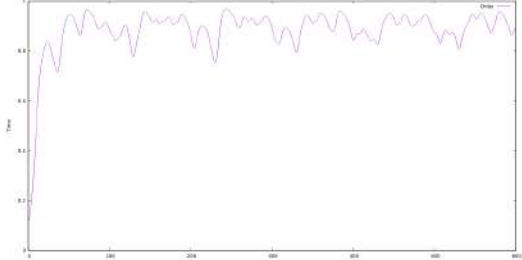
Finally, Figures 36c and 37c show that the phases of each group look synchronized whenever the frequencies of that group are synchronized. The oscillators within the group that did not synchronize in frequency are at some moments synchronized in phase and at other moments not synchronized in phase. These oscillators cause the oscillations seen in the plots of the order parameter of each group apart (see Figures 34b and 34c).



(a) Order parameter for all oscillators ($n = 100$ and $K = 0.315$).



(b) Order parameter for the oscillators with modus 0.2 ($n_1 = 50$ and $K = 0.315$)



(c) Order parameter for the oscillators with modus 0.5 ($n_2 = 50$ and $K = 0.315$).

Figure 34: Order parameter for the Kuramoto model with coupling $K = 0.315$.

Figure 35: Time frequency analysis for $K = 0.315$

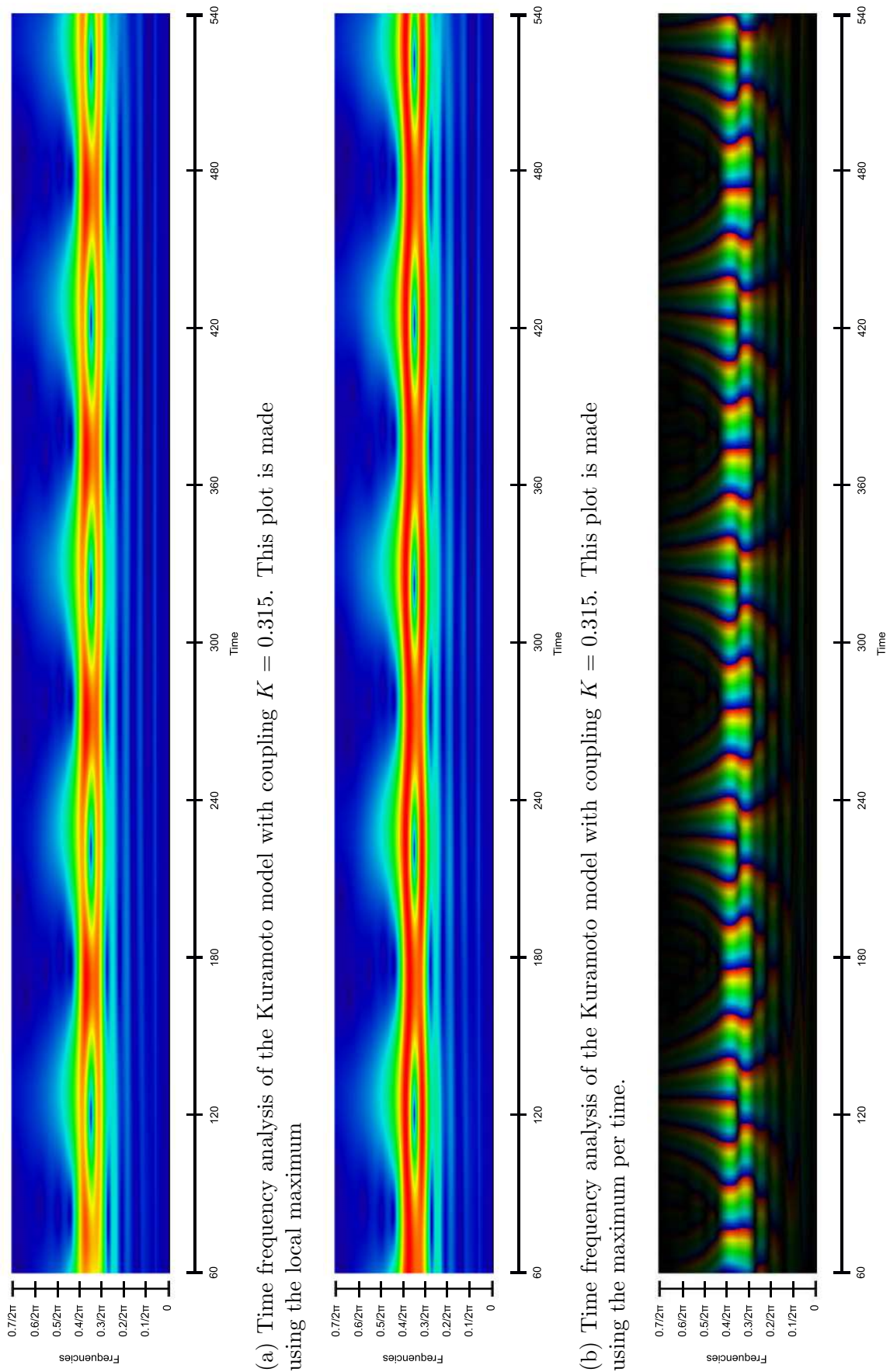


Figure 36: Time frequency analysis for the first group of oscillators (modus is $0.2/2\pi$) with coupling $K = 0.315$

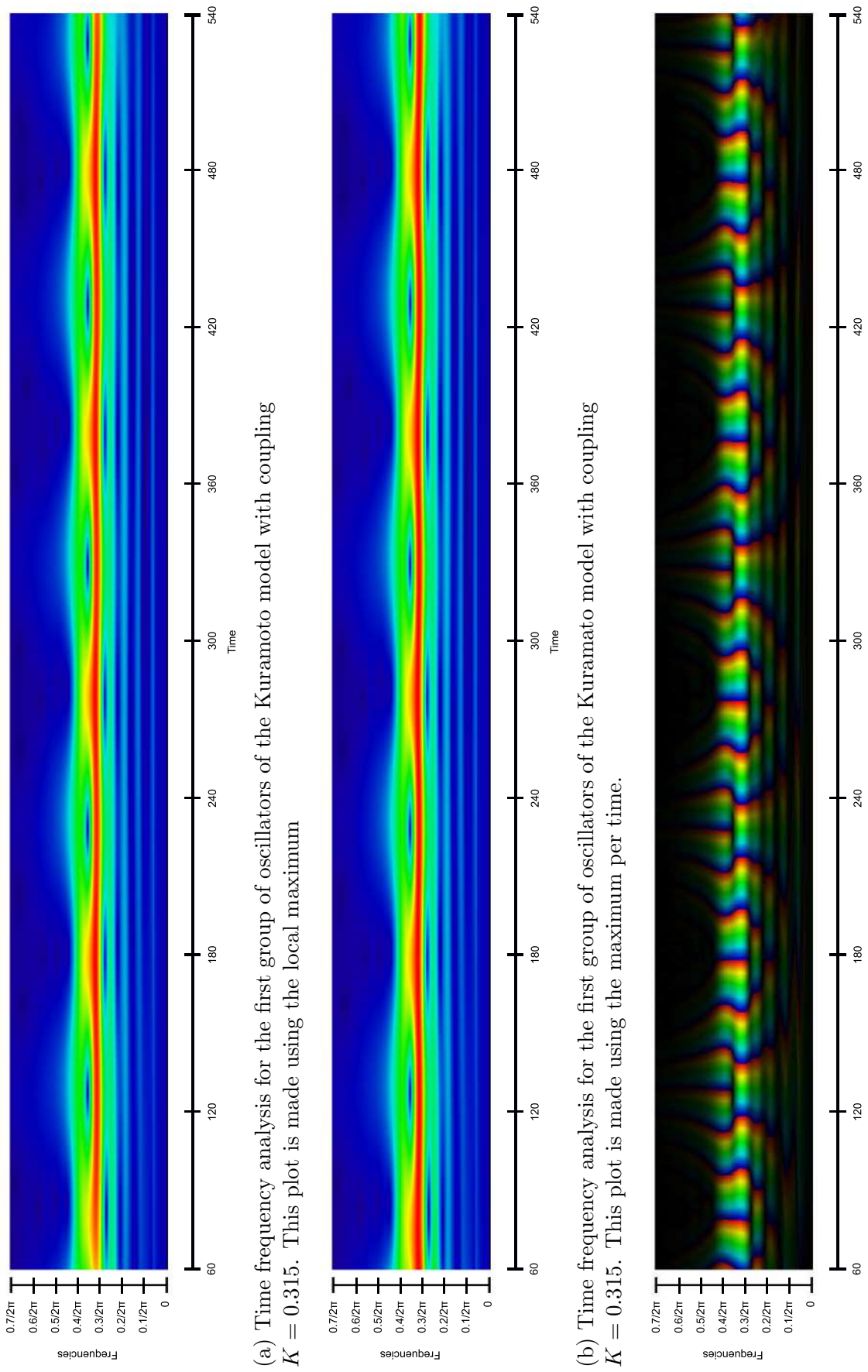
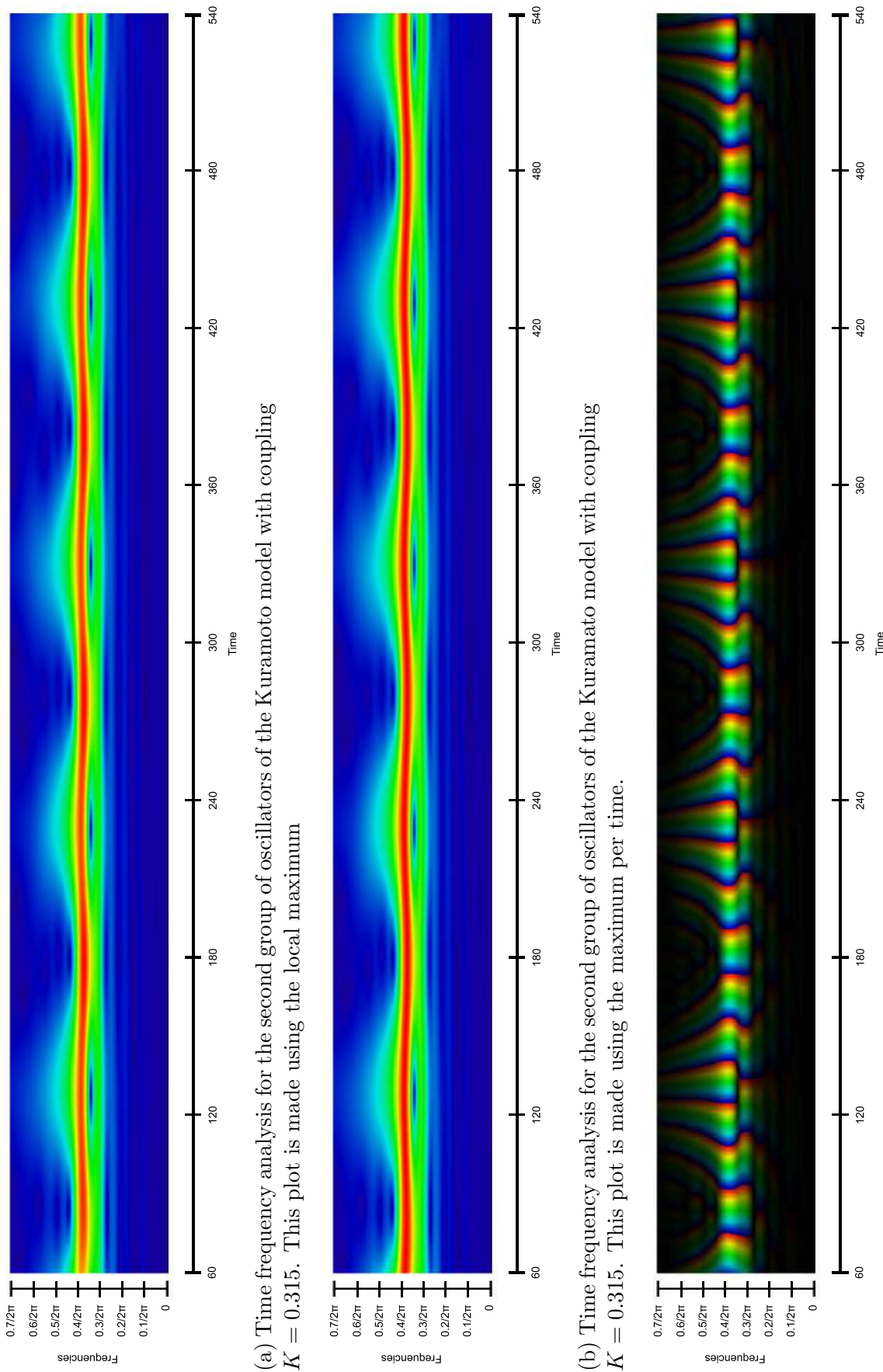
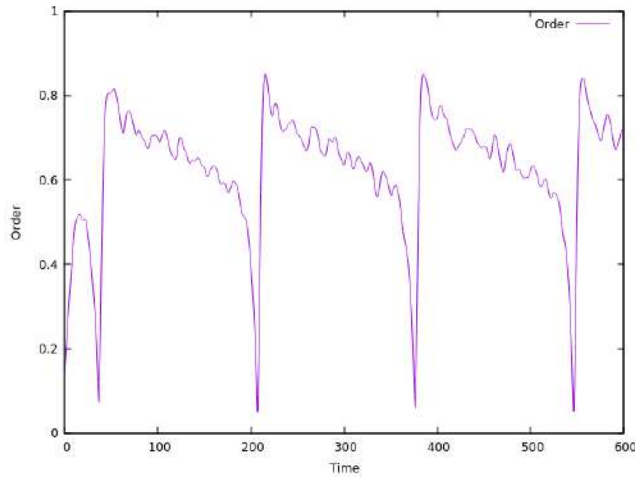


Figure 37: Time frequency analysis for the second group of oscillators (modus is $0.5/2\pi$) with coupling $K = 0.315$

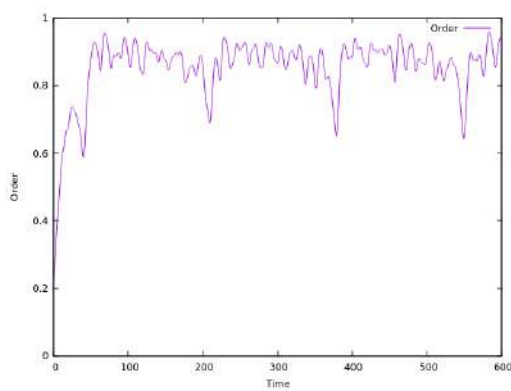


We increased the coupling again a bit ($K = 0.32$) and we found that the order parameter oscillates even less (see Figure 38a). There is a total of 4 oscillations of the order parameter. Again the peaks and minima are in agreement with the time frequency analysis. Hence, the phases and frequencies (de)synchronize at the same moment. The same pattern can be seen in the plot of the phase of the wavelet transform. (Figure 39c).

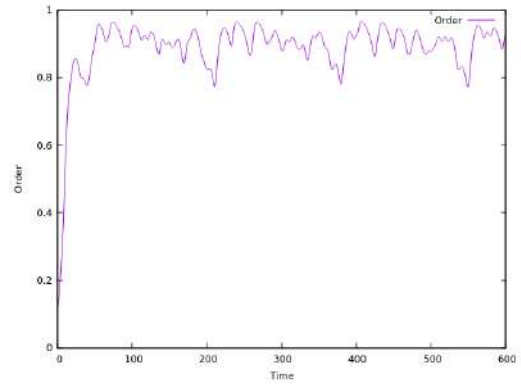
Figures 40 and 41 show the time frequency plots of each group separately. These plots are very similar to the time frequency plot of all oscillators (i.e. Figure 39). There are however some small differences. The frequencies of the first group of oscillators are still a bit lower and the frequencies of the second group of oscillators are a bit higher. Observe that combining the figures of the time frequency analysis obtained using the maximum per time for both groups (i.e. Figures 40b and 41b) gives exactly the time frequency analysis for both groups of oscillators together. Finally the plot of the phase of the wavelet transform shows that the phases of both groups are synchronized whenever the frequencies are synchronized (see Figures 40c and 41c). At 190 time units and at 360 time units the phases of both groups are a bit desynchronized, because the frequencies are desynchronized as well. This is also visible in the plot of the order parameter.



(a) Order parameter for all oscillators ($n = 100$ and $K = 0.32$).



(b) Order parameter for the oscillators with modus 0.2 ($n1 = 50$ and $K = 0.32$)



(c) Order parameter for the oscillators with modus 0.5 ($n2 = 50$ and $K = 0.32$).

Figure 38: Order parameter for the Kuramoto model with coupling $K = 0.32$.

Figure 39: Time frequency analysis for $K = 0.32$

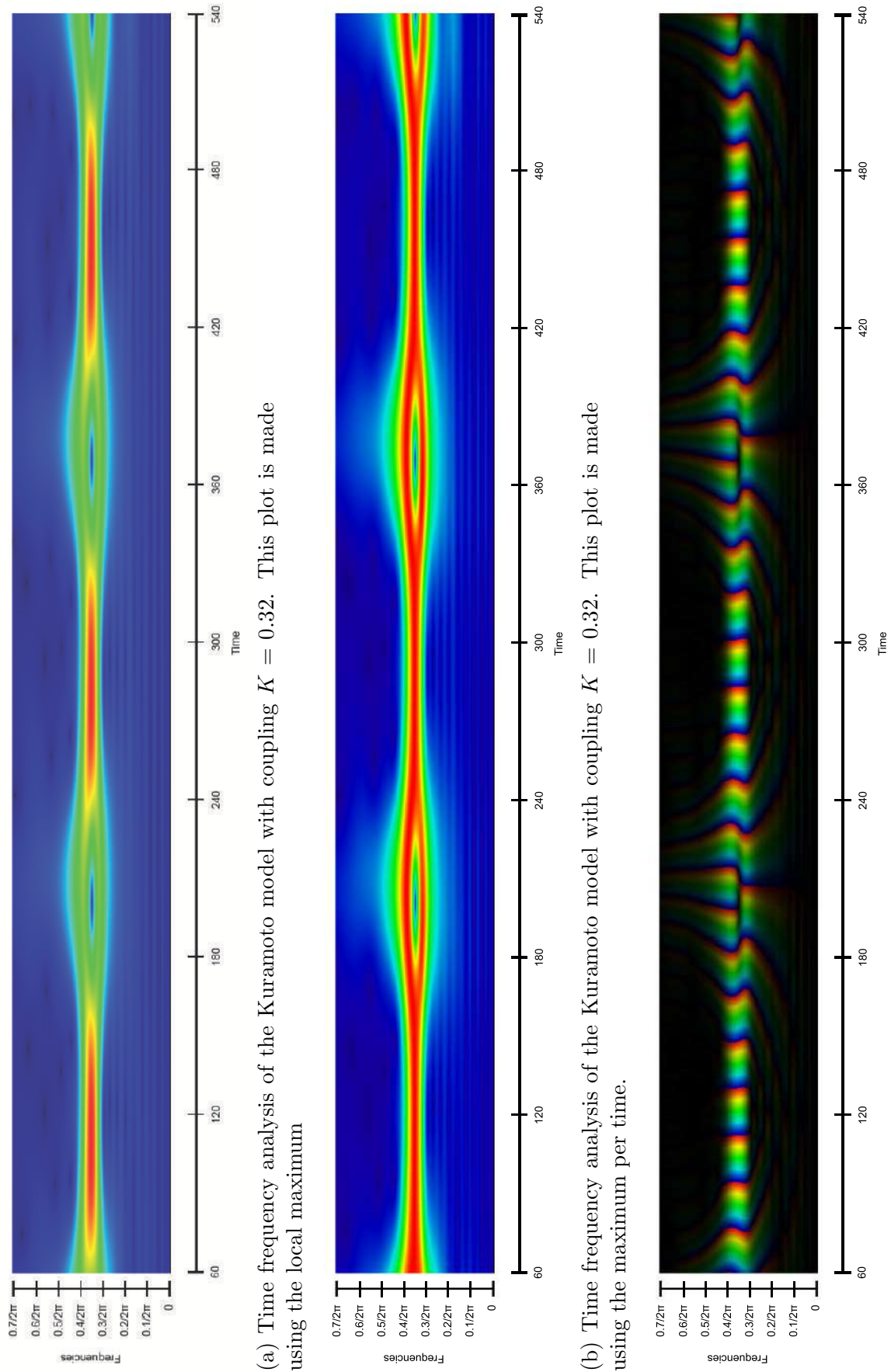


Figure 40: Time frequency analysis for the first group of oscillators (modus is $0.2/2\pi$) with coupling $K = 0.32$

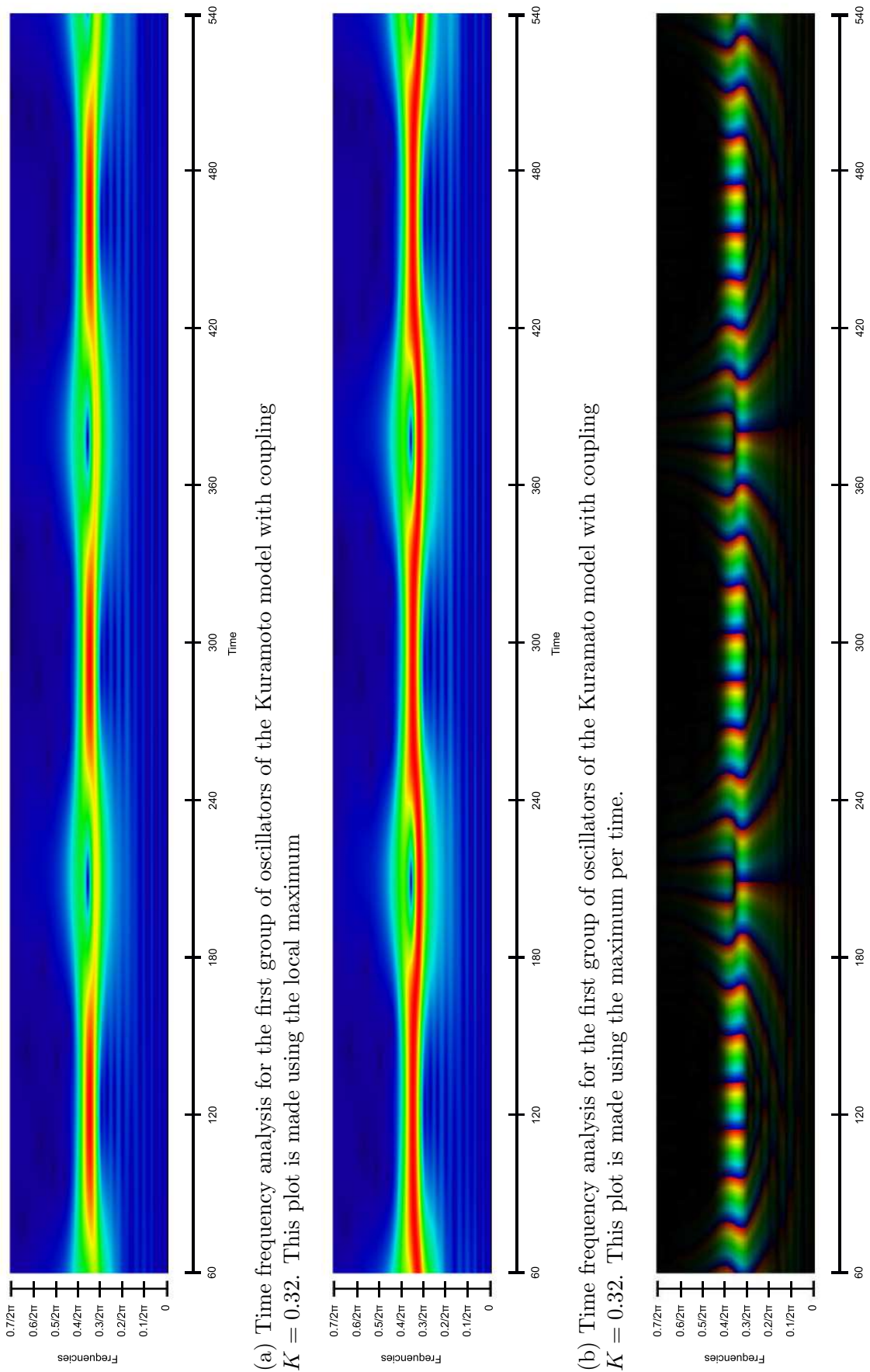
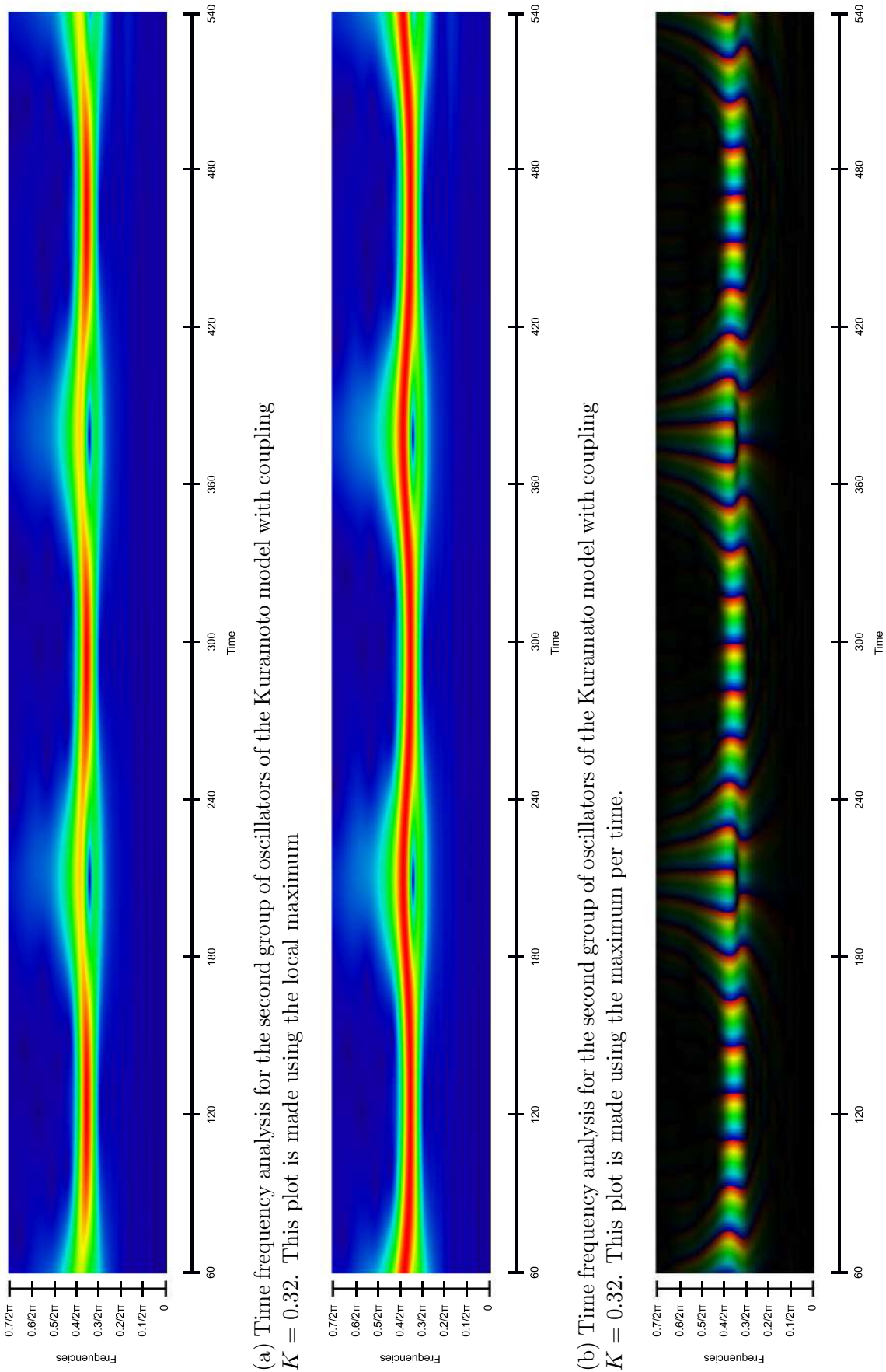
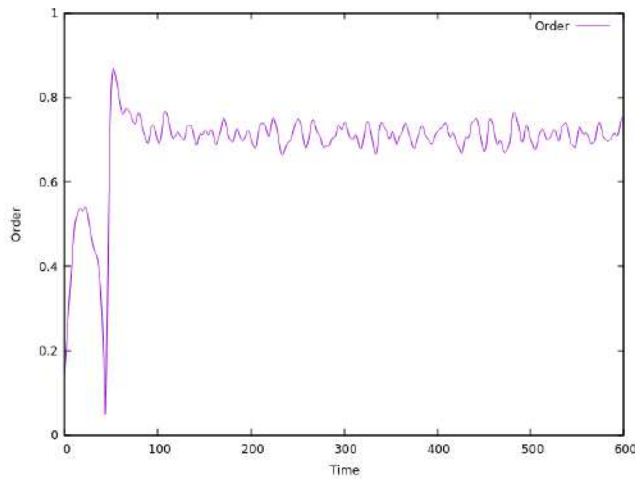


Figure 41: Time frequency analysis for the second group of oscillators (modus is $0.5/2\pi$) with coupling $K = 0.32$

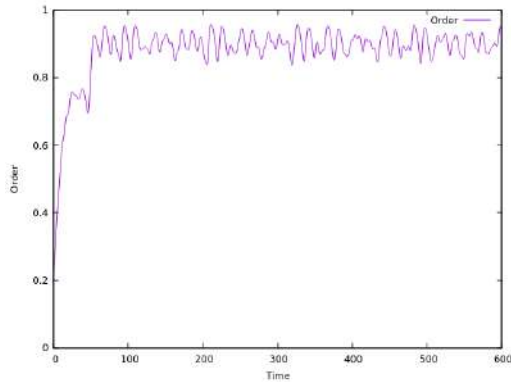


We expect that increasing the coupling even further will lead to a state where both populations of oscillators merge into one population of oscillators. In this stage, we expect the order parameter to show partial synchronization. Moreover, we still expect the order parameter to oscillate but with a smaller amplitude. To check our expectations we increase the coupling to $K = 0.325$. Figure 42a shows the order parameter for all oscillators. As expected we find that the oscillations of the order parameter have a smaller amplitude. In the beginning there is one point in time where the order parameter shows a clear minimum. At that point of time the frequencies of the two groups clearly did not merge into one group of frequencies. Unfortunately, this process can not be seen in the time frequency plot as the first 60 time units are not shown in the time frequency plot, because it may happen that the wavelet is not fully contained in the interval of the first 60 time units. After $t = 70$ the phases (and thus the frequencies too) of the oscillators are partially synchronized. This result is also clearly visible in the time frequency plots (see Figure 43).

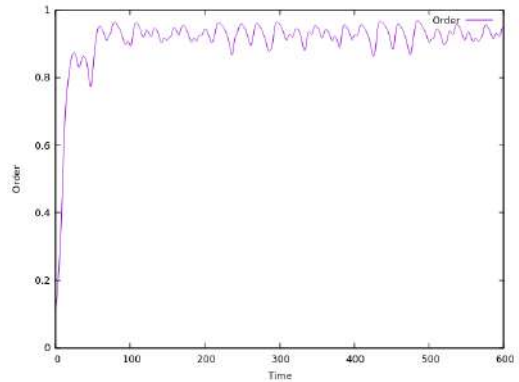
Time frequency analysis per group shows that the frequency of each group converged to the frequency of the other group ending up at a frequency of $0.35/2\pi$ (see Figure 44a and 45a). This is exactly the middle of the starting points of the modus we chose for both groups. Note that in the beginning, the process of synchronization is still ongoing; in the first group the frequencies increase between time 60 and 90 and in the second group we see a decrease of the frequencies. This is even more visible in the time frequency plots obtained by taking the maximum per time (i.e. in Figures 44b and 45b). Figures 44c and 45c show that the phases of both groups are synchronized.



(a) Order parameter for all oscillators ($n = 100$ and $K = 0.325$).



(b) Order parameter for the oscillators with modus 0.2 ($n_1 = 50$ and $K = 0.325$)



(c) Order parameter for the oscillators with modus 0.5 ($n_2 = 50$ and $K = 0.325$).

Figure 42: Order parameter for the Kuramoto model with coupling $K = 0.325$.

Figure 43: Time frequency analysis for $K = 0.325$

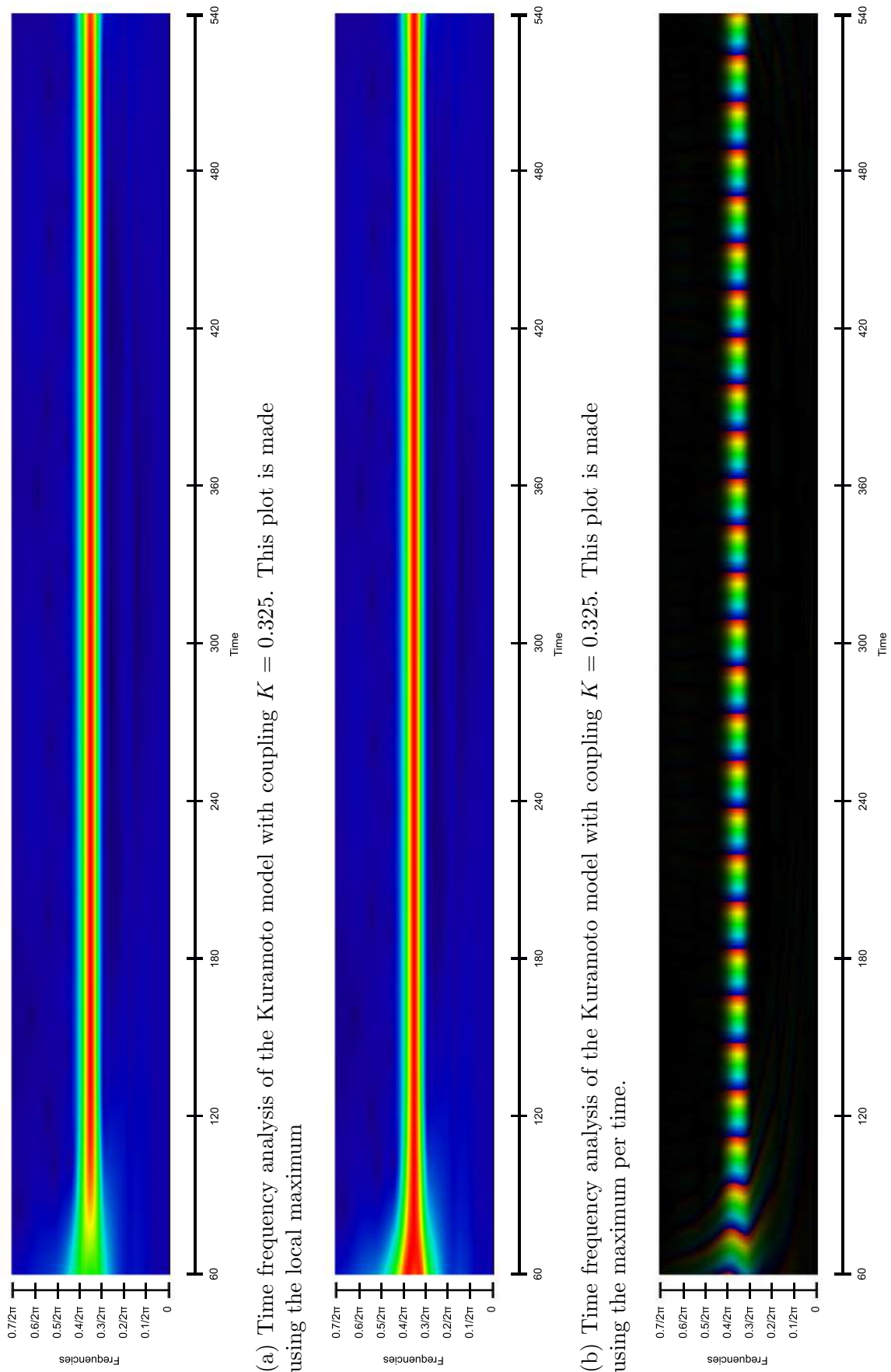


Figure 44: Time frequency analysis for the first group of oscillators (modus is $0.2/2\pi$) with coupling $K = 0.325$

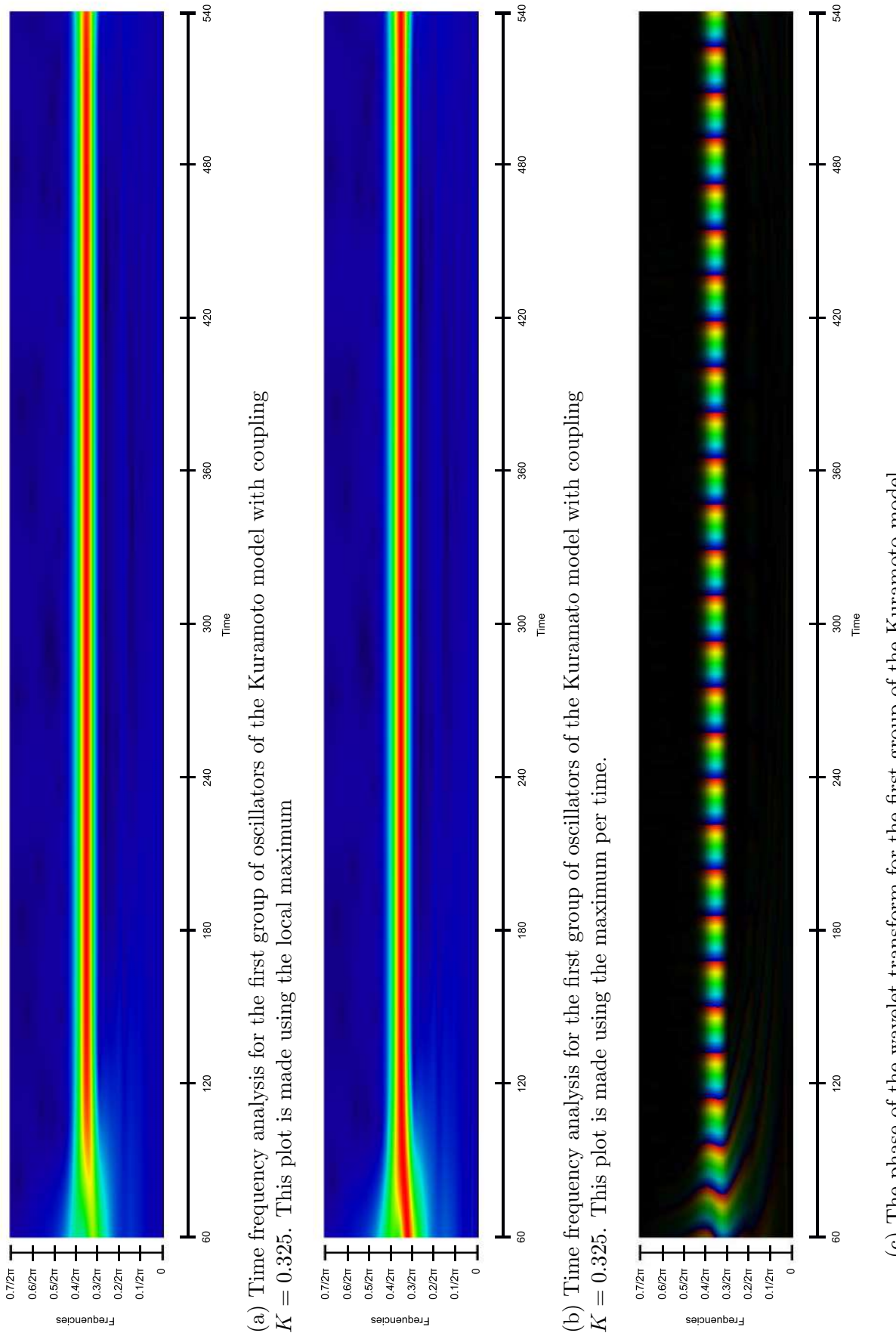
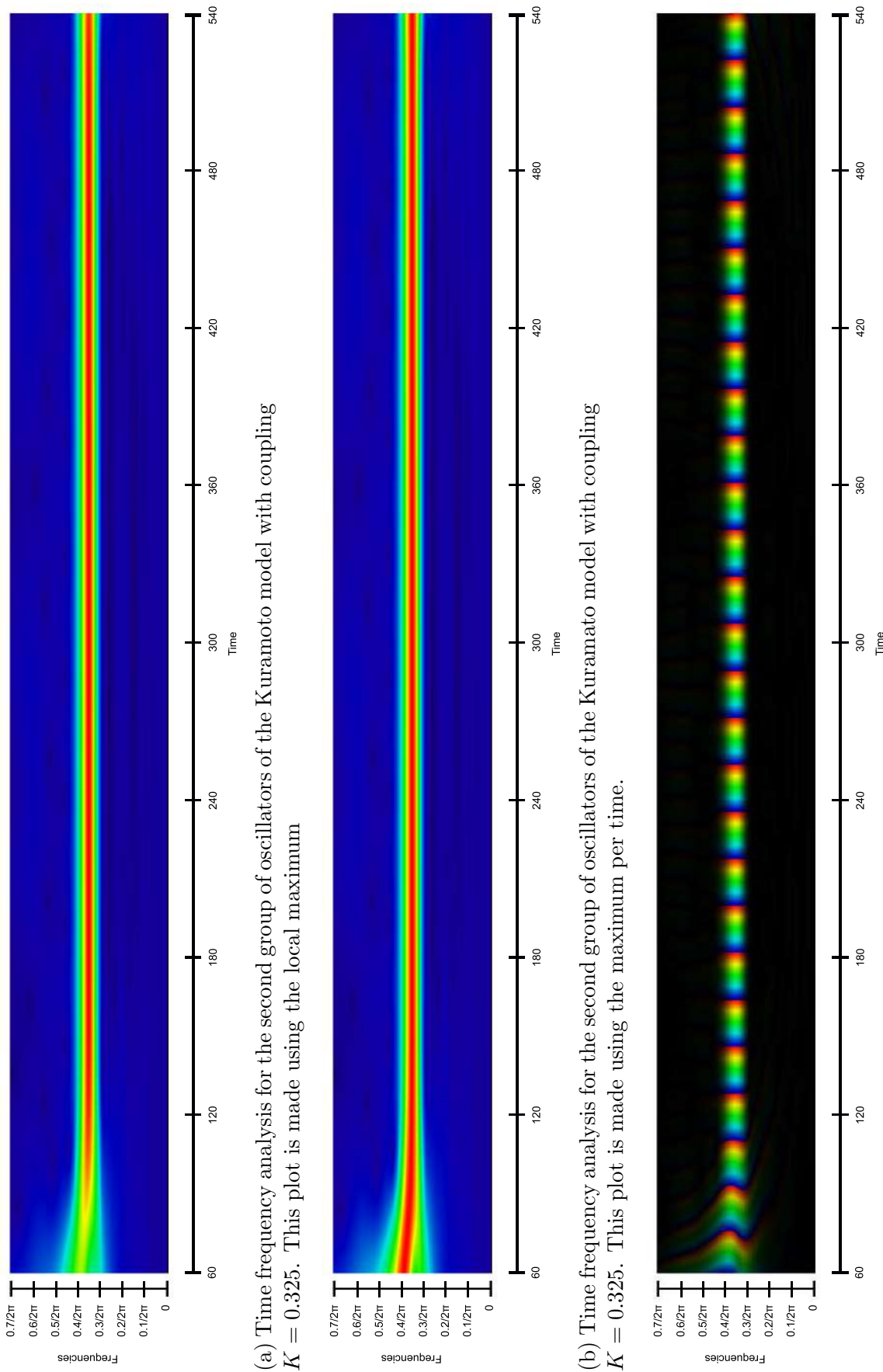


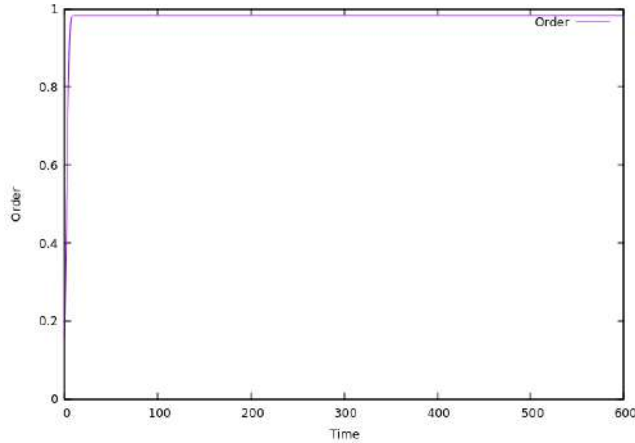
Figure 45: Time frequency analysis for the second group of oscillators (modus is $0.5/2\pi$) with coupling $K = 0.325$



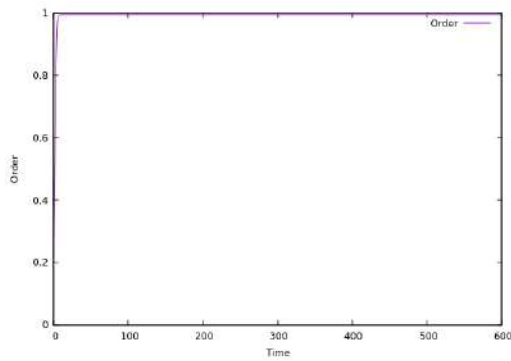
Finally, we increase the coupling to $K = 1.0$. We expect all oscillators to be synchronized. Thus, we expect to see an order parameter that is almost one. Moreover, in the time frequency plot we expect to see synchronized frequencies and phases. As shown in Figure 46a the phases are almost perfectly synchronized. Furthermore, the time frequency analysis of the phases confirms this (see Figure 47c). At last the time frequencies plots for both methods show synchronization of the frequencies.

The time frequency analysis of both groups separately look exactly the same as the time frequency analysis of all oscillators together (see Figures 48 and 49). Hence, the two groups merged into one group of oscillators. The frequencies of the oscillators synchronized within 60 time units. According to Figures 48c and 49c the phases of each of the groups synchronized also within 60 time units. Moreover, note the resemblance between these plots and the plot of the phase of the wavelet transform.

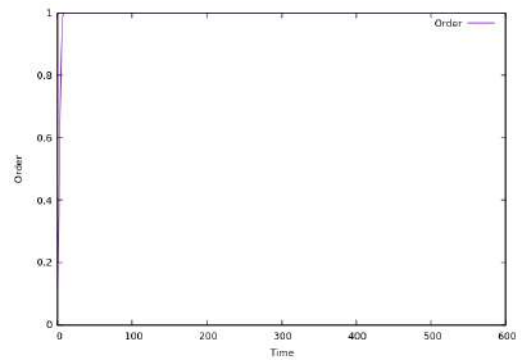
In short, we can conclude that it is possible that two groups of oscillators synchronize and start to form one group of oscillators. For two groups of oscillators with modus 0.2 and 0.5 and scale 0.015 we found a critical value of $K_c = 0.325$. We saw how the oscillators started to synchronize as we approached this critical value. As the coupling went to the critical value we saw that the oscillators moved as a group to the other group of oscillators. Hence, we saw a group process rather than a individual process. Finally, we noted that whenever synchronization took place it happened fast and in the beginning. This is not so surprising as it is well known that for the Kuramoto model the order parameter increases exponentially in the beginning for $K > K_c$. Thus, the process of synchronization is always at the beginning.



(a) Order parameter for all oscillators ($n = 100$ and $K = 1.0$).



(b) Order parameter for the oscillators with modulus 0.2 ($n_1 = 50$ and $K = 1.0$)



(c) Order parameter for the oscillators with modulus 0.5 ($n_2 = 50$ and $K = 1.0$).

Figure 46: Order parameter for the Kuramoto model with coupling $K = 1.0$.

Figure 47: Time frequency analysis for $K = 1.0$

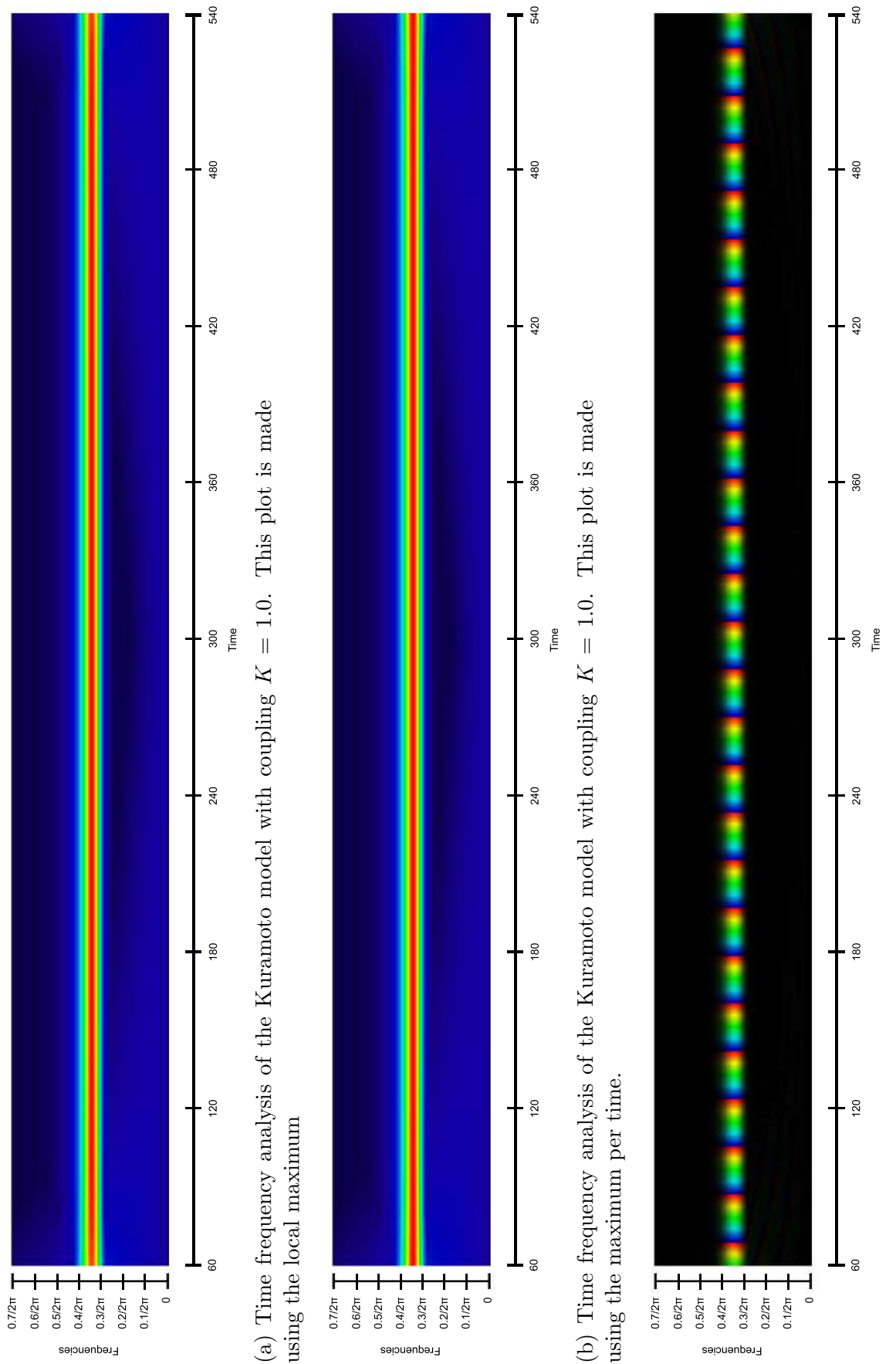


Figure 48: Time frequency analysis for the first group of oscillators (modus is $0.2/2\pi$) with coupling $K = 1.0$

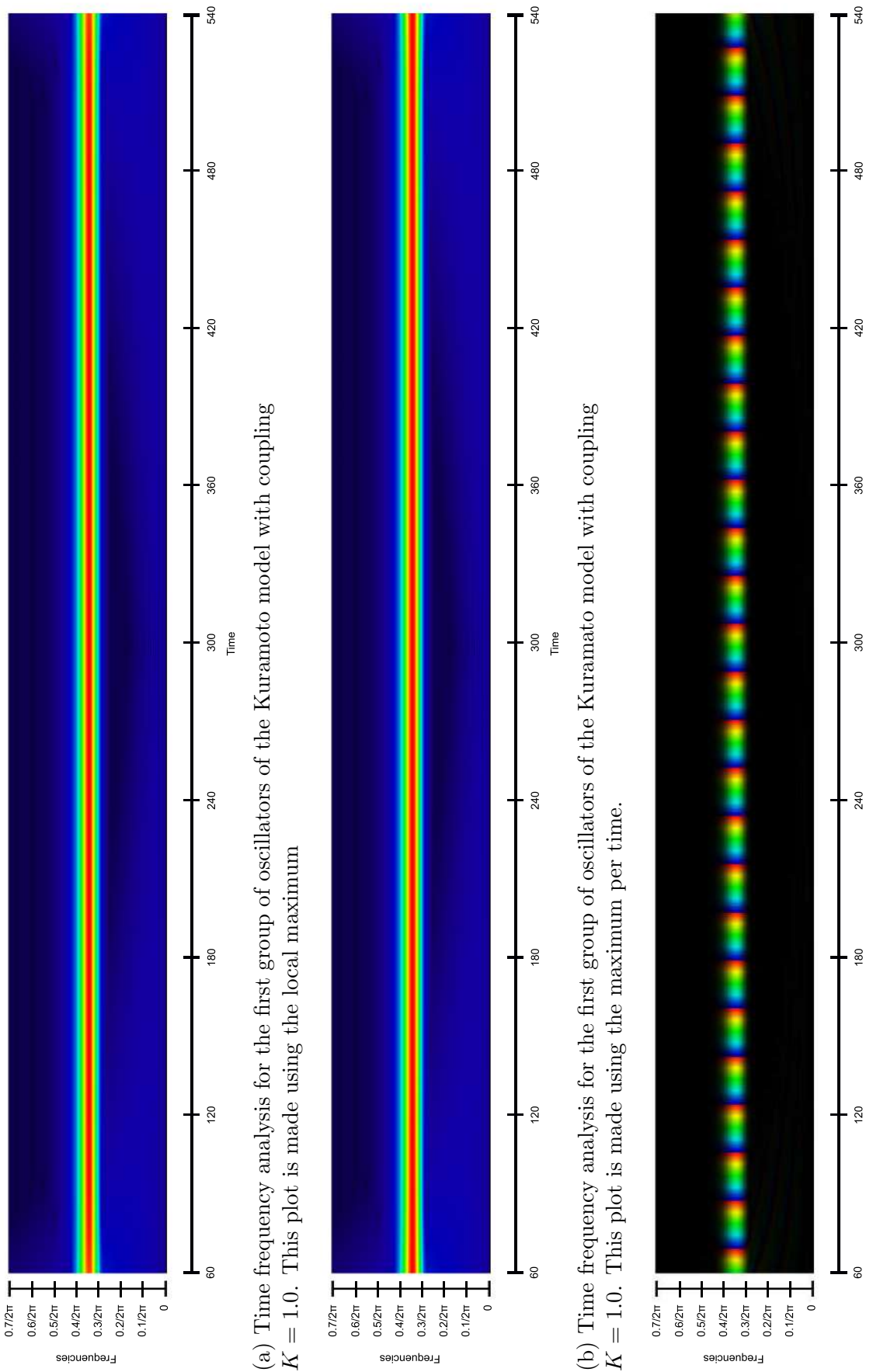
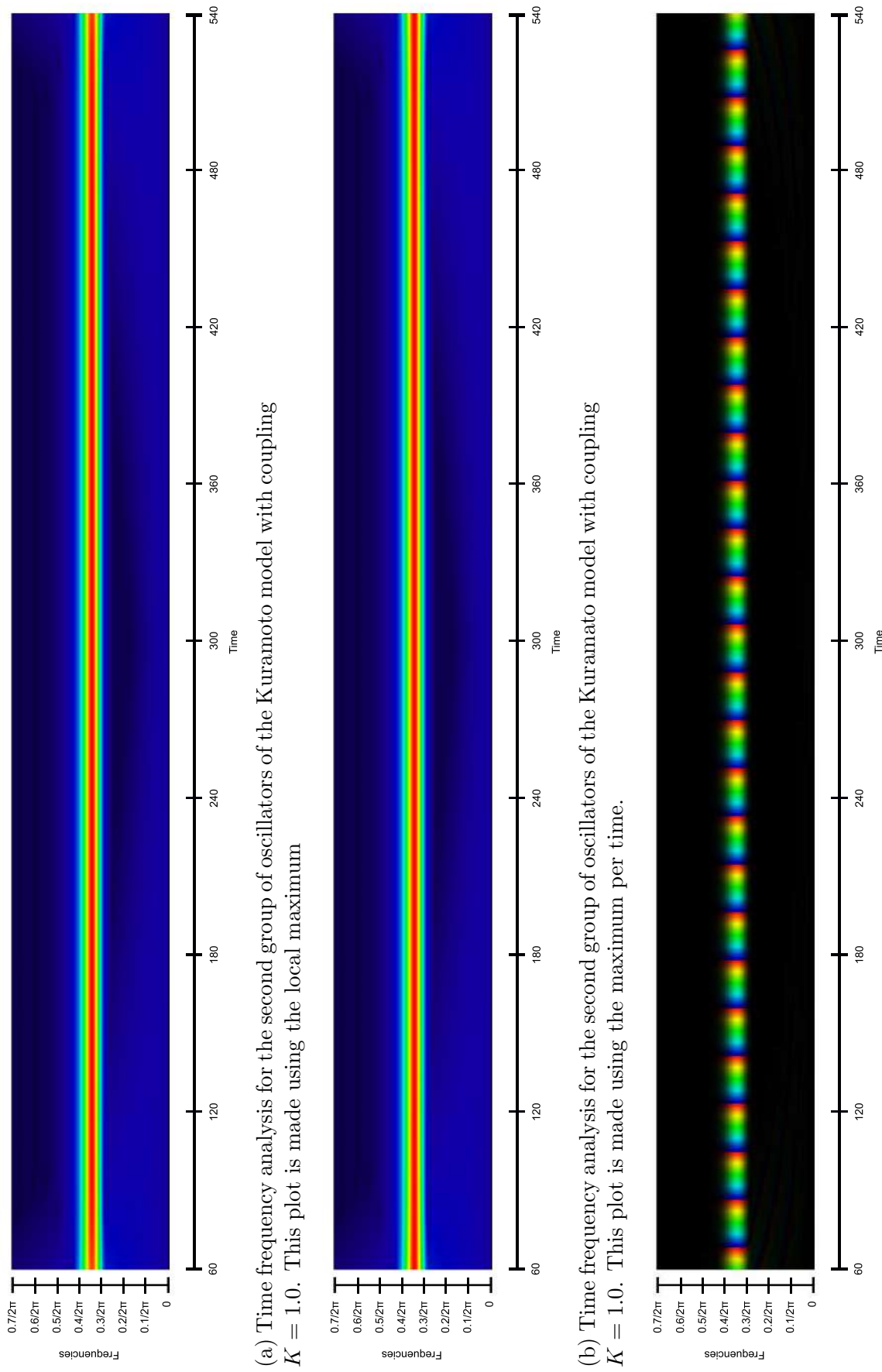


Figure 49: Time frequency analysis for the second group of oscillators (modus is $0.5/(2\pi)$) with coupling $K = 1.0$



7 Time frequency analysis of chimera states

In Section 4 we discussed chimera states as a state in which a nonlocally coupled array of oscillators splits into two groups; one group is perfectly synchronized while the other group is incoherent. In this Section we will show the numerical results of the chimera states that we obtained and apply a time frequency analysis to these state.

To obtain chimera states we programmed Equations (73) and integrated this system for different values of A , β and N . Furthermore, we set $\omega = 0.2$. We obtained chimera states for $N = 2$, $N = 4$ and $N = 100$ using the parameter values $A = 0.1$ and $A = 0.4$ with $\beta = 0.025$. Note that N denotes the group size of one group. Hence, the total number of oscillators is $2N$.

7.1 Two groups of two oscillators

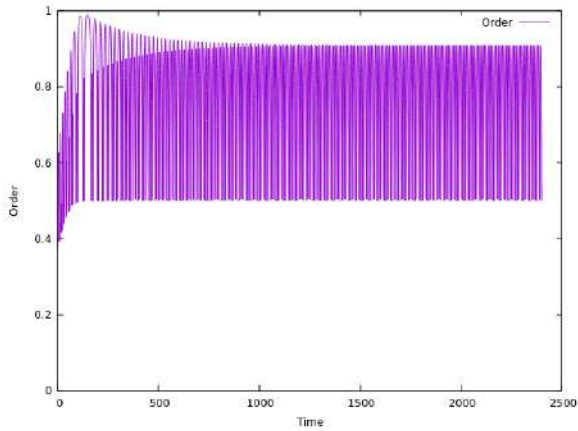
We start with $N = 2$, $A = 0.1$ and $\beta = 0.1$. Figure 50 shows the trajectories of the order parameter for both groups of $N = 2$. There are four plots; Figure 50a shows the trajectory of the order parameter for both groups together. Figure 50b shows the trajectory of the order parameter for the synchronized group of oscillators. Figure 50c shows the trajectory of the order parameter for the incoherent group of oscillators. Finally, Figure 50d shows the trajectory of the order parameter for the incoherent group more closely examined. Figure 50a shows clearly that the phases of both groups are not synchronized. Moreover, Figure 50b shows that after 200 time units the first group is (almost) perfectly synchronized. The second group oscillates heavily (see Figure 50c).

We did three time frequency analyses per group; one for the frequencies using the local maximum, one for the frequencies using the maximum per time and one for the phases. Moreover, there are three groups; one group consists of all oscillators, one group consists of the synchronized oscillators and one group is incoherent. Figure 51 shows the time frequency analysis of all four oscillators. Observe in Figures 51a and 51b that after 350 time units there are just two frequencies, of which the lowest frequency is the most common one. Furthermore note that whenever the frequencies stabilize the order parameter stabilizes too (see Figures 50 and 51). In Figure 50 the order parameter for all oscillators oscillates quite heavily which indicates that the phases are not coherent, this is in agreement with the time frequency analysis for the phases. Next to this Figure 54a shows the trajectories of the phases for all oscillators. Note that everywhere there are three oscillators synchronized, and one fails to synchronize. Furthermore, observe that this one oscillator that fails to synchronize, differs from time to time.

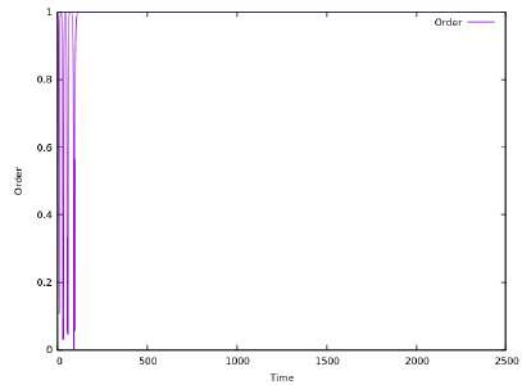
In Figure 52 we show the time frequency analysis of the order parameter for the syn-

chronized group. Figure 50b shows that after approximately 125 time units the phases are (almost) perfectly synchronized. However, Figure 52c shows that at that moment the phases are not synchronized. This is not what we expected. Therefore we look more closely at the trajectory of the phases (see Figure 54a). In Figure 54b one can find the trajectory of the oscillators from the synchronized group. Observe that the oscillators are perfectly synchronized according to this plot as well. In Figure 52b it is even more clear that there should be oscillators present in this group (of $N = 2$) that have a frequency different than $0.025/2\pi$, however according to Figure 54b this is not the case. We looked further into the numerical values of the phases and found that there are some minor differences between the phases. Therefore a possible, but not likely explanation for the pattern in Figure 52 is that the oscillators with different phases try to correct for the difference by going faster or slower. Hence, they cause the different frequencies seen in Figure 52.

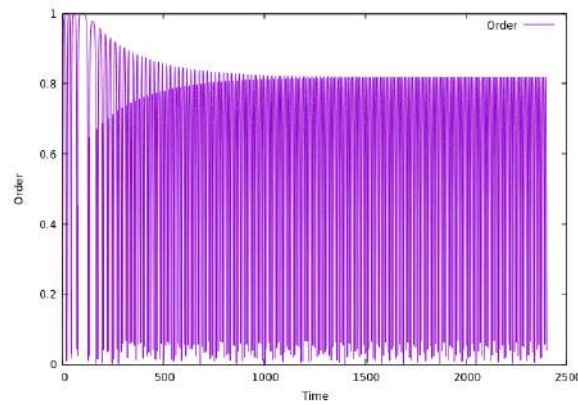
Finally, Figure 53 shows the time frequency analysis for the incoherent group of oscillators. In this plot it looks like that around time 650 there are two frequencies, $0.025/2\pi$ and $0.38/2\pi$, from which the lower one is the most common. Figure 54c confirms that there are more than one frequencies. However, it is not necessary that each frequency belongs to one oscillators. Furthermore, observe the agreements between Figures 50c, 53c and 54c, there are points in time in which the phases are synchronized pretty well, and there are points in time in which they are completely different.



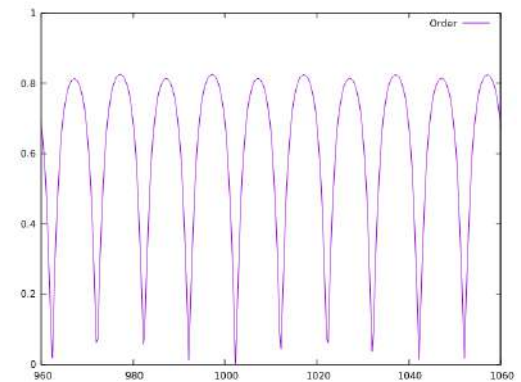
(a) The order parameter of a chimera state for all four oscillators.



(b) The order parameter for the synchronized group.



(c) The order parameter for the incoherent group.



(d) The order parameter for the incoherent group zoomed in.

Figure 50: Order parameter for a chimera state with $N = 2$, $A = 0.1$ and $\beta = 0.025$

Figure 51: Time frequency analysis for the chimera state with $N = 2$, $A = 0.1$ and $\beta = 0.025$

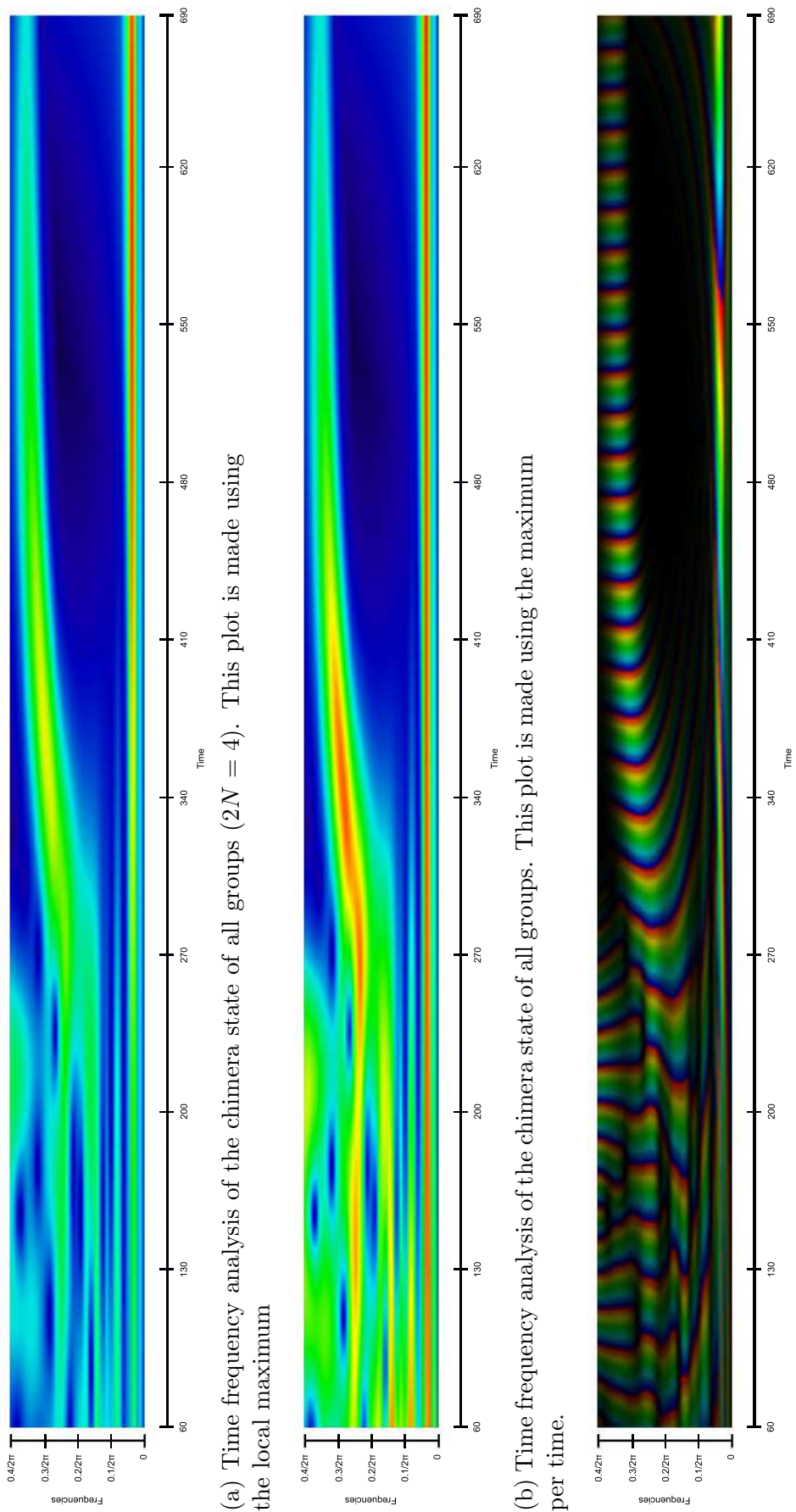


Figure 52: Time frequency analysis of the chimera state for the synchronized group with $N = 2$, $A = 0.1$ and $\beta = 0.025$

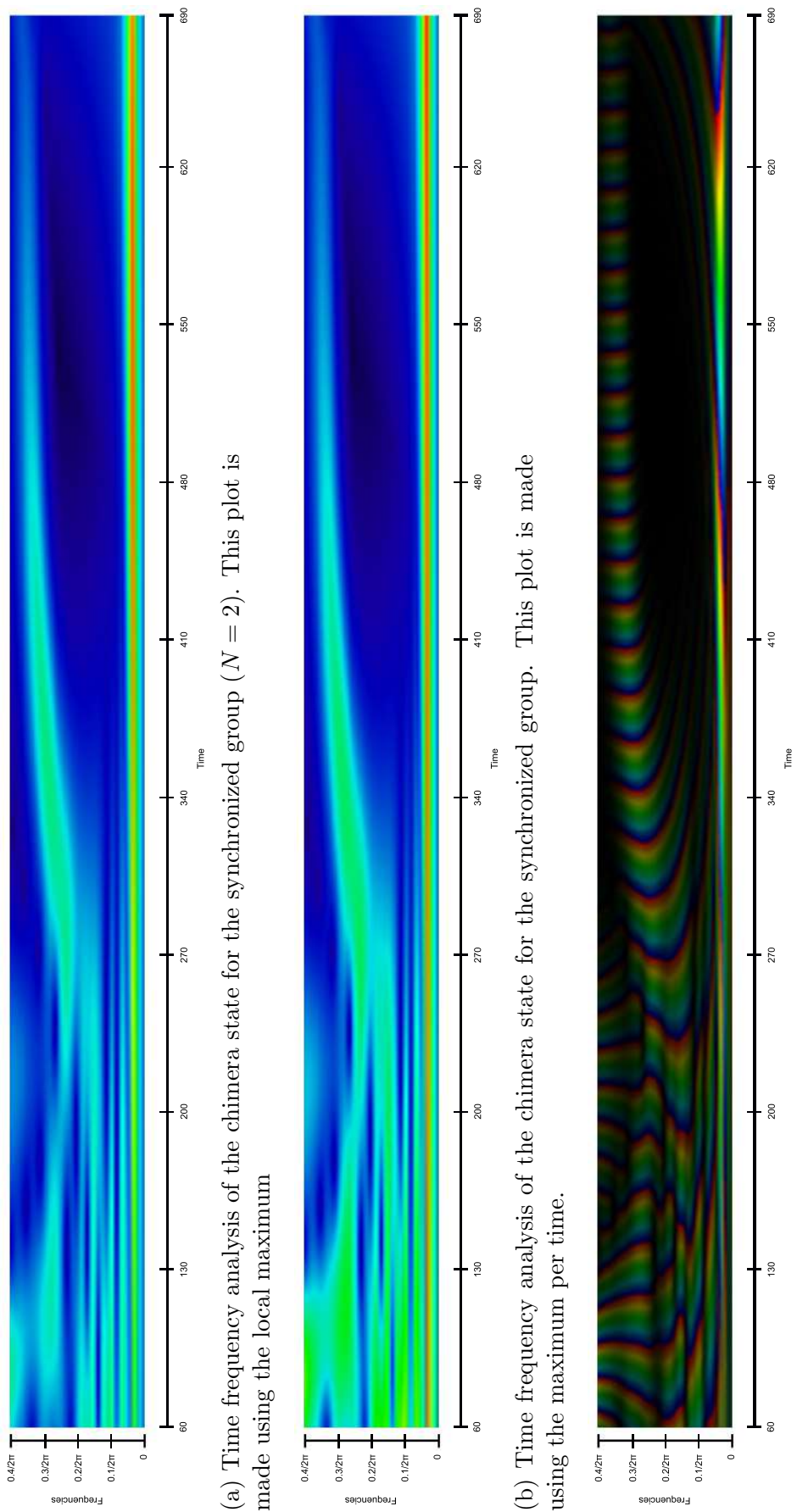
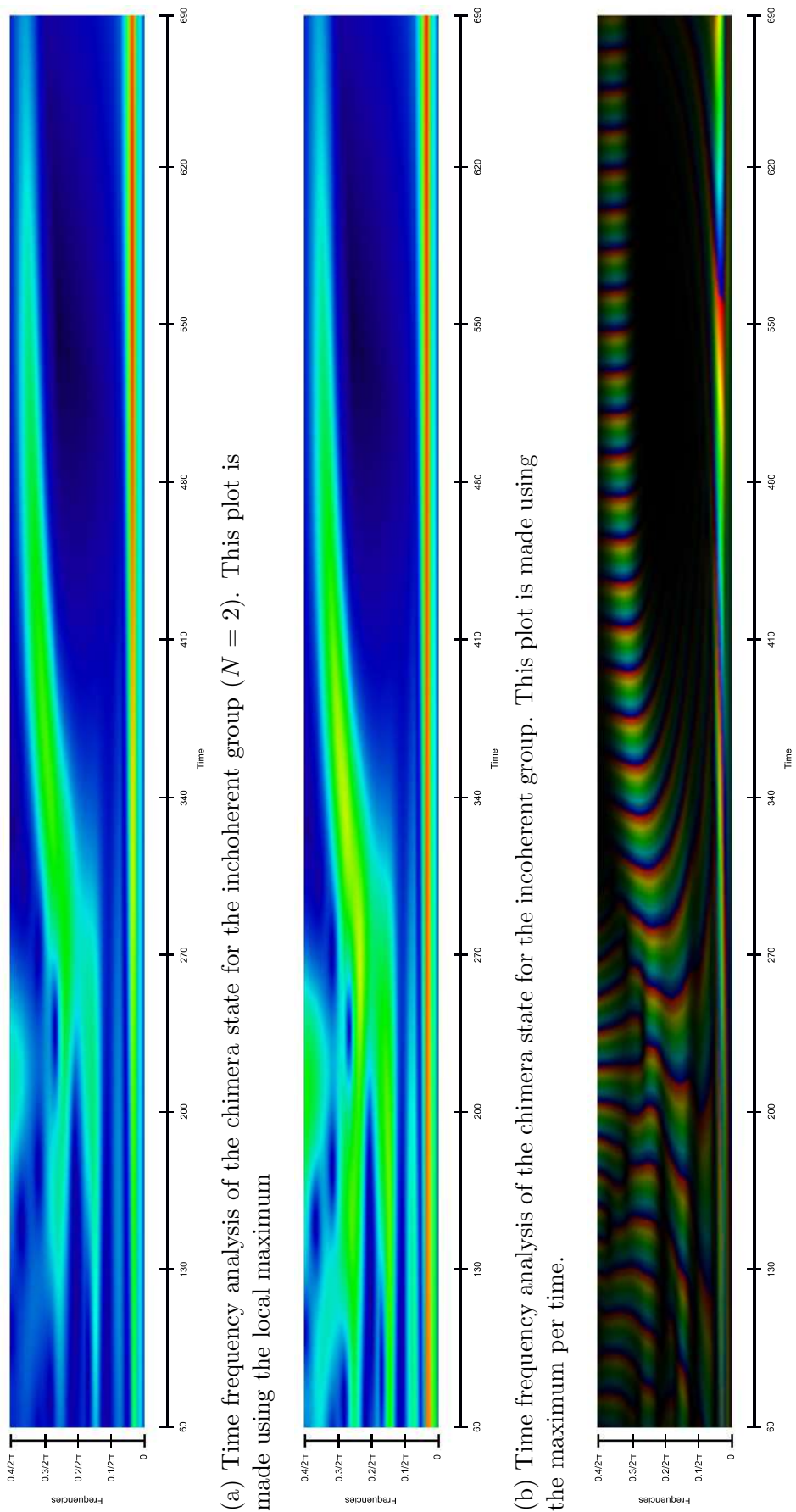
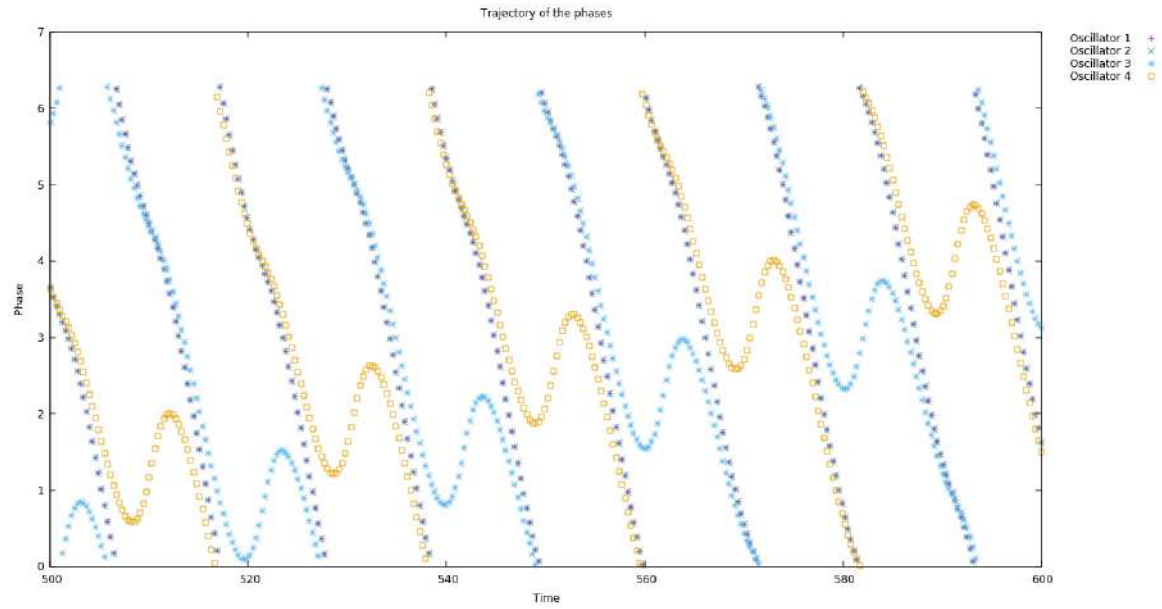
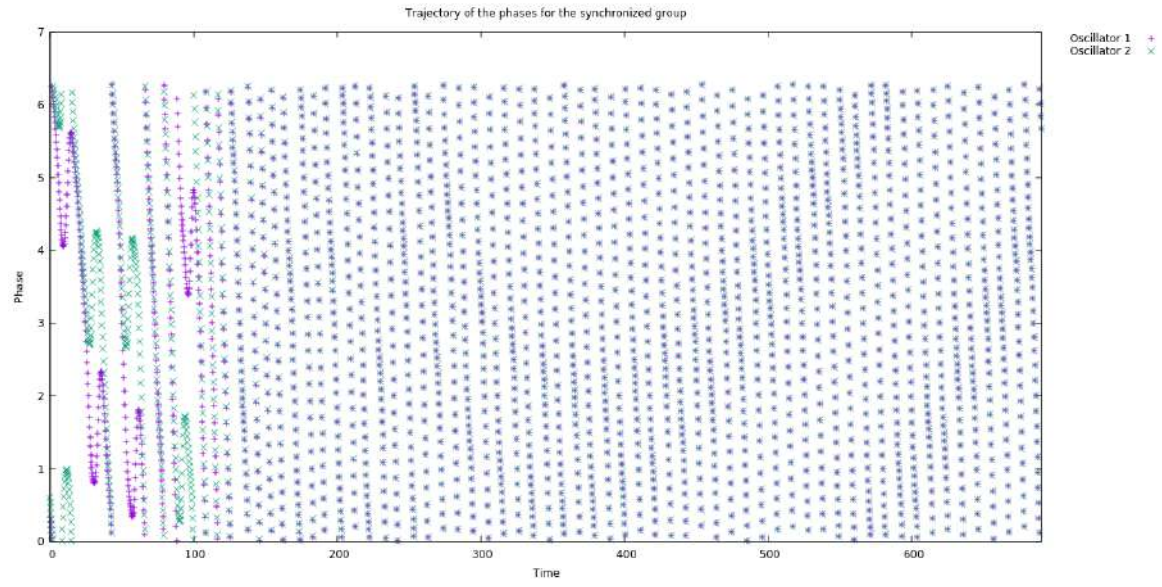


Figure 53: Time frequency analysis of the chimera state for the incoherent group with $N = 2$, $A = 0.1$ and $\beta = 0.025$

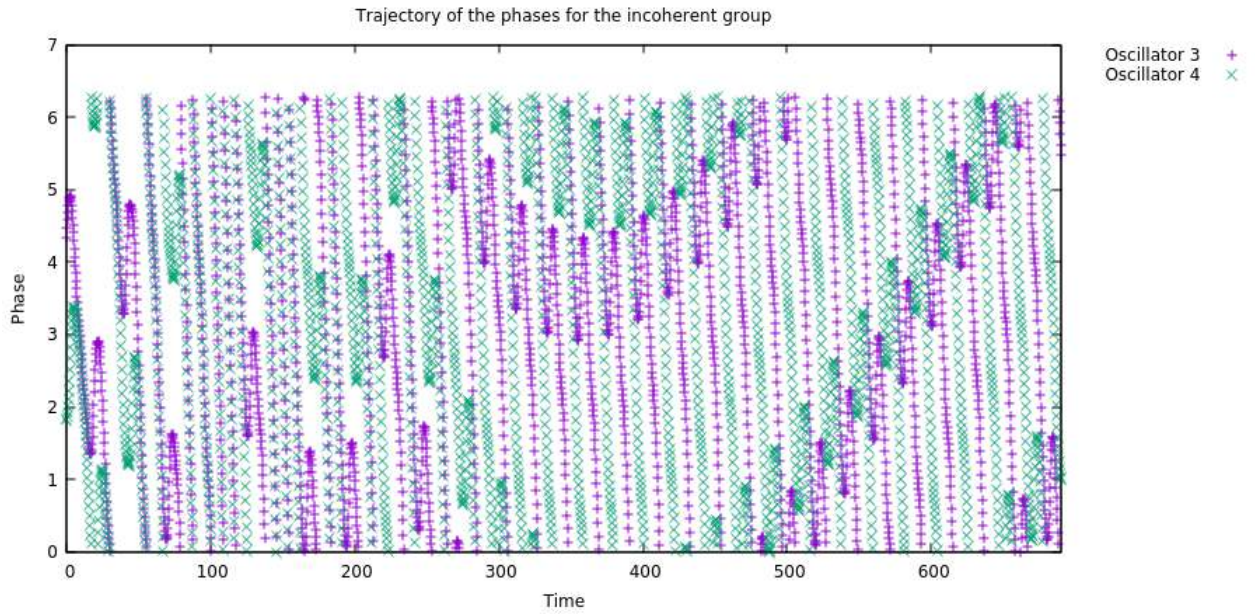




(a) Trajectory of the phases for all oscillators. The first half of oscillators belongs to the synchronized group while the second half belongs to the incoherent group.



(b) Trajectory of the phases for the synchronized group.



(c) Trajectory of the phases for the incoherent group.

Figure 54: Trajectory of the phases.

The next step is to increase A above the Hopf bifurcation. We set $A = 0.4$. Recall that according to Panaggio, Abrams, Ashwin and Laing (2016) the oscillating state that one obtains above the Hopf bifurcation in the case of $N \rightarrow \infty$ was not stable for smaller group sizes. Therefore, we expect that in this case both groups will synchronize. Figure 55 shows that this is indeed the case.

The time frequency analysis shows that after 550 time units the frequencies of all oscillators synchronized (see Figure 56). Note that at the beginning of the time frequency analysis the signal looks stronger than in the end. We do not have an explanation for this. Moreover, Figure 56b shows that there is still one oscillator desynchronized in the end. This is not in agreement with the plot of the order parameter (Figure 55a) and the trajectories of the phases (Figure 59a). This could be explained by the fact that the phases are not yet perfectly synchronized (i.e. there are non visible differences in the phases) and that the frequencies try to correct for this. However, to us this explanation is quite unlikely as the differences in the phases are rather small.

Figure 57 shows the time frequency analysis for the first group of oscillators. Observe that in the end the frequencies look synchronized. Note that again the signal is stronger at the beginning than in the end. The time frequency analysis that is made using the maximum per time shows that at the end the frequencies synchronized (see Figure 57b), however it looks like there is one oscillator with a higher frequency too. This is also visible in the plot

of the phase of the wavelet transform (Figure 57c). As discussed before we do not see this in the plot of the order parameter or in the trajectory of the phases. The numerical values of the phases show some small differences. Therefore, it might be, even though we think it is rather unlikely, that the phases who are not perfectly synchronized try to synchronize by adjusting their frequencies. Observe that the time frequency analysis for the second group of oscillators (Figure 58) looks very similar to the one for the first group of oscillators. Moreover, the order parameters per group show the same pattern. Hence, we conclude the same for the second group of oscillators.

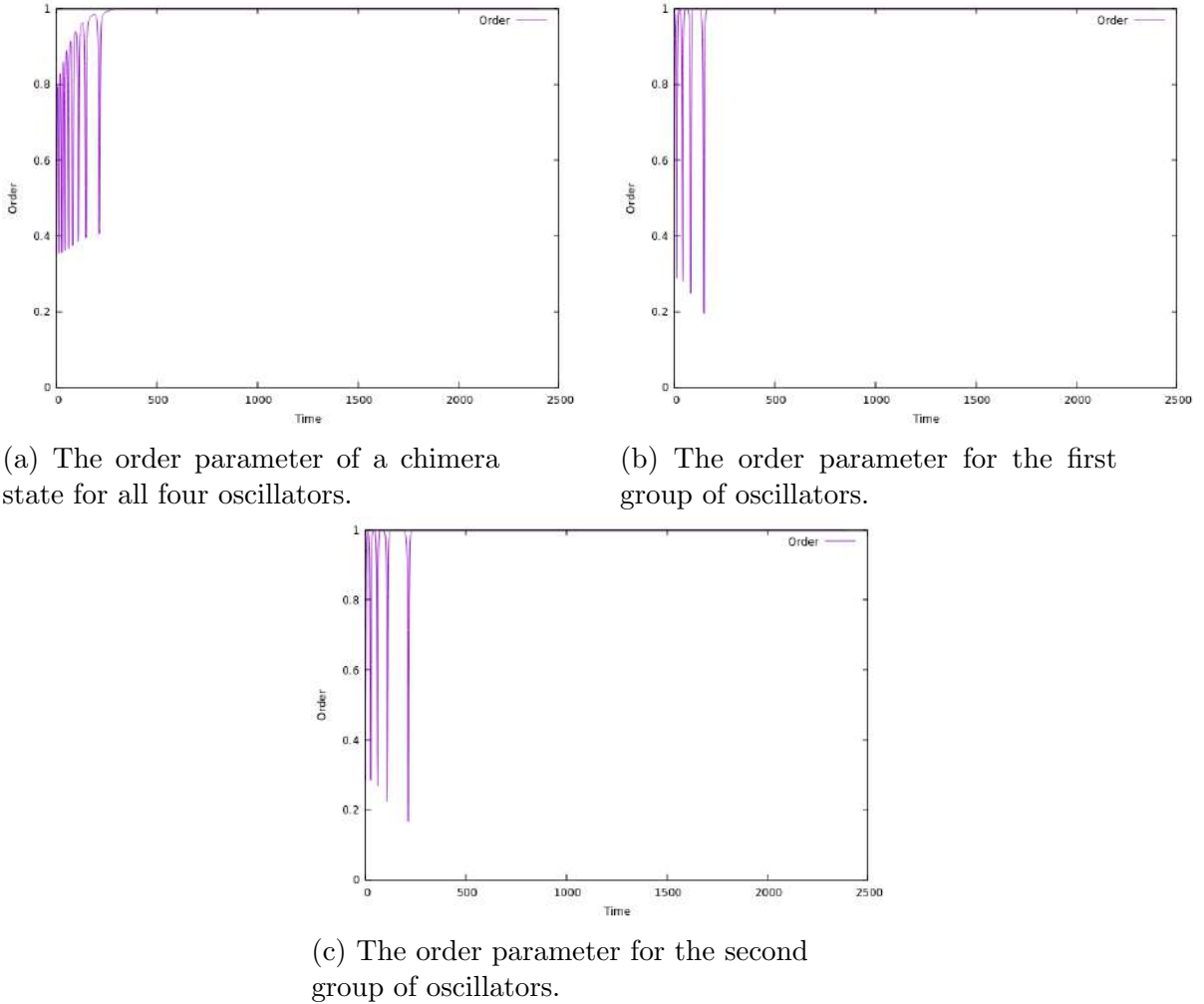


Figure 55: Order parameter for a chimera state with $N = 2$, $A = 0.4$ and $\beta = 0.025$

Figure 56: Time frequency analysis for the chimera state with $N = 2$, $A = 0.4$ and $\beta = 0.025$

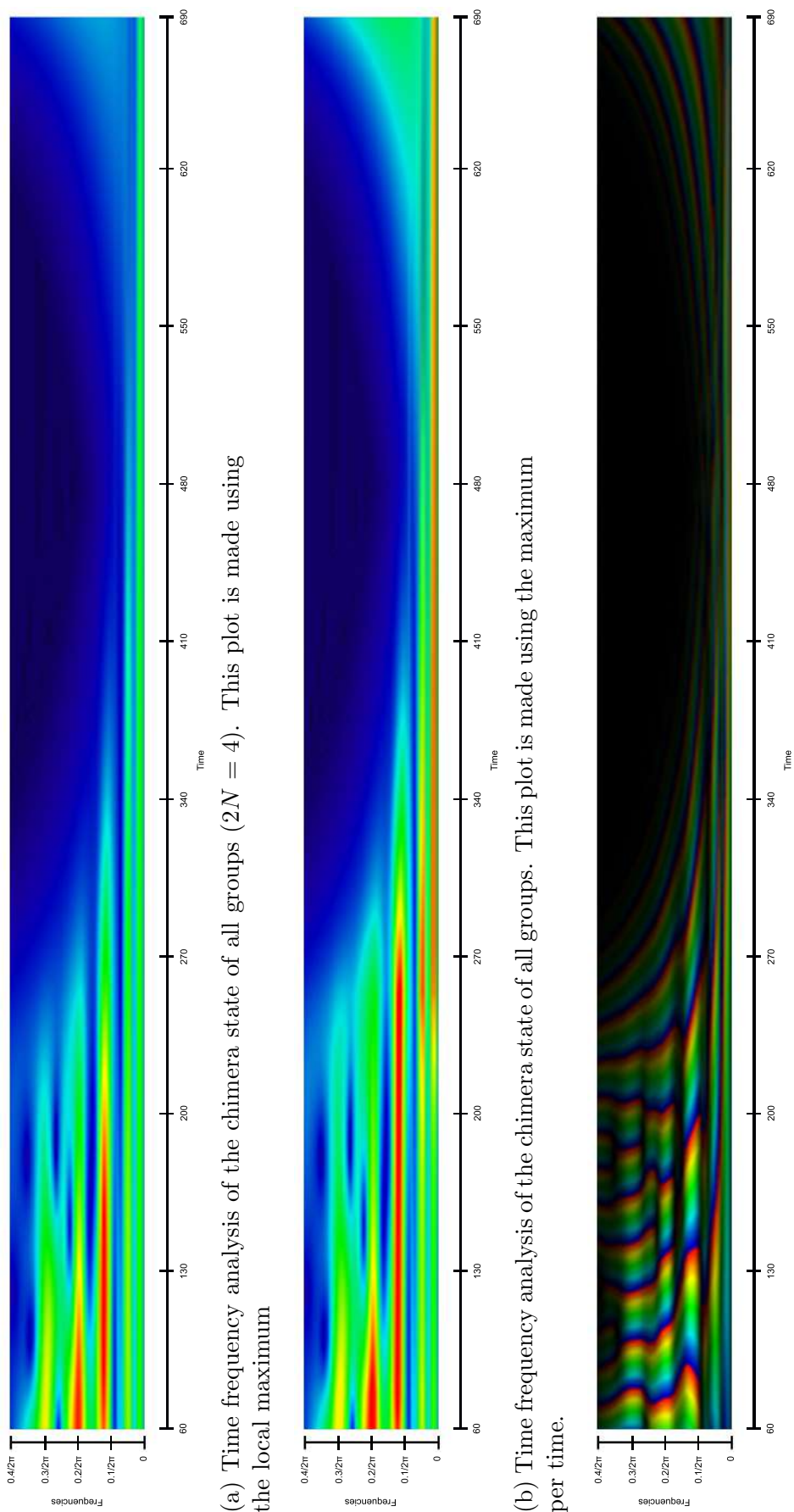


Figure 57: Time frequency analysis of the chimera state for the synchronized group with $N = 2$, $A = 0.4$ and $\beta = 0.025$

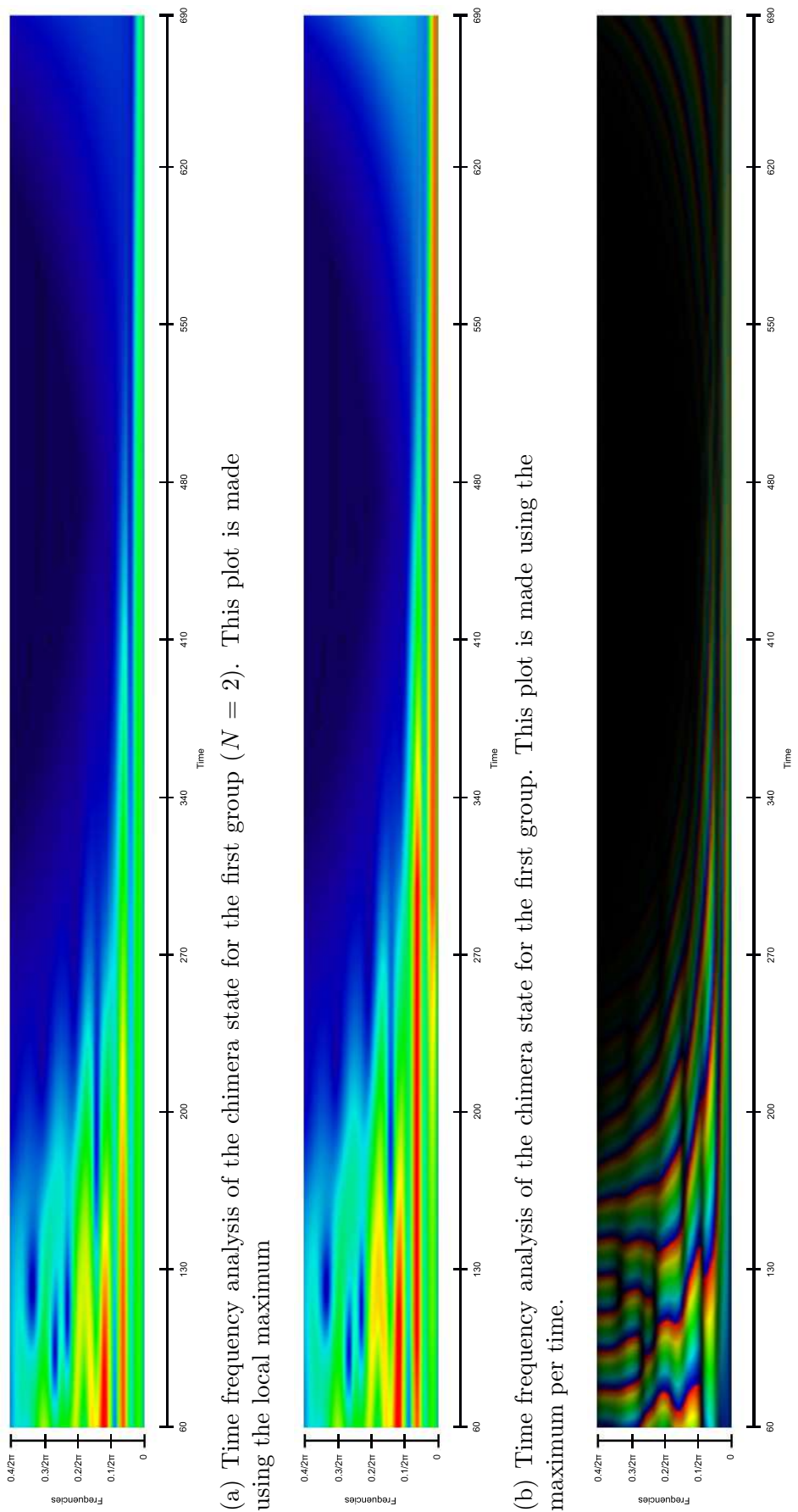
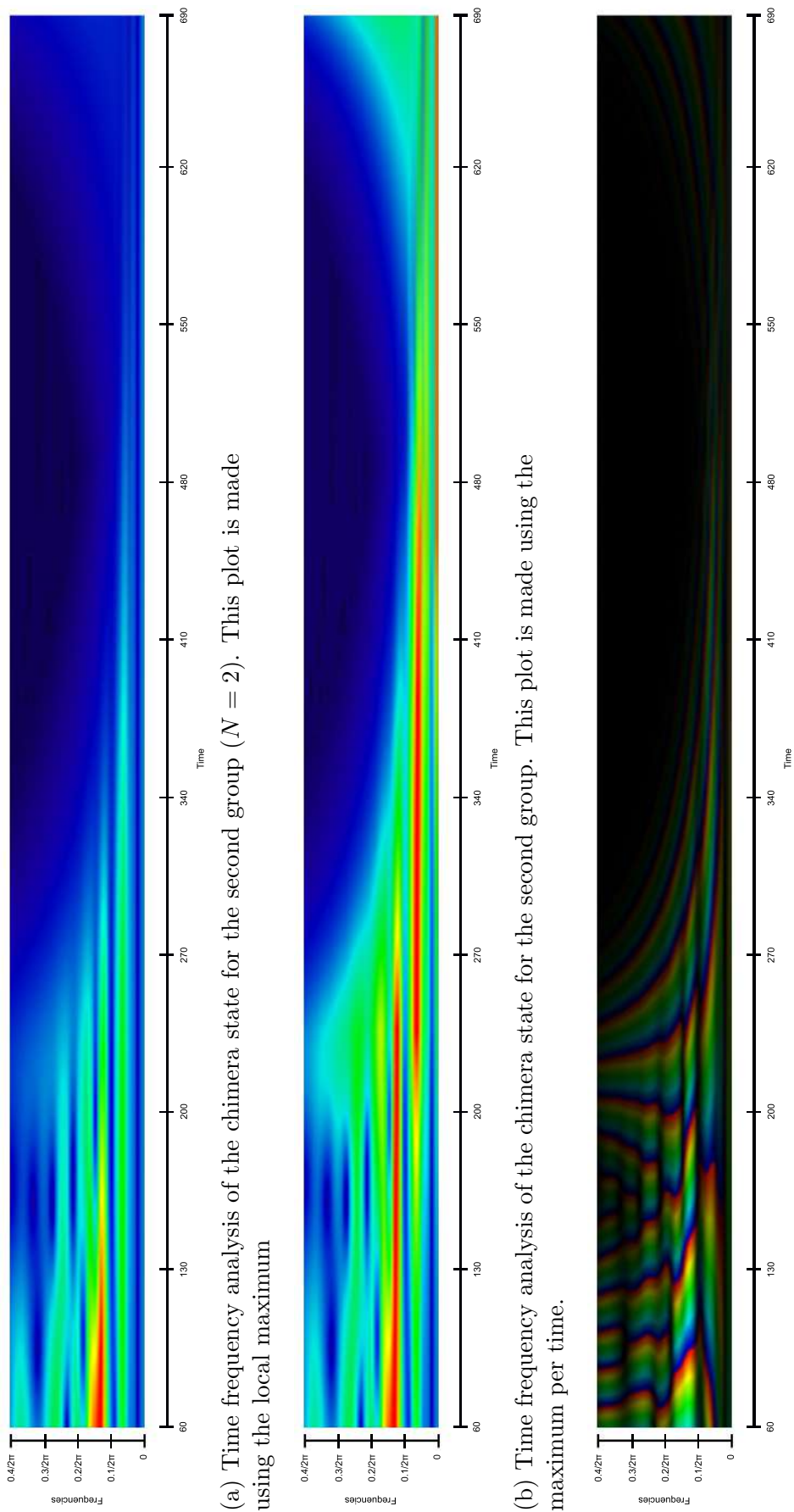
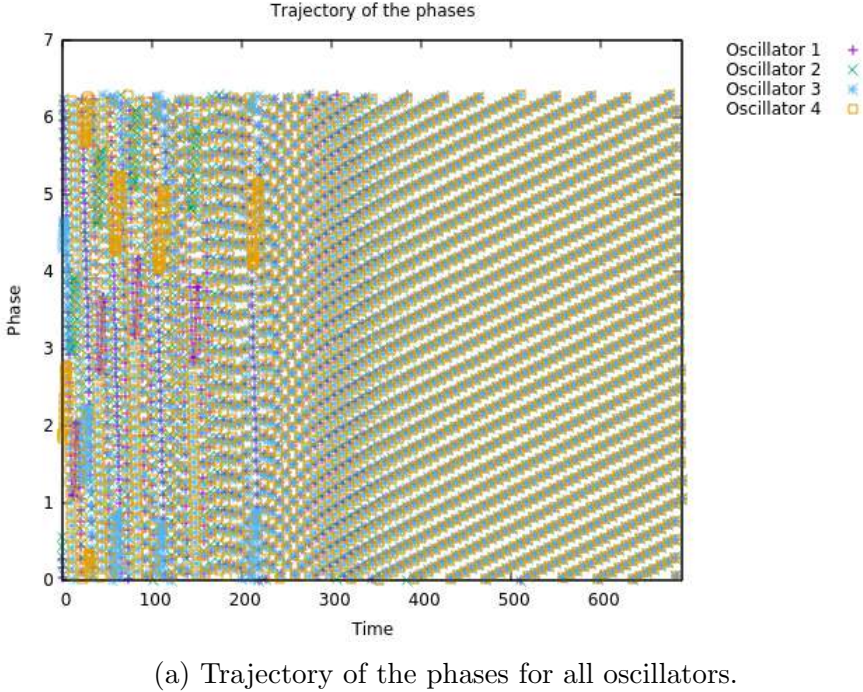


Figure 58: Time frequency analysis of the chimera state for the second group with $N = 2$, $A = 0.4$ and $\beta = 0.025$





(a) Trajectory of the phases for all oscillators.

7.2 Two groups of four oscillators

In the previous subsection we looked at two groups of two oscillators with different inter and intra coupling strengths. In this section we will double the group sizes to $N = 4$ and again observe the states for different A . We start with $A = 0.1$ and $\beta = 0.025$. We expect to find a chimera state that oscillates, which is in agreement with the research of Panaggio, Abrams, Ashwin and Laing (2016).

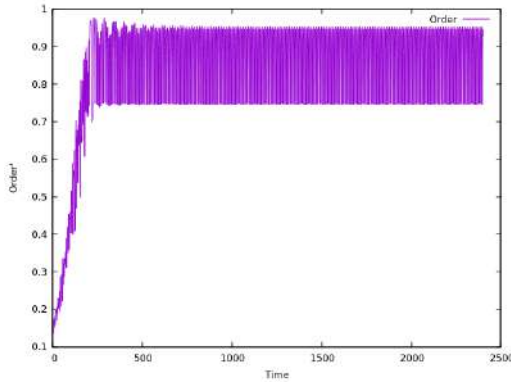
Figure 60 shows the order parameter of our analyses. Note that the first group of oscillators is synchronized (Figure 60b), while the second group is incoherent and shows oscillations (see Figure 60c). The zoomed in plot of the order parameter for the incoherent group show that these oscillations are in agreement with the work of Panaggio, Abrams, Ashwin and Laing (2016).

The time frequency analysis of all eight oscillators shows that there are three frequencies present: one around $0.01/2\pi$ one around $0.2/2\pi$ and one around $0.3/2\pi$. Most oscillators have a frequency around $0.2/2\pi$. Moreover, observe in Figure 61c that whenever the order parameter stabilizes (around 420) the time frequency analysis shows only those three frequencies. According to the time frequency plot of the phases the phases are not synchronized between those three frequencies.

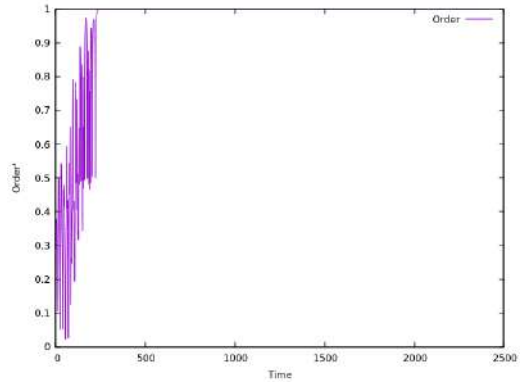
Figure 62 shows the time frequency analysis of the order parameter for the synchronized group. Note that after 400 time units the time frequency analysis shows that in the end there are two frequencies present. This is quite remarkable as the phases are almost perfectly

synchronized at this point (see Figure 60b and the trajectories 64b). The only explanation we have for this is that there are still some small differences between the phases of the oscillators (not visible in Figure 64b) and that the oscillators with different phases try to correct for the difference by going faster or slower. However, we think that this explanation is rather unlikely.

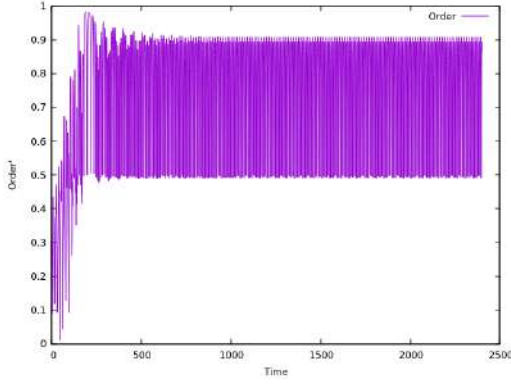
Figure 63 shows the time frequency analysis of the incoherent group. Note that in the end there are just three frequencies left; $0.025/2\pi$, $0.1/2\pi$, $0.2/2\pi$. The phases do not look synchronized for the oscillators with these frequencies (see Figure 63c). This is even clearer in Figure 64 which shows the trajectories of the phases. Furthermore, Figure 64a shows a remarkable pattern. It appears that there are always seven oscillators synchronized and just one is out of sync with the rest. However, this one oscillator that is out of sync switches. Note that this oscillator is always from the incoherent group.



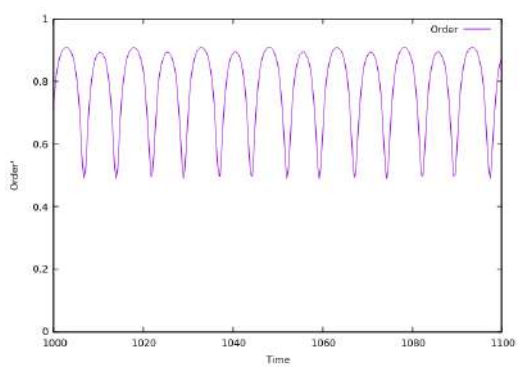
(a) The order parameter of a chimera state for all eight oscillators.



(b) The order parameter for the synchronized group.



(c) The order parameter for the incoherent group.



(d) The order parameter for the incoherent group zoomed in.

Figure 60: Order parameter for a chimera state with $N = 4$, $A = 0.1$ and $\beta = 0.025$

Figure 61: Time frequency analysis for the chimera state with $N = 4$, $A = 0.1$ and $\beta = 0.025$

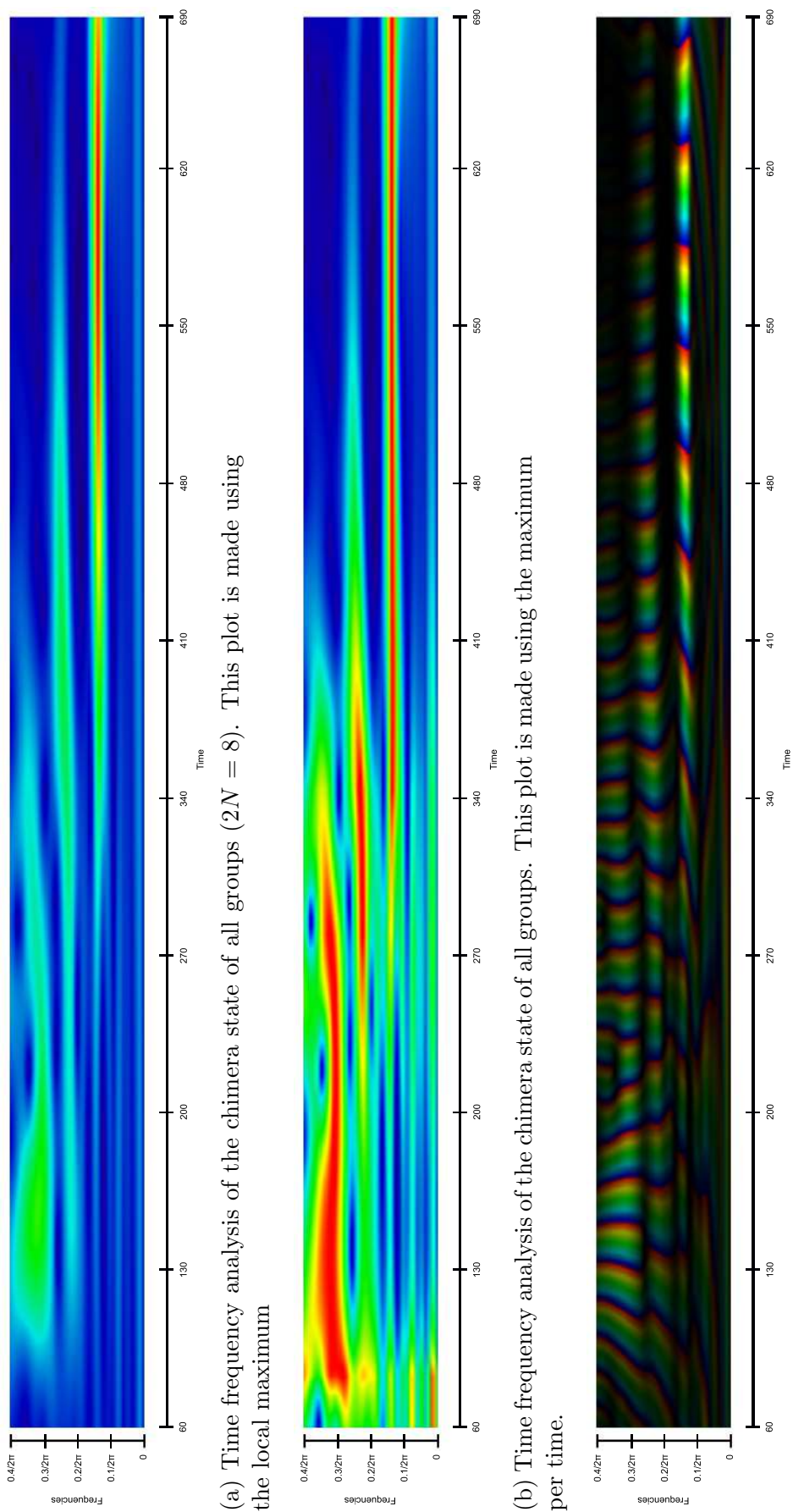


Figure 62: Time frequency analysis of the chimera state for the synchronized group with $N = 4$, $A = 0.1$ and $\beta = 0.025$

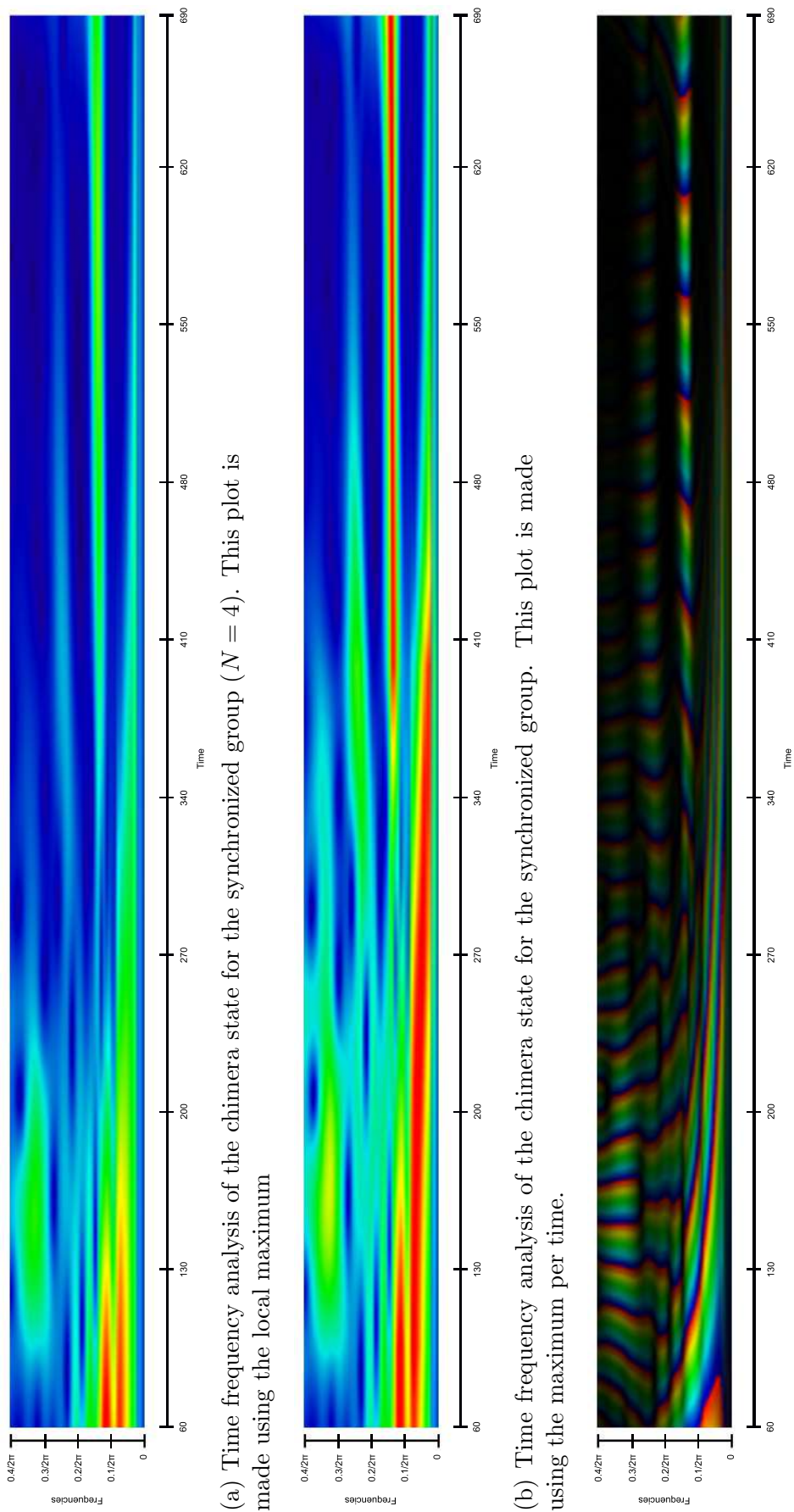
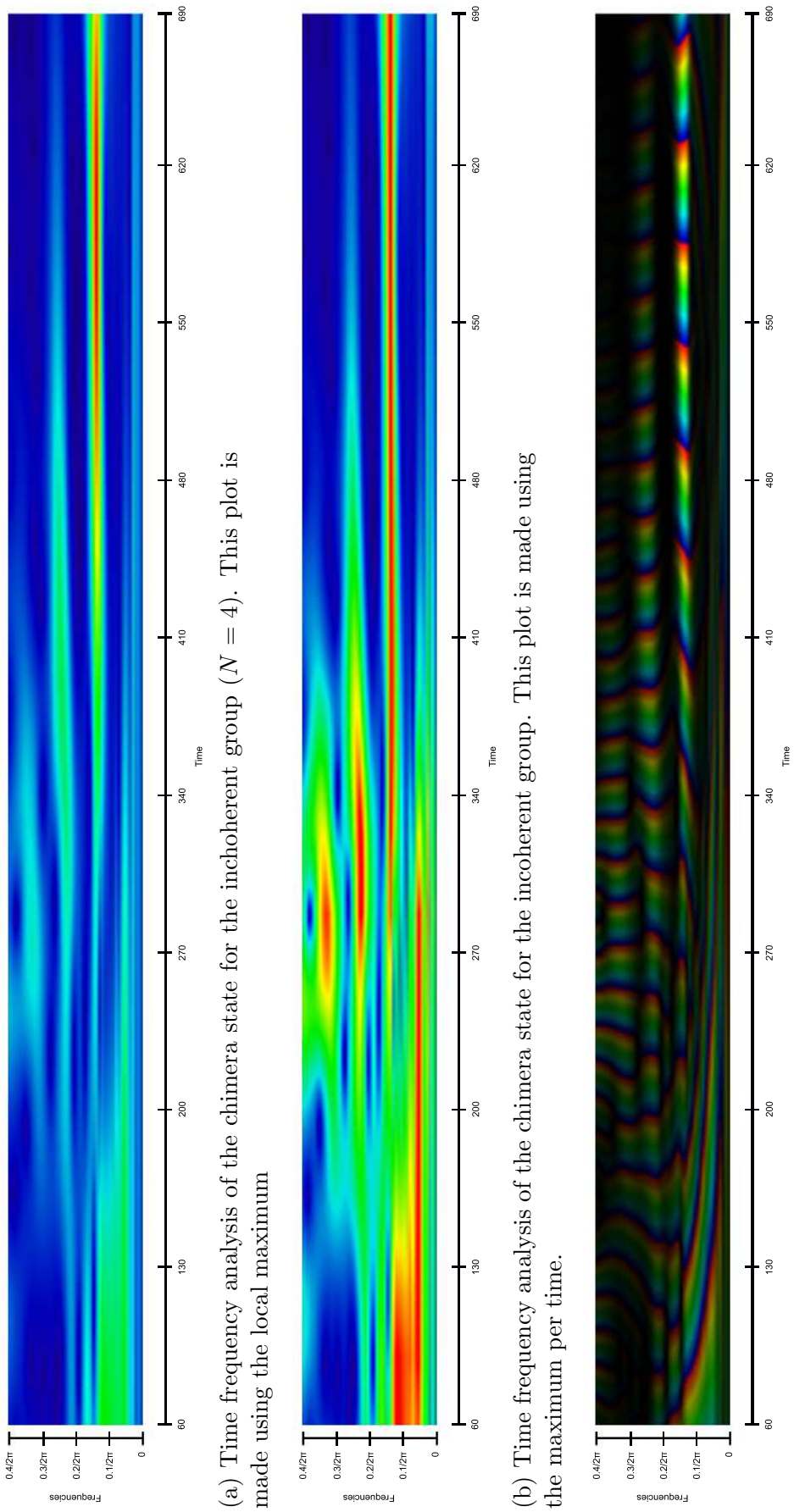
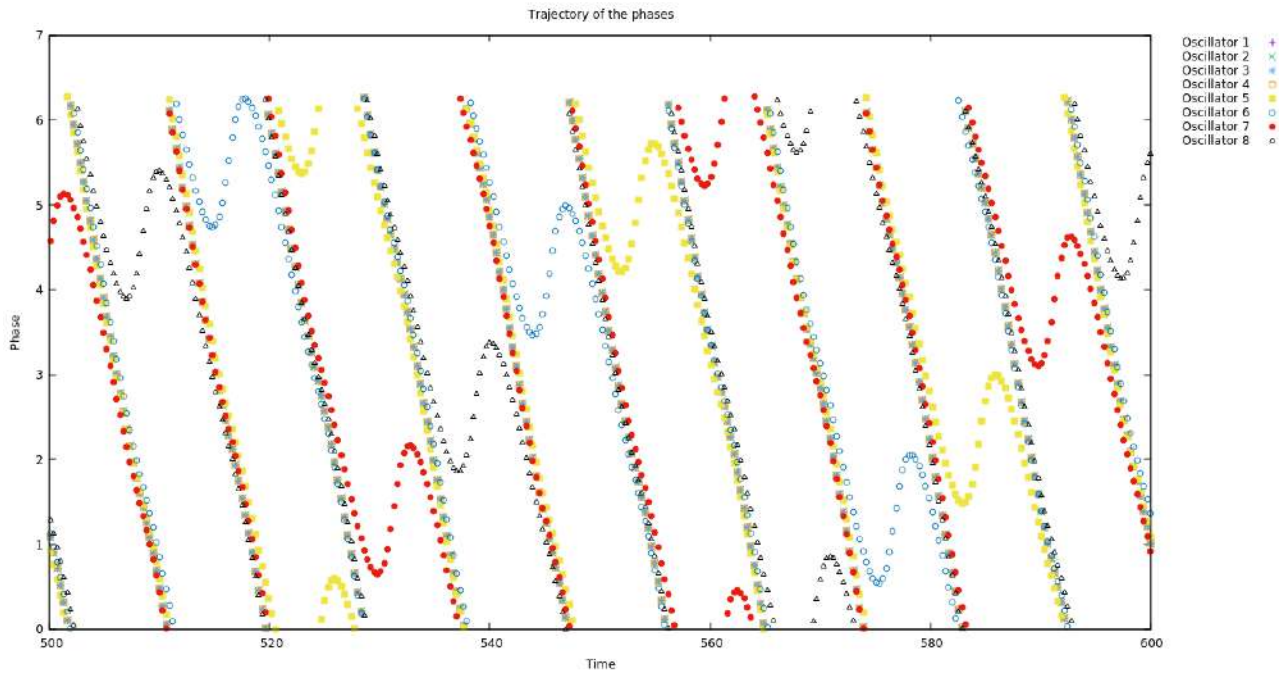
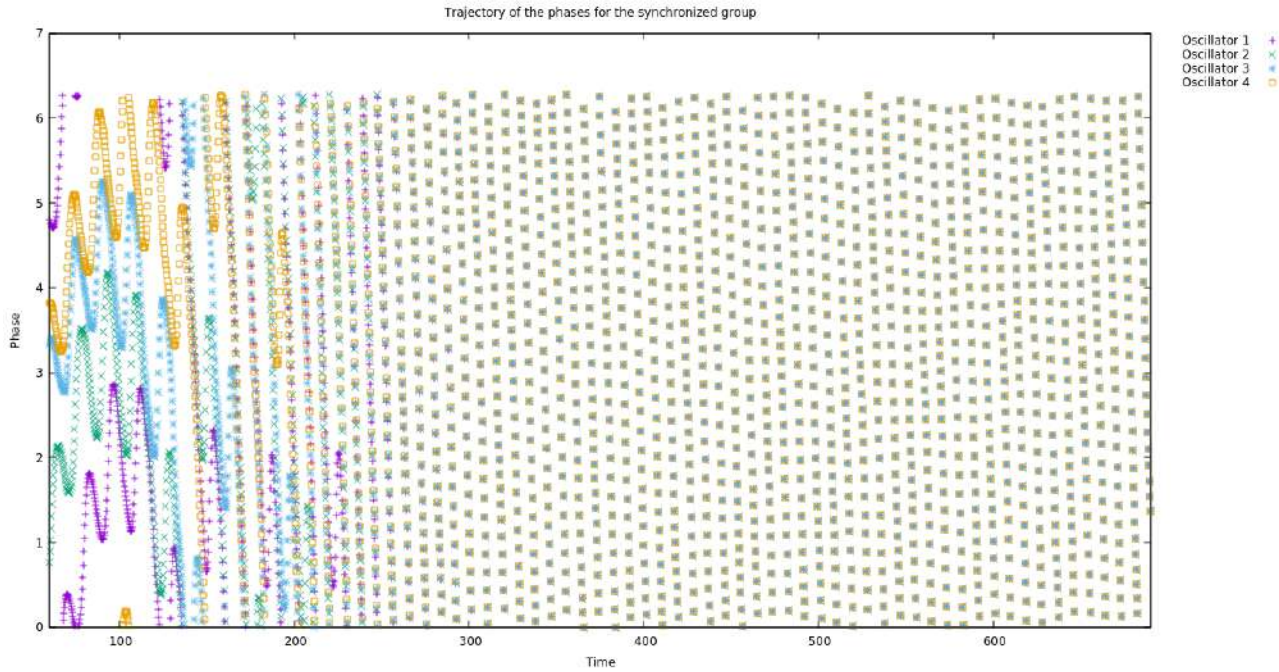


Figure 63: Time frequency analysis of the chimera state for the incoherent group with $N = 4$, $A = 0.1$ and $\beta = 0.025$

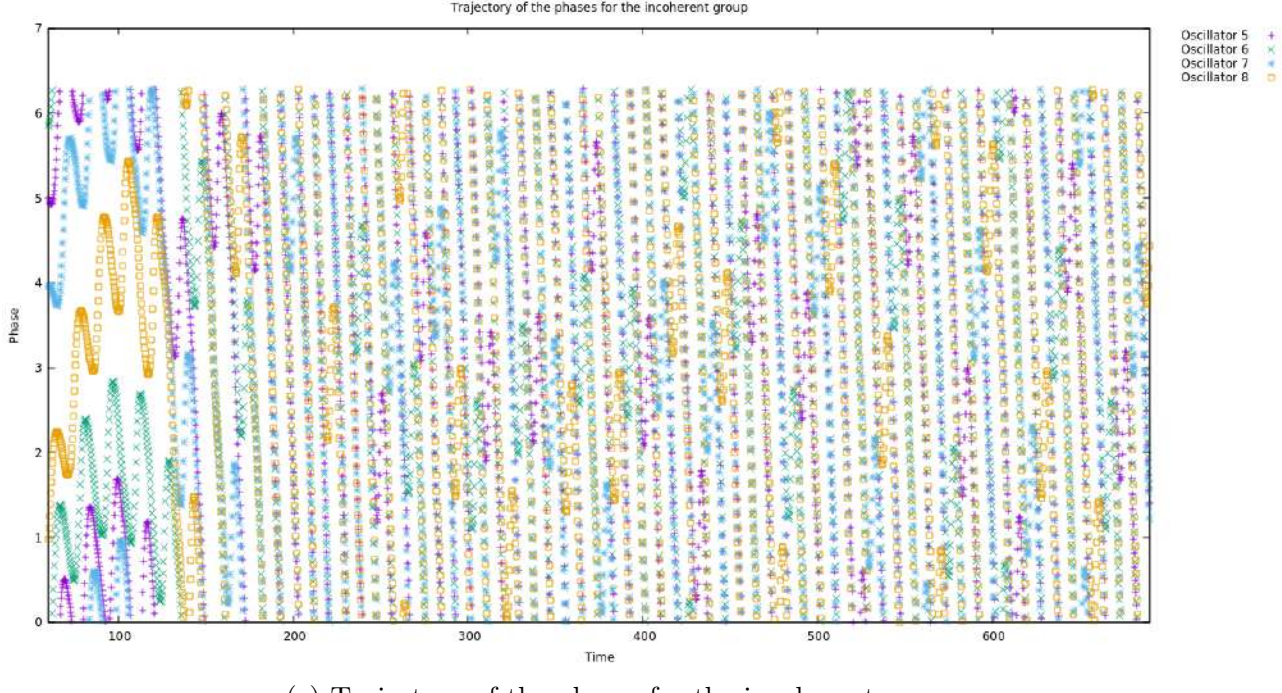




(a) Trajectory of the phases for all oscillators. The first half of oscillators belongs to the synchronized group while the second half belongs to the incoherent group.



(b) Trajectory of the phases for the synchronized group.



(c) Trajectory of the phases for the incoherent group.

Figure 64: Trajectory of the phases.

Next we increase A to 0.4 which is above the Hopf bifurcation. Again we expect to find that the breathing chimera, which exists for $N \rightarrow \infty$, is not stable for small groups. Hence, we expect to see that both groups synchronized in phase and frequency. Figure 65a shows that the phases are indeed synchronized, however sometimes there is a drop in the synchrony and the oscillators become incoherent. Note that it takes relatively long for the phases to synchronize. Figure 65b shows the order parameter for the first group of oscillators. Note that the phases of this group of oscillators are synchronized around 300 time units, but then around 700 they suddenly desynchronize. In Figure 65c one can find the order parameter for the second group of oscillators. The order parameter of this group oscillates quite heavily, but in the end it stabilizes to one.

Figure 66 shows the time frequency analysis for all eight oscillators. Note that we only show the first 690 time units and that the phases did not synchronize yet during this time according to the plot of the order parameter (Figure 65b). This is also visible in the time frequency analysis as the frequencies are clearly incoherent (see Figure 66a). The time frequency analysis with a plot that is made using the maximum per time also shows that the frequencies are incoherent (see Figure 66b). Figure 66c shows the phase of the wavelet transform. This plot also confirms that the phases are incoherent. Figure 69a shows the trajectory of the phases for the last 100 time units of the time frequency analysis. This plot

clearly shows that the phases are incoherent.

Next, we look at the time frequency analysis for the first group of oscillators. Note that the frequencies synchronize partly but then desynchronizes around 620 (see Figure 67). This is in agreement with the plot of the order parameter. Moreover, observe the similarities between Figure 67a and Figure 67b. Finally, note in Figure 67c how the phases synchronize from 340 time units onwards. This is clearly visible in the trajectory of the phases for the first group of oscillators (Figure 69b). The phases desynchronize shortly after 690 time units (not shown here).

At last we will take a look at the time frequency analysis for the second group of oscillators (Figure 68). Recall that the order parameter oscillated for the second group of oscillators. The time frequency analysis of this group shows that the frequencies are incoherent (see Figure 68). Note the similarities between Figure 68a and Figure 68b. Furthermore, observe in Figure 68c that the phases are incoherent. This is also visible in the trajectories of the phases for the second group of oscillators (Figure 69c).

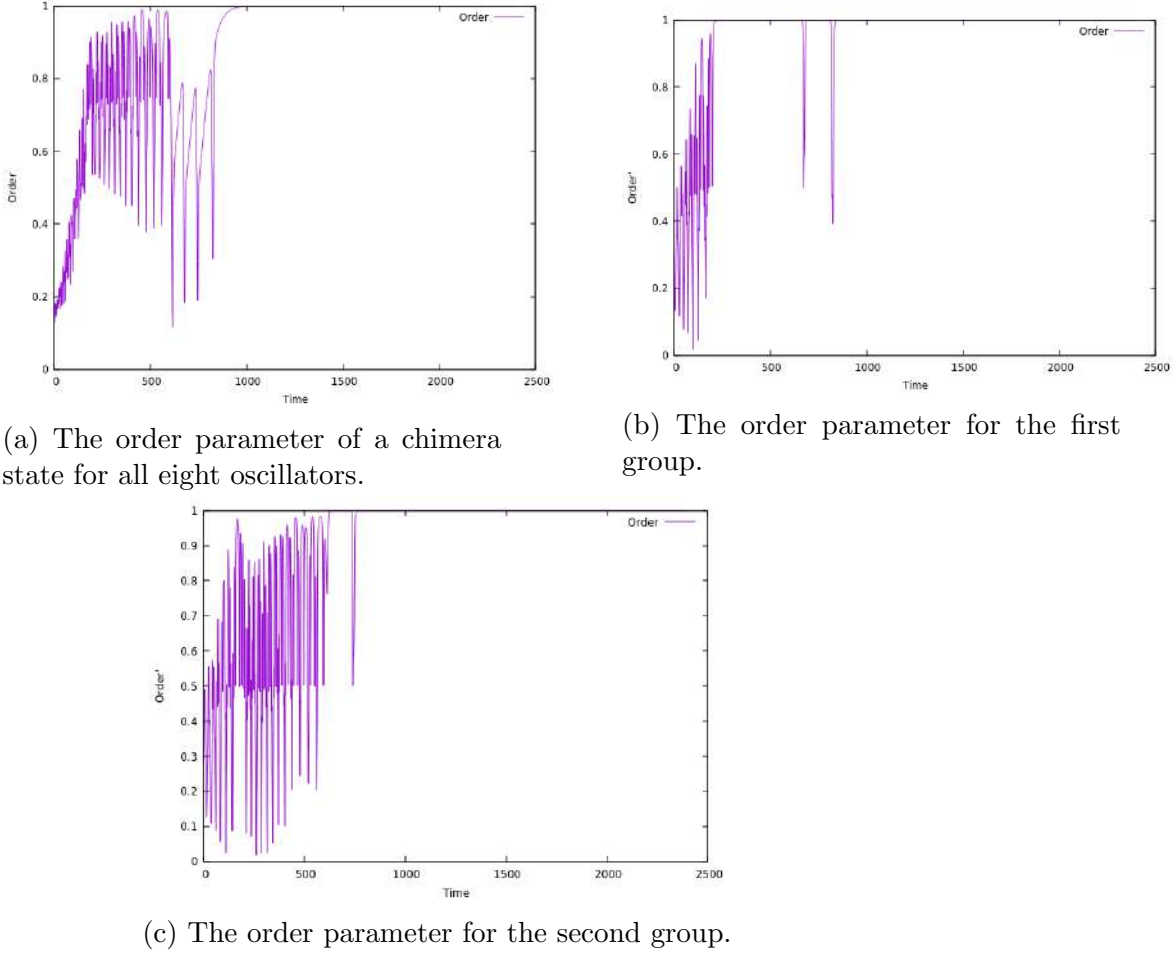


Figure 65: Order parameter for a chimera state with $N = 4$, $A = 0.1$ and $\beta = 0.025$

Figure 66: Time frequency analysis for the chimera state with $N = 4$, $A = 0.4$ and $\beta = 0.025$

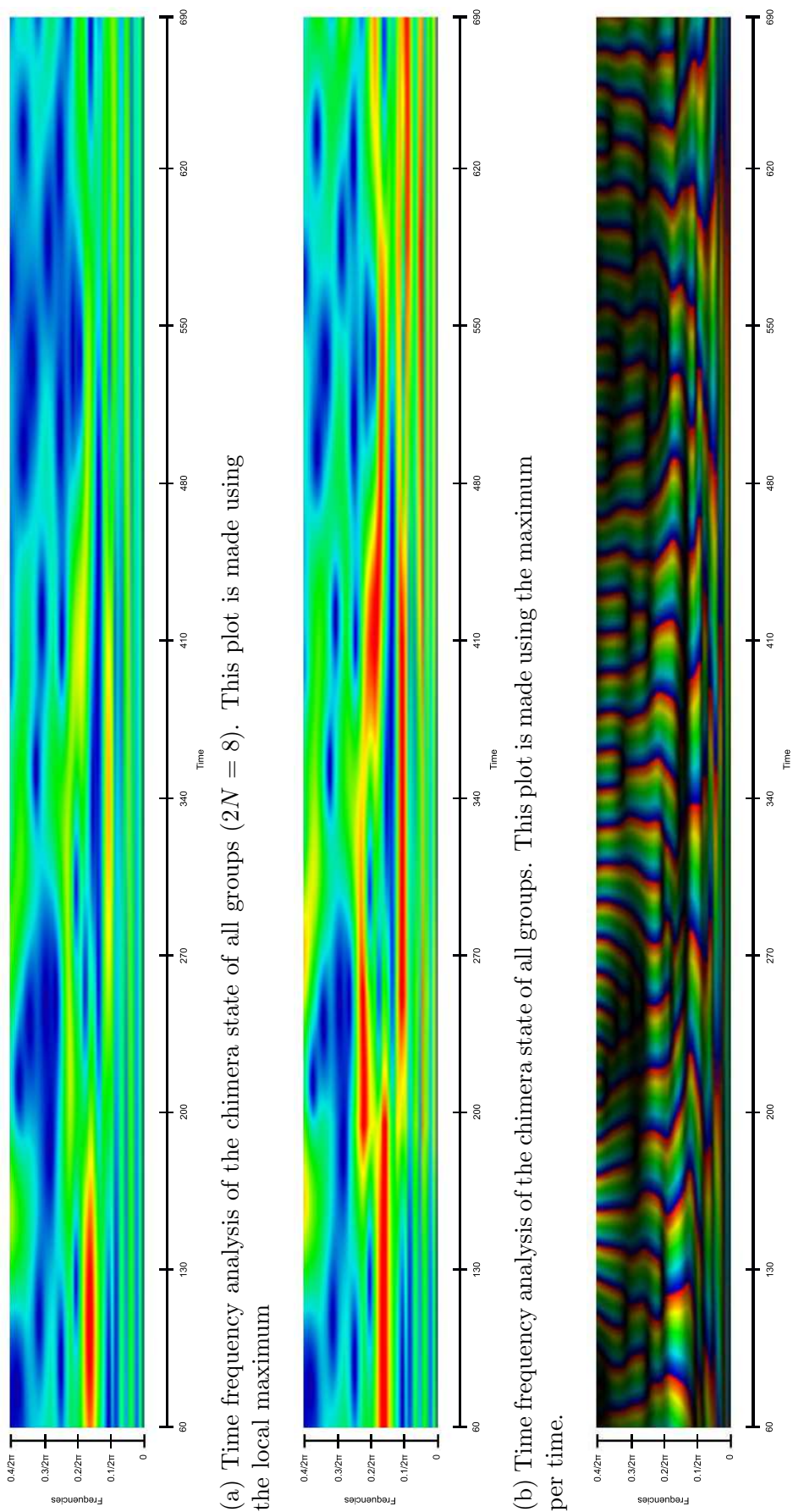


Figure 67: Time frequency analysis of the chimera state for the first group of oscillators with $N = 4$, $A = 0.4$ and $\beta = 0.025$

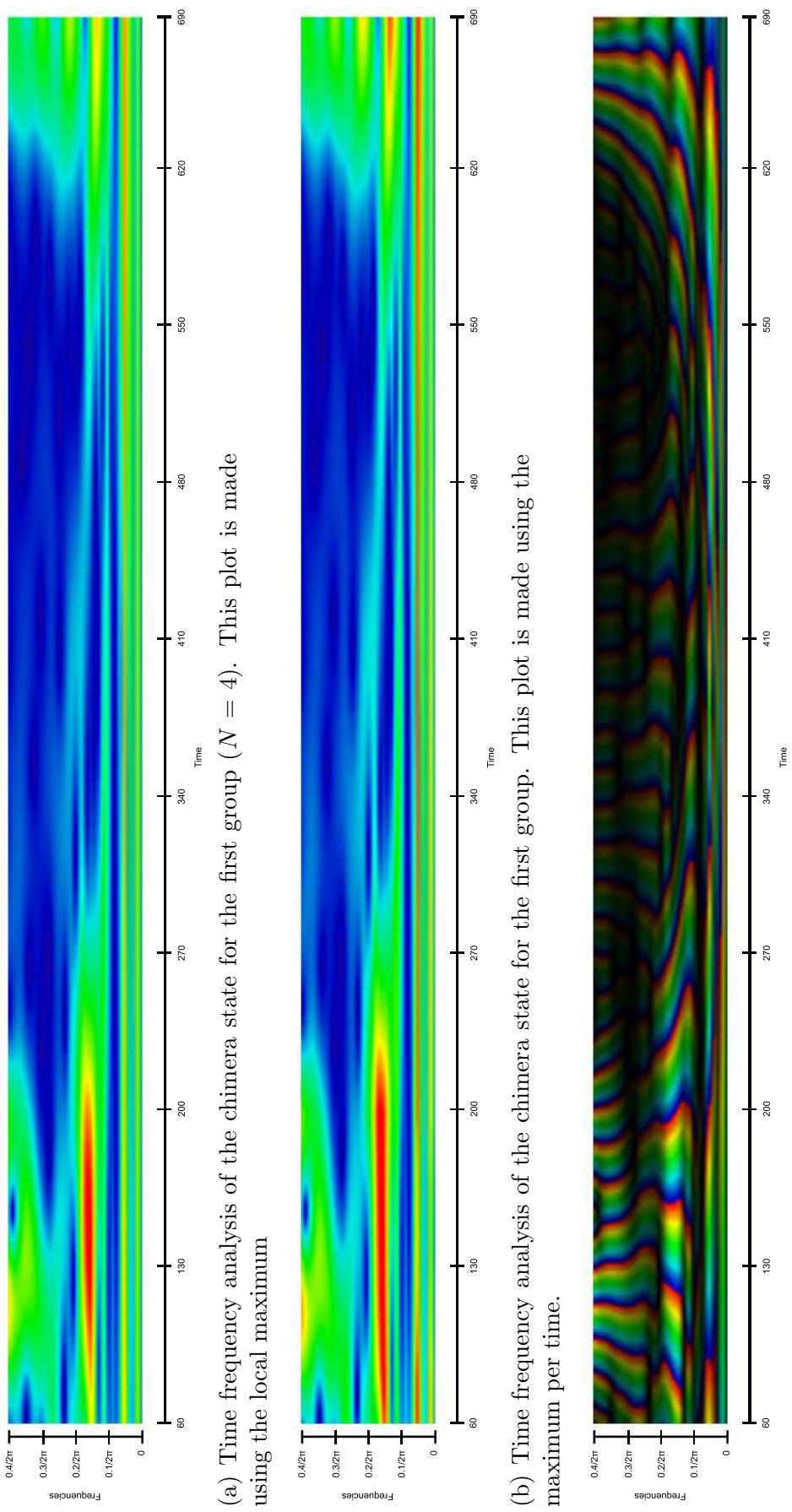
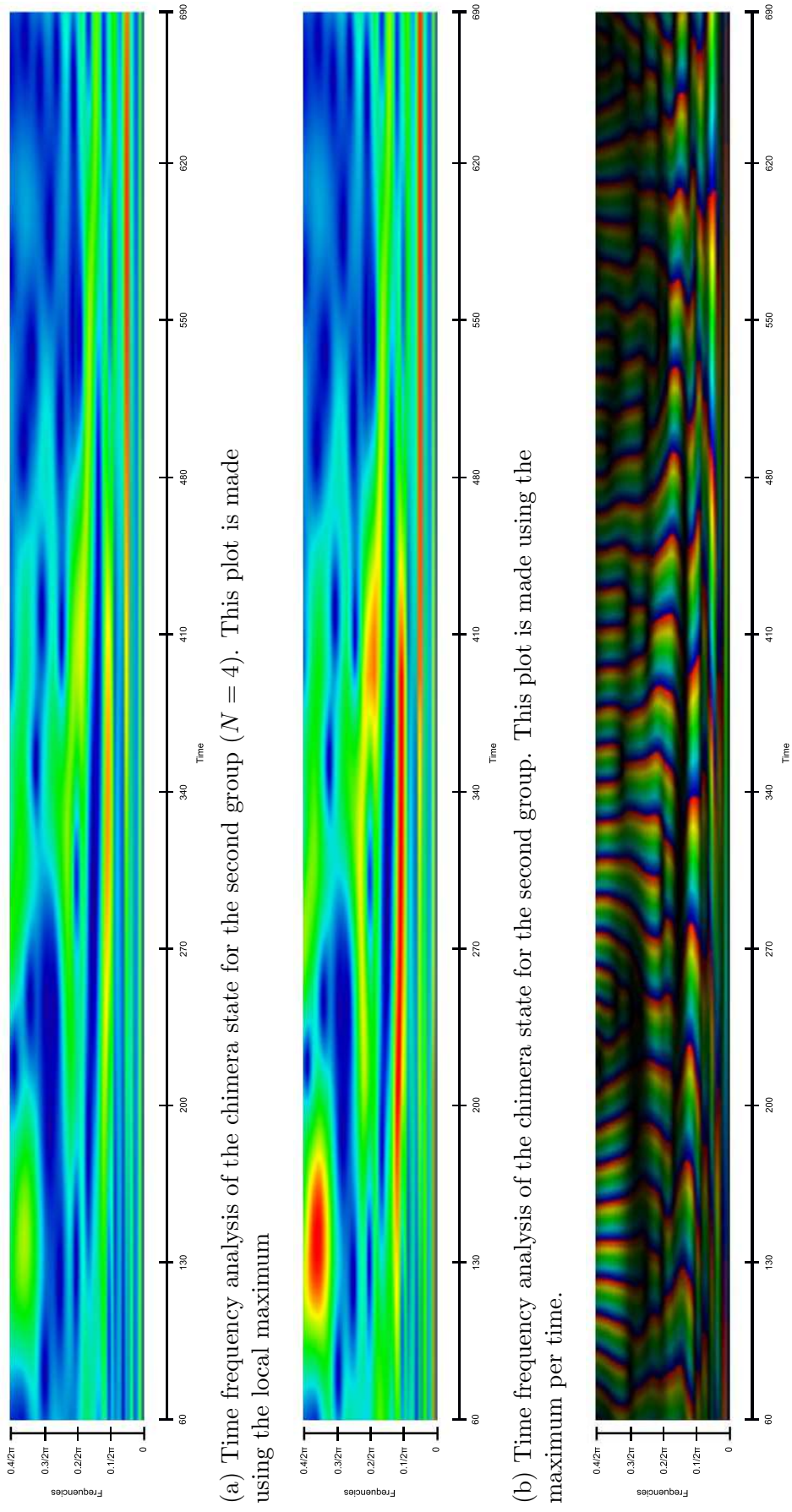
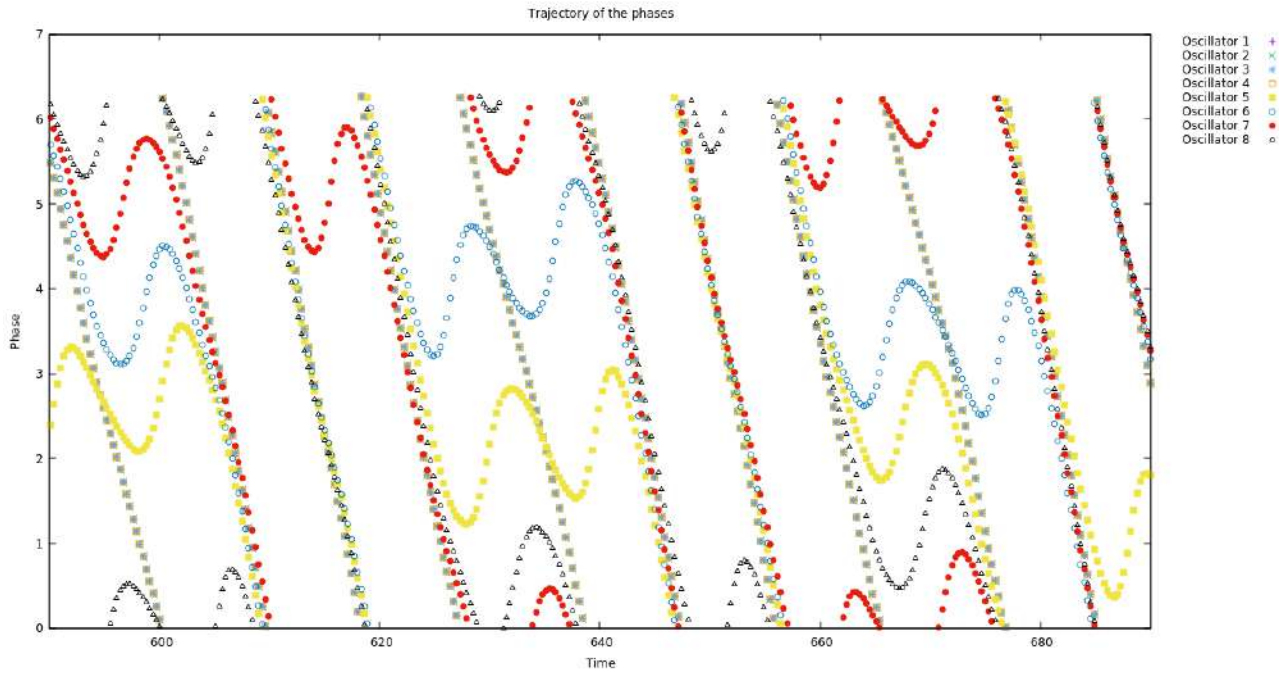
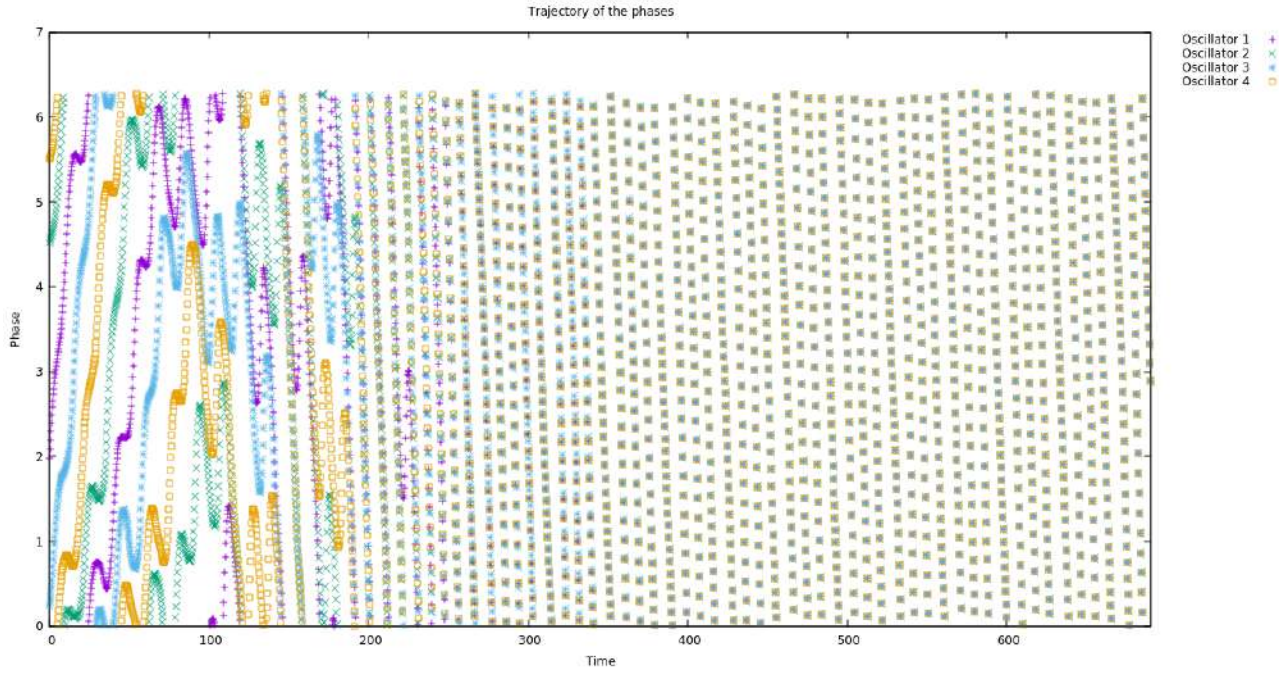


Figure 68: Time frequency analysis of the chimera state for the second group of oscillators with $N = 4$, $A = 0.4$ and $\beta = 0.025$

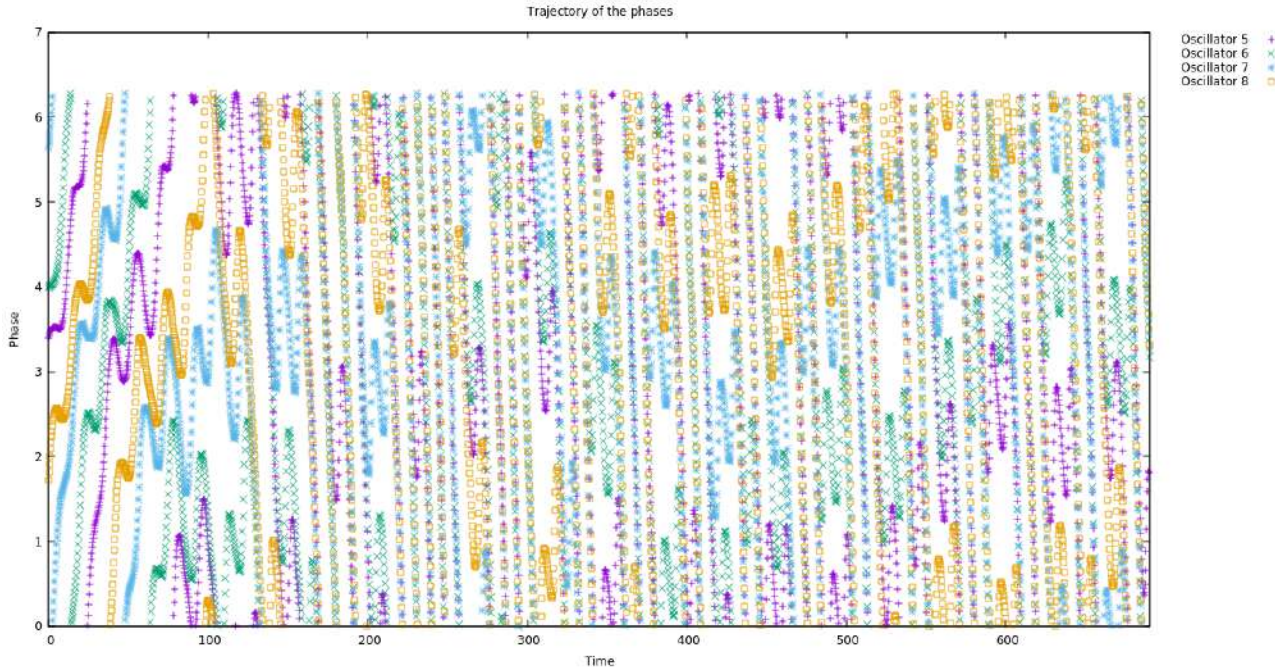




(a) Trajectory of the phases for all oscillators.



(b) Trajectory of the phases for the first group of oscillators.



(c) Trajectory of the phases for the second group of oscillators.

Figure 69: Trajectory of the phases.

7.3 Two groups of hundred oscillators

Finally, we will analyze the chimera state with two groups of hundred oscillators. We will compare this to the $N \rightarrow \infty$ case of Panaggio, Abrams, Ashwin and Laing (2016). We will start with analyzing the case of $A = 0.1$ and $\beta = 0.025$. For this case Panaggio, Abrams, Ashwin and Laing found a stable chimera.

In our analysis we found a oscillating chimera. The oscillations of this chimera were small and we expect that they are due to a finite size effect. Therefore, we expect that whenever $N \rightarrow \infty$ the oscillations disappear.

Figure 71 shows the time frequency analysis for all oscillators ($2N = 200$). The frequencies are not completely incoherent but also not perfectly synchronized. Especially the time frequency plot made using the maximum per time makes this very clear (see Figure 71b). Moreover, Figure 71c shows that at some moments the phases are coherent, while at other moments they are incoherent. This is confirmed by the trajectory of the phases (see Figure 74a).

Figure 72 shows the time frequency analysis for the synchronized group. Note that after approximately 400 time units this group synchronizes (almost) perfectly. Moreover, Figure 74b which shows the trajectory of the phases, confirms this. However, in the time frequency analysis it does not look like the frequencies synchronized perfectly. As mentioned earlier

we do not have an explanation for this. Looking at the numerical values of the phases we found that there were some small differences between them. It might be that the oscillators with different phases try to correct for the difference by going faster or slower. However, we do not think this is very likely.

In Figure 73 one can find the time frequency analysis of the incoherent group. Note that in this group the frequencies did synchronize into three groups of frequencies (see Figures 73a and 73b). Moreover, in Figure 73c the phases look partly synchronized. This confirmed by the plot of the order parameter 70c and the plot of the trajectories of the phases 74c.

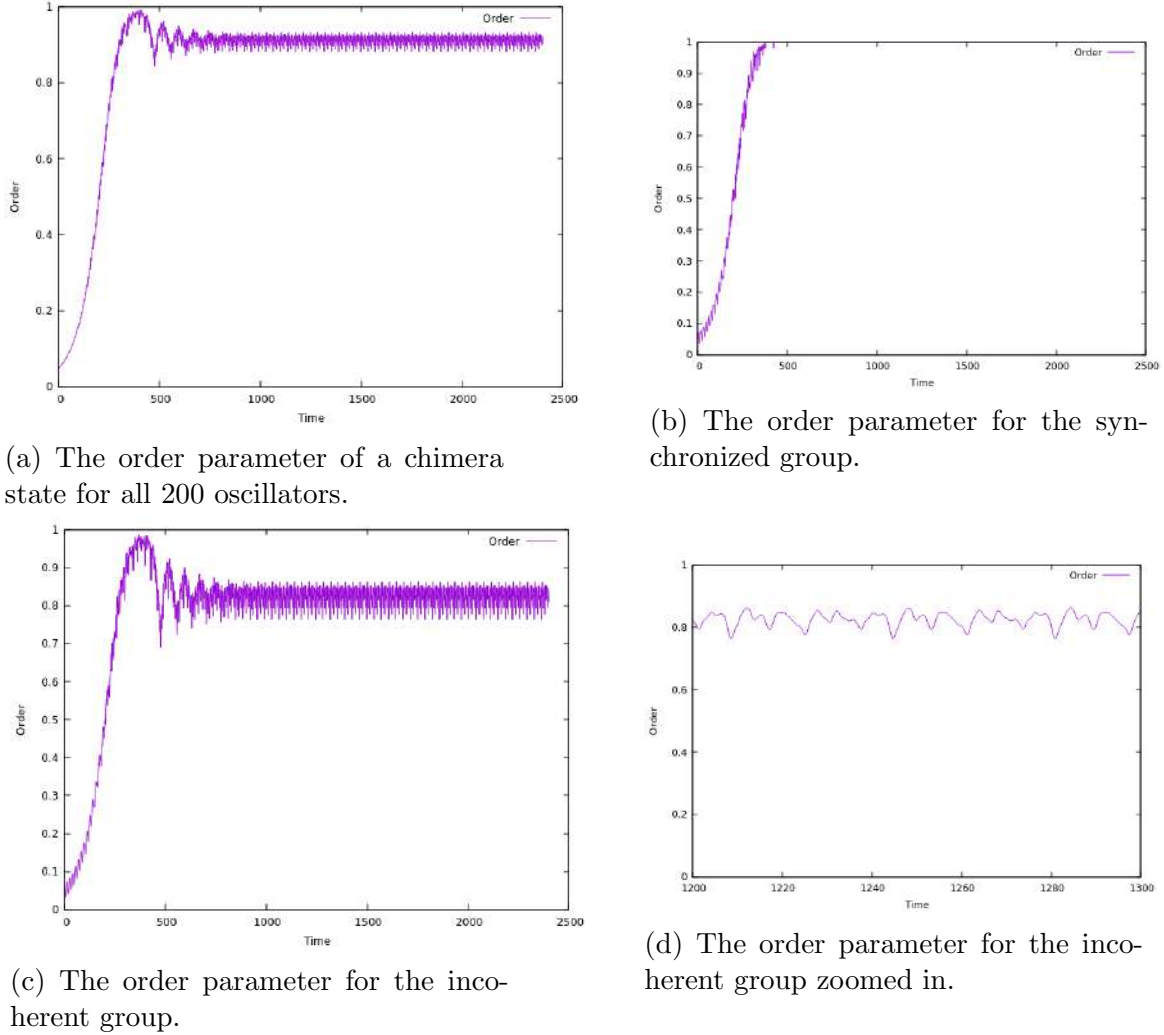


Figure 70: Order parameter for a chimera state with $N = 100$, $A = 0.1$ and $\beta = 0.025$

Figure 71: Time frequency analysis for the chimera state with $N = 100$, $A = 0.1$ and $\beta = 0.025$. The x -axis represents the time and starts from 60 and ends at 1080 in steps of 54. The y -axis represents the frequencies and starts at 0 and ends at $0.4/2\pi$ in steps of $0.1/2\pi$.

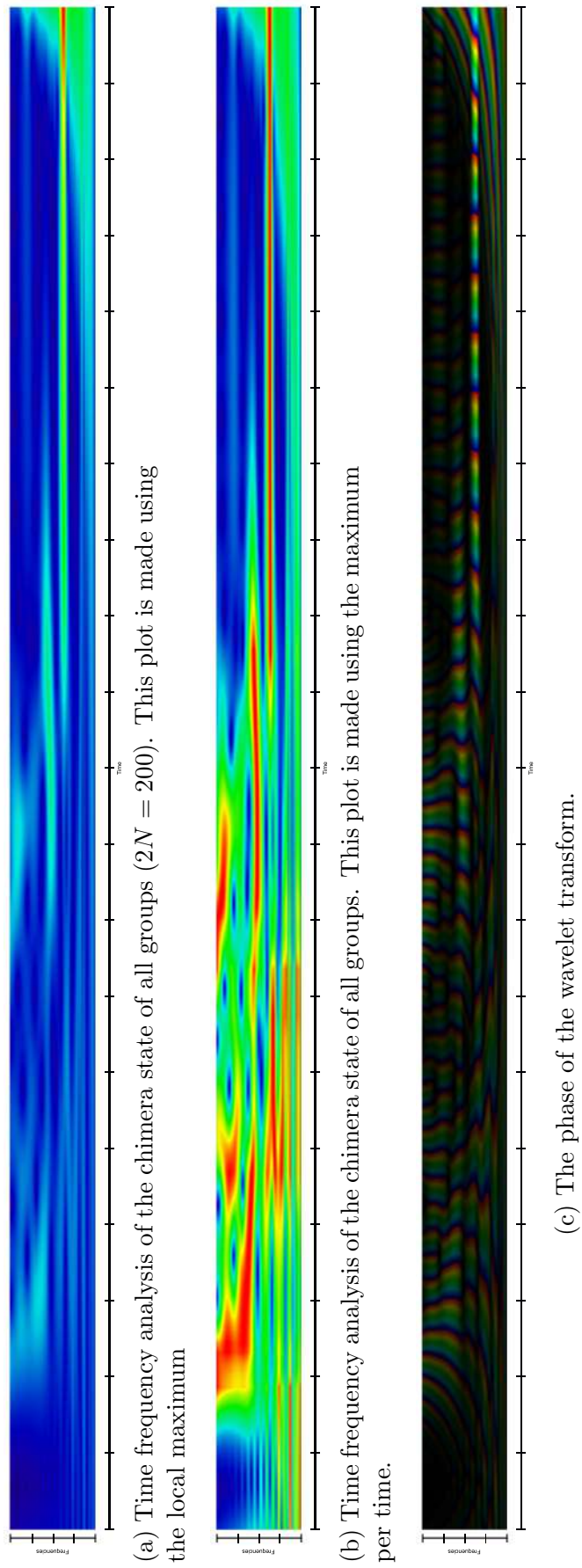


Figure 72: Time frequency analysis of the chimera state for the synchronized group with $N = 100$, $A = 0.1$ and $\beta = 0.025$. The x -axis represents the time and starts from 60 and ends at 1080 in steps of 54. The y -axis represents the frequencies and starts at 0 and ends at $0.4/2\pi$ in steps of $0.1/2\pi$.

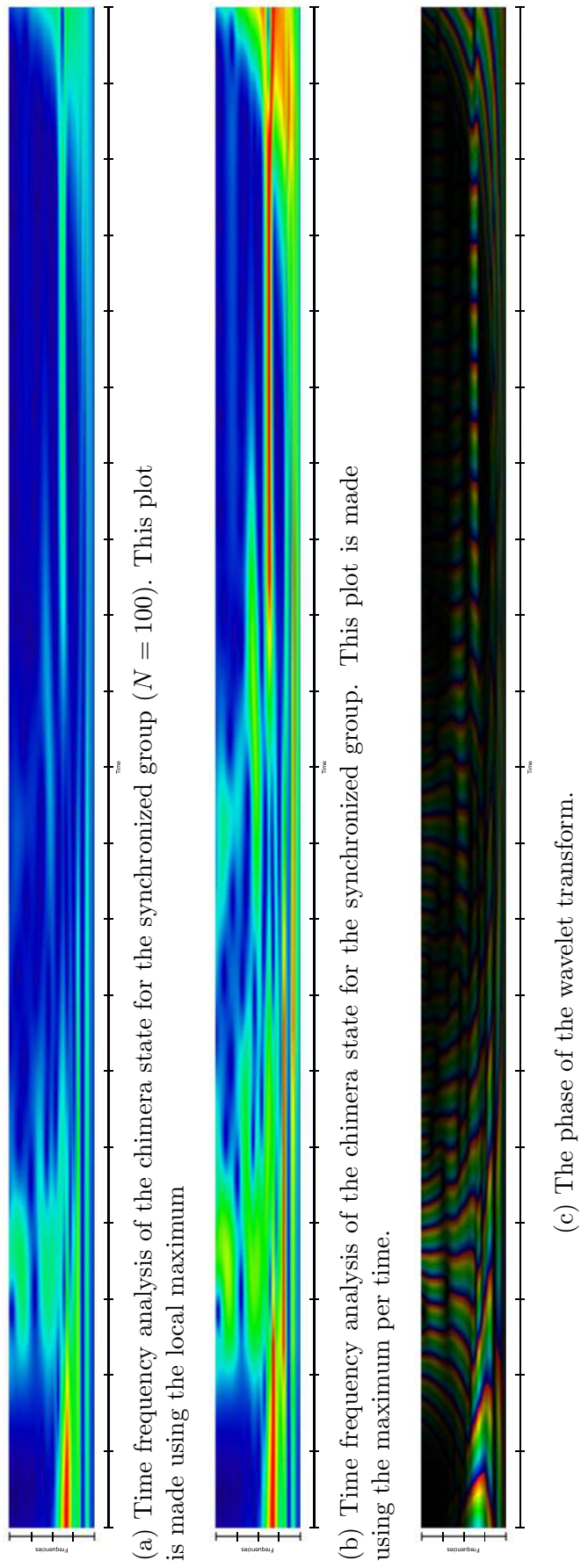
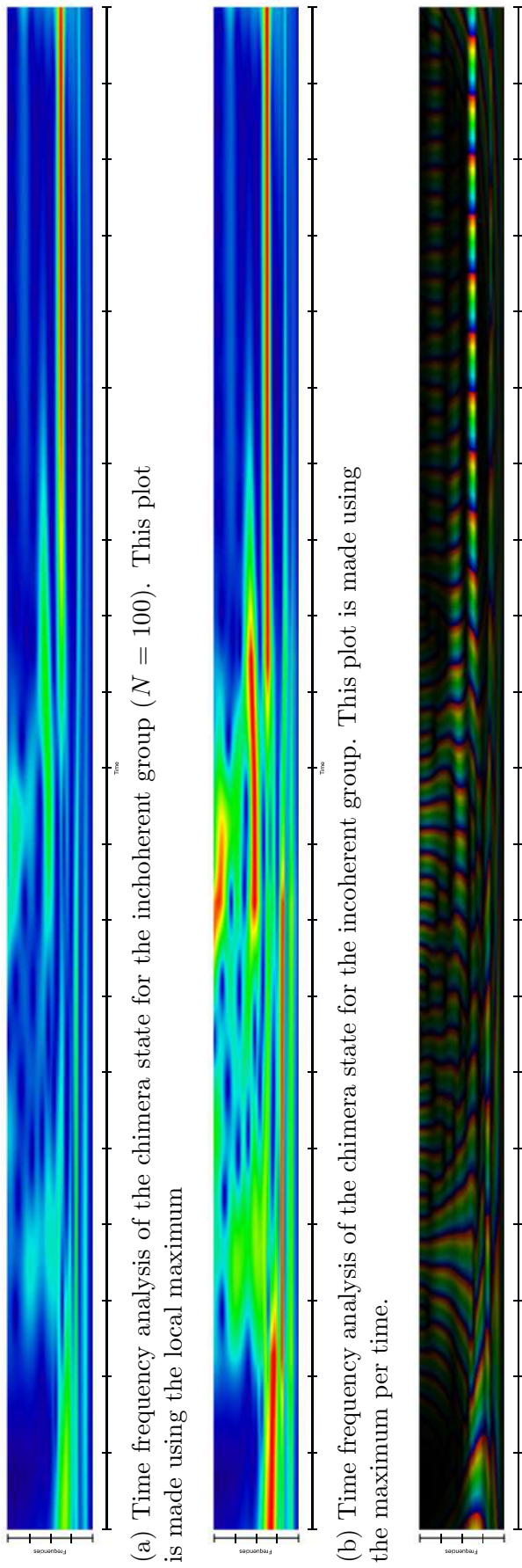


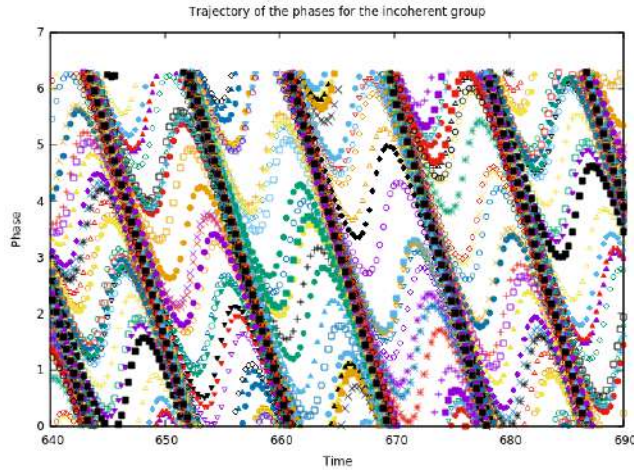
Figure 73: Time frequency analysis of the chimera state for the incoherent group with $N = 100$, $A = 0.1$ and $\beta = 0.025$. The x -axis represents the time and starts from 60 and ends at 1080 in steps of 54. The y -axis represents the frequencies and starts at 0 and ends at $0.4/2\pi$ in steps of $0.1/2\pi$.



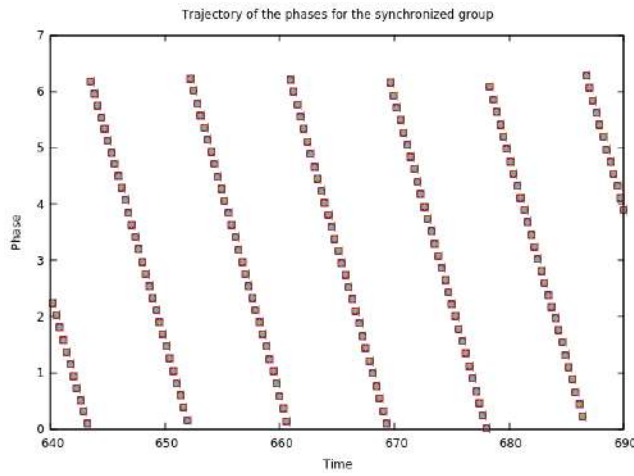
(a) Time frequency analysis of the chimera state for the incoherent group ($N = 100$). This plot is made using the local maximum

(b) Time frequency analysis of the chimera state for the incoherent group. This plot is made using the maximum per time.

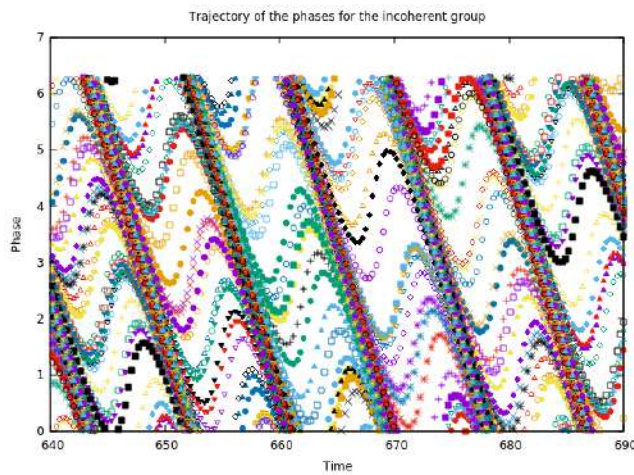
(c) The phase of the wavelet transform.



(a) Trajectory of the phases for all oscillators. The first half of oscillators belongs to the synchronized group while the second half belongs to the incoherent group.



(b) Trajectory of the phases for the synchronized group.



(c) Trajectory of the phases for the incoherent group.

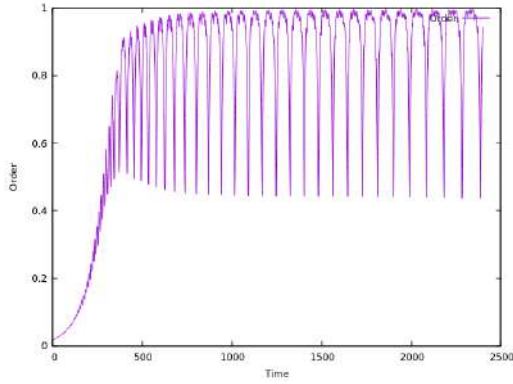
Figure 74: Trajectory of the phases.

At last we will look at the case of $A = 0.4$, $\beta = 0.025$ and $N = 100$. We will compare our results of the order parameter with the order parameter of the $N \rightarrow \infty$ case obtained by Panaggio, Abrams, Ashwin and Laing (2016). We expect to find a breathing chimera. Figure 75c shows that the order parameter for the incoherent group is indeed a breathing chimera. On the top of each oscillations there is some disturbance, this might be due to a finite size effect.

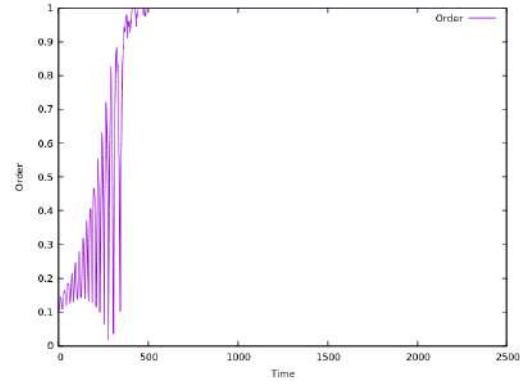
Figure 76 shows the time frequency analysis for all 200 oscillators. According to the order parameter the phases are mostly incoherent (see Figure 75a). This is confirmed by the plot of the trajectories for the phases (see Figure 79a). The time frequency analysis shows that the frequencies are incoherent (Figures 76a and 76b). Moreover, the phases look mostly incoherent, together with some brief moments of synchronization.

In Figure 76a one can find the time frequency analysis for the synchronized group. Observe that the frequencies did not synchronize. However, they have just a small spread and their mean is small too. The phases do not look perfectly synchronized in Figure 76c. Moreover, the signal looks quite weak. This in contrary with the plot of the order parameter and the trajectory of the phases (Figures 75b and 79b). Therefore, we looked more closely at the phases and found out that there is a real small difference between them. Hence, it could be, although we think it is quite unlikely, that the oscillators with different phases try to correct for the difference by going faster or slower. This might be the reason of the spread of the frequencies and the weakness of the signal. Moreover, as the differences in the phases are this small this is not visible in both Figure 75b and 79b.

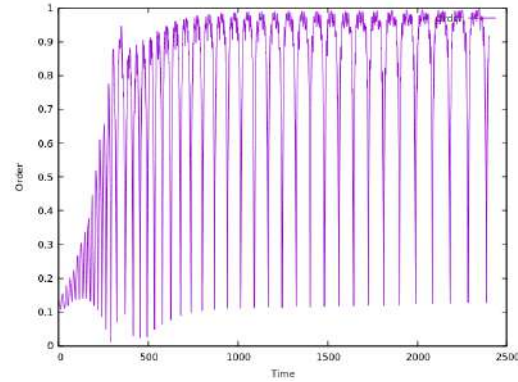
Figures 78a and 78b shows that the frequencies are incoherent for the second group of oscillators. This is as expected as order parameter oscillates heavily. These oscillations are also visible in the time frequency plot of the phases (see Figure 78c). Moreover, Figure 79c shows that the majority of the oscillators are synchronized. There are a few oscillators out of sync with the rest.



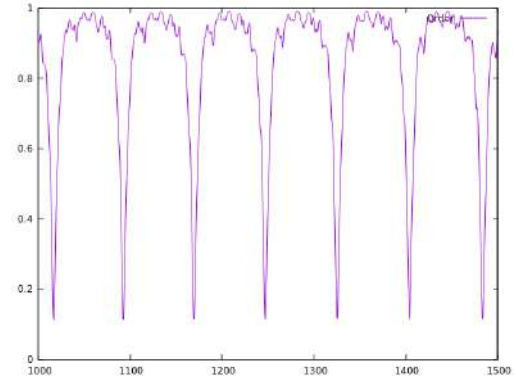
(a) The order parameter of a chimera state for all 200 oscillators.



(b) The order parameter for the synchronized group.



(c) The order parameter for the incoherent group.



(d) The order parameter for the incoherent group zoomed in.

Figure 75: Order parameter for a chimera state with $N = 100$, $A = 0.4$ and $\beta = 0.025$

Figure 76: Time frequency analysis for the chimera state with $N = 100$, $A = 0.4$ and $\beta = 0.025$. The x -axis represents the time and starts from 60 and ends at 1080 in steps of 54. The y -axis represents the frequencies and starts at 0 and ends at $0.4/2\pi$ in steps of $0.1/2\pi$.

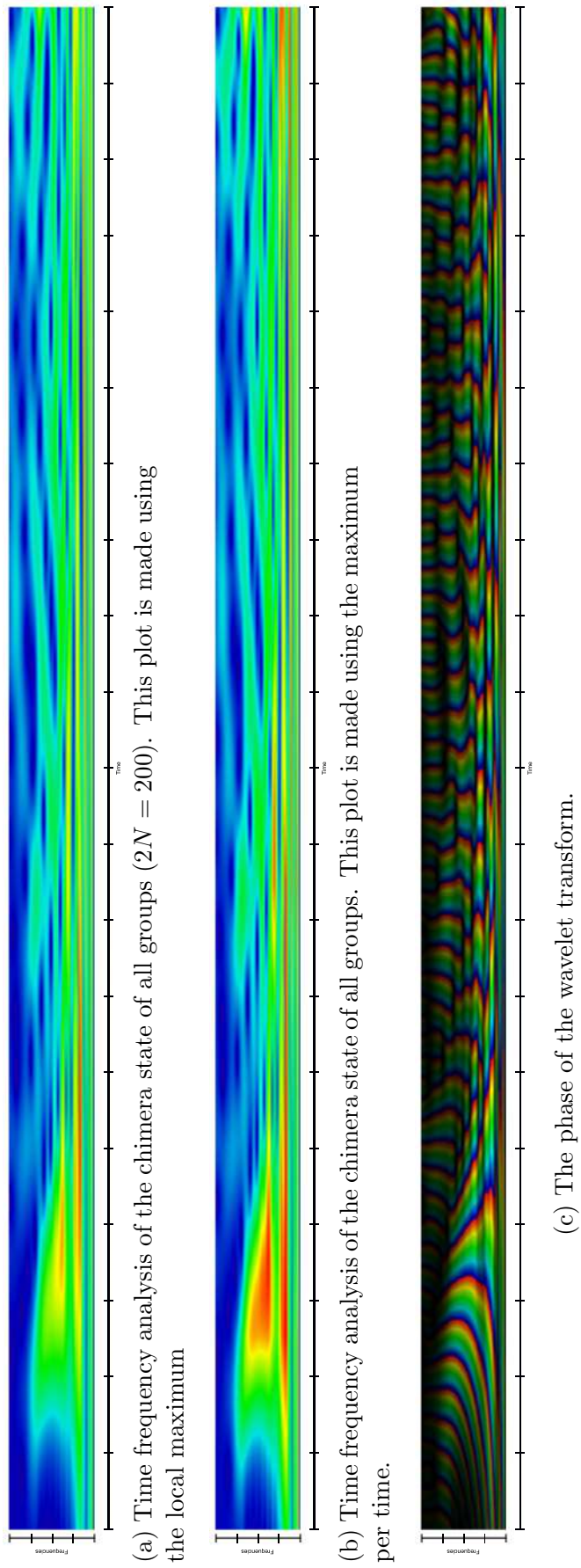


Figure 77: Time frequency analysis of the chimera state for the synchronized group with $N = 100$, $A = 0.4$ and $\beta = 0.025$. The x -axis represents the time and starts from 60 and ends at 1080 in steps of 54. The y -axis represents the frequencies and starts at 0 and ends at $0.4/2\pi$ in steps of $0.1/2\pi$.

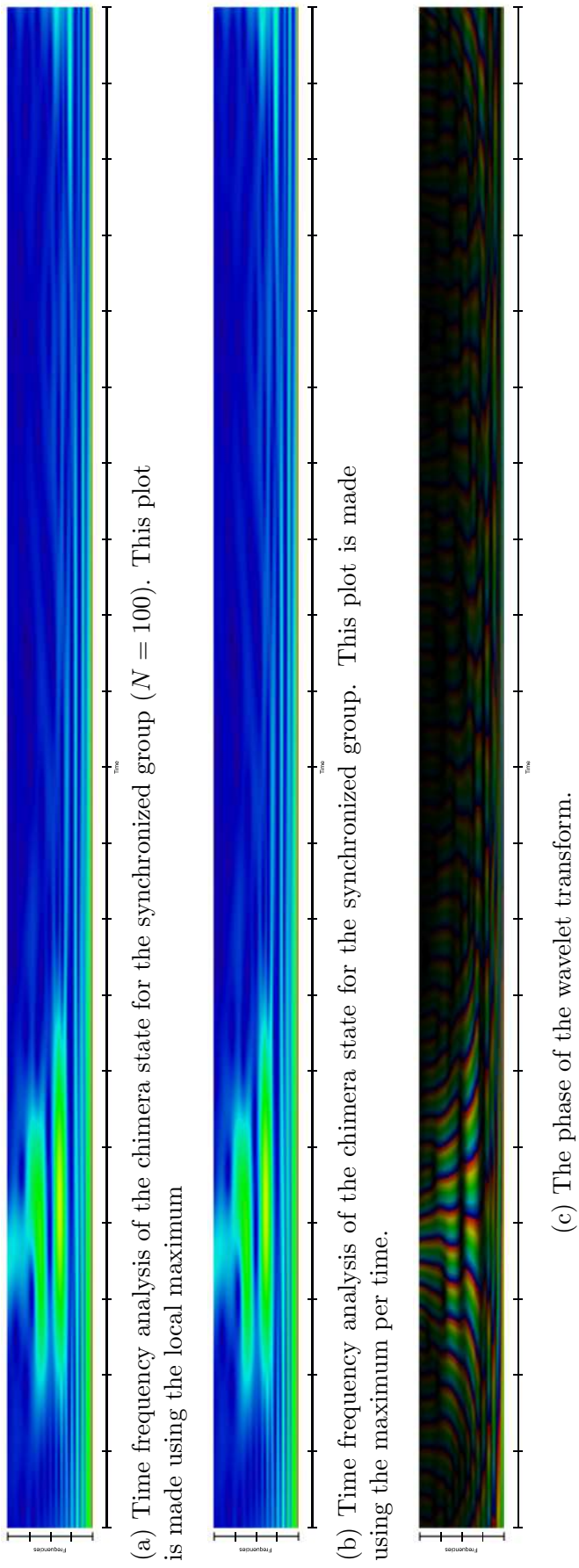
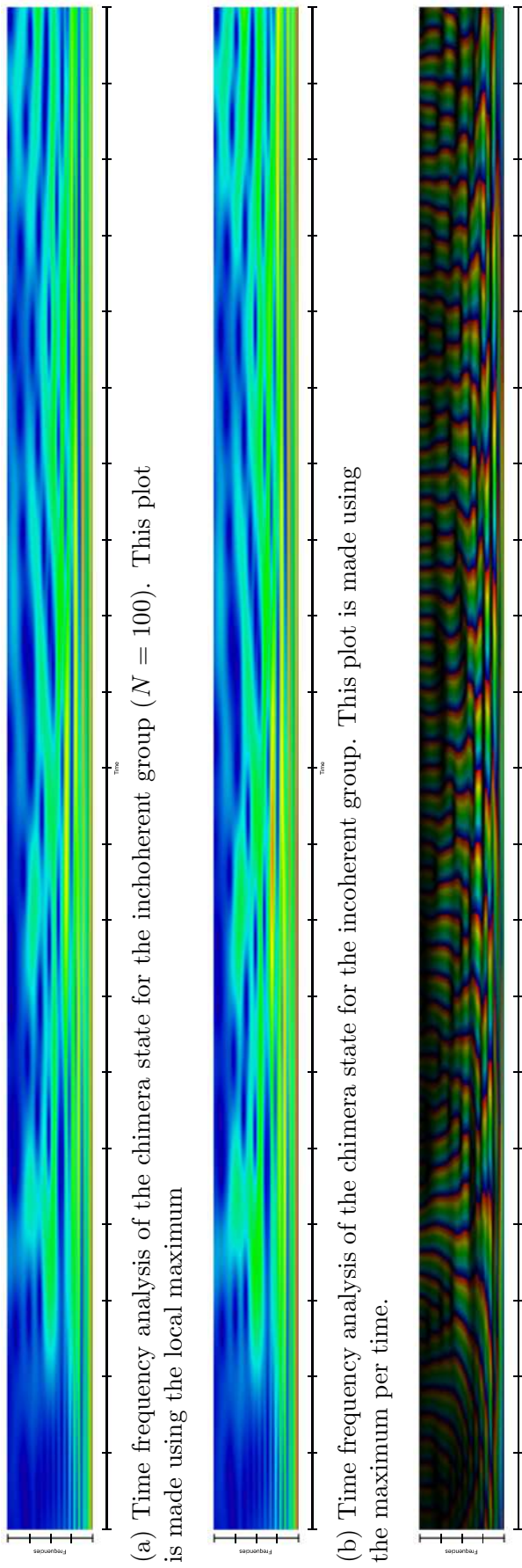
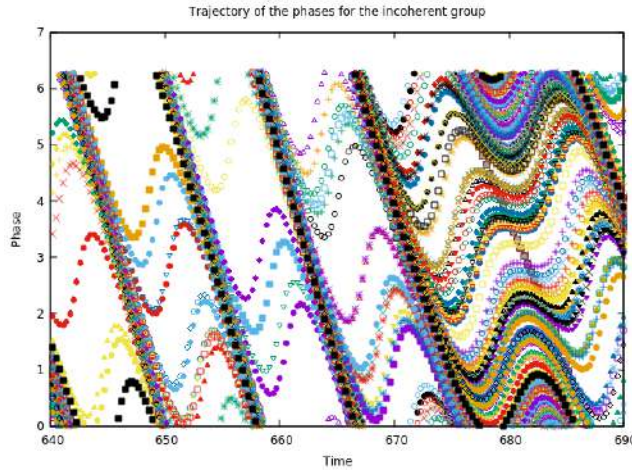
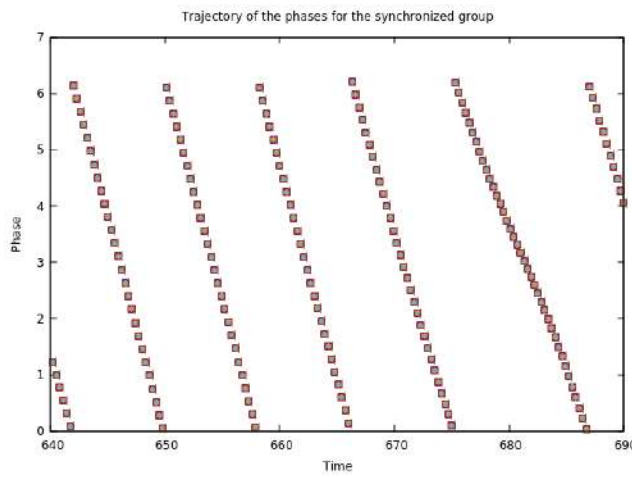


Figure 78: Time frequency analysis of the chimera state for the incoherent group with $N = 100$, $A = 0.4$ and $\beta = 0.025$. The x -axis represents the time and starts from 60 and ends at 1080 in steps of 54. The y -axis represents the frequencies and starts at 0 and ends at $0.4/2\pi$ in steps of $0.1/2\pi$.

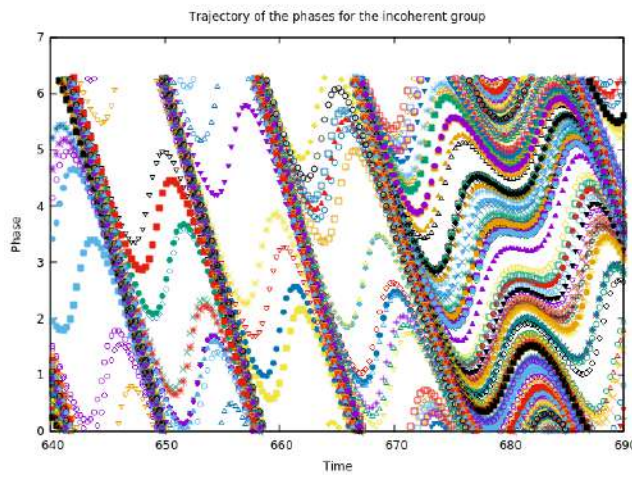




(a) Trajectory of the phases for all oscillators. The first half of oscillators belongs to the synchronized group while the second half belongs to the incoherent group.



(b) Trajectory of the phases for the synchronized group.



(c) Trajectory of the phases for the incoherent group.

Figure 79: Trajectory of the phases.

8 Poincaré sections

In the previous section we analyzed chimera states using time frequency analysis. In this section we will look more closely at the stability of chimera states for groups of $N = 4$, with $0.28 \leq A \leq 0.35$ and $\beta = 0.1$. According to the work of Panaggio, Abrams, Ashwin and Laing (2016) these parameter values have to give a stable limit cycle and an unstable fixed point. We will thrive to confirm the work of Panaggio, Abrams, Ashwin and Laing (2016) and extend this work by doing a time frequency analysis.

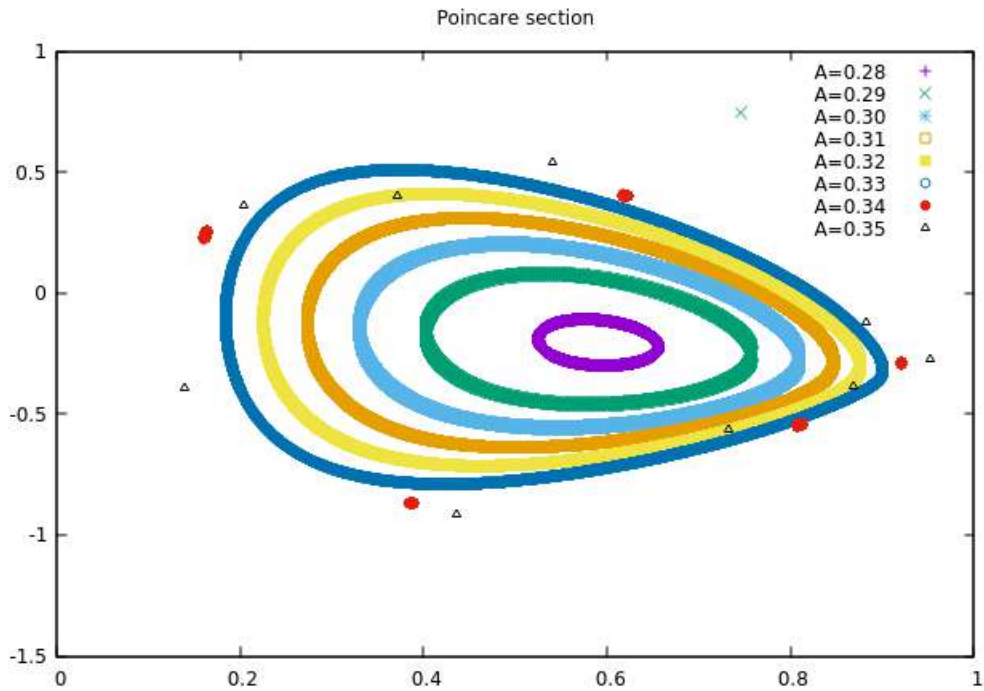
Hence, we placed a Poincaré section at $\Psi = \pi$ and recorded the values of ρ and Δ . These values of ρ and Δ were obtained by integrating System (73), where γ_2 was given by (74). We record the time step in which $\Psi < \pi$ and in which $\Psi > \pi$. Hence, we check in which time step the Poincaré section is crossed. Suppose now that $\Psi(t_k) < \pi < \Psi(t_{k+1})$. We want to know the values of ρ and Δ whenever $\Psi = \pi$. These values can be found by integrating the following system over Ψ from $\Psi(t_{k+1})$ to π :

$$\begin{aligned} \frac{d\Delta}{d\Psi} &= \frac{dt}{d\Psi} \frac{d\Delta}{dt} \\ \frac{d\rho}{d\Psi} &= \frac{dt}{d\Psi} \frac{d\rho}{dt} \\ \frac{d\Psi}{d\Psi} &= 1, \end{aligned} \tag{79}$$

using the following initial conditions: $\Delta(t_{k+1})$, $\rho(t_{k+1})$ and $\Psi(t_{k+1})$. Observe that System (79) can easily be obtained using System (73). The above method is referred to as the Hénon trick.

We programmed this in C++ (see Section A) and let the program run for different values of A (from 0.28 to 0.35) with 20,000,000 steps. We plotted the last 90% of the points on the Poincaré section in order to obtain the stable limit cicle. We expected to find a similar figure as obtained by Panaggio, Abrams, Ashwin and Laing (2016) (see Figure 4b). The results are shown in Figure 80. Our results confirm that the Hopf bifurcation is supercritical. Figure 80 shows the same pattern for $A = 0.28$ to $A = 0.33$ as Figure 4b. However, the points on the section for $A = 0.34$ and $A = 0.35$ are not exactly the same. In our Poincaré section we see resonance for $A = 0.34$. Furthermore, for $A = 0.35$ we only had 10 intersections of the Poincaré section. Hence, it looks like the points on the Poincaré section for $A = 0.35$ did not converge yet. We expect to find resonance too for $A = 0.35$. Note that Panaggio, Abrams, Ashwin and Laing (2016) found resonance points for $A = 0.35$ but not for $A = 0.34$. For $A = 0.34$ they found a stable limit cycle. We do not have an explanation for this.

Figure 80: Poincaré section obtained by running our program (see Section A).



The next step is to apply a time frequency analysis to the trajectory of Δ and ρ . We defined the signal as $\rho + i\Delta$. We expect to find two different frequencies; one of Δ and one of ρ . These signals together form a two dimensional torus, which is projected on the Poincaré section. We calculated the time frequency analysis for 20,000,000 steps of 0.01.

Figure 81: Time Frequency analysis for the trajectories of Δ and ρ , with $N = 4$, $A = 0.32$ and $\beta = 0.025$.

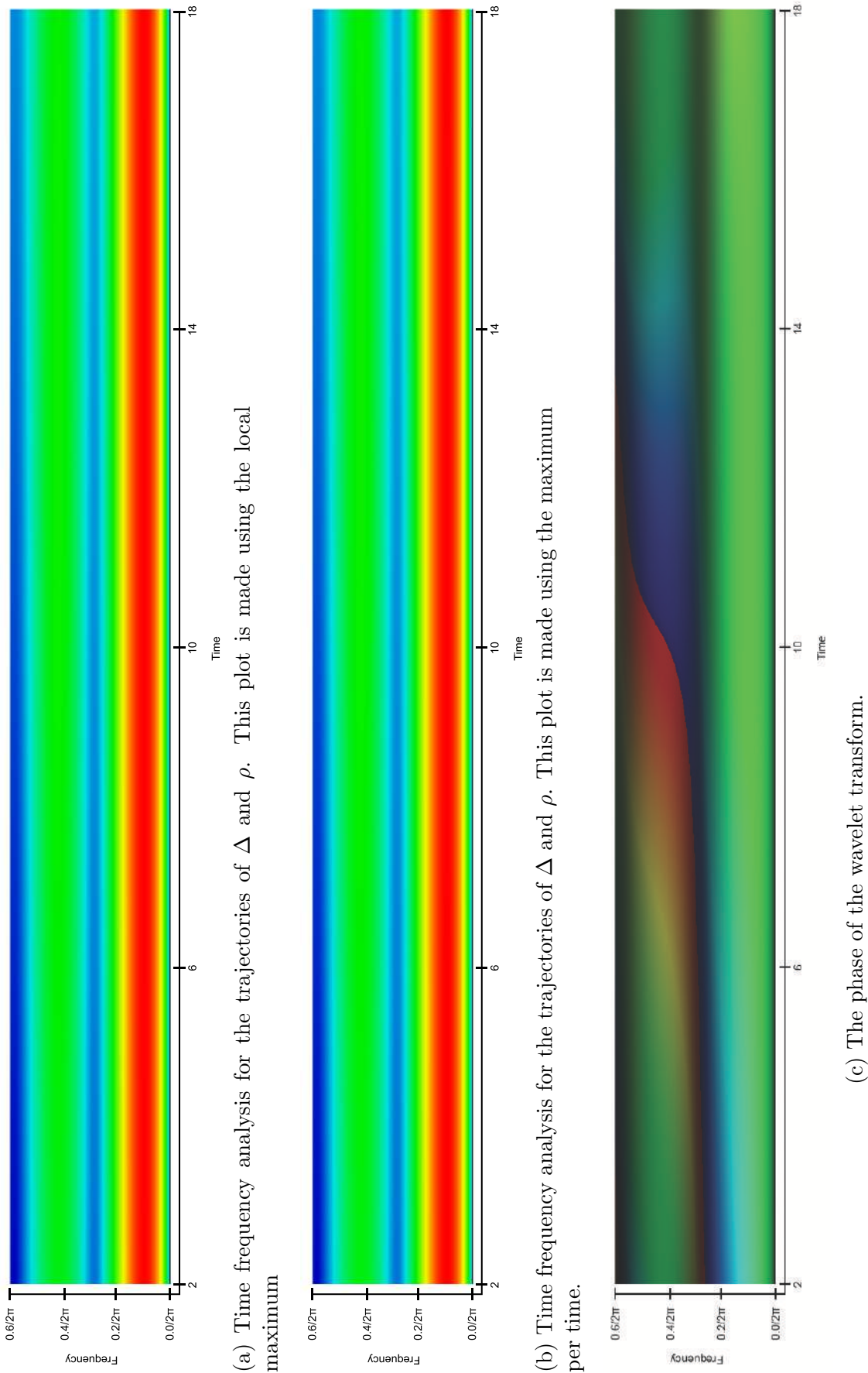


Figure 81 shows the time frequency analysis for $A = 0.32$, $\beta = 0.025$ and $N = 4$. As expected, we see two frequencies; one for each variable. Observe that the time frequency analysis plot with the local maximum looks the same as with the maximum per time. Moreover, note that the frequencies already synchronized within the first 2 time units. Finally, Figure 81c shows that the phases of the oscillator with the lowest frequency change very slowly, and the phases of the oscillator with a higher frequency change faster. Hence, Figure 81c explains the great number of points we had to take (20,000,000) to create the Poincaré section.

We also performed a time frequency analysis for $A = 0.28$, $A = 0.29$, $A = 0.30$, $A = 0.31$, $A = 0.33$, $A = 0.34$ and $A = 0.35$, with $N =$ and $\beta = 0.025$ (not shown here). These time frequency analyses look the same as Figure 81. Hence, the limit cycle grows with A , but the frequencies remain the same.

9 Discussion

In this research we studied the Kuramoto model extensively. Moreover, we thrived to get more insight in time frequency analysis as a method to detect synchronization. We started by calculating the critical coupling of the Kuramoto model. After the coupling is increased above the critical coupling the order parameter should equal $\sqrt{1 - K_c/K}$ (Strogatz, 2000). After this we analyzed the stability of the distribution of the oscillators and showed that the distribution of the oscillators for the incoherent state is neutrally stable for $K < K_c$ and unstable for $K > K_c$. Next to this we analyzed the stability of the order parameter using the Ott Antonsen Ansatz. We found stability for $R = 0$ whenever $K < K_c$. In the case that $K > K_c$, the branch $R = 0$ was unstable. Furthermore, we found that the branch of the locked state was stable for $K > K_c$. Moreover, for $K < K_c$ this branch did not exist. Using numerical simulations, we confirmed that whenever $K < K_c$ $R \approx 0$ and whenever $K > K_c$ $R = \sqrt{1 - K_c/K}$. However, there were some small differences, which we expect to be due to a finite size effect.

Moreover, we reduced the Kuramoto model from a N-dimensional model to a three dimensional model using the Watanabe and Strogatz Ansatz (1994). This three dimensional model has some problems, whenever $\gamma = 0$. One of these problems is a singularity. More researched is required to regularize this singularity.

We performed a time frequency analysis on the Kuramoto model for one population of oscillators and two populations of oscillators. For one population of oscillators we found that whenever the frequencies synchronize the phases synchronize too. Hence, whenever $K > K_c$ the frequencies synchronize too. Furthermore, whenever $K = 0$ we expected to find a line

that is approximately straight and has a horizontal orientation for the wavelet transform in the plot with the maximum per time. However, we did not find a straight line and we hypothesized that this has to do with the fluctuation in the order parameter R .

For two populations of oscillators we saw that the frequencies first synchronize per population and eventually to each other. The order parameter showed severe oscillations whenever we increased K from zero onwards. The plot of the phase of the wavelet transform showed clearly that these oscillations were caused by the two groups having different frequencies. Increasing K even further resulted in synchronization for both the phases and the frequencies. Hence, we found numerically a critical value for the coupling in case of two populations of oscillators. However, we were not yet able to relate this value to the spread within and between the populations like the critical value of one population of oscillators. Therefore, we suggest that further research could be done in finding the critical value for multiple populations of oscillators analytically.

Next to this we looked further into chimera states. We discussed the reduced equation for chimera states. Moreover, we discussed the bifurcations of chimera states for different number of oscillators per group. Subsequently we thrived to obtain chimera states for these group sizes N and different parameters A . Recall that the time frequency analysis of the synchronized population often showed multiple frequencies and we did not have an explanation for this.

One remarkable discovery for the chimera states, is that for the phases of the incoherent groups there are just a few oscillators incoherent to the rest. Moreover, the incoherent oscillators become coherent at some points and at these points in time other oscillators become incoherent.

To find out more about the bifurcations of the chimera state with 4 oscillators we looked at a Poincaré map. We confirmed that the Hopf bifurcation is supercritical. We found resonance whenever the difference between the intragroup coupling and the intergroup coupling was big (bigger than 0.68). We expected this for the highest difference, but not for smaller differences as according to Panaggio, Abrams, Ashwin and Laing (2016) this should have been a limit cycle.

Moreover, we did a time frequency analysis with the trajectories of the two phase variables obtained from the reduced system for the chimera states (System 73). These trajectories formed the limit cycles on the Poincaré section. We found two frequencies, which are the frequencies of the trajectories of a two dimensional torus. Finally, we concluded that when the difference between the intragroup coupling and the intergroup coupling increases the limit cycle grows, but the frequencies stay the same.

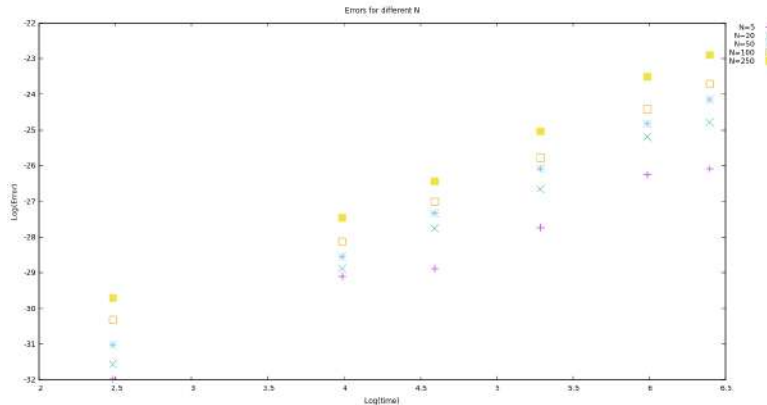
9.1 Numerical correctness

To test the numerical correctness of the numerical integration that we used we wrote a program in C++. This program integrates the System 1 from an initial value that is between 0 and 2π over a time T . The result of this integral will be the initial value of the integral of the negative counterpart of System 1, that is

$$\dot{\theta}_i = -\omega_i - \sum_{j=1}^N \frac{K}{N} \sin(\theta_j - \theta_i), \quad i = 1, \dots, N. \quad (80)$$

This system will be integrated over a time T . If the integration is perfect, the result of this integral should equal the begin value of the integral of System 1. We found that, as expected, the two norm of the errors increased with the group size N and with the number of time units. Moreover, we found small errors for all different situations. Figure 82 shows the two norm of the error of the numerical integration for different group sizes and number of time units with $K = 0$.

Figure 82: The two norm of the errors of the numerical integration for different group sizes and number of time units. Note how the error grows for bigger groups and more time units



9.2 Advantages and disadvantages of the wavelet transform

Another goal of this research was to find advantages and disadvantages of the wavelet transform. Recall that in Section 5 we discussed that the time frequency analysis gives us the opportunity to find information in both the frequency and time domain. Moreover, unlike the windowed Fourier transform the wavelet transform adjusts the window size to the signal. Therefore the time and frequency resolution is mostly better than in the windowed Fourier transform. Hence, the wavelet transform can give us a lot of information about the frequen-

cies of the signals in time. For example the wavelet transform showed for the chimera state with $N = 100$, $A = 0.1$ and $\beta = 0.025$ that the incoherent group has just three frequencies in the end.

A problem with the wavelet transform can be the choice of the signal. For the Kuramoto model this is quite straightforward as we can represent it using the order parameter. However, for other systems this might not be this easy. For example, we did a time frequency analysis for $\rho + \Delta i$, but we could have done also a time frequency analysis for $\rho e^{\Delta i}$ as ρ is related to the degree of synchrony in the group (R) and Δ is related to the mean phase ϕ . The results of the wavelet transform might be different. Hence, it is difficult to choose a signal for the wavelet transform and one has to be careful while interpreting the results of the wavelet transform for a given signal.

9.3 Conclusion and further research direction

In conclusion the dynamics of the Kuramoto model is very rich. Different phenomenon can be found while studying the Kuramoto model, like synchronization, partial synchronization, phase locking and chimera states. These phenomenon can be related back to nature quite easily. Moreover, by introducing time-varying natural frequencies, time-varying coupling and different connective arrangements the Kuramoto model provides a realistic picture of synchronization in the brain (Cumin & Unsworth, 2006). The different connective arrangements of the Kuramoto model could be a fruitful avenue for future research. For example Chiba and Medvedev (2016) found a critical coupling for other connectivity arrangements. The critical coupling of these systems could be numerically confirmed using the wavelet transform. Moreover, the presence of chimera states could be researched in these systems as well.

Another interesting step in further research would be to look at the second order Kuramoto model (Rodrigues, Peron & Ji, 2016). One possibility is to apply the time frequency analysis to this model. Another possibility would be to look for chimera states and apply the time frequency analysis to these states.

Hence, from our research we conclude that the wavelet transform is a very helpful tool. Focusing on the wavelet transform with a plot obtained using the local maximum one can easily see the development of the frequencies of a signal. Moreover, the plot of the wavelet transform obtained using the maximum per time can tell us exactly what kind of frequency is present and in what amount for each moment. Both can be very helpful in practice as the measurement of frequencies is very important for different fields of science. For example people with epilepsy can benefit from this as an epileptic attack is nothing more than

desynchronization and synchronization of large neuronal populations in the brain (Jiruska, de Curtis, Jefferys, Schevon, Schiff & Schindler, 2013). Hence, more information about the process of synchronization can be very helpful. However, a disadvantage of the wavelet transform is that it is difficult to find a signal which represents all the trajectories. For example it is difficult to find a signal which represents the activity of the neurons in the brain.

In short, there is still a lot of work left in the research of the Kuramoto model and its applications. Moreover, the wavelet transform would be a very useful tool in this research. We are convinced that further research in the Kuramoto model and the wavelet transform as a tool to detect synchronization would give us interesting, fascinating and most of all useful results for the future.

References

- Abrams, D. M., Mirollo, R., Strogatz, S., and Wiley, D. (2008). Solvable model for chimera states of coupled oscillators. *Physical Review Letters*, 101(8).
- Abrams, D. M. and Strogatz, S. H. (2004). Chimera states for coupled oscillators. *Phys. Rev. Lett.*, 93:174102.
- Acebrón, J. A., Bonilla, L. L., Pérez Vicente, C. J., Ritort, F., and Spigler, R. (2005). The kuramoto model: A simple paradigm for synchronization phenomena. *Rev. Mod. Phys.*, 77:137–185.
- Bonilla, L. L., Pérez Vicente, C. J., Ritort, F., and Soler, J. (1998). Exactly solvable phase oscillator models with synchronization dynamics. *Phys. Rev. Lett.*, 81:3643–3646.
- Carmona, R., Hwang, W.-L., and Torrsani, B. (1998). *Practical Time-Frequency Analysis*. Academic press.
- Chiba, H. and Medvedev, G. S. (2016). The mean field analysis for the kuramoto model on graphs i. the mean field equation and transition point formulas.
- Daido, H. (1996). Multibranch entrainment and scaling in large populations of coupled oscillators. *Phys. Rev. Lett.*, 77:1406–1409.
- Gao, R. and Yan, R. (2011). *Wavelets: Theory and Applications for Manufacturing*. Springer.
- Jiruska, P., de Curtis, M., Jefferys, J. G. R., Schevon, C. A., Schiff, S. J., and Schindler, K. (2013). Synchronization and desynchronization in epilepsy: controversies and hypotheses. *The Journal of Physiology*, 591(4):787–797.
- Kaiser, G. (1994). *A friendly guide to wavelets*. Boston etc.: Birkhauser.
- Kuramoto, Y. (1984). *Chemical Oscillations, Waves, and Turbulence*. Springer Berlin Heidelberg.
- Mirollo, R. E. and Strogatz, S. H. (1990). Amplitude death in an array of limit-cycle oscillators. *Journal of Statistical Physics*, 60(1):245–262.
- Mirollo, R. E. and Strogatz, S. H. (2005). The spectrum of the locked state for the kuramoto model of coupled oscillators. *Physica D: Nonlinear Phenomena*, 205(1):249 – 266.
- Oukil, W., Kessi, A., and Thieullen, P. (2016). Synchronization hypothesis in the winfree model. *Dynamical Systems*, 32(114).

- Peleš, S. and Wiesenfeld, K. (2003). Synchronization law for a van der pol array. *Phys. Rev. E*, 68:026220.
- Pikovsky, A. and Rosenblum, M. (2008). Partially integrable dynamics of hierarchical populations of coupled oscillators. *Phys. Rev. Lett.*, 101:264103.
- Rodrigues, F., Peron, T., Ji, P., and Kurths, J. (2016). The kuramoto model in complex networks. *Physics Reports*, 610:1 – 98.
- Strogatz, S. H. (2000). From kuramoto to crawford: exploring the onset of synchronization in populations of coupled oscillators. *Physica D: Nonlinear Phenomena*, 143(14):1 – 20.
- Strogatz, S. H. and Mirollo, R. E. (1991). Stability of incoherence in a population of coupled oscillators. *Journal of Statistical Physics*, 63(3):613–635.
- Unsworth, C., Cumin, D., and of Auckland. Department of Engineering Science, U. (2006). *Generalising the Kuramoto Model for the Study of Neuronal Synchronisation in the Brain*. Report (University of Auckland. Faculty of Engineering). Department of Engineering Science, University of Auckland.
- Watanabe, S. and Strogatz, S. H. (1994). Constants of motion for superconducting josephson arrays. *Physica D: Nonlinear Phenomena*, 74(3):197 – 253.
- Wiener, N. (1961). *Cybernetics or control and communication in the animal and the machine*. New York etc.: M.I.T. Press and Wiley., 2 edition.
- Wiener, N. (1966). *Nonlinear problems in random theory*. Cambridge: The MIT Press.

A Appendix: Integration of the system

This program, made in C++, integrates the Kuramoto model and calculates the order parameter.

```
#include <iostream>
#include <iomanip>
#include <cmath>
#include <complex>
#include "nr.h"

using namespace std;

const int n=250;

double w1_array[n];
double w_array[n];
int runtime= 12000;
double K=0;
double phistart_array[n];

// Driver for routine odeint

DP dxsav; // defining declarations
int kmax,kount;
Vec_DP *xp_p;
Mat_DP *yp_p;

int nrhs; // counts function evaluations

void derivs(const DP t, Vec_I_DP &yvector, Vec_O_DP &dydx)
{
    int i=0;
    int k=0;
    nrhs++;
}
```

```

        for(i=0; i<n; i++){
            dydx[i] = w_array[i];
            for(k=0;k<n;k++){
                dydx[i] += K/n*sin(yvector[k]-yvector[i]);
            }
        }

    }

DP mod_2_PI(DP x)
{while (x<=0) {
x += 2.0*M_PI;
}while (x>2*M_PI) {
x -= 2.0*M_PI;
}return x;
}

int main(void)
{
const int N=n, KMAX=100;
int nbad,nok;
DP eps=1.0e-7,h1=1.0e-10,hmin=0.0,x1=0.0,x2=0.0, dx=0.3;
DP x1max = runtime*dx;
Vec_DP ystart(N);
Vec_DP ystart_old(N);
int i=0;
int idum = -2 ;

ofstream outfile_w("omega.dat");
ofstream outfile_p("phases.dat");

//std:: default_random_engine generator;
//std:: normal_distribution<double> distribution(2.5,1.0);

for(i=0;i<n;i++){
w1_array[i] = NR::ran3(idum);
}

```

```

w_array[i] = 0.3 + 0.025*tan(M_PI*(w1_array[i]-0.5));
outfile_w<<w_array[i]<<" "<<endl;
cout << "w[" << i << "] : " << w_array[i] << " ";
}

cout << endl;

//std::default_random_engine generator2;
//std::uniform_real_distribution<double> distribution2(0,2*M_PI);

for(i=0;i<n;i++){
ystart[i]= NR::ran3(idum)*2*M_PI; // distribution2(generator2);
outfile_p<< ystart[i]<<" "<<endl;
}
outfile_w . close();
outfile_p . close();

nrhs=0;
dxsav=(x2-x1)/2.0;
kmax=KMAX;
xp_p=new Vec_DP(KMAX);
yp_p=new Mat_DP(N,KMAX);

ofstream outfile_s("trajectory.dat");
ofstream outfile_o("order.dat");
ofstream outfile_or("Rorder.dat");

for(x1=0;x1<x1max;x1+=dx){
x2 = x1 + dx;
cout << "time: " << x1 << " " << x2 <<endl;

NR::odeint(ystart,x1,x2,eps,h1,hmin,nok,nbad,derivs,NR::rkqs);

for(i=0;i<n;i++){
ystart[i]=mod_2_PI(ystart[i]);
}
outfile_s << x1;
}

```

```

complex<double> im=-1;
im = sqrt(im);
for(i=0;i<n;i++){
    outfile_s<<" "<< ystart[i];
}
outfile_s << endl;

complex<double> order= exp(im*ystart[0]);
for(i=1;i<n;i++){
    order += exp(im*ystart[i]);
}
double realorder = real(order)/n;
double imagorder= imag(order)/n;
double order1= sqrt(realorder*realorder + imagorder*imagorder);

outfile_o << x1 << " "<< realorder << " "<< imagorder << " " << endl;

outfile_or << x1 << " "<< order1 << endl;
}

outfile_s.close();
outfile_o.close();
outfile_or.close();

int length = runtime/dx+1;

cout << "length order.dat=" << length << endl;

delete yp_p;
delete xp_p;

return 0;
}

```

B Appendix: Integration of the system for chimera states

This program is made in C++ and integrates the System 70 and 71. Moreover, it finds the order parameter for both groups and the order parameter of all oscillators together.

```
#include <iostream>
#include <iomanip>
#include <cmath>
//#include <random>
#include <complex>
//#include <std>
#include "nr.h"

using namespace std;

const int n1=4;
const int n2=4;
const int n=n1+n2;

double w = 0.2;
int runtime= 8000;
double A= 0.1;
double b= 0.025;
double phistart_array[n];

// Driver for routine odeint

DP dxsav; // defining declarations
int kmax,kount;
Vec_DP *xp_p;
Mat_DP *yp_p;

int nrhs; // counts function evaluations

void derivs(const DP t, Vec_I_DP &yvector, Vec_O_DP &dydx)
{
```

```

int i=0;
int j=n1+1;
int k=0;
nrhs++;

for(i=0; i<n1; i++){
    dydx[i] = w;
    for(j=0; j<n1; j++){
        dydx[i] -= (1.0+A)/n *cos(yvector[i]-yvector[j]-b);
    }
    for(j=n1; j<n; j++){
        dydx[i] -= (1.0-A)/n *cos(yvector[i]-yvector[j]-b);
    }
}

for(i=n1; i<n; i++){
    dydx[i] = w;
    for(j=n1; j<n; j++){
        dydx[i] -= (1.0+A)/n *cos(yvector[i]-yvector[j]-b);
    }
    for(j=0; j<n1; j++){
        dydx[i] -= (1.0-A)/n *cos(yvector[i]-yvector[j]-b);
    }
}

}

DP mod_2_PI(DP x)
{while (x<=0) {
x += 2.0*M_PI;
}while (x>2*M_PI) {
x -= 2.0*M_PI;
}return x;
}

```

```

int main(void)
{
const int N=n, KMAX=100;
int nbad,nok;
DP eps=1.0e-7,h1=1.0e-10,hmin=0.0,x1=0.0,x2=0.0, dx=0.3;
DP x1max = runtime*dx;
Vec_DP ystart(N);
Vec_DP ystart_old(N);
int i=0;
int idum = -1;

ofstream outfile_v("phases.dat");

//std:: default_random_engine generator;
//std:: normal_distribution<double> distribution(2.5,1.0);

//std::default_random_engine generator2;
//std::uniform_real_distribution<double> distribution2(0,2*M_PI);
for(i=0;i<n;i++){
    ystart[i]= NR::ran3(idum)*2*M_PI;

    outfile_v<< ystart[i]<<" "<<endl;
}

outfile_v.close();

nrhs=0;
dxsav=(x2-x1)/2.0;
kmax=KMAX;
xp_p=new Vec_DP(KMAX);
yp_p=new Mat_DP(N,KMAX);

ofstream outfile_s("trajectory.dat");

```

```

ofstream outfile_o("order.dat");
ofstream outfile_or("Rorder.dat");
ofstream outfile_q("orderfirst");
ofstream outfile_r("Rorderfirst");
ofstream outfile_t("ordersecond");
ofstream outfile_u("Rordersecond");

for(x1=0;x1<x1max;x1+=dx){
    x2 = x1 + dx;
    cout << "time: " << x1 << " " << x2 << endl;
    NR::odeint(ystart,x1,x2,eps,h1,hmin,nok,nbad,derivs,NR::rkqs);

    for(i=0;i<n;i++){
        ystart[i]=mod_2_PI(ystart[i]);
    }

    outfile_s << x1;
    complex<double> im=-1;
    im = sqrt(im);
    for(i=0;i<n;i++){
        outfile_s<<" "<< ystart[i];
    }
    outfile_s << endl;

    complex<double> order= exp(im*ystart[0]);
    for(i=1;i<n;i++){
        order += exp(im*ystart[i]);
    }

    double realorder = real(order)/n;
    double imagorder= imag(order)/n;
    double order1= sqrt(realorder*realorder + imagorder*imagorder);

    outfile_o << x1 << " " << realorder << " " << imagorder << " " << endl;

    outfile_or << x1 << " "<< order1 << endl;

    complex<double> orderd= exp(im*ystart[0]);
}

```

```

        for(i=1;i<n1;i++){
            orderd += exp(im*ystart[i]);
        }

        double realorder1 = real(orderd)/n1;
        double imagorder1= imag(orderd)/n1;
        double order11= sqrt(realorder1*realorder1 + imagorder1*imagorder1);

        outfile_q << x1 << " " << realorder1 << " " << imagorder1 << " " << endl;

        outfile_r << x1 <<" " << order11 << endl;

        complex<double> orders= exp(im*ystart[n1]);
        for(i=n1+1;i<n;i++){
            orders += exp(im*ystart[i]);
        }

        double realorder2 = real(orders)/n2;
        double imagorder2 = imag(orders)/n2;
        double order12= sqrt(realorder2*realorder2 + imagorder2*imagorder2);

        outfile_t << x1 << " " << realorder2 << " " << imagorder2 << " " << endl;

        outfile_u << x1 <<" " << order12 << endl;
    }

    outfile_s.close();
    outfile_o.close();
    outfile_or.close();
    outfile_q.close();
    outfile_r.close();
    outfile_t.close();
    outfile_u.close();

    int length = runtime/dx+1;

    cout << "lenght order.dat=" << length << endl;

```

```
delete yp_p;  
delete xp_p;  
  
return 0;  
}
```

C Appendix: Calculating the wavelet transform

This program, made in C, computes the wavelet transform of the signal $\frac{1}{N} \sum_{i=1}^N Re^{i\theta_i}$.

```
#include <math.h>
#include <stdio.h>

#define epsilon 0.04

/* parameters for the morlet wavelet */
#define sigma 2.0
#define lambda 1.0
#define ntmax 2000 /* 4000 */

FILE *out,*out1,*out2, *out3, *in, *out_main,*out_freq;

double morlet_re(double);
double morlet_im(double);

double wave_trans(double, int, double *,double *, double *);
double wave_trans_phase(double, int, double *,double *, double *);

double maxis(double,double);
double minis(double,double);
double theta(double,double,double);

int main(void){

    double eps=1.e-5;
    double h1=1.e-1, hmin=0,t1,t2,tmin=0., tmax=440000.;
```

```

int nvar=6, nok, nbad;

int nt;

double omega;

/* for the wavelet transform*/

double omega_x0,omega_y0,omega_z0;

double wave_trans_x,wave_trans_y,wave_trans_z,wave_trans_0,
wave_trans_phase_0,wave_trans_sub,wave_trans_top;

double omegamin =0.15/(2*M_PI) , omegamax = 0.45/(2*M_PI), domega;

int nomega,nomegamax = 200; /*5000*/

int nb,nbmin,nbmax;

double x_array[ntmax];
double px_array[ntmax];
double t_array[ntmax];

double omega_x0_array[ntmax];

nbmin = 200; //margins left and right
nbmax = ntmax - nbmin;

domega = (omegamax-omegamin)/nomegamax;

printf("%f %f %f\n",omegamin,omegamax,domega);

```

```

double xstart[nvar];

printf("epsilon: %f\n", epsilon);

/* reads trajectory from order.dat produced by orderpM.cpp */

FILE*in_order = fopen("order.dat", "r");

for(int k=0; k<ntmax; k++){
    fscanf(in_order,"%lf %lf %lf", &t_array[k], &x_array[k], &px_array[k]);
    printf("%lf %lf %lf \n", t_array[k], x_array[k], px_array[k]); }

/* output for dat_2_ppm.C */

int I201 = nbmin + 1;
int I601 = ntmax - 2*nbmin + 1;

out1 = fopen("out.dat","w");
out2 = fopen("out2.dat","w");
fprintf(out1, "%d %d \n", I201, I601);
fprintf(out2, "%d %d \n", I201, I601);

for(nb=nbmin; nb<=nbmax; nb++){
    printf("nb=%d\n", nb);
    for(nomega=0; nomega<=nmegamax;nomega++){
        fprintf(out1, "%d %d ", nb, nomega);
        fprintf(out2, "%d %d ", nb, nomega);
        omega_x0 = omegamin + nomega*(omegamax-omegamin)/nmegamax;

        wave_trans_0 = wave_trans(omega_x0, nb, x_array, px_array,
        t_array);
        fprintf(out1," %f\n", wave_trans_0);
        wave_trans_phase_0 = wave_trans_phase(omega_x0,
        nb, x_array, px_array, t_array);
        fprintf(out2," %f\n", wave_trans_phase_0);
    }
}

```

```

}

fclose(out1);
fclose(out2);
} /* end main */

double morlet_re(double t){
return 1./sigma/sqrt(2.*M_PI)*cos((2*M_PI*lambda*t))*exp(-t*t/(2.*sigma*sigma));}

double morlet_im(double t){
return 1./sigma/sqrt(2.*M_PI)*sin((2*M_PI*lambda*t))*exp(-t*t/(2.*sigma*sigma));}

double maxis(double x, double y){

if(x>=y)
    return x;
else
    return y; }

double minis(double x, double y){

if(x<=y)
    return x;
else
    return y; }

double wave_trans(double omega, int nb, double *array_signal , double
*array_signal_H , double *array_t){
    double dt, a, b, tmin, tmax, mean=0., trans, trans_re=0., trans_im=0.;
    double *array_si;
    int nt;

a = (lambda + sqrt( lambda*lambda + 1./(2.*M_PI*M_PI*sigma*sigma)))/(2.*omega);
b = array_t[nb];

tmin = b - 3.*sqrt(2)*sigma*a;

```

```

tmax = b + 3*sqrt(2)*sigma*a;

/* determine wavelet transform */

dt = array_t[2] - array_t[1];

for(nt=(int) maxis(0., tmin/dt -2); nt<= (int)
minis(ntmax, tmax/dt +2); nt++){
trans_re += (array_signal[nt] * morlet_re((array_t[nt] - b)/a)
+ array_signal_H[nt] * morlet_im((array_t[nt]-b)/a) )/sqrt(a) *dt ;

trans_im += (array_signal_H[nt]*morlet_re((array_t[nt]-b)/a)
- array_signal[nt] * morlet_im((array_t[nt]-b)/a) )/sqrt(a) * dt; }

trans= sqrt(trans_re*trans_re + trans_im*trans_im);

return trans;
} /* end wave_trans */

double wave_trans_phase(double omega, int nb, double *array_signal ,
double *array_signal_H , double *array_t){

double dt, a, b, tmin, tmax, mean=0., trans, trans_re=0., trans_im=0.;
double *array_si;
int nt;
double phase = 0.0;

a = (lambda + sqrt( lambda*lambda + 1./(2.*M_PI*M_PI*sigma*sigma)))/(2.*omega);
b = array_t[nb];

tmin = b - 3.*sqrt(2)*sigma*a;
tmax = b + 3*sqrt(2)*sigma*a;

```

```

/* determine wavelet transform */

dt = array_t[2] - array_t[1];

for(nt=(int) maxis(0., tmin/dt -2); nt<= (int)
minis(ntmax, tmax/dt +2); nt++){
trans_re += (array_signal[nt] * morlet_re((array_t[nt] - b)/a)
+ array_signal_H[nt] * morlet_im((array_t[nt]-b)/a) )/sqrt(a) *dt ;

trans_im += (array_signal_H[nt]*morlet_re((array_t[nt]-b)/a) - array_signal[nt]
* morlet_im((array_t[nt]-b)/a) )/sqrt(a) * dt; }

trans= sqrt(trans_re*trans_re + trans_im*trans_im);

phase = atan2(trans_im,trans_re);

return phase;
} /* end wave_trans_phase */

double theta(double q, double p, double h){
double phi, thetais;

phi = acos(q/pow(4.*h, 0.25));

thetais = M_PI/2.;

if(q>=0 && p>=0)
return 2*M_PI-thetais;
else if(p>0 && q<=0)
return 2*M_PI - (M_PI - thetais);
else if(p<0 && q<=0)
return 2*M_PI - (thetais + M_PI);
else
return 2*M_PI - (2.*M_PI-thetais);
}

```

D Appendix: Plot of the wavelet transform

This program, made in C, assigns colors to the wavelet transform and creates a plot of the time frequency analysis.

```
#include <iostream>
#include <iomanip>
#include <cmath>
#include <fstream>

using namespace std;

void hsv2rgb (double h, double s, double v, double *r, double *g, double *b)
{
    double q,p,f,t;
    int i;

    if (s==0){
        *r = *g = *b = v;
    }
    else{
        h = h / 60;
        i = (int)(h);
        f = h - i;
        p = v * (1 - s);
        q = v * (1 - (s * f));
        t = v * (1 - (s * (1 - f)));
    }

    switch(i){
        case 0: *r = v; *g = t; *b = p;break;
        case 1: *r = q; *g = v; *b = p;break;
        case 2: *r = p; *g = v; *b = t;break;
    }
}
```

```

        case 3: *r = p; *g = q; *b = v;break;
        case 4: *r = t; *g = p; *b = v,break;
        case 5: *r = v; *g = p; *b = q;break;
    }
}

int main(void)
{
    double max_fxy=-1.E-10,min_fxy=1.E10;
    int Nx,Ny;
    double x,y,fxy;

    // find maximum and minimum values

    ifstream infile( "out.dat" );

    if( infile )
    {
        // # grid points in x and y direction

        infile >> Nx >> Ny;

        for( int ny=1 ; ny<=Ny ; ny++ )
            for( int nx=1 ; nx<=Nx ; nx++ )
            {
                infile >> x >> y >> fxy;

                max_fxy = fxy > max_fxy ? fxy : max_fxy;

```

```

        min_fxy = fxy < min_fxy ? fxy : min_fxy;
    }
}

else
{
    cout << "file could not be opened";
    return (-1);
}

infile.close();

cout << "Nx : " << Nx << " Ny : " << Ny << "\n";
cout << "Min : " << min_fxy << " Max : " << max_fxy << "\n";

ifstream infile_2( "out.dat" );
ofstream outfile( "out.ppm" );

outfile << "P3\n\n" << Nx << " " << Ny << "\n\n" << "255\n\n" ;

if( infile_2 )
{
// # grid points in x and y direction

    infile_2 >> Nx >> Ny;

    double r,g,b;

    for( int ny=1 ; ny<=Ny ; ny++ )
        for( int nx=1 ; nx<=Nx ; nx++ )
        {
            infile_2 >> x >> y >> fxy;

            double r,g,b;

```

```

    hsv2rgb( (max_fxy-fxy)/(max_fxy-min_fxy)
              *250,1.0,1.0,&r,&g,&b);

    outfile << (int)( pow(fabs((fxy-min_fxy)/
        (max_fxy-min_fxy)),0.1)* 255*r) << " ";
    outfile << (int)( pow(fabs((fxy-min_fxy)/
        (max_fxy-min_fxy)),0.1)* 255*g) << " ";
    outfile << (int)( pow(fabs((fxy-min_fxy)/
        (max_fxy-min_fxy)),0.1)* 255*b) << "\n";

}

else
{
    cout << "file could not be opened";
    return (-1);
}

infile_2.close();
outfile.close();

return 0;
}

```

E Appendix: Poincaré map

This program is made in C++ and finds the intersections of ρ and δ with the Poincaré section $\psi = \pi$.

```
#include <iostream>
#include <iomanip>
#include "nr.h"

using namespace std;

const int N = 4;
const DP A = 0.28;
const DP Beta = 0.1;
const DP x22 = M_PI;
complex<double> im=-1;

int runtime= 20000000;

// Driver for routine odeint

DP dxsav; // defining declarations
int kmax,kount;
Vec_DP *xp_p;
Mat_DP *yp_p;

int nrhs; // counts function evaluations

// Declaration variable funtions

DP gamma2(const DP rho2, const DP psi2)
{
    im = sqrt(im);
```

```

complex<double> imNumber = (double)1 + ((1-pow(rho2,2))*pow(-rho2*exp(-im*psi2),N))
/((double)1-pow(-rho2*exp(-im*psi2),N));
DP tempReturn = real(imNumber);
return tempReturn; }

DP mod_2_PI(DP x)
{while (x<=0) {
x += 2.0*M_PI;
}while (x>2*M_PI) {
x -= 2.0*M_PI;
}return x;
}

DP mod_2_PI_PI(DP x)
{while (x<=-M_PI) {
x += 2.0*M_PI;
}while (x>M_PI) {
x -= 2.0*M_PI;
}return x;
}

void derivs(const DP t, Vec_I_DP &yvector, Vec_O_DP &dydx)
{ DP rho2 = yvector[0];
  DP delta = yvector[1];
  DP psi2 = yvector[2];

  nrhs++;
  DP gamma2Var = gamma2(rho2,psi2);

  dydx[0] = (1-pow(rho2,2))/4 *((1+A)*rho2*gamma2Var*sin(Beta)
+ (1-A) *sin(Beta + delta));
  dydx[1] = ((1+A)/2)*(-cos(Beta) + ((1+pow(rho2,2))/(2*rho2))
*gamma2Var*rho2*cos(Beta))

+ ((1-A)/2)*(-rho2*gamma2Var*cos(Beta-delta) + ((1+pow(rho2,2))
/(2*rho2))*cos(Beta+delta));

```

```

dydx[2] = -((1-pow(rho2,2))/(4*rho2))* ((1+A)*rho2*gamma2Var*cos(Beta)
+(1-A)*cos(Beta+delta));
}

void derivs2(const DP t, Vec_I_DP &yvector, Vec_O_DP &dydx)
{
DP rho2 = yvector[0];
DP delta = yvector[1];
DP psi2 = yvector[2];
nrhs++;

DP gamma2Var = gamma2(rho2,psi2);

// rho2_psi
dydx[0]= ((1-pow(rho2,2))/4 *((1+A)*rho2*gamma2Var*sin(Beta) +
(1-A) *sin(Beta + delta)))/(-((1-pow(rho2,2))/(4*rho2))*(
((1+A)*rho2*gamma2Var*cos(Beta) +(1-A)*cos(Beta+delta)));
// delta_psi
dydx[1]= (((1+A)/2)*(-cos(Beta) +
((1+pow(rho2,2))/(2*rho2))*gamma2Var
*rho2*cos(Beta)) + ((1-A)/2)*(-rho2*gamma2Var*cos(Beta-delta)
+ ((1+pow(rho2,2))/(2*rho2))*cos(Beta+delta)))
/(-((1-pow(rho2,2))/(4*rho2))* ((1+A)*rho2*gamma2Var*cos(Beta)
+(1-A)*cos(Beta+delta)));
// psi2_psi
dydx[2]= 1;

}

int main(void)
{
const int KMAX=100;
int i,nbad,nok;

```

```

DP eps=1.0e-8,h1=0.1,hmin=0.0,x1=1.0,x2=10.0, dx=0.01;
DP x1max = runtime*dx;
Vec_DP ystart(N);
Vec_DP ystart2(N);

ystart[0]= 0.5;
ystart[1]= 0.25;
ystart[2]= M_PI;

nrhs=0;
dxsav=(x2-x1)/20.0;
kmax=KMAX;
xp_p=new Vec_DP(KMAX);
yp_p=new Mat_DP(N,KMAX);
Vec_DP &xp=*xp_p;
Mat_DP &yp=*yp_p;

ofstream outfile_y("Poincarre.dat");
ofstream outfile_x("Poincarretime.dat");
ofstream outfile_m("PoincarreFinal.dat");
int Count = 0, Count_min=1000;
for(x1=0;x1<x1max;x1+=dx){
    cout << ystart[2] << endl;

    x2 = x1 + dx;

    DP Psi2old = M_PI;
    if (x1 > 0) {
        Psi2old = ystart[2];
    }
    outfile_x << x1 << " " << mod_2_PI_PI(ystart[0]) << " " <<
    mod_2_PI_PI(ystart[1]) << " " << endl;
    NR::odeint(ystart,x1,x2,eps,h1,hmin,nok,nbad,
               derivs,NR::rkqs);
}

```

```

        for(i=0;i<N;i++){
            ystart[i]=mod_2_PI(ystart[i]);
        }

        if(Psi2old< M_PI && ystart[2]>M_PI){

            Count+= 1;
            ystart2[0]= ystart[0];
            ystart2[1]= ystart[1];
            ystart2[2]= ystart[2];

            DP x12 = ystart[2];

NR::odeint(ystart2,x12,x22,eps,h1,hmin,nok,nbad,derivs2, NR::rkqs);
//outfile_y.open("Poincarre.dat");
    outfile_y << mod_2_PI_PI(ystart2[0]) << " " <<
    mod_2_PI_PI(ystart2[1]) << " " << ystart2[2]
    << " " << endl;

//if(Count>Count_min){
outfile_m << x1 << " " << mod_2_PI_PI(ystart2[0]) << " " <<
mod_2_PI_PI(ystart2[1]) << " " << endl;
//}

}

outfile_y.close();
outfile_x.close();
outfile_m.close();
delete yp_p;
delete xp_p;

```

```
return 0;  
}
```

F Appendix: Calculating the two norm of the error for the numerical integration

The following program is made in C++ and calculates the 2-norm of the error made with the integration. This is done by comparing the value of the integrated Kuramoto model to the value obtained by back integration of the same system with a minus in front.

```
#include <iostream>
#include <iomanip>
#include <cmath>
//#include <random>
#include <complex>
//#include <std>
#include "nr.h"

using namespace std;

const int n=250;
int countmin;
int countplus;

double w1_array[n];
double w_array[n];
int runtime= 2000;
double K=0;
double phistart_array[n];
double sum;
double norm1 =0;

// Driver for routine odeint

DP dxsav; // defining declarations
int kmax,kount;
Vec_DP *xp_p;
Mat_DP *yp_p;
```

```

int nrhs; // counts function evaluations

void derivs(const DP t, Vec_I_DP &yvector, Vec_O_DP &dydx)
{
    int i=0;
    int k=0;
    nrhs++;

    for(i=0; i<n; i++){
        dydx[i] = w_array[i];
        for(k=0;k<n;k++){
            dydx[i] += K/n*sin(yvector[k]-yvector[i]);
        }
    }
    //cout << "dydx[1] : " << dydx[1] << endl;
}

void derivs2(const DP t, Vec_I_DP &yvector, Vec_O_DP &dydx)
{
    int i=0;
    int k=0;
    nrhs++;

    for(i=0; i<n; i++){
        dydx[i] = - w_array[i];
        for(k=0;k<n;k++){
            dydx[i] -= K/n*sin(yvector[k]-yvector[i]);
        }
    }
    //cout << "dydx[1] : " << dydx[1] << endl;
}

DP mod_2_PI(DP x)
{while (x<=0) {
x += 2.0*M_PI;
}

```

```

countplus++;
}while (x>2*M_PI) {
x -= 2.0*M_PI;
countmin--;
}return x;
}

DP mod_2_PI_PI(DP x)
{while (x<=-M_PI) {
x += 2.0*M_PI;
}while (x>M_PI) {
x -= 2.0*M_PI;
}return x;
}

int main(void)
{
const int N=n, KMAX=100;
int nbad,nok;
DP eps=1.0e-7,h1=1.0e-10,hmin=0.0,x1=0.0,x2=0.0, dx=0.3;
DP x1max = runtime*dx;
Vec_DP ystart(n);
Vec_DP ystart2(n);
Vec_DP ystart1(n);
DP error(n);
Vec_DP ystart_old(n);
int i=0;
int idum = -2 ;

ofstream outfile_w("omega.dat");
ofstream outfile_p("phases.dat");

for(i=0;i<n;i++){
w1_array[i] = NR::ran3(idum);
w_array[i] = 0.3 + 0.025*tan(M_PI*(w1_array[i]-0.5));
outfile_w<<w_array[i]<<" "<<endl;
}
}

```

```

    cout << "w[" << i << "] : " << w_array[i] << " ";
}

cout << endl;

for(i=0;i<n;i++){
    ystart[i]= NR::ran3(idum)*2*M_PI;
    outfile_p<< ystart[i] <<" "<<endl;
    ystart1[i]=ystart[i];
}

outfile_w . close();
outfile_p . close();

nrhs=0;
dxsav=(x2-x1)/2.0;
kmax=KMAX;
xp_p=new Vec_DP(KMAX);
yp_p=new Mat_DP(N,KMAX);

ofstream outfile_s("trajectory.dat");
ofstream outfile_o("order.dat");
ofstream outfile_or("Rorder.dat");
ofstream outfile_e("error.dat");

for(x1=0;x1<x1max;x1+=dx){
    x2 = x1 + dx;
    cout << "time: " << x1 << " " << x2 <<endl;
    NR::odeint(ystart,x1,x2,eps,h1,hmin,nok,nbad,derivs, NR::rkqs);

    outfile_s << x1;
    complex<double> im=-1;
    im = sqrt(im);
    for(i=0;i<n;i++){
        outfile_s<<" "<< ystart[i];}
    outfile_s << endl;
}

```

```

complex<double> order= exp(im*ystart[0]);
    for(i=1;i<n;i++){
order += exp(im*ystart[i]);}
    double realorder = real(order)/n;
    double imagorder= imag(order)/n;
    double order1= sqrt(realorder*realorder + imagorder*imagorder);

    outfile_o << x1 << " "<< realorder << " "<< imagorder
<< " " << endl;

outfile_or << x1 <<" "<< order1 << endl;

}

for(i=0;i<n;i++){
ystart2[i]=ystart[i];
}

for(x1=0;x1<x1max;x1+=dx){

x2 = x1 + dx;
NR::odeint(ystart2,x1,x2,eps,h1,hmin,nok,nbad,derivs2,NR::rkqs);
}

for(i=0;i<n;i++){
cout<<"ystart1:"<< ystart1[i] <<endl;
cout<< "ystart2:" <<mod_2_PI(ystart2[i]) <<endl;
}

for(i=0;i<n;i++){
error = ystart1[i] - ystart2[i];
cout<< "error:" << " " << error <<" "<<endl;
outfile_e<<" "<< error<< " " << endl;
sum+=(error*error);
}

```

```
norm1 =sqrt(sum);

cout << "\n Result of norm: "<< norm1 << "log(norm): "
<< log(norm1);

outfile_s.close();
outfile_o.close();
outfile_or.close();
outfile_e.close();

int length = runtime/dx+1;

cout << "lenght order.dat=" << length << endl;

delete yp_p;
delete xp_p;

return 0;
}
```

G Animation

This program makes an animated plot in Matlab. The animated plot shows the oscillators of two groups running around on the unit circle and displays the order parameter of both group as well.

```
clear; close all;

% Create data trajectory
matrixData = dlmread('trajectory.dat');
averageData = dlmread('order.dat');
averageData1 = dlmread('orderfirst');
averageData2 = dlmread('ordersecond');
timeColum = matrixData(:,1);
plot(cos(timeColum), sin(timeColum));
dots = zeros(1,21);
hold on

axis square

% Draw initial figure
figure(1);
set(gcf, 'Renderer', 'OpenGL');
xlim([-1.5,1.5]);
ylim([-1.5,1.5]);

% Draw dots
for j=2:5
    xPos = cos(matrixData(1,j));
    yPos = sin(matrixData(1,j));

    dots(1,j) = plot(xPos, yPos, 'o', 'MarkerSize', 10,
        'MarkerFaceColor', 'b');
    set(dots(1,j), 'EraseMode', 'normal');
end

for j=6:9
```

```

xPos = cos(matrixData(1,j));
yPos = sin(matrixData(1,j));

dots(1,j) = plot(xPos, yPos, 'o', 'MarkerSize', 10,
'MarkerFaceColor', 'g');
set(dots(1,j), 'EraseMode', 'normal');
end

% Draw average
averageX = averageData(1,2);
averageY = averageData(1,3);

% Draw line to average
lineX=[0 averageX];
lineY=[0 averageY];
lineToAverage = line(lineX,lineY, 'LineWidth', 1, 'Color', 'r');

averageDot = plot(averageX, averageY, 'o', 'MarkerSize', 10,
'MarkerFaceColor', 'r');
set(averageDot, 'EraseMode', 'normal');

% Draw average1
averageX1 = averageData1(1,2);
averageY1 = averageData1(1,3);

% Draw line to average1
lineX1=[0 averageX1];
lineY1=[0 averageY1];
lineToAverage1 = line(lineX1,lineY1, 'LineWidth', 1, 'Color', 'b');

averageDot1 = plot(averageX1, averageY1, 'o', 'MarkerSize', 10,
'MarkerFaceColor', 'b');
set(averageDot1, 'EraseMode', 'normal');

% Draw average2
averageX2 = averageData2(1,2);

```

```

averageY2 = averageData2(1,3);

% Draw line to average2
lineX2=[0 averageX2];
lineY2=[0 averageY2];
lineToAverage2 = line(lineX2,lineY2, 'LineWidth', 1, 'Color', 'g');

averageDot2 = plot(averageX2, averageY2, 'o', 'MarkerSize', 10,
'MarkerFaceColor', 'g');
set(averageDot2, 'EraseMode', 'normal');

% Animation Loop
for i=2:1001
    % Dots animation
    for k=2:9
        x = cos(matrixData(i,k));
        y = sin(matrixData(i,k));

        set(dots(1,k), 'XData', x);
        set(dots(1,k), 'YData', y);
        drawnow;
    end

    %AverageDot animation
    averageX = averageData(i,2);
    averageY = averageData(i,3);

    lineX=[0 averageX];
    lineY=[0 averageY];
    set(lineToAverage, 'XData', lineX);
    set(lineToAverage, 'YData', lineY);

    set(averageDot, 'XData', averageX);
    set(averageDot, 'YData', averageY);

```

```

drawnow;

% AverageDot animation
averageX1 = averageData1(i,2);
averageY1 = averageData1(i,3);

lineX1=[0 averageX1];
lineY1=[0 averageY1];
set(lineToAverage1, 'XData', lineX1);
set(lineToAverage1, 'YData', lineY1);

set(averageDot1, 'XData', averageX1);
set(averageDot1, 'YData', averageY1);
drawnow;

% AverageDot animation
averageX2 = averageData2(i,2);
averageY2 = averageData2(i,3);

lineX2=[0 averageX2];
lineY2=[0 averageY2];
set(lineToAverage2, 'XData', lineX2);
set(lineToAverage2, 'YData', lineY2);

set(averageDot2, 'XData', averageX2);
set(averageDot2, 'YData', averageY2);
drawnow;
end

```